Non-Covalent Interactions in Polymeric Materials: From Ionomers to Polymer Blends

Lin Ju

Dissertation submitted to the faculty of the Virginia Polytechnic Institute and State University in partial fulfillment of the requirements for the degree of

Doctor of Philosophy
In
Chemistry

Robert B. Moore, Chair
Timothy E. Long
Michael J. Bortner
John B. Matson

August 14, 2019
Blacksburg, VA

Keywords: phosphonated ionomers, compatibilization of polymer blends, plasticization of poly(vinyl alcohol), deep eutectic solvent, structure-morphology-property relationship

Non-Covalent Interactions in Polymeric Materials: From Ionomers to Polymer Blends

Lin Ju

ABSTRACT

Conventional studies of ionomers have focused on ionomers bearing monovalent carboxylate or sulfonate pendant ions. There are relatively fewer studies on ionomers containing multivalent pendant ions, such as divalent phosphonate. In this dissertation, poly(ethylene terephthalate) (PET) and polystyrene ionomers with divalent phosphonate pendant ions have been synthesized, and the influence of divalent phosphonate pendant ions on the structure-morphology-property relationship has been compared to the ionomers with monovalent sulfonate pendant ions. The phosphonate groups generated a stronger physically crosslinked network in phosphonated ionomers as compared to sulfonated analogues. Higher plateau modulus, longer relaxation time, and significantly higher zero-shear viscosity were noted for phosphonated ionomers by a dynamic melt rheology study. Compared to the ionic aggregates generated from sulfonate groups, larger ionic aggregates with associated phosphonate groups have been observed. Furthermore, phosphonated ionomers displayed significantly higher glass transition temperatures than sulfonated ionomers.

Ionomers have proven to be attractive, interfacially active compatibilizers for a number of polymer blend systems because of specific interactions that may develop between the ionic groups and complementary functional groups on other polar polymers within the blends. The successful compatibilization of polyester/polyamide blends (prepared by solution mixing and melt blending methods) using phosphonated PET

ionomers as a minor-component compatibilizer has been demonstrated. The phase-separated polyamide domain dimension decreased with increasing mol % phosphonated monomers and this decrease was attributed to the specific interactions between the ionic phosphonate groups on the polyester ionomer and the amide linkages of polyamide. More importantly, the divalent phosphonate pendant ions are more effective at compatibilizing polyester/polyamide blends in comparison to the monovalent sulfonate pendant ions. Phosphonated PET ionomer-compatibilized polyester/polyamide blends required 6 times fewer ionic monomers to achieve domain dimension < 1 μm as compared to sulfonated PET-containing blends.

Deep eutectic solvents (DES) have been reported to be the next generation solvents due to the superior biocompatibility, biodegradability, and sustainability as compared to ionic liquids. Two types of deep eutectic solvents, choline chloride : malic acid (ChCl:MA) and L-arginine : levulinic acid (Arg:LA), have been demonstrated as effective plasticizers for poly(vinyl alcohol) (PVOH) films. The plasticization effects on the properties of PVOH films were evidenced by lower crystallizability and improved film ductility. In addition, ChCl:MA deep eutectic solvent was more effective in plasticizing PVOH as compared to propylene glycol, one of the most widely studied alcohol-type plasticizers. From an applied perspective, DES-plasticized PVOH film is a promising candidate in the packaging market of heath-related products.

Non-Covalent Interactions in Polymeric Materials: From Ionomers to Polymer Blends

Lin Ju

GENERAL AUDIENCE ABSTRACT

Non-covalent interactions play an important role on the structure-morphology-property relationship of polymeric materials. Divalent phosphonate pendant ions provide interesting effects on the properties of ionomer and polymer blends as compared to the monovalent sulfonate pendant ions. Ionomers containing phosphonate pendant ions exhibit a significantly stronger physically crosslinked network as compared to sulfonated ionomers. Compared to monovalent sulfonate groups, the divalent phosphonate groups are more effective at compatibilizing polymer blends. Furthermore, the compatibilized poly(ethylene terephthalate)-based blends exhibit improved optical and oxygen barrier properties compared to the base blend without compatibilizer, signifying potential benefits in packaging industry.

Poly(vinyl alcohol) is one of the most widely used packaging materials for food, medicine, detergent, etc. The incorporation of deep eutectic solvents as plasticizers significantly improved film ductility. In addition, the plasticization effect for choline chloride-based deep eutectic solvent is more profound than one of the most widely studied alcohol-type plasticizers, propylene glycol. The effective plasticization of poly(vinyl alcohol) using deep eutectic solvents confirmed the potential for future applications in the packaging market of health-related product.

ACKNOWLEDGEMENTS

Firstly, I would like to thank and acknowledge Dr. Robert Moore. He is the best advisor one could ever have for his/her PhD study. I sincerely appreciate his guidance and mentorship during my PhD career. His enthusiasm towards innovation and his scientific curiosity have motivated me to dig deeper into my research. Every research project, group meeting presentation, and manuscript revision have prepared me to be an independent researcher. All the achievements I have obtained during my PhD study would not be possible without his patience, encouragement, and continuous supports. I would like to thank my committee members, Dr. Timothy E. Long, Dr. Michael J. Bortner, and Dr. John B. Matson, for their insightful comments and continuous help during all the committee meetings. Dr. Long's expertise in the field of polyester furnished me with an in-depth understanding of the phosphonated polyester ionomers studied in this dissertation. Dr. Bortner provided valuable comments on the polymer blends work from an engineering perspective. Dr. Matson's "synthesis and reaction of macromolecules" class was so interesting that drove my career interests in the wonderful world of polymers. I also thank Dr. Donald Baird for the great discussion and collaboration on melt rheology analysis.

I am very fortunate to be a member of the Moore Research Group (MoRG), and enjoyed my graduate life with many brilliant students. I would like to thank our group members Dr. Samantha Talley, Dr. Lindsey Anderson, Kristen Felice Noble, and Gregory Fahs for their helps and great suggestions on my projects. I learned writing skills from Sam and Kristen as well as presentation skills from Lindsey. Greg taught me how to play with laser light scattering, and was always patient when explaining the scattering theory.

It was a pleasure to work with Christina Orsino, Melissa Novy, Glenn Spiering, Garrett Godshall, and Zahra Mansouri. Christy and Melissa became my lovely friends after working together in the lab. Glenn is our new scattering and extrusion expert and helped with solving difficult scattering problems. I passed my lab safety officer position along with officer badge to Garrett. There is no doubt that he will do a great job on our lab safety. Special thanks to Dr. Bruce Orler, who taught me how to use DSC and analyze data in my first year. I appreciate all their supports and wish them successful careers.

I am thankful for all the collaborators contributed to this dissertation. Dr. Ryan Mondschein, Johanna Vandenbrande, and Clay Arrington helped with oxygen permeability measurements. Even though gas permeability tests took a long time, we finally yielded good results after several months. I would like to thank Dr. Joseph Dennis and Dr. Katherine Heifferon for training in the PET synthesis. Joe was like sunshine, brightening up my fume hood every time he came to our lab to help with my reactions. I also thank Ryan Carrazzone and Dong Guo for GPC and TGA analysis, respectively. All these people are not only collaborators, but also the best teammates on the softball field. They always encouraged me and told me I did a great job no matter how bad I was. Most of them graduated and left Blacksburg, but I still miss these exciting nights on the softball field.

I acknowledge funding from the Institute for Advanced Learning and Research (IALR) and the Proctor and Gamble Company (P&G) that supported my research assistantship for most of my graduate school years. I appreciate all the collaborations and discussions with Freddy Barnabas, Lorri Bacca, and Marcela Valenzuela from P&G for sharing their knowledge of deep eutectic solvent and poly(vinyl alcohol) films. I also

would like to thank Jeremy Beach from IALR for extrusion training and troubleshooting. Special thanks to Eastman Chemical Company for awarding me the 2017 fellowship to support my graduate career.

I would like to thank my manager, Jignesh Sheth, and my mentor, Benjamin Biber, for their guidance and support during summer internship at the Henkel Corporation, Bridgewater, NJ. Jignesh opened the door to the world of adhesive for me. I miss those days staying with Joann Sutyak, Bristee Das, Jocelyne Yuen, and Jenny Plummer. I look forward to being back in Princeton and playing escape room with them again. I would like to thank Eric Silverberg for giving me the opportunity for an onsite interview after a phone interview and for sharing his career experience in the field of pressure sensitive adhesives. I appreciate the morning coffee time with Michael Harwell at Bollo's, and sincerely thank him for sharing his industrial experience and providing suggestions about career path. Special thanks to James Nowicki. He is such a charming, knowledgeable guy with enthusiasm in life. I am fortunate to become a friend of his, and we are following each other on "Strava" since we all like running. Thanks for all the thumbs up he gave on every running record I broke. I appreciate all the great discussions with Charles Paul, Cristina Dejesus, Clay Kellam, and Wu Suen for sharing their knowledge of adhesives and career path in industry.

I am very appreciative for Prof. Zhenghu Xu in SDU and Prof. Jessica Hoover in WVU. I started to work in Prof. Xu's lab when I was a sophomore. He opened the door to the world of organic chemistry for me, and was always patient on teaching me how to run TLC plates and how to "run columns". I would like to thank Prof. Hoover for her mentorship in the project of copper-catalyzed coupling reactions and her guidance on

how to give presentations. Even though I am not researching organic chemistry, all the knowledge and lab skills I learned will definitely benefit my career. I appreciate for Junsi Gu from Dow Chemical Company for sharing his experience in industry and offering helpful suggestions about graduate study. I sincerely acknowledge Dr. Keren Zhang, Dr. Justin Sirrine, and Dr. Yifan Dong for sharing their experience on their graduate careers.

Finally and most importantly, I am forever grateful to my parents, my lovely sister, and my dearest fiancé for their unconditional love and forever support. My father is a talented, courageous men, and always stays persistent to achieve his goals. He is a superman and also my hero. I still remember the spirit he told me during hiking when I was a kid. When flash floods occur, you should never give up and move forward. That moment was imprinted on my head, and I am not scared of any obstacles in my life. My mother always taught me to be a courageous girl and always stay optimistic. My parents gave my sister and me the names of “Lu” and “Lin”, and wish us to be happy, keep curiosity about the world, achieve our dreams, and live a wonderful life. I must thank my sister for giving “lucky spray” to support me during every milestone exam. Thanks to my cat, Pipi /`pi:pi:/, for bringing me numerous funny moments. He is such a cute, smart, and lovely cat. He knows how to play “piano”, shake hands, high five, and open the bedroom door when I locked him out. He is my Pokémon, like Pikachu. We will experience all the adventures in the future. I am grateful to my fiancé, Tianran Chen, for his quiet, warm, and endless love. I was very lucky to meet you six years ago, and I wish I could have met you earlier. You are such a humorous guy that I never get bored when staying with you. I am happy to have you in my life as my Mr. Right.

Life is short, but is colorful because we all have dreams. Everyone I met on my way to my dreams is like the sunshine that brightens up the road. I am so fortunate to meet everyone and have you in my life. I sincerely wish you all happiness and success in life.

Table of Content

List of Figures

List of Tables

Attributions

Prof. Robert B. Moore
Professor of Chemistry Department at Virginia Tech and the author's research advisor

Prof. Donald G. Baird
Professor of the Department of Chemical Engineering and collaborators on Chapters 3, 4, and 5

Prof. Timothy E. Long
Professor of Chemistry Department at Virginia Tech and collaborator on Chapters 3, 6, and 7

Prof. Guoliang Liu
Professor of the Department of Chemistry at Virginia Tech and collaborator on Chapters 8 and 9

Dr. Joseph M. Dennis
Past graduate student in Prof. Timothy E. Long's research group who contributed to Chapters 3 and 6

Dr. Katherine V. Heifferon
Past graduate student in Prof. Timothy E. Long's research group who contributed to Chapters 3 and 6

Tianran Chen
Graduate student in Prof. Donald G. Baird's research group who contributed to Chapters 3, 4, and 5

Juan Pretelt
Graduate student in Prof. Donald G. Baird's research group who contributed to Chapter 3.

Glenn A. Spiering
Graduate student in Prof. Robert B. Moore's research group who contributed to Chapter 5.

Dr. Ryan J. Mondschein
Past graduate student in Prof. Timothy E. Long's research group who contributed to Chapter 7

Johanna A. Vandenbrande
Graduate student in Prof. Timothy E. Long's research group who contributed to Chapter 7

Clay B. Arrington
Graduate student in Prof. Timothy E. Long's research group who contributed to Chapter 7

Zahra Mansouri
Graduate student in Prof. Robert B. Moore's research group who contributed to Chapter 8

Dong Guo
Graduate student in Prof. Guoliang Liu's research group who contributed to Chapters 8 and 9

List of Abbreviations

PET = poly(ethylene terephthalate)

PPET = phosphonated poly(ethylene terephthalate)

DSC = differential scanning calorimetry

SPET = sulfonated poly(ethylene terephthalate)

$t_{1/2}$ = crystallization half-time

T_g = glass transition temperature

T_{cc} = cold crystallization temperature

T_m = melting temperature

T_c = crystallization temperature

HFIP = hexafluoro-2-propanol

ΔH_m = enthalpy of melting

ΔH_{cc} = enthalpy of cold crystallization

ΔH_c = enthalpy of crystallization

X_c = degree of crystallinity

η^* = complex viscosity

SAXS = small angle X-ray scattering

η_0 = zero-shear viscosity

ω = frequency

G' = storage modulus

G'' = loss modulus

LRC = Leibler-Rubinstein-Colby (LRC) theory

TTS = time-temperature superposition

τ_{rep} = reptation time

SPS = sulfonated polystyrene

PPS = phosphonated polystyrene

MXD6 = poly(m-xylylene adipamide)

LVE = linear viscoelastic

T_r = reference temperature

η = melt viscosity

M_w = weight average molecular weight

M_n = number average molecular weight

PDI = polydispersity index

R_1 = radius of the spherical aggregate

R_{ca} = radius of closet approach

$2R_{is}$ = average center- to-center aggregate separation

QCC = quadrupolar coupling constant

M_e = entangle molecular weight

G_N = plateau modulus in storage modulus

E_a = activation energy

PC-OM = phase contrast optical microscopy

SALLS = small angle laser light scattering

PETG = amorphous polyester composed of terephthalic acid and ethylene glycol with a portion of the glycol units substituted with cyclohexanedimethanol

SDD = sample-to-detector distance

λ = wavelength of incident light

FTIR = fourier transform infrared spectroscopy

SEM = scanning electron microscope

TEM = transmission electron microscopy

OTR = oxygen transmission rate

P = gas permeability

D = gas diffusivity

S = gas solubility

PVOH = poly(vinyl alcohol)

DES = deep eutectic solvent

ChCl = choline chloride

MA = DL-malic acid

PG = propylene glycol

TGA = thermogravimetric analysis

DMA = thermal mechanical analysis

$T_{d,\ 5\ wt\%}$ = the temperature at which 5 wt% weight loss is observed

Arg = L-arginine

LA = Levulinic acid

NADES = natural deep eutectic solvent

RH = relative humidity

Chapter 1. Introduction

1.1 Dissertation Overview

This dissertation details the stronger effects of divalent phosphonate pendant ions on the properties of ionomers and polyester/polyamide blends as compared to monovalent sulfonate groups. The plasticization of poly(vinyl alcohol) films using deep eutectic solvents (DES) is also depicted. Chapter 2 reviews current progress in the synthesis and properties of ionomers bearing divalent phosphonate pendant ions, along with the theories and strategies of the compatibilization of polymer blends. Chapter 3 to 4 mainly focus on the synthesis of phosphonated poly(ethylene terephthalate) (PPET) ionomers, and the comparison to sulfonated PET (SPET) analogues. Chapter 5 details the synthesis of polystyrene ionomers containing the same mol% of sulfonated and phosphonated ionic monomers and the evaluation of structure-morphology-property relationship for these two series of polystyrene ionomers. Chapter 6 and 7 describe the application of PPET ionomers as minor-component compatibilizers in polyester/polyamide blends prepared by solution mixing and melt blending methods. Chapter 8 and 9 detail the investigation of deep eutectic solvents as plasticizers in poly(vinyl alcohol) films.

Chapter 3 details the synthesis of phosphonated ionic monomer and the melt polymerization to produce phosphonated PET ionomers. This chapter also reports the structure-property relationship for these phosphonated PET ionomers at low ionic contents (0.5-4.0 mol%). The incorporation of phosphonate groups provides strong physical crosslinks in PET ionomers, thus imparting higher melt viscosity and enhanced

mechanical properties as compared to pure PET. Chapter 4 investigates the thermal properties and linear viscoelastic behaviors of PPET ionomers as compared to SEPT analogues. Crystallization behavior and crystallization kinetics were studied to evaluated their thermal properties. Time-temperature superposition principle was applied in dynamic melt rheology measurements to evaluate the influence of pendant ions on the linear viscoelastic behaviors of PET ionomers.

Chapter 5 studies the effects of monovalent sulfonate and divalent phosphonate pendant ions on the thermal, morphological, and dynamic rheological properties of polystyrene ionomers. The glass transition temperature and microphase-separated morphology between sulfonated and phosphonated polystyrene ionomers were evaluated. Oligomeric polystyrene ionomers with molecular weight below the chain entangle molecular weight were synthesized in order to isolate the effect ionic associations on the linear viscoelastic properties of polystyrene ionomers.

Chapter 6 describes the investigation of compatibilization effects of phosphonated PET ionomers in amorphous polyester/polyamide blends prepared by solution mixing method. The phase-separated morphology and the phase-separated domain dimensions were evaluated, and were compared to sulfonated PET ionomers with monovalent sulfonate groups. The specific interactions between the ionic groups and the polar amide linkages of polyamide were studied. Chapter 7 reports the compatibilization effect of phosphonated PET ionomers in PET/MXD6 melt blends. The phase-separated MXD6 domain size was characterized to evaluate the effectiveness of phosphonate ionic groups on the morphology of polyester/polyamide blend systems. Optical and oxygen barrier

properties were evaluated on biaxially stretched films to probe the potential of these compatibilized blends for future packaging applications.

Chapter 8 reports the plasticization effect of choline chloride : malic acid deep eutectic solvents (ChCl:MA DES) on the thermal and tensile properties, as well as water absorption, of polyvinyl alcohol films. The plasticization effects for ChCl:MA DES were compared to a widely used alcohol-type plasticizer, propylene glycol. In Chapter 9, a novel natural DES, arginine : levulinic acid (Arg:LA), was synthesized. The relationship between plasticization effect and the molar ratio of Arg and LA was investigated.

Finally, Chapter 10 provides the overall conclusion regarding the structure-morphology-property relationships of phosphonated ionomers and DES-plasticized PVOH films. Chapter 11 suggests future directions to continue the research efforts on novel ionomers design and the evaluation of their potential applications.

Chapter 2. Introduction to Ionomers Bearing Phosphonate Pendant Ions and Compatibilization of Polymer Blends

2.1 Ionomers Bearing Phosphonate Pendant Ions

2.1.1 Introduction

Ionomers are charged polymers that contain minor amounts (typically < 15 mol%) of covalently attached ionic functionalities incorporated into or pendant to the polymer backbones.[1-3] The term "ionomer" was originally proposed by DuPont to describe random copolymers of ethylene and methacrylic, or acrylic acid, partially or completely neutralized with alkali metals or zinc (M-PEMA, where the first M represents the cation).[4, 5] The M-PEMA ionomers were first commercialized in 1964 by DuPont under the trade name Surlyn®. During the past half-century, various types of ionomers have been developed and applied in numerous fields.[2, 6-17] The incorporated polar ionic groups, surrounded by a less polar matrix, tend to form nanometer-sized ionic aggregates due to the attractive Coulombic interactions between the ion pairs.[18] These ionic aggregates act as physical crosslinks that significantly alter the physical, mechanical, optical, dielectric, and dynamic properties of a polymer.[2, 19-27]

Ionomers bearing monovalent carboxylate and sulfonate pendant ions are the most widely studied ionomers in the literature.[1, 3, 18, 22, 28-30] Relatively fewer studies have focused on ionomers containing the multivalent functionality, such as divalent phosphonate. This review will focus on the synthesis methodology of ionomers bearing phosphonate pendant ions and their physical properties. The comparison of the effects of

monovalent sulfonate and divalent phosphonate pendant ions on the physical properties of ionomers will also be discussed in this review.

2.1.2 Synthesis Methodology

To prepare ionomers containing phosphonate pendant ions, two main methods exist: direct polymerization of phosphonated monomers, and post-polymerization phosphonation of existing polymers. Both routes will be discussed in detail below.

2.1.2.1 Direction Polymerization of Phosphonated Monomers

Phosphonated ionomers with aliphatic backbone are usually prepared by free-radical polymerization of phosphonate-containing monomers. A wide range of polyelectrolytes with phosphorus ionic groups were prepared with various acidic forms (**Figure 1A**).[31] Weiss and coworkers[30, 32] developed a facile route for preparing styrene-based phosphonated ionomers, i.e., poly(styrene-*co*-vinylphophonate) (SVP) copolymers. SVP copolymers in the phosphonate ester form were synthesized by free radical polymerization with styrene and diethyl vinylphosphonate esters (DEVP) in toluene initiated by tetrabutyl hydroperoxide. The ester groups of the copolymers were hydrolyzed to phosphonic acid groups, and the sodium and zinc salts ionomers were obtained by further neutralization (**Figure 2.1B**). Kwei and coworkers[33, 34] prepared poly(styrene-*co*-4-vinylbenzenephosphonic acid diethyl ester) (PSVBDEP) by bulk radical polymerization of styrene with 4-vinylbenzenephosphonic acid diethyl ester (VBDEP). 2,2'-Azobis(isobutyronitrile) (AIBN) was utilized as an initiator for this type of reaction. The acid form, poly(styrene-*co*-4-vinylbenzenephosphonic acid) (PSVBA), was prepared by hydrolysis of PSVBDEP in dioxane saturated with concentrated hydrochloric acid (**Figure 2.1C**). Another type of reaction to provide phosphonated ionomers with aliphatic backbone was via ring opening polymerization. A new ionic diol,

1,2-dihydroxypropylphosphonic acid (DPPA), was synthesized from epibromohydrin and triethyl phosphite, and was subsequently used as a chain extender diol in the two-step synthesis of polyurethane ionomers (**Figure 2.2**).[35]

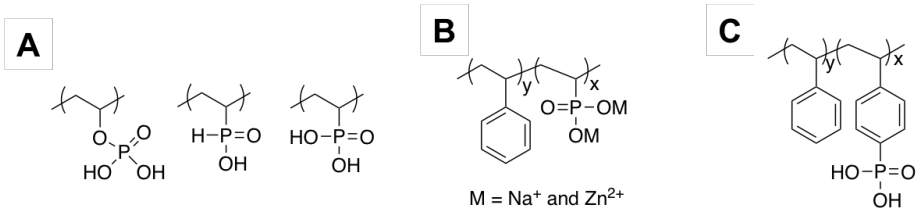

Figure 2.1. Chemical structures of (A) polyelectrolytes with phosphorus ionic groups,[31] (B) poly(styrene-co-vinylphophonate) (SVP) ionomers,[30,32] and (C) poly(styrene-co-4-vinylbenzenephosphonic acid) (PSVBA) ionomers.[33,34]

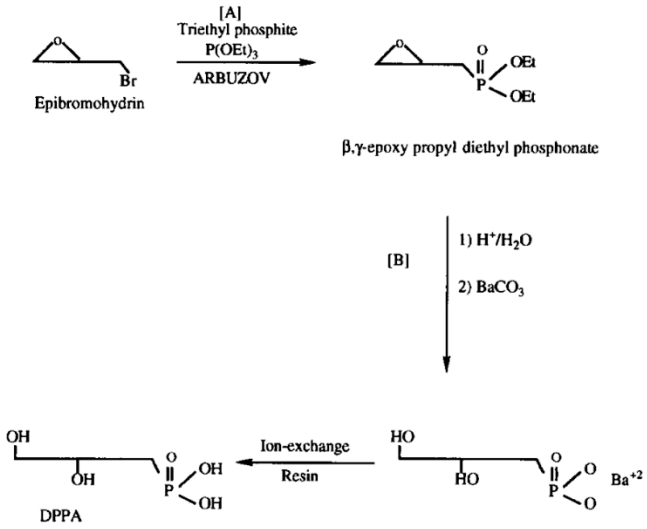

Figure 2.2. Synthesis of 1,2-dihydroxypropylphosphonic acid (DPPA). Reprinted from reference 35. Copyright 1994 Butterworth-Heinemann Ltd.

Literatures available for polymerization of phosphonated monomers to ionomers with aromatic polymer backbone were quite limited due to the complexity and difficulties in synthesis methodology. An aromatic polyelectrolyte bearing phosphonic acids was

synthesized from the synthetic route depicted in **Figure 2.3A**.[36] Poly(phenylenephosphonic acid ester) was generated by nickel-catalyzed Arbuzov reaction of an aryliodide with triethyl phosphite. The aromatic rings were then linked together at the chlorinated positions by nickel-catalyzed reductive coupling in the presence of metallic zinc. The phosphonic acid esters were then hydrolyzed with concentrated HCl to provide the acid form in the final step. Banerjee et al.[37] reported an easy synthesis strategy of phosphonic acid-containing diphosphonated poly(ether ether ketone) (P-PEEK) by polycondensation of difluoro benzophenone and phosphonated bisphenol A (BPA). Phosphonation of BPA was carried out by monophosphoazylation followed by rearrangement in the presence of organolithium compound at -78 °C (**Figure 2.3B**). In the field of polyester ionomers, the synthesis of a phosphonated poly(ethylene terephthalate) ionomer in Na^+ form (Na^+-PPET) was reported in a patent in 1962 by DuPont.[38] Melt polycondensation with ethylene glycol, dimethyl terephthalate, and the phosphonate ionic monomer yielded Na^+-PPET ionomers (**Figure 2.3C**) that were processed into textile fibers with an affinity for basic type dyes, such as colored cationic organic substances containing sulfonium, oxonium, or quaternary ammonium functional groups. However, the yield of the essential phosphonated isophthalate monomer was reported to be only 15%, which apparently limited subsequent comprehensive structure-property relationship investigations. Recently, Moore and coworkers[39] modified the synthetic pathway to the phosphonated isophthalate monomers, and the yield of pure monomers was improved by 300%. This greatly improved yield enabled the synthesis of Na^+-PPET ionomers in a large scale.

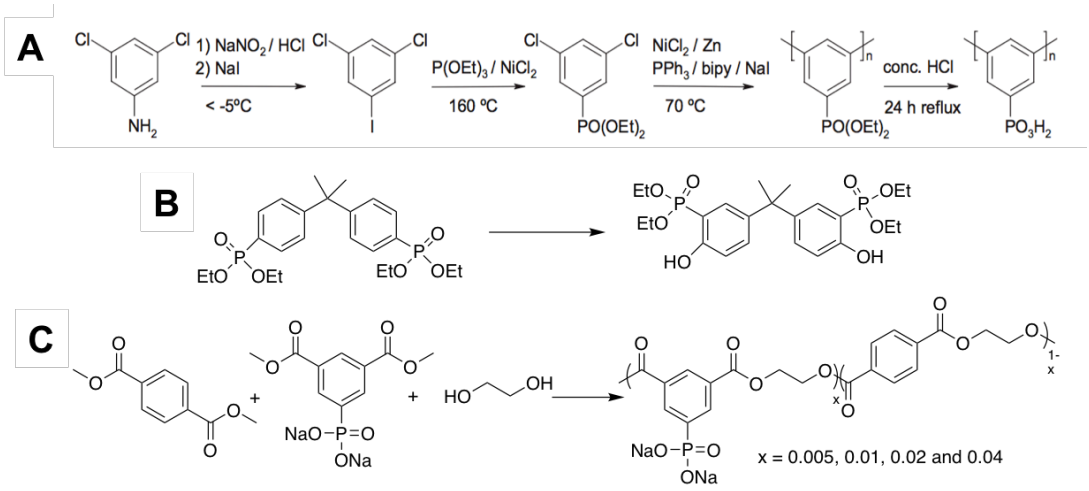

Figure 2.3. (A) Synthesis of poly(phenylenephosphonic acid). Reprinted from reference 36. Copyright 2007 WILEY-VCH Verlag GmbH & Co. KGaA, Weinheim. (B) Synthesis of phosphonated bisphenol A (BPA). Reprinted from reference 37. Copyright 2014 High Performance Polymers. (C) Synthesis of phosphonated poly(ethylene terephthalate) ionomer in Na^+ form (Na^+-PPET). Reprinted from reference 39. Copyright 2018 Elsevier Ltd.

2.1.2.2 Post-Polymerization Phosphonation of Existing Polymers

Modification of existing polymers using phosphonating agents is a useful route to provide phosphonated ionomers. Poly(vinyl alcohol) (PVOH) and poly(ethylene glycol) (PEG) have been reported to react with phosphoryl chloride ($POCl_3$) to generate phosphonyl dichloride groups via chlorophosphonylation.[40] Phosphonic acid form was realized by further hydrolysis.[40] Azuma and MacKnight[41] developed a method to introduce phosphonate side groups to poly(pentenamer) (PP) by free-radical grafting of dimethyl phosphite onto the C=C bonds of PP to generate the dimethyl ester form (PP-PO). The corresponding acid derivative was prepared by bubbling hydrochloric acid

(HCl) gas through a dilute solution of the ester-form PP-PO, and further neutralization using cesium hydroxide provided cesium salt form.

The incorporation of phosphonic acid groups by direct phosphonation of unfunctionalized aromatic polymers required harsh reaction conditions. Lewis acid-activated phosphorus trichloride (PCl_3) was employed to arylphosphonate the aromatic moieties in electron-rich polymers, such as polystyrene or polysulfones.[42, 43] However, the arylphosponation of polystyrene was accompanied by insuppressible crosslinking issue because of the reactive aryl-PCl_2 intermediates and the weak electrophilicity of PCl_3 that require long reaction times. In other works, various approaches have been applied to catalytic arylphosphonation of brominated high performance polymers, e.g., PEEK, PSU, poly(ether sulfones) (PES), and poly(phenyl sulfone) (PPSU) (**Figure 2.4**).[43-47] Brominated-aromatics react with diethylphosphite to generated the coupled C-P bonds via Palladium-catalyzed Michaelis-Arbuzov reactions. Recently, arylphsphonation using $NiCl_2$ and commercial trialkylphosphites or tris(trimethylsilyl)phosphite substantially improved reaction conditions in weakly coordinating, higher-boiling-point solvents, such as diphenyl ether, diphenylketone, and diphenylsolfone.[43, 48]

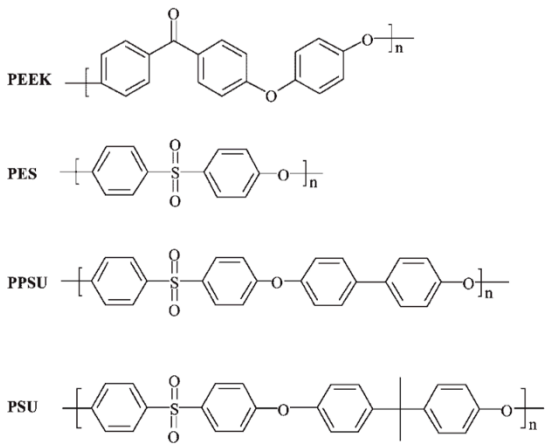

Figure 2.4. Higher performance polymers employed in Ni-catalyzed arylphosphonation. Reprinted from reference 43. Copyright 2007 WILEY-VCH Verlag GmbH & Co. KGaA, Weinheim.

2.1.3 Physical Properties

2.1.3.1 Thermal Properties

The Glass Transition Temperature. The incorporation of phosphonate pendant ions in polymers leaded to an increased glass transition temperature (T_g)[30, 32, 49-51] as commonly seen in carboxylated and sulfonated ionomers.[1, 2, 21, 22, 29, 52, 53] This higher T_g compared to nonionic control is attributed to a reduction in chain mobility from the physical cross-links formed by dipole-dipole interactions between the polar ion pairs. In addition, the effect of anionic pendant ions, i.e., thioglycolate, phosphonate, carboxylate, and sulfonate, on the glass transition temperatures (T_g) of poly(pentenamer) ionomers (**Figure 2.5A**) with the concentration of ionic functionalities up to 19 mol% was evaluated by MacKnight and Earnest using differential scanning calorimetry (DSC).[50] **Figure 2.5B** displays the plot of T_g as a function of mol% ionic functionalities. Poly(pentenamer) ionomers bearing divalent phosphonate groups exhibited the highest T_g

as compared to the monovalent sulfonate and carboxylate-containing analogues. With increasing the mol% of ionic functionalities, the difference of T_g between each composition became more distinct. The higher T_g for phosphonated poly(penenamer) ionomers suggested the divalent phosphonate groups generated stronger electrostatically-crosslinked physical network that provides a more profound effect on restricting the mobility of polymer chains. Therefore, a higher T_g was observed for the ionomers containing the divalent phosphonate pendant ions as compared to the monovalent pendant ions-containing analogues.

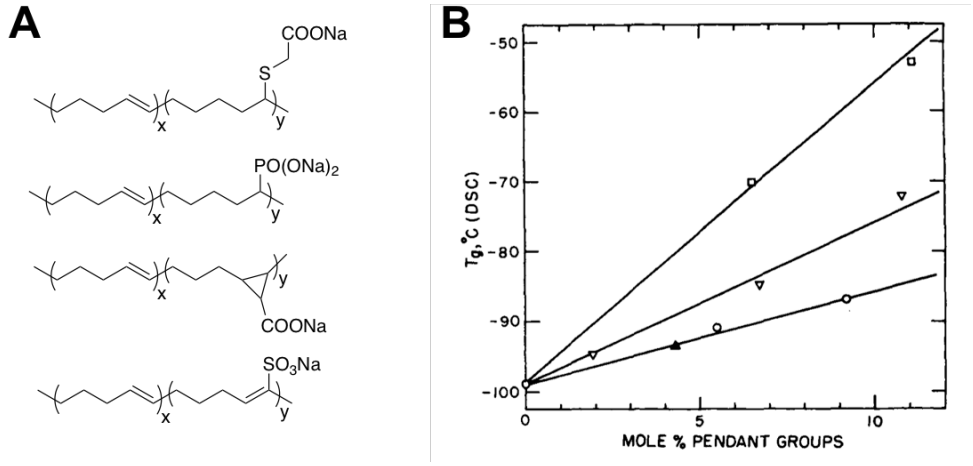

Figure 2.5. (A) Chemical structures representing poly(penenamer) ionomers bearing thioglycolate, phosphonate, carboxylate, and sulfonate pendant ions; (B) Glass transition temperatures (T_g) for poly(penenamer) ionomers bearing sodium thioglycolate (open circle symbols), cesium phosphonate (open square symbol), cesium carboxylate (filled triangle symbols), and sodium sulfonate (open triangle symbols) pendant ions as a function of mol% of ionic functionalities. Reprinted from reference 50. Copyright 1981 John Wiley & Sons, Inc.

Crystallizability and Crystallization Kinetics. Our group[39] synthesized phosphonated poly(ethylene terephthalate) ionomers in Na^+ form (Na^+-PPET) with low ionic monomer contents (0.5-4.0 mol%), and investigated their crystallizability and crystallization kinetics by using DSC. With increasing ionic content, heating thermograms exhibited decreased melting temperature (T_m) and degree of crystallinity (X_c), and the subsequent cooling scans showed decreased crystallization temperature (T_c), as commonly seen in other semicrystalline polymers.[53, 54] Upon cooling from the melt, the phosphonate ionic groups acting as structural defects that are rejected from the growing crystalline interface. Thus, with an increasing defect content, both T_m and X_c decreased as a consequence of decreased average length of crystallizable segments and limited lamellar thickness. In addition, the interactions between the interactive defects (phosphonate pendant ions) restrict chain mobility during the time scale of cooling cycle, which retards the crystallization phenomenon to lower temperatures. Moreover, the effect of phosphonate pendant ions on the crystallization behavior of Na^+-PPET ionomers was further evaluated using DSC isothermal crystallization experiments over a rang of controlled crystallization temperatures. Avrami analysis indicated that at the same isothermal crystallization temperature, the crystallization rate decreased with increasing ionic content, which further confirmed lower crystallizability. However, the comparison of crystallization behaviors between sulfonated and phosphonated ionomers has not been reported.

2.1.3.2 Dynamic Mechanical Behavior

Weiss and coworkers[30, 32] reported the synthesis of poly(styrene-*co*-vinylphosphonate) (SVP) copolymers and investigated the dynamic mechanical behaviors

as compared to sulfonated polystyrene (SPS) ionomers at the same level of ionic functionality (**Figure 2.6**). **Figure 2.7** depicts the dynamic mechanical behaviors, including storage modulus (*E'*) and tan δ, of the ester, acid, Na^+, and Zn^{2+} forms of SVP copolymers along with the Na^+ and Zn^{2+} forms of SPS. *E'* of phosphonated copolymers increased in the order of ester < acid < Na^+ = Zn^{2+}. In addition, SVP in the ester form failed to show rubbery plateau, but SVP in both Na^+ and Zn^{2+} forms exhibited significant plateau region persisted for a wide temperature range (**Figure 2.7A**). These observations suggested the physical crosslinks generated between phosphonate ion pairs were stronger and more temperature resistant than the hydrogen bonding interactions formed between phosphonic acid groups. Furthermore, it is important to note that the comparison between SVP and SPS indicated the SVP ionomers in both Na^+ and Zn^{2+} forms at the same ionic functionality displayed a higher rubbery plateau modulus and a more extended plateau region than SPS analogues (**Figure 2.7A**). Even though the acid strength of the phosphonic acid (pK_{a1} ~ 2-3; pK_{a2} ~7) is less than that of the sulfonic acid (pK_a ~ 1), SVP bearing divalent phosphonate pendant ions possessed stronger physical crosslinked network than SPS functionalized with the monovalent sulfonate groups.

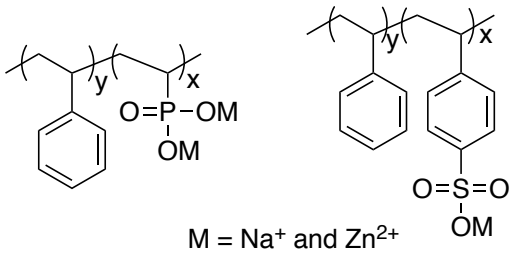

Figure 2.6. Chemical structures of poly(styrene-*co*-vinylphosphonate) (SVP) (left) and sulfonated polystyrene (SPS) (right) ionomers in Na^+ and Zn^{2+} forms.

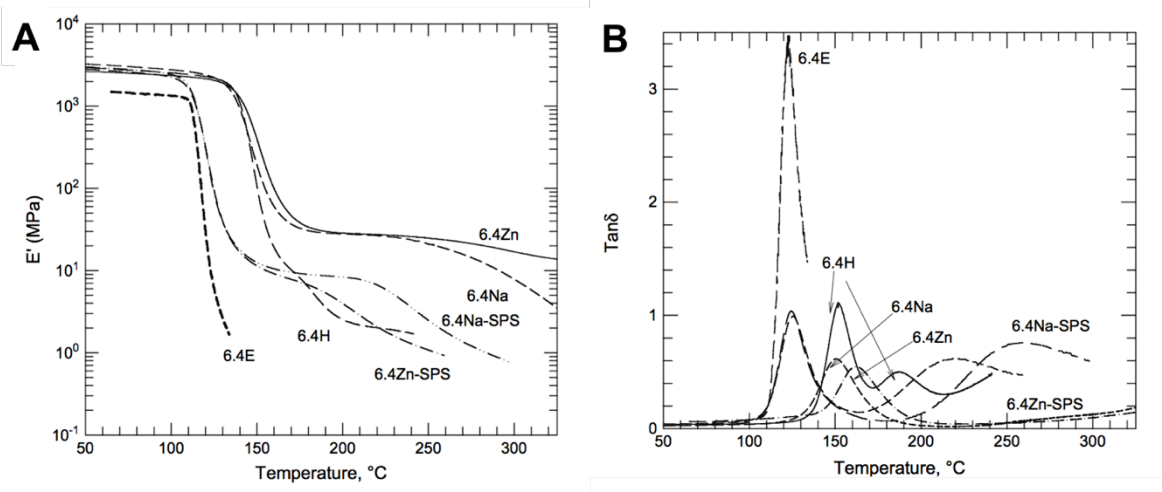

Figure 2.7. (A) Storage modulus (*E'*) and (B) tan δ for 6.4 mol% functionalized SVP copolymers in the ester, acid, Na^+, and Zn^{2+} forms along with SPS ionomers in the Na^+ and Zn^{2+} forms. f = 1 Hz, 2 °C/min. Reprinted from reference 30. Copyright 2007 Elsevier Ltd.

Ionomers often exhibit two principle relaxations in the tan δ versus temperature response: a lower temperature peak due to the glass transition of the hydrocarbon matrix and a higher temperature peak due to a transition of an ion-rich microphase.[55, 56] Unlike SPS ionomers exhibiting two relaxations, SVP only showed one tan δ along the measured temperature range (**Figure 2.7B**). It is possible that the ionic phase relaxation in these ionomers occurs above 300 °C. Due to the degradation issue of these ionomers, this assumption was not confirmed in the literature. Nevertheless, in agreement with DSC results, the investigation of tan δ further confirmed the higher T_g for SVP containing divalent phosphonate pendant ions as compared to SPS bearing monovalent sulfonate ions.

2.1.3.3 Morphological Properties

The microphase-separated morphologies of SVP ionomers were examined by using small-angle X-ray scattering (SAXS).[32] The plot of scattering intensity versus q for SVP ionomers in Na^+ and Zn^{2+} form is shown in **Figure 2.8**. The single, broad scattering peak seen in **Figure 2.8** for each sample except 2.4 mol% SVP ionomers is designated as ionic peak corresponding to the formation of ionic aggregates, as commonly seen in other ionomers.[53, 57-60] The intensity of the ionic peak increased as the ion content increased, and the position of the peak shifted to higher q. The increase in the position of the scattering peak, q_{max}, suggested a decreased interdomain spacing (d_{max}) based on Bragg's law. Generally, d_{max} for SVP in Zn^{2+} form was smaller than that for SVP in the Na^+ form. Additionally, a clear peak was not observed in the scattering profile for 2.4 mol% Na^+-SVP, while a distinct shoulder was found for the 2.4 mol% Zn^{2+}-SVP, which is due to the enhanced electron density by the incorporation of the Zn^{2+} cation. However, the radius of the spherical aggregate and the average center-to-center aggregate separation were not calculated, and no systematic comparison between phosphonate and sulfonate analogues has been evaluated.

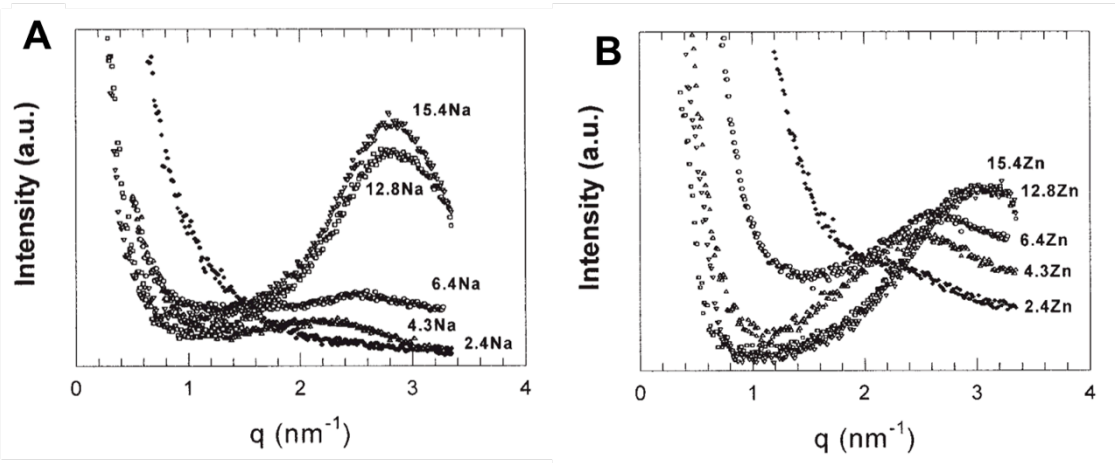

Figure 2.8. Small-angle X-ray scattering profile for (A) Na^+-SVP and (B) Zn^{2+}-SVP ionomers. Reprinted from reference 32. Copyright 2004 Wiley Periodicals, Inc.

2.1.3.4 Other Physical Properties

Our group[39] studied the melt rheology of phosphonated PET ionomers in the Na^+ form (Na^+-PPET) at various ionic contents (0.5-4.0 mol%) via a frequency sweep (0.1-100 rad/s) in the melt state at 280 °C. Na^+-PPET ionomers exhibited increased complex viscosity as a result of increased ionic content. In addition, a crossover of storage modulus (*G'*) and loss modulus (*G''*) was observed for all the Na^+-PPET ionomers, and the corresponding crossover frequency shifted to lower frequency with increasing ionic content, indicative of an enhanced effect of physical crosslinked network attributed to the strong electrostatic associations between phosphonated units on the polymer chains. Additionally, unlike most sulfonated ionomers, ionomers bearing phosphonate pendant ions, e.g., phosphonated PET ionomers[39] and phosphonated high performance polymers (PEEK, PSU, PES, and PPSU)[43-47] have been shown to exhibit a poor solubility in most of the organic solvents and organic acids even at high temperatures (> 100 °C).

2.1.4 Summary

Ionomers bearing divalent phosphonate pendant ions can be synthesized by two ways: direct polymerization of phosphonated monomers and post-polymerization phosphonation of existing polymers. The incorporated phosphonate groups exhibited profound effects on the thermal, dynamic mechanical, morphological and linear viscoelastic properties of polymers. Phosphonated ionomers exhibited lower crystallizability and slower crystallization kinetics. A rubbery plateau, indicative of the presence of physical crosslinks, has been observed in storage modulus from dynamic mechanical analysis. However, no studies have focused on systematic comparison of sulfonated and phosphonated ionomers. The evaluation of the influence of monovalent sulfonate and divalent phosphonate pendant ions on the physical properties of ionomers has not been reported.

2.2 Compatibilization of Polymer Blends

2.2.1 Introduction to Polymer Blends

A polymer blend is a physical mixture of two or more polymers that have been blended together to create a new material with different physical properties.[61] Generally, polymer blends can be divided into three major classes based on their thermodynamic phase behavior: miscible, immiscible and compatible blends.[62, 63] Miscible blends are inherently mixed on a molecular level. This behavior is associated with a negative free energy of mixing, and is often composition and/or temperature independent. An immiscible blend shows phase separation at all compositions and temperatures and a positive free energy of mixing. A compatible polymer blend refers to an immiscible blend exhibiting macroscopically uniform physical properties, and often shows good mechanical properties (toughness, tensile strength, etc.) due to reduced interfacial tension and enhanced interfacial adhesion.

Increasing market pressure is driving the need to develop more economic polymer materials with better properties (toughness, tensile strength, barrier properties, etc.). Polymer blending has attracted attention as a potential solution in the development of low-cost high-performance materials. The reasons for selecting this approach fall into two categories: property combination and cost dilution.[62] Most polymer blend products succeed because of a combination or a balance of properties rather than because of any single characteristic. In addition, low-performance polymer A and high-cost, high-performance polymer B are blended to result in a series of lower-performance materials which can compete with other materials because of cost dilution. Therefore, polymer blending is a way of producing cheaper materials using limited amounts of the normally

expensive polymers to provide the maximum synergy of improved properties and lower costs.[64]

Compared to the development and commercialization of a new polymer, which usually require many years and are extremely costly, polymer blending is inexpensive to adapt and time-effective to commercialize. The time to commercialize polymer alloys and blends (PAB) was reduced to less than one year vs. 8-10 or more years for the synthesis of a new polymer.[64] Thus, blending technology is greatly desired to expand the performance capabilities of blends under specific conditions (e.g., mechanical, chemical, thermal, electrical). However, a key issue is that most polymers are immiscible. Phase behavior of a polymer blend is governed by the specific interactions between these polymer components. Thermodynamics and kinetics of phase separation, compatibilization strategies, and characterization of polymer blends will be discussed in the following sections.

2.2.2 Thermodynamics and Kinetics of Phase Separation

2.2.2.1 Thermodynamics of Mixing

Conditions of Mixing. Polymer blends exhibit immiscibility or miscibility with profound phase separation and various levels of mixing in between the extremes. Solubility of one component in another is governed by the free energy of mixing (**Equation 2.1**). There are two primary requirements for the miscibility of two components.[65, 66] First, a negative free energy change is characteristic of spontaneous processes. A negative ΔG_M indicates that the mixing process will occur spontaneously (**Equation 2.1**). Second, a plot of ΔG_M vs. volume fraction should be concave up.[6] The

change in the free energy of mixing with respect to the composition must meet the prerequisite in **Equation 2.2**:

$$\Delta G_M = \Delta H_M - T\Delta S_M \quad (2.1)$$

where ΔH_M and ΔS_M are the enthalpy and entropy of mixing.

$$\frac{\partial^2 \Delta G_M}{\partial \phi_i^2} > 0 \quad (2.2)$$

where ϕ_i is the volume fraction of either component.

Flory-Huggins Theory of Mixing. In 1941, Flory[67] and Huggins[68] published the following equation:

$$\Delta G_M = kT(n_1 ln\phi_1 + n_2 ln\phi_2 + \phi_1\phi_2\chi_{12}) \quad (2.3)$$

where, n_1 and n_2 are the number of moles, and ϕ_1 and ϕ_2 are the volume fractions of components 1 and 2, respectively, and χ_{12} is the interaction parameter. This equation describes the miscible behavior of a mixture and can be expressed in terms of free energy of mixing per mole of lattice sites by Flory-Huggins lattice model. The first two terms represent the combinatorial entropy of mixing, and the final term comes from the enthalpy of interaction. Entropic contribution is generally negligible for most polymer blends due to low configurational entropy inherent in high molecular weight polymers (**Equation 2.4**). Thus, enthalpic contribution to the free energy of mixing becomes the driving force for miscibility for most polymer mixtures.[69-71] In addition, due to the effects of differences in molecular size, and anomalous entropic contribution, Flory-Huggins model is unable to predict the miscibility of many polymer mixtures that exhibit lower critical solution temperature (LCST) behavior, and another approach must be taken.[72, 73]

$$\Delta S_M = -k\left(\frac{\phi_1}{N_1} ln\phi_1 + \frac{\phi_2}{N_2} ln\phi_2\right) \quad (2.4)$$

where N_1 and N_2 are the degrees of polymerization of components 1 and 2, respectively.

It is often necessary to utilize a polymer pair that possesses the capability of forming specific intermolecular interactions in order to achieve miscibility. These specific interactions include hydrogen bonding, ion-dipole, dipole-dipole, ionic, and van der Waals interactions.[74] Miscibility can be obtained by either increasing the strength of specific interactions or by increasing the fraction of interacting groups. As illustrated in **Figure 2.9**,[75] ΔG_m is positive throughout the composition range for polystyrene (PS)/polyamide-6 (PA6) blends, whereas the blends of PA6 and lithium sulfonated polystyrene (LiSPS) ionomer having 12.0 mol% lithium sulfonate groups exhibit negative ΔG_m throughout the composition range. This indicates an enhanced miscibility with increased strength of ionic interaction.

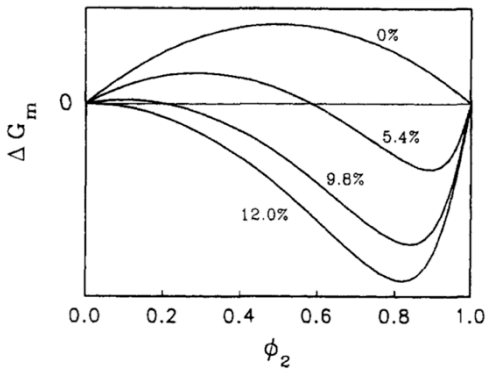

Figure 2.9. Profile of ΔG_m for polystyrene (PS)/polyamide-6 (PA6) blends with various ionic contents. Reprinted from reference 75. Copyright 1992 American Chemical Society.

2.2.2.2 Phase Diagrams of Polymer Blends

For blends exhibiting a significant region of miscibility, state of phase separation can be described as a function of either composition or temperature. Several types of

phase behaviors with regard to temperature and composition are outlined in **Figure 2.10**.[76]

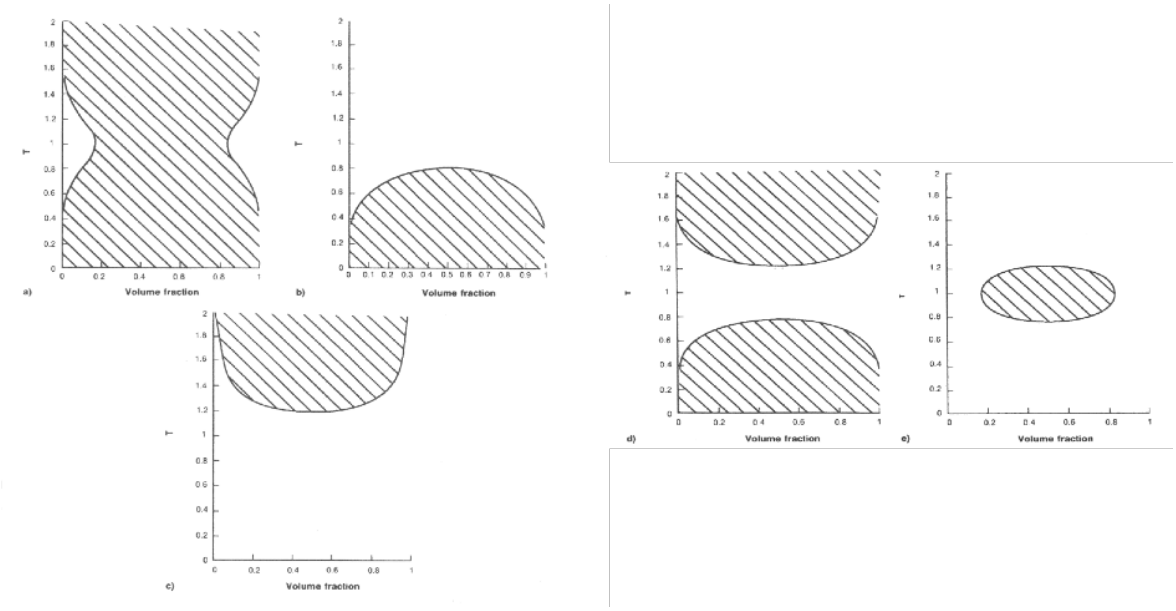

Figure 2.10. Polymer blend phase diagram types: (A) Hourglass; (B) UCST; (C) LCST; (D) UCST/LCST; E) Loop. Light area represents miscible region while shaded area represents immiscible region. Reprinted from reference 76. Copyright 1996 Hanser.

a) The hourglass curve describes a blend system that is miscible only at very low concentrations of one polymer in the other. Thus, "miscibility window" is quite narrow and often an immiscible blend is one in which the window is too small to detect.

b) The critical point on a phase diagram that separates a two-phase system at low temperature from a one-phase system at high temperature is called an upper critical solution temperature (UCST). This type of phase behavior is that the blend is immiscible at low temperatures, but after passing above the upper critical solution temperature (UCST), the blend becomes miscible at all.

c) A more common phase behavior in blends of high polymers involving specific interactions is the presence of a lower critical solution temperature (LCST), below which the blend system is miscible for all compositions. In this type of behavior, an increase in temperature provides ample energy to the system to overcome any type of specific interactions between the polymers in the blend.

d) The phase behavior illustrated in Figure 2d involves combination of UCST and LCST. LCST lies above UCST, and the region of miscibility is between the two critical temperatures.

e) Phase behavior of loop has never been seen for any polymer blend and is rarely encountered in small molecule mixtures.

2.2.2.3 Phase Separation Mechanism

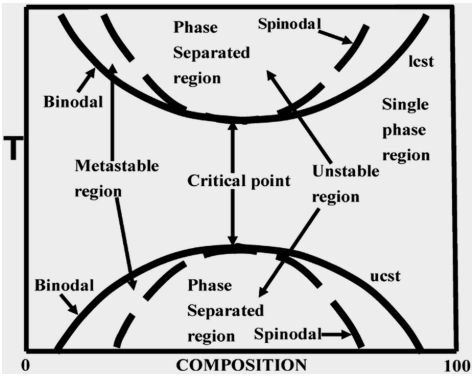

Figure 2.11. Phase diagram of LCST and UCST blends. Reprinted from reference 77. Copyright 1994 American Chemical Society.

Nucleation and Growth. The region between binodal and spinodal curves is metastable for phase separation (**Figure 2.11**).[76, 77] Domains smaller than a critical size will remix with the matrix. On the other hand, domains that are bigger than critical size will form nuclei for separated phase, which will grow with time until the whole sample is separated into two phases. Metastable region is characterized as "nucleation and growth".

Nucleation and growth process is the same as those for the growth of crystals from a liquid by nucleation.[17]

Spinodal Decomposition. In the region bordered by spinodal curve, phase separation is spontaneous because there is no need for a nucleated domain of one phase or the other.[76, 77] The second derivative of the free energy with respect to composition is negative in this region, and so all fluctuations from the average composition will grow to equilibrium phase compositions, driven by a reduction in the overall free energy of mixing.

2.2.2.4 Interfacial Tension and Morphology

Interfacial tension of fully co-continuous polymer blend structures is predicted in a model developed by Willemse and coworkers.[78, 79] During mixing, domains of each component are deformed by the applied flow field, which results in elongated particles of the dispersed phase. Conditions in the model developed by Willemse and coworkers are established for the stability of elongated particles.[78] The lower limit of volume fraction of the minor phase necessary for phase co-continuity (ϕ_{cc}) can be calculated by Equation 5:

$$\frac{1}{\phi_{cc}} = 1.38 + 0.0213\left(\frac{\eta_m \dot{\gamma}}{\sigma} R_0\right)^{4.2} \tag{2.5}$$

where η_m is the matrix viscosity at the blending conditions, $\dot{\gamma}$ is the shear rate, σ is the interfacial tension and R_0 is the radius of the minor phase. With the lower limit for phase co-continuity proportional to interfacial tension, a decrease in interfacial tension leads to a broader co-continuous region.[79] Experimental results confirmed the incorporation of a compatibilizer in polyethylene/PA6 blends reduces phase domain dimensions and shifts morphology from droplet/matrix to co-continuous due to a reduction in the interfacial tension between blend components.[80, 81]

2.2.3 Compatibilization Strategies

2.2.3.1 Addition of Block and Graft Copolymers

Emulsification of polymer blends has been proposed as the most efficient process for obtaining a fine phase morphology and good mechanical properties. The addition of block or graft copolymers represents the most extensively researched approach to compatibilization. Block and graft copolymers containing segments chemically identical to blend components locate preferentially at blend interfaces.[82] Diblock copolymers consisting of poly(pentadecalactone) (PPDL) and poly(L-lactide) (PLLA) were synthesized and applied as compatibilizers for high-density polyethylene (HDPE)/PLLA blends and linear low-density polyethylene (LLDPE)/PLLA blends. The compatibilized blends exhibited a steep decrease in particle size of the dispersed phase.[83] In addition, the use of grafted copolymers is another possible route for controlling phase morphology and mechanical properties of immiscible polymer blends. Lodge and Hillmyer reported polyethylene-graft-poly(methyl methacrylate) (PE-g-PMMA) copolymers as compatibilizers for binary PE/PMMA blends. Even at compatibilizer loading as low as 1 wt%, the average droplet size of PMMA was highly decreased.[84] However, these copolymers are often not commercially available or only available at high cost, and need to be tailor-made for a particular blend.[82]

2.2.3.2 Addition of Reactive Polymers

A polymer chemically identical to one of blend components is modified by incorporating functional (or reactive) units, which chemically react with the second blend component in the melt. Reactive polymers are generated by free radical copolymerization or by melt grafting of reactive groups onto chemically inert polymer chains.[85] The addition of end-reactive polymers or polymers carrying pendant reactive groups generates

reactive block or graft copolymers. Ethylene-glycidyl methacrylate-methyl acrylate terpolymer (PEGMMA, Lotader) was utilized as a compatibilizer in polylactide/polypropylene (PLA/PP) blends.[86] Successful compatibilization was achieved by coupling PEGMMA to the end groups of PLA. Additionally, reactive comb (RC) polymers were synthesized by copolymerizing methyl methacrylate (MMA) with glycidyl methacrylate (GMA) and carboxyl-terminated poly(methyl methacrylate) (PMMA-COOH). With only 1 wt % of RC polymers in an immiscible poly(l-lactic acid)/poly(vinylidene fluoride) (PLLA/PVDF) system, domain sizes were significantly reduced, and the uniformity of dispersed PVDF phase in PLLA matrix was enhanced.[87]

2.2.3.3 Addition of Low Molecular Weight Chemicals

The actual compatibilizer, a branched, block or grafted copolymer, is formed during reactive blending process by the addition of low molecular weight chemicals.[82] Dicumylperoxide as a low molecular weight chemical was added in the melt to initiate melt grafting reactions of poly(ethylene octene) (POE) and glycidyl methacrylate (GMA). POE-g-GMA was generated during reactive blending, and acted as effective compatibilizer in POE/PLA blends, leading to a better wetting of the dispersed phase.[88]

2.2.3.4 Addition of Ionomers

lonomers are polymeric species carrying a relatively low number of pendant ionic groups per chain. While carboxylate groups have been used to create ionomers, another common form of functionalization involves sulfonation of polymer backbone followed by neutralization of the generated sulfonic acid groups with a variety of counterions, ranging from monovalent (Na^+, Li^+, K^+) and divalent (Zn^{2+}, Mn^{2+}, Ca^{2+}) metals to quaternary alkyl ammoniums.[82] The ionic groups on the ionomer interact with the polar constituents

of the blended polymers, whereas the nonionic backbone of the ionomer is compatible with the less polar constituents.[82]

The compatibilization effects of several ionomers, including polystyrene,[89-92] polyethylene[93-97] and polyester ionomers,[98-100] on various types of polymer blends have been investigated. The incorporation of ionomers have been shown to effectively compatibilize immiscible polymer blends.[109-119] Ionomers have proven to be attractive, interfacially-active compatibilizers for a number of blend systems because of specific interactions that may develop between the ionic groups and complementary functional groups on other polar polymers within the blend.[101-106] These specific interactions tend to decrease the interfacial tension between the dissimilar polymers, leading to reduced phase dimensions and enhanced phase stability that inhibit coalescence during melt processing.[107, 108] In addition, the compatibilization effect is strongly dependent on the counterion type of the ionomer. Divalent counterions (Zn^{2+}, Mn^{2+}, Ca^{2+}) are more effective at compatibilizing polymer blends as compared to monovalent counterions (Na^{+}, Li^{+}, K^{+}).[109, 110, 107]

2.2.3.5 Compatibilization of Polyester/Polyamide Blends

Polyesters (e.g. poly(ethylene terephthalate) (PET)) are widely used polymers in the food and beverage packaging industry. The oxygen barrier properties of PET are acceptable for many food and beverage products. However, improvements are needed to meet the requirements for packaging highly oxygen-sensitive foods and beverages. Various methods have been investigated to reduce the inherent oxygen permeability of PET as a passive polymer.[120] These methods include structural manipulation,[121-123] copolymerization,[124-126] and the used of nanocomposites.[127-129] Such strategies have

provided limited improvements of barrier properties. In the case of nanocomposites, the formation of haze and nanoparticle agglomeration, as well as phase separation between nanoparticles and PET matrix, continue to be very challenging problems.[120]

Blending with high barrier polymers significantly improves the oxygen barrier properties of PET films and containers. This strategy is usually convenient, cheaper, and less time-consuming than the development of new polymers by synthesis.[130] PET has been blended with high barrier polymers such as ethylene vinyl alcohol copolymer (EVOH) and semi-aromatic polyamides. However, the moisture sensitivity of EVOH is an obstacle for achieving improved barrier properties in humid atmospheres.[131] Aromatic polyamides with high thermal and mechanical properties as well as good processability are less moisture sensitive compared to EVOH, and their melting temperatures are close to that of PET. Therefore, a special semi-aromatic polyamide, poly(*m*-xylene adipamide) (MXD6), has attracted attention.[132] Blends of PET and MXD6 showed good clarity due to incompatibility, and hence produced a multiphase blend.[133] The key to make PET/MXD6 blends useful with improved gas barrier property is to enhance their compatibility.[120] Studies on improvements of compatibility between polyester and polyamide have been focused on interchange reactions,[134-136] to generate copolymers that serve as interfacial compatibilizers,[97-99] or the incorporation of functional groups capable of forming intermolecular interactions.[90-92] These methods will be discussed in further detail below.

Compatibilization via Interchange Reaction. When polycondensate systems (e.g., polyester-polyester, polyamide-polyamide, and polyester-polyamide) are blended in the melt, ester-ester,[137-139] amide-amide,[140, 141] and ester-amide[136, 142] interchange

reactions occur. The generated copolymers improved compatibility and interfacial adhesion between blend components with reduced domain dimensions of the dispersed phase.[134-136] For PET/poly(amide-6,6) blends, the formation of block copolymers via ester-amide interchange reactions during blending process improves compatibility of the two homopolymers. However, thermal degradation, and extensive interchange reactions are shown to lower the mechanical properties of blends.[134, 136]

Addition of Maleic Anhydride-Grafted Copolymers. Moore and coworkers reported the photoinitiated grafting of maleic anhydride (MA) onto polypropylene (PP) performed in both solution and melt with the use of benzophenone (BP) as initiator.[143] The generated MA-g-PP has been shown to be effective compatibilizer in nylon 6/liquid crystalline polymer (LCP) blends.[144] Electron microscopy showed reduced domain dimension of dispersed phase and confirmed the influence of compatibilizer on blend morphology. However, the application of MA-grafted copolymers is limited to the functionalities of incorporated compatibilizers, which must have a suitable reactivity to go across melt phase boundary during short blending time.[144, 145]

Addition of Bifunctional Epoxy Resins. Bifunctional epoxy resins have been investigated to compatibilize PBT/polyamide blends.[146-148] The epoxy resin has the first chance to react with PBT, then with PA66, due to the lower melting temperature of PBT than that of polyamide. The in situ generated PBT-epoxy-polyamide terpolymers act at the interface, reducing the domain dimensions of dispersed phase and greatly enhancing the mechanical properties of polymer blends.

Addition of Ionomers as Minor-Component Compatibilizers. Small amounts of an ionomer have been added to compatibilize polyester/polyamide blends. Sulfonated

polyester ionomers are widely used compatibilizers in the blends of polyester and polyamide.[107, 149-152] It is known to interact strongly with polyamides, establishing a network structure in which sulfonate anions coordinate to amide N-H groups, meanwhile, counterions complex to amide and carbonyl groups.[107, 153] Except ion-dipole interaction, transesterification reactions also played a role in compatibilization.[101, 154] More importantly, the addition of small amount of ionomer dramatically reduced dispersed-domain dimensions and enhanced tensile modulus and stress.[107, 149-151, 153]

2.2.4 Characterization of Polymer Blends

2.2.4.1 Phase Contrast Optical Microscope (PC-OM)

Optical microscopy has been used to study the microscopic phase behavior of blends with the resolution of up to 0.3 μm. The use of optical microscope under phase-contrast mode results in enhanced resolution of refractive index differences between blend components and allows a clearer investigation of phase-separated domains and domain dimensions compared to that under normal mode. Study of the phase-separated domain dimensions as a function of compatibilizer incorporation provides useful insight into the effectiveness of the employed compatibilization technique. As the incorporation of the compatibilizer, sulfonated polyester ionomer (SPET), goes higher, a trend of reduced domain dimension in compatibilized polyester/polyamide blends is obtained (**Figure 2.12**).[107]

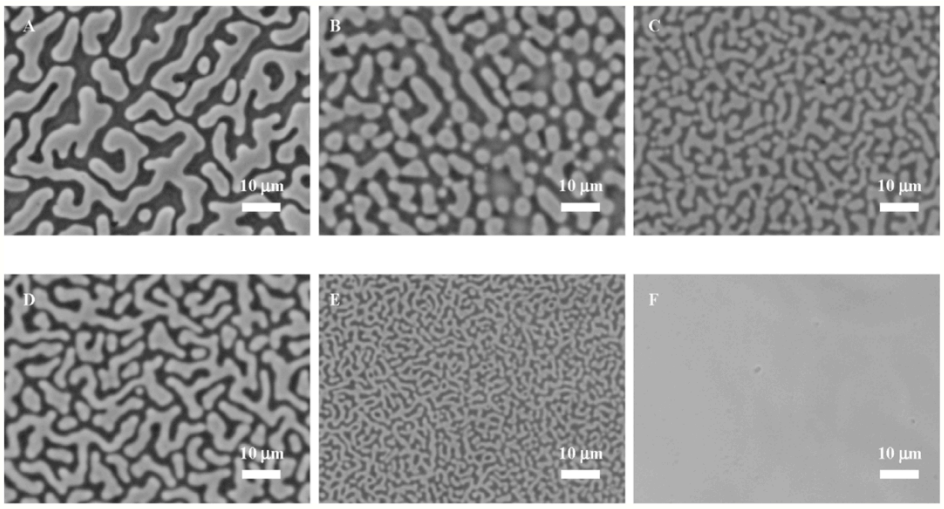

Figure 2.12. Phase contrast optical microscopy of T40/PETG/1.9SPETG solution blends. Blends ratios were set by weight. (A) 50/50/0; (B) 50/48/2; (C) 50/45/5; (D) 50/40/10; (E) 50/35/15; (F) 50/25/25. Scale bar 10 µm. Reprinted from reference 107. Copyright 2004 Wiley InterScience.

2.2.4.2 Scanning Electron Microscopy (SEM)

Scanning electron microscopy (SEM) is a widely used technique in the analysis of phase separation behavior of polymer blends with a much higher resolution (up to 10 nm) compared with PC-OM. SEM is based on scattered electrons, and focuses on the sample's surface, providing a 3D image. **Figure 2.13** shows the SEM micrographs of fracture surface micrographs of the injection molded blends: polyamide/polyester (T40/PETG) binary blends and the ternary blends with polyamide/polyester/sulfonated polyester ionomer (T40/PETG/3.0SPETG).[107] Uncompatibilized T40/PETG blend showed gross phase separation with a wide range of domain sizes. An increase of ionomer incorporation resulted in a continued decrease in dimensions of the dispersed phase (**Figure 2.13**).[107]

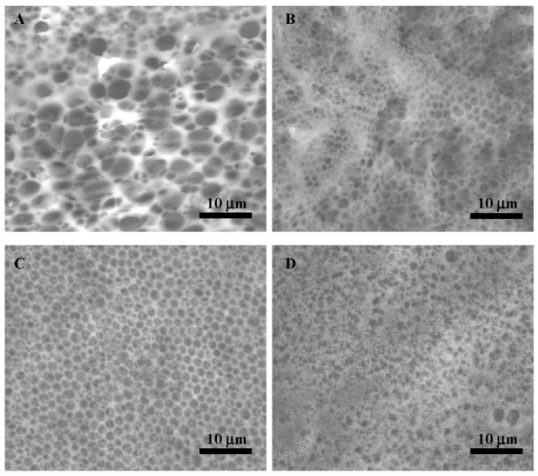

Figure 2.13. Electron micrographs showing the effect of ionomer incorporation on the blend morphology of T40/PETG/3.0SPETG blends. (A) 50/50/0; (B) 50/45/5; (C) 50/40/10; (D) 50/25/25. Scale bar 10 µm. Reprinted from reference 107. Copyright 2004 Wiley InterScience.

2.2.4.3 Transmission Electron Microscopy (TEM)

Another microscopic technique used to evaluate phase separation behavior of polymer blend systems is transmission electron microscopy (TEM). TEM is based on transmitted electrons, and focuses on the details about internal composition, providing a 2D image. TEM possesses a higher resolution (0.2 nm) than SEM (10 nm). This technique involves thin sectioning of polymer samples using an ultramicrotome equipped with either a glass or diamond knife. Following microtoming, the samples must be stained with chemicals such as Br_2, OsO_4, or RuO_4 to enhance contrast between polymer blend phases.[155]

TEM was used to examine morphologies of nylon 6/ABS blends compatibilized with a styrene/maleic anhydride copolymer containing 25 mol% maleic anhydride (SMA 25).[156] **Figure 2.14** shows the TEM photomicrographs for a series of nylon 6/ABS/SMA

25 blends. Large ABS domains are clearly apparent in the uncompatibilized nylon 6/ABS blend, and most ABS domains contain numerous rubber particles (**Figure 2.14a**). The number of rubber particles per cluster is significantly diminished when the concentration of SMA 25 copolymer in ABS phase is increased (**Figures 2.14b-e**).[156]

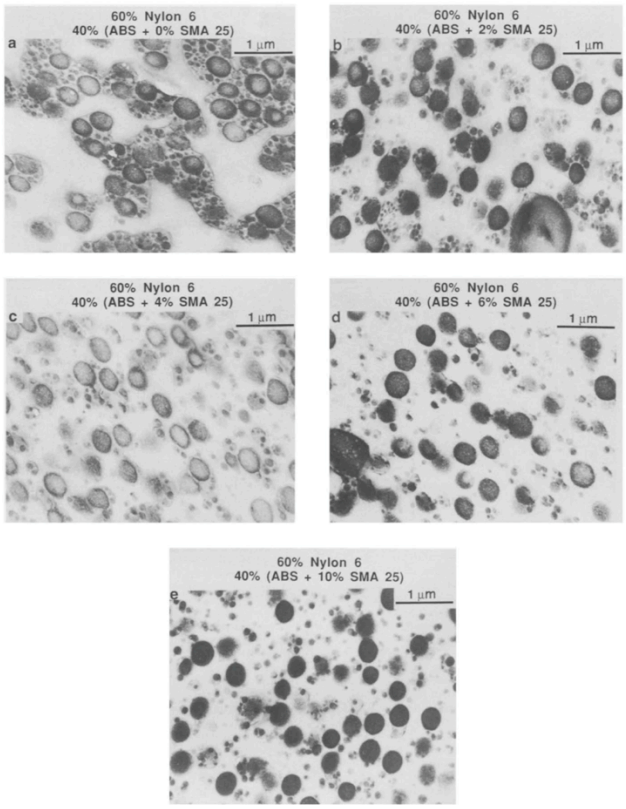

Figure 2.14. TEM photomicrographs for 60% nylon 6 blends with BL-65 (ABS) containing (a) 0%, (b) 2%, (c) 4%, (d) 6% and (e) 10% SMA 25 copolymer in the ABS phase. Blends ratios were set by weight. The samples were dual stained with OsO_4 and RuO_4. Reprinted from reference 156. Copyright 1994 Butterworth-Heinemann Ltd.

2.2.4.4 Small Angle Laser Light Scattering (SALLS)

SALLS can be used to investigate phase-separated domain dimension of polymer blends. The formation of phase-separated domains in a polymer blend is observed as a

halo in a SALLS experiment with the size of the halo being inversely proportional to the size of the phase-separated domains. In **Figure 2.15**, as the incorporation of ionomer goes higher, the domain dimensions go smaller and the halos become larger, indicating blends are more compatible.[107]

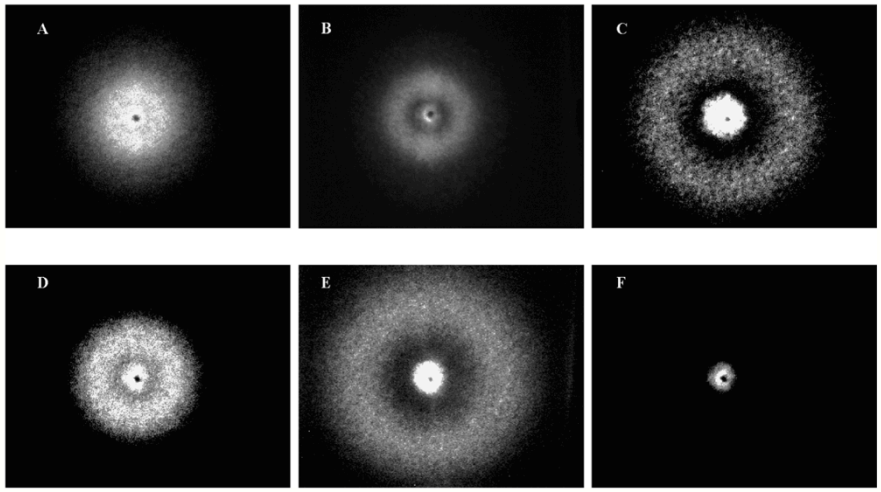

Figure 2.15. Small angle laser light scattering (SALLS) images of T40/PETG/1.9SPETG solution blends. Blends ratios were set by weight. (A) 50/50/0; (B) 50/48/2; (C) 50/45/5; (D) 50/40/10; (E) 50/35/15; (F) 50/25/25. Scale bar 10 μm. Reprinted from reference 107. Copyright 2004 Wiley InterScience.

2.2.4.5 Small Angle X-ray Scattering (SAXS)

The utilization of scattering experiments to investigate heterogeneous systems has been widely applied to a variety of samples ranging from semi-crystalline polymers to ionomers and polymer blends. Small angle x-ray scattering (SAXS) technique have been proven very useful in a wide variety of applications due to their ability to probe much smaller size scales with a shorter wavelength irradiant beam.

Zou and coworkers utilized SAXS to investigate the compatibilization effect of a block copolymer, styrene-maleic anhydride copolymers (SMA), on the thickness of the interfacial region of the blends of polycarbonate (PC) and acrylonitrile-ethylene-propylene-diene-styrene (AES).[157] With increasing SMA content, interfacial layer thickness detected by SAXS reaches minimum value, and then goes higher. Lower-viscosity AES particles turned to lager domains during processing,[57-158] which explained the increased interfacial thickness at higher compatibilizer level.

2.2.4.6 Thermal Properties of Polymer Blends

Differential Scanning Calorimetry (DSC) is commonly employed to investigate the effects of blending and ionic functionality on the thermal properties of polymer blend components. Investigations can include DSC experiments of evaluating glass transition temperature (T_g),[159-166] melting temperature (T_m),[167] and degree of crystallinity as well as isothermal experiments of studying the crystallization kinetics.[132] T_g and T_m of polymer blends will be discussed below.

Glass Transition Temperature. Utilization of DSC to investigate the glass transition temperature (T_g) of polymer blends is one of the simplest and most common methods to determine miscibility. The appearance of two glass transition temperatures indicates the presence of two heterogeneous phases, while a single T_g is indicative of miscibility.[159-166] The simplest representation of such a relationship is given by Flory-Fox equation:[155]

$$\frac{1}{T_g} = \frac{w_1}{T_{g1}} + \frac{w_2}{T_{g2}} \tag{2.6}$$

which describes T_g of a blend as a function of the weight percent (w_i) and glass transition temperature (T_{gi}) of the individual blend component. The compatibility of polymer blends can be investigated by observing whether the blend shows a positive or negative deviation from the above linear dependence of glass transition temperature.

Melting Temperature. Another method used to determine the degree of mixing in a polymer blend system containing at least one crystallizable component involves the investigation of crystalline melting temperature (T_m) of a semicrystalline component in the blend. The presence of a miscible amorphous polymer in a blend serves to decrease chemical potential of crystallizable polymer, resulting in a depression in melting point of crystallizable component, which has been modeled by Nishi and Wang:[167]

$$\frac{1}{T_m} - \frac{1}{T_m^\circ} = -\frac{RV_2}{\Delta H_f V_1}\chi\phi_1^2 \qquad (2.7)$$

where T_m and T_m° are the equilibrium melting points of the crystalline material in the blend and the pure crystallizable component, respectively, R is the universal gas constant; ΔH_f is the heat of fusion per mole of crystallizable polymer, V_1 and V_2 are the volumes of noncrystallizable and crystallizable components, respectively, ϕ_1 is the mass fraction of noncrystallizable polymer, and χ is the polymer/polymer interaction parameter. For χ'*s* less than zero, polymer/polymer interactions result in an equilibrium melting point depression. The smaller the value of χ, the greater the polymer/polymer interactions and the greater melting point depression.[168, 169]

2.2.4.7 Fourier Transform Infrared Spectroscopy (FT-IR)

FT-IR spectroscopy is a very useful technique for studying intermolecular interactions present in a polymer blend. Specific intermolecular interactions often lead to compatibility, if not miscibility, between polymer pairs and FT-IR is very useful to study

and to determine the interactions between blend components that drive miscibility.[107, 170, 171] In **Figure 2.16**,[107] as the molar ratio of sulfonate to amide approaches 1:1 in the blends of sulfonated polyester ionomers and polyamide (Na-mSIP and T40), the intensity of another carbonyl stretching peak at 1610 cm^{-1} increases and a second SO_3^- stretching vibration is observed at 1060 cm^{-1}, indicating an interaction involving the carbonyl of polyamide and the SO_3^- of the ionomer.

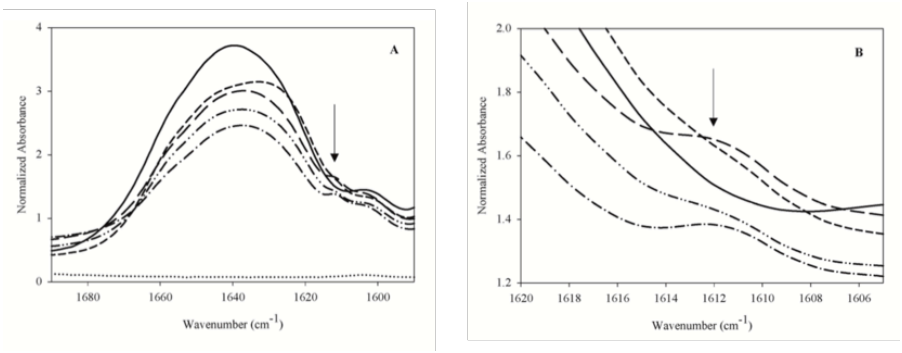

Figure 2.16. FT-IR spectroscopy of T40/m-SIP blends (blended on mol:mol ratio of sulfonate:amide) showing interaction between sulfonate group and amide linkage. (A) Carbonyl stretching and (B) expanded view of extra vibration. (—) T40, (- - - -) Na-SIP, (– – -) 0.25:1, (— - - —) 0.5:1, (— —) 0.75:1, (— - —) 1:1. Reprinted from reference 107. Copyright 2004 Wiley InterScience.

2.2.5 Summary

Compatibilization is a widely used technique to effectively compatibilize immiscible blends by reducing interfacial tension and enhancing interfacial adhesion. Various types of compatibilizers have been developed for different blend systems. Ionomers have proven to be attractive, interfacially active compatibilizers for a number of blend systems because of specific interactions that may develop between the ionic

groups and complementary functional groups on other polar polymers within the blend. These specific interactions tend to decrease the interfacial tension between the dimensions and enhanced phase stability that inhibits coalescence during melt processing. Among all the studied compatibilizers, small amount of ionomers has been shown to effectively compatibilize the dissimilar polymer components, leading to significantly decreases phase-separated domain dimension and highly improved mechanical properties.

2.3 References

1. Lundberg, R. D., Elastomers and fluid applications. In Ionomers: Synthesis, structure, properties and applications, Tant, M. R.; Mauritz, K. A.; Wilkes, G. L., Eds. Springer Netherlands: Dordrecht, 1997; pp 477-501.
2. Tant, M. R.; Mauritz, K. A.; Wilkes, G. L., Ionomers: synthesis, structure, properties and applications. Springer Science & Business Media: 2012.
3. Zhang, L.; Brostowitz, N. R.; Cavicchi, K. A.; Weiss, R., Perspective: Ionomer research and applications. Macromolecular Reaction Engineering 2014, 8 (2), 81-99.
4. Rees, R., Ionomers: A New Thermoplastic. Modern Plast 1964, 42, 98-102.
5. Rees, R.; Vaughan, D., Physical structure of ionomers. Polymer preprints. American Chemical Society. Division of Polymer Chemistry 1965, 6, 287.
6. Eisenberg, A.; Kim, J. S., Introduction to Ionomers. Wiley: 1998.
7. Heitner-Wirguin, C., Recent advances in perfluorinated ionomer membranes: structure, properties and applications. Journal of membrane Science 1996, 120 (1), 1-33.
8. Kerres, J. A., Development of ionomer membranes for fuel cells. Journal of Membrane Science 2001, 185 (1), 3-27.
9. Kusoglu, A.; Weber, A. Z., New Insights into Perfluorinated Sulfonic-Acid Ionomers. Chemical Reviews 2017, 117 (3), 987-1104.
10. Wilson, C. L.; Oscar, S., Foamed polyester resin laminated products and method of making same. U.S. Patent US3170832A: 1965.
11. Gao, Z.; Molnar, A.; Eisenberg, A., Blend compatibilization. In Ionomers, Springer: 1997; pp 390-443.
12. Hamama, H.; Burrow, M.; Yiu, C., Effect of dentine conditioning on adhesion of resin-modified glass ionomer adhesives. Australian dental journal 2014, 59 (2), 193-200.

13. Hsiao, K. J.; Lee, S. P.; Kong, D. C.; Chen, F. L., Thermal and mechanical properties of poly (trimethylene terephthalate)(PTT)/cationic dyeable poly (trimethylene terephthalate)(CD-PTT) polyblended fibers. Journal of applied polymer science 2006, 102 (2), 1008-1013.
14. Huang, C.; Young, N. P.; Grant, P. S., Spray processing of TiO 2 nanoparticle/ionomer coatings on carbon nanotube scaffolds for solid-state supercapacitors. Journal of Materials Chemistry A 2014, 2 (29), 11022-11028.
15. Longworth, R.; Nagel, H., Packaging. In Ionomers, Springer: 1997; pp 365-389.
16. Sezinando, A.; Linares Serrano, M.; Morales Pérez, V.; García Muñoz, R. A.; Ceballos, L.; Perdigão, J., Chemical Adhesion of Polyalkenoate-based Adhesives to Hydroxyapatite. Journal of Adhesive Dentistry 2016, 18 (3).
17. Ugo, P.; Moretto, L. M.; Vezza, F., Ionomer-Coated Electrodes and Nanoelectrode Ensembles as Electrochemical Environmental Sensors: Recent Advances and Prospects. ChemPhysChem 2002, 3 (11), 917-925.
18. Eisenberg, A.; Hird, B.; Moore, R., A new multiplet-cluster model for the morphology of random ionomers. Macromolecules 1990, 23 (18), 4098-4107.
19. Eisenberg, A., Ion-containing polymers: physical properties and structure. Elsevier: 2012; Vol. 2.
20. MacKnight, W.; Earnest, T., The structure and properties of ionomers. Journal of Polymer Science: Macromolecular Reviews 1981, 16 (1), 41-122.
21. Orler, E. B.; Calhoun, B. H.; Moore, R. B., Crystallization kinetics as a probe of the dynamic network in lightly sulfonated syndiotactic polystyrene ionomers. Macromolecules 1996, 29 (18), 5965-5971.
22. Orler, E. B.; Moore, R. B., Influence of ionic interactions on the crystallization of lightly sulfonated syndiotactic polystyrene ionomers. Macromolecules 1994, 27 (17), 4774-4780.
23. Tant, M. R.; Wilkes, G. L., An overview of the viscous and viscoelastic behavior of ionomers in bulk and solution. Polymer Reviews 1988, 28 (1), 1-63.
24. Choi, U. H.; Lee, M.; Wang, S.; Liu, W.; Winey, K. I.; Gibson, H. W.; Colby, R. H., Ionic conduction and dielectric response of poly (imidazolium acrylate) ionomers. Macromolecules 2012, 45 (9), 3974-3985.
25. Mauritz, K. A., Dielectric relaxation studies of ion motions in electrolyte-containing perfluorosulfonate ionomers. 4. Long-range ion transport. Macromolecules 1989, 22 (12), 4483-4488.
26. Nguyen, T.-Q.; Schwartz, B. J., Ionomeric control of interchain interactions, morphology, and the electronic properties of conjugated polymer solutions and films. The Journal of chemical physics 2002, 116 (18), 8198-8208.
27. Yakuphanoglu, F.; Erten, H., Refractive index dispersion and analysis of the optical constants of an ionomer thin film. Optica applicata 2005, 35 (4).
28. Kang, H.; Lin, Q.; Armentrout, R. S.; Long, T. E., Synthesis and characterization of telechelic poly (ethylene terephthalate) sodiosulfonate ionomers. Macromolecules 2002, 35 (23), 8738-8744.
29. Weiss, R.; Yu, W.-C., Viscoelastic behavior of very lightly sulfonated polystyrene ionomers. Macromolecules 2007, 40 (10), 3640-3643.
30. Wu, Q.; Weiss, R., Viscoelastic properties of poly (styrene-co-vinylphosphonate) ionomers. Polymer 2007, 48 (26), 7558-7566.

31. Sandler, S., Polymer syntheses. Elsevier: 2012; Vol. 1.
32. Wu, Q.; Weiss, R., Synthesis and characterization of poly (styrene-co-vinyl phosphonate) ionomers. Journal of Polymer Science Part B: Polymer Physics 2004, 42 (19), 3628-3641.
33. Zhuang, H.; Pearce, E. M.; Kwei, T., Miscibility Studies of Poly (styrene-co-4-vinylbenzenephosphonic acid diethyl ester) with Poly (p-vinylphenol). Macromolecules 1994, 27 (22), 6398-6403.
34. Zhuang, H.; Pearce, E. M.; Kwei, T., Self-association in poly (styrene-co-4-vinylbenzenephosphonic acid) and miscibility of its blends. Polymer 1995, 36 (11), 2237-2241.
35. Kakati, D.; Gosain, R.; George, M., New polyurethane ionomers containing phosphonate groups. Polymer 1994, 35 (2), 398-402.
36. Rager, T.; Schuster, M.; Steininger, H.; Kreuer, K. D., Poly (1, 3-phenylene-5-phosphonic Acid), a Fully Aromatic Polyelectrolyte with High Ion Exchange Capacity. Advanced Materials 2007, 19 (20), 3317-3321.
37. Banerjee, S.; Kar, K. K.; Ghorai, M. K.; Das, S., Synthesis of polyether ether ketone membrane with pendent phosphonic acid group and determination of proton conductivity and thermal stability. High Performance Polymers 2015, 27 (4), 402-411.
38. Iannicelli, J., Metallic phosphonate containing polyester. US Patent 3,052,653.: 1962.
39. Ju, L.; Pretelt, J.; Chen, T.; Dennis, J. M.; Heifferon, K. V.; Baird, D. G.; Long, T. E.; Moore, R. B., Synthesis and characterization of phosphonated Poly (ethylene terephthalate) ionomers. Polymer 2018, 151, 154-163.
40. Wilson, A. D., Developments in Ionic Polymers—2. Springer Science & Business Media: 2012.
41. Rahrig, D.; Azuma, C.; MacKnight, W., Dynamic mechanical and dielectric properties of phosphonylated polypentenamers and their hydrogenated derivatives. Journal of Polymer Science: Polymer Physics Edition 1978, 16 (1), 59-80.
42. Alexandratos, S. D.; Strand, M. A.; Quillen, D. R.; Walder, A. J., Synthesis and characterization of bifunctional phosphinic acid resins. Macromolecules 1985, 18 (5), 829-835.
43. Bock, T.; Möhwald, H.; Mülhaupt, R., Arylphosphonic Acid-Functionalized Polyelectrolytes as Fuel Cell Membrane Material. Macromolecular Chemistry and Physics 2007, 208 (13), 1324-1340.
44. Hirao, T.; Masunaga, T.; Ohshiro, Y.; Agawa, T., A novel synthesis of dialkyl arenephosphonates. Synthesis 1981, 1981 (01), 56-57.
45. Hirao, T.; Masunaga, T.; Yamada, N.; Ohshiro, Y.; Agawa, T., Palladium-catalyzed new carbon-phosphorus bond formation. Bulletin of the Chemical Society of Japan 1982, 55 (3), 909-913.
46. Jakoby, K.; Peinemann, K.; Nunes, S. P., Palladium-Catalyzed Phosphonation of Polyphenylsulfone. Macromolecular Chemistry and Physics 2003, 204 (1), 61-67.
47. Miyatake, K.; Hay, A. S., New poly (arylene ether) s with pendant phosphonic acid groups. Journal of Polymer Science Part A: Polymer Chemistry 2001, 39 (21), 3770-3779.

48. Bock, T.; Mülhaupt, R.; Möhwald, H., Halogen-Free Polyarylphosphonates and Polyelectrolyte Membranes for PEMFC by Nickel-Catalyzed Phosphonylation with Silylated Phosphates. Macromolecular rapid communications 2006, 27 (24), 2065-2071.
49. Allcock, H. R.; Hofmann, M. A.; Ambler, C. M.; Lvov, S. N.; Zhou, X. Y.; Chalkova, E.; Weston, J., Phenyl phosphonic acid functionalized poly [aryloxyphosphazenes] as proton-conducting membranes for direct methanol fuel cells. Journal of Membrane Science 2002, 201 (1-2), 47-54.
50. MacKnight, W.; Earnest Jr, T. R., The structure and properties of ionomers. Journal of Polymer Science: Macromolecular Reviews 1981, 16 (1), 41-122.
51. Rikukawa, M.; Sanui, K., Proton-conducting polymer electrolyte membranes based on hydrocarbon polymers. Progress in Polymer Science 2000, 25 (10), 1463-1502.
52. Anderson, L. J.; Yuan, X.; Fahs, G. B.; Moore, R. B., Blocky Ionomers via Sulfonation of Poly (ether ether ketone) in the Semicrystalline Gel State. Macromolecules 2018, 51 (16), 6226-6237.
53. Orler, E. B.; Yontz, D. J.; Moore, R. B., Sulfonation of syndiotactic polystyrene for model semicrystalline ionomer investigations. Macromolecules 1993, 26 (19), 5157-5160.
54. Marx, C. L.; Cooper, S. L., The crystallinity of ionomers. Journal of Macromolecular Science, Part B: Physics 1974, 9 (1), 19-33.
55. Osborn, S. J.; Hassan, M. K.; Divoux, G. M.; Rhoades, D. W.; Mauritz, K. A.; Moore, R. B., Glass transition temperature of perfluorosulfonic acid ionomers. Macromolecules 2007, 40 (10), 3886-3890.
56. Yeo, S. C.; Eisenberg, A., Physical properties and supermolecular structure of perfluorinated ion-containing (Nafion) polymers. Journal of applied polymer science 1977, 21 (4), 875-898.
57. Gebel, G.; Moore, R. B., Small-angle scattering study of short pendant chain perfuorosulfonated ionomer membranes. Macromolecules 2000, 33 (13), 4850-4855.
58. Page, K. A.; Landis, F. A.; Phillips, A. K.; Moore, R. B., SAXS analysis of the thermal relaxation of anisotropic morphologies in oriented Nafion membranes. Macromolecules 2006, 39 (11), 3939-3946.
59. Wu, D. Q.; Chu, B.; Lundberg, R. D.; MacKnight, W. J., Small-angle x-ray scattering (SAXS) studies of sulfonated polystyrene ionomers. 2. Correlation function analysis. Macromolecules 1993, 26 (5), 1000-1007.
60. Zhang, K.; Fahs, G. B.; Drummey, K. J.; Moore, R. B.; Long, T. E., Doubly-Charged Ionomers with Enhanced Microphase-Separation. Macromolecules 2016, 49 (18), 6965-6972.
61. Parameswaranpillai, J.; Thomas, S.; Grohens, Y., Polymer Blends: State of the Art, New Challenges, and Opportunities. In Characterization of Polymer Blends, Wiley-VCH Verlag GmbH & Co. KGaA: 2014; pp 1-6.
62. Paul, D. R., Control of phase structure in polymer blends. In Functional Polymers, Springer: 1989; pp 1-18.
63. Sabzi, F.; Boushehri, A., Compatibility of polymer blends. I. Copolymers with organic solvents. Journal of Applied Polymer Science 2006, 101 (1), 492-498.

64. Scobbo, J. J.; Goettler, L. A., Applications of Polymer Alloys and Blends. In Polymer Blends Handbook, Utracki, L. A., Ed. Springer Netherlands: Dordrecht, 2003; pp 951-976.
65. Folkes, M.; Hope, P., Polymer blends and alloys. Springer: 1993.
66. Utracki, L.; Walsh, D.; Weiss, R., Polymer Alloys, Blends, and Ionomers. POLYMER 1989, 1, 22.
67. Flory, P. J., Thermodynamics of high polymer solutions. The Journal of Chemical Physics 1941, 9 (8), 660-660.
68. Huggins, M. L., Solutions of long chain compounds. The Journal of chemical physics 1941, 9 (5), 440-440.
69. Barlow, J.; Paul, D., The importance of enthalpic interactions in polymeric systems. Polymer Engineering & Science 1987, 27 (20), 1482-1494.
70. Flory, P. J., Principles of polymer chemistry. Cornell University Press: 1953.
71. Riedl, B.; Prud'homme, R. E., The determination of the thermodynamic interaction parameter χ in polymer blends. Polymer Engineering & Science 1984, 24 (17), 1291-1299.
72. Ten Brinke, G.; Karasz, F. E., Lower critical solution temperature behavior in polymer blends: compressibility and directional-specific interactions. Macromolecules 1984, 17 (4), 815-820.
73. Uriarte, C.; Eguiazabal, J.; Llanos, M.; Iribarren, J.; Iruin, J., Miscibility and phase separation in poly (vinyl methyl ether)/poly (bisphenol A hydroxy ether) blends. Macromolecules 1987, 20 (12), 3038-3042.
74. Paul, D.; Newman, S., Polymer Blends, Academic. New York 1978, 2.
75. Molnar, A.; Eisenberg, A., Miscibility of polyamide-6 with lithium or sodium sulfonated polystyrene ionomers. Macromolecules 1992, 25 (21), 5774-5782.
76. Datta, S.; Lohse, D. J., Polymeric comptabilizers. 1996.
77. Utracki, L., Thermodynamics and kinetics of phase separation. Interpenetrating polymer networks 1991, 77-123.
78. Willemse, R.; De Boer, A. P.; Van Dam, J.; Gotsis, A., Co-continuous morphologies in polymer blends: a new model. Polymer 1998, 39 (24), 5879-5887.
79. Willemse, R.; De Boer, A. P.; Van Dam, J.; Gotsis, A., Co-continuous morphologies in polymer blends: the influence of the interfacial tension. Polymer 1999, 40 (4), 827-834.
80. Jafari, S.; Pötschke, P.; Stephan, M.; Warth, H.; Alberts, H., Multicomponent blends based on polyamide 6 and styrenic polymers: morphology and melt rheology. Polymer 2002, 43 (25), 6985-6992.
81. Mekhilef, N.; Favis, B. D.; Carreau, P. J., Morphological stability, interfacial tension, and dual-phase continuity in polystyrene-polyethylene blends. Journal of Polymer Science Part B: Polymer Physics 1997, 35 (2), 293-308.
82. Koning, C.; Van Duin, M.; Pagnoulle, C.; Jerome, R., Strategies for compatibilization of polymer blends. Progress in Polymer Science 1998, 23 (4), 707-757.
83. Pepels, M. P.; Hofman, W. P.; Kleijnen, R.; Spoelstra, A. B.; Koning, C. E.; Goossens, H.; Duchateau, R., Block Copolymers of "PE-Like" Poly (pentadecalactone) and Poly (l-lactide): Synthesis, Properties, and

Compatibilization of Polyethylene/Poly (l-lactide) Blends. Macromolecules 2015, 48 (19), 6909-6921.
84. Xu, Y.; Thurber, C. M.; Lodge, T. P.; Hillmyer, M. A., Synthesis and Remarkable Efficacy of Model Polyethylene-graft-poly(methyl methacrylate) Copolymers as Compatibilizers in Polyethylene/Poly(methyl methacrylate) Blends. Macromolecules 2012, 45 (24), 9604-9610.
85. Xanthos, M.; Dagli, S., Compatibilization of polymer blends by reactive processing. Polymer Engineering & Science 1991, 31 (13), 929-935.
86. Xu, Y.; Loi, J.; Delgado, P.; Topolkaraev, V.; McEneany, R. J.; Macosko, C. W.; Hillmyer, M. A., Reactive Compatibilization of Polylactide/Polypropylene Blends. Industrial & Engineering Chemistry Research 2015, 54 (23), 6108-6114.
87. Dong, W.; Wang, H.; He, M.; Ren, F.; Wu, T.; Zheng, Q.; Li, Y., Synthesis of Reactive Comb Polymers and Their Applications as a Highly Efficient Compatibilizer in Immiscible Polymer Blends. Industrial & Engineering Chemistry Research 2015, 54 (7), 2081-2089.
88. Feng, Y.; Hu, Y.; Yin, J.; Zhao, G.; Jiang, W., High impact poly(lactic acid)/poly(ethylene octene) blends prepared by reactive blending. Polymer Engineering & Science 2013, 53 (2), 389-396.
89. O'Connell, E. M.; Peiffer, D. G.; Root, T. W.; Cooper, S. L., Morphological studies of lightly sulfonated polystyrene using 23Na NMR: effects of polydispersity in molecular weight. Macromolecules 1996, 29, 2124-2130.
90. O'Connell, E. M.; Root, T. W.; Cooper, S. L., Morphological studies of lightly-sulfonated polystyrene using 23Na NMR 1. Effects of sample composition. Macromolecules 1994, 27, 5803-5810.
91. O'Connell, E. M.; Root, T. W.; Cooper, S. L., Morphological studies of lightly-sulfonated polystyrene using 23Na NMR 2. Effects of solution casting. Macromolecules 1995, 28, 3995-3999.
92. O'Connell, E. M.; Root, T. W.; Cooper, S. L., Morphological studies of lightly-sulfonated polystyrene using 23Na NMR 3. Effects of humidification and annealing. Macromolecules 1995, 28, 4000-4006.
93. Kim, S. H.; Kim, J. S., Effects of low matrix glass transition temperature on the cluster formation of ionomers having two ion pairs per ionic repeat unit. Macromolecules 2003, 36, 1870-1875.
94. Kim, S. H.; Kim, J. S., Relationships between the glass transition temperatures and the type of cations in poly(ethyl acrylate) ionomers. Macromolecules 2003, 36, 2382-2386.
95. Winey, K. I.; Laurer, J. H.; Kirkmeyer, B. P., Ionic Aggregates in Partially Zn-Neutralized Poly(ethylene-ran-methacrylic acid) Ionomers: Shape, Size, and Size Distribution. Macromolecules 1999, 33, 507-513.
96. Yoshimizu, H.; Tsujita, Y., Applications of NMR spectroscopy to the structure and ionic aggregates of ionomers. Ann. Rep. NMR Spec. 2001, 44, 1-22.
97. Willis, J. M.; Favis, B. D.; Lavallee, C., J. Mat. Sci. 1993, 28 (7), 1749-1757.
98. Gorda, K. R.; Peiffer, D. G., Properties of sulfonated PBT. J. Polym. Sci.: Polym. Phys. 1992, 30, 281-292.

99. Connelly, R. W.; McConkey, R. C.; Noonan, J. M.; Pearson, G. H., Melt rheology of ion-containing polymers. I. Effect of ionic content in a model polyesterionomer. J. Polym. Sci.: Polym. Phys. 1982, 20, 259-268.
100. Berti, C.; Celli, A.; Colonna, M.; Fabbri, P.; Fiorini, M.; Marianucci, E., Modification of PET by reactive blending with sulfonated esters. 1. Synthesis and characterization of PET-ionomer. Macromol. Symp. 2001, 176, 211.
101. Boykin, T. L.; Moore, R. B., The role of specific interactions and transreactions on the compatibility of polyester ionomers with poly (ethylene terephthalate) and nylon 6, 6. Polymer Engineering & Science 1998, 38 (10), 1658-1665.
102. Dutta, D.; Weiss, R.; He, J., Compatibilization of blends containing thermotropic liquid crystalline polymers with sulfonate ionomers. Polymer 1996, 37 (3), 429-435.
103. Eisenberg, A.; Hara, M., A review of miscibility enhancement via ion-dipole interactions. Polymer Engineering & Science 1984, 24 (17), 1306-1311.
104. Rajagopalan, P.; Kim, J. S.; Brack, H. P.; Lu, X.; Eisenberg, A.; Weiss, R.; Risen Jr, W. M., Molecular interpretation of miscibility in polyamide-6 blends with alkali ionomers of sulfonated polystyrene. Journal of Polymer Science Part B: Polymer Physics 1995, 33 (3), 495-503.
105. Feng, Y.; Weiss, R.; Karim, A.; Han, C.; Ankner, J. F.; Kaiser, H.; Peiffer, D. G., Compatibilization of polymer blends by complexation. 2. Kinetics of interfacial mixing. Macromolecules 1996, 29 (11), 3918-3924.
106. Hara, M.; Eisenberg, A., Miscibility enhancement via ion-dipole interactions. 1. Polystyrene ionomer/poly (alkylene oxide) systems. Macromolecules 1984, 17 (7), 1335-1340.
107. Gemeinhardt, G. C.; Moore, A. A.; Moore, R. B., Influence of ionomeric compatibilizers on the morphology and properties of amorphous polyester/polyamide blends. Polymer Engineering & Science 2004, 44 (9), 1721-1731.
108. Sullivan, M.; Weiss, R., Characterization of blends of an amorphous polyamide with lightly sulfonated polystyrene ionomers. Polymer Engineering & Science 1992, 32 (8), 517-523.
109. Lu, X.; Weiss, R. A., Development of miscible blends of polyamide-6 and manganese sulfonated polystyrene using specific interactions. Macromolecules 1991, 24, 4381.
110. Lu, X.; Weiss, R. A., Specific interactions and ionic aggregation in miscible blends of nylon-6 and zinc sulfonated polystyrene ionomers. Macromolecules 1992, 25, 6185-6189.
111. Molnar, A.; Eisenberg, A., Miscibility of polyamide-6 with lithium or sodium sulfonated polystyrene ionomers. Macromolecules 1992, 25, 5774-5782.
112. Molnar, A.; Eisenberg, A., Miscibility of carboxylated and sulfonated polystyrene ionomers with polyamides-66, -610, and -11. Polymer 1993, 34 (9), 1918-1924.
113. Rajagopalan, P.; Kim, J. S.; Brack, H. P.; Lu, X.; Eisenberg, A.; Weiss, R. A.; Risen, W. M., Molecular interpretation of miscibility in polyamide-6 blends with alkali ionomers of sulfonated polystyrene. J. Polym. Sci.: Polym. Phys. 1995, 33, 495-503.

114. Feng, Y.; Schmidt, A.; Weiss, R. A., Compatibilization of polymer blends by complexation. 1. Spectroscopic characterization of ion-amide interactions in ionomer/polyamide blends. Macromolecules 1996, 29, 3909-3917.
115. Feng, Y.; Weiss, R. A.; Han, C. C., Compatibilization of polymer blends by complexation. 3. Structure pinning during phase separation of ionomer/polyamide blends. Macromolecules 1996, 29, 3925-3930.
116. Feng, Y.; Weiss, R. A.; Karim, A.; Han, C. C.; Ankner, J. F.; Kaiser, H.; Peiffer, D. G., Compatibilization of polymer blends by complexation. 2. Kinetics of interfacial mixing. Macromolecules 1996, 29, 3918-3924.
117. Deimede, V. A.; Fragou, K. V.; Koulouri, E. G.; Kallitsis, J. K.; Voyiatzis, G. A., Miscibility behavior of polyamide 11/sulfonated polysulfone blends using thermal and spectroscopic techniques. Polymer 2000, 41, 9095-9101.
118. Ghebremeskel, Y.; J., F.; Garton, A., The Use of Near Infrared (NIR) Spectroscopy to Study Specific Interactions in Polymer Blends. J. Polym. Sci.: Part B: Polym. Phys. 1994, 32, 383-386.
119. Yoshikawa, K.; Molnar, A.; Eisenberg, A., Rheological Properties of Blends of Lithium- or Sodium-Sulfonated Polystyrene Ionomers with Polyamide 6. Polym. Eng. Sci. 1994, 34 (13), 1056-1064.
120. Mahajan, K.; Lofgren, E. A.; Jabarin, S. A., Development of active barrier systems for poly(ethylene terephthalate). Journal of Applied Polymer Science 2013, 129 (4), 2196-2207.
121. Lin, J.; Shenogin, S.; Nazarenko, S., Oxygen solubility and specific volume of rigid amorphous fraction in semicrystalline poly (ethylene terephthalate). Polymer 2002, 43 (17), 4733-4743.
122. Natu, A.; Lofgren, E.; Jabarin, S., Effect of morphology on barrier properties of poly (ethylene terephthalate). Polymer Engineering & Science 2005, 45 (3), 400-409.
123. Qureshi, N.; Stepanov, E.; Schiraldi, D.; Hiltner, A.; Baer, E., Oxygen-barrier properties of oriented and heat-set poly (ethylene terephthalate). Journal of Polymer Science Part B: Polymer Physics 2000, 38 (13), 1679-1686.
124. Polyakova, A.; Connor, D.; Collard, D.; Schiraldi, D.; Hiltner, A.; Baer, E., Oxygen-barrier properties of polyethylene terephthalate modified with a small amount of aromatic comonomer. Journal of Polymer Science Part B: Polymer Physics 2001, 39 (16), 1900-1910.
125. Polyakova, A.; Liu, R.; Schiraldi, D.; Hiltner, A.; Baer, E., Oxygen-barrier properties of copolymers based on ethylene terephthalate. Journal of Polymer Science Part B: Polymer Physics 2001, 39 (16), 1889-1899.
126. Polyakova, A.; Stepanov, E.; Sekelik, D.; Schiraldi, D.; Hiltner, A.; Baer, E., Effect of crystallization on oxygen-barrier properties of copolyesters based on ethylene terephthalate. Journal of Polymer Science Part B: Polymer Physics 2001, 39 (16), 1911-1919.
127. Chang, J.-H.; Kim, S. J.; Joo, Y. L.; Im, S., Poly (ethylene terephthalate) nanocomposites by in situ interlayer polymerization: the thermo-mechanical properties and morphology of the hybrid fibers. Polymer 2004, 45 (3), 919-926.

128. Saujanya, C.; Imai, Y.; Tateyama, H., Structure and thermal properties of compatibilized PET/expandable fluorine mica nanocomposites. Polymer Bulletin 2002, 49 (1), 69-76.
129. Wen, J.; Mark, J., Mechanical properties and structural characterization of poly (dimethylsiloxane) elastomers reinforced with zeolite fillers. Journal of materials science 1994, 29 (2), 499-503.
130. Doudou, B. B.; Dargent, E.; Grenet, J., Relationship between Draw Ratio and Strain-Induced Crystallinity in Uniaxially Hot-Drawn PET MXD6 Films. Journal of plastic film and sheeting 2005, 21 (3), 233-251.
131. Samios, C. K.; Kalfoglou, N. K., Compatibilization of poly (ethylene-co-vinyl alcohol)(EVOH) and EVOH/HDPE blends with ionomers. Structure and properties. Polymer 1998, 39 (16), 3863-3870.
132. Hu, Y.; Prattipati, V.; Mehta, S.; Schiraldi, D.; Hiltner, A.; Baer, E., Improving gas barrier of PET by blending with aromatic polyamides. Polymer 2005, 46 (8), 2685-2698.
133. Cahill, P. J.; Chen, S. Y., Oxygen scavenging condensation copolymers for bottles and packaging articles. Google Patents: 2000.
134. Evstatiev, M.; Schultz, J.; Petrovich, S.; Georgiev, G.; Fakirov, S.; Friedrich, K., In situ polymer/polymer composites from poly (ethylene terephthalate), polyamide-6, and polyamide-66 blends. Journal of applied polymer science 1998, 67 (4), 723-737.
135. Ellis, T. S., Polyamide–polyester blends: An estimation of the amide–ester interaction. Journal of Polymer Science Part B: Polymer Physics 1993, 31 (9), 1109-1125.
136. Pillon, L.; Utracki, L., Compatibilization of polyester/polyamide blends via catalytic ester-amide interchange reaction. Polymer Engineering & Science 1984, 24 (17), 1300-1305.
137. Godard, P.; Dekoninck, J.; Devlesaver, V.; Devaux, J., Molten bisphenol-A polycarbonate-poly (ethylene terephthalate) blends. I. Identification of the reactions. Journal of Polymer Science Part A: Polymer Chemistry 1986, 24 (12), 3301-3313.
138. Mondragon, I.; Nazabal, J., Control of interchange reactions of polycarbonate/polyarylate blends and their influence on physical behavior. Journal of applied polymer science 1986, 32 (8), 6191-6207.
139. Otera, J., Ester-Interchange Reactions. In Esterification, Wiley-VCH Verlag GmbH & Co. KGaA: 2004; pp 173-174.
140. Takeda, Y.; Paul, D., The effect of physical interactions on melt-phase homogenization of mixtures of poly (m-xylene adipamide) with aliphatic polyamides induced by interchange reactions. Polymer 1992, 33 (18), 3899-3907.
141. Beste, L.; Houtz, R., Amide interchange reactions. Journal of Polymer Science 1952, 8 (4), 395-407.
142. Pillon, L.; Utracki, L.; Pillon, D., Spectroscopic study of poly (ethylene terephthalate)/poly (amide-6, 6) blends. Polymer Engineering & Science 1987, 27 (8), 562-567.

143. Pan, B.; Viswanathan, K.; Hoyle, C. E.; Moore, R. B., Photoinitiated grafting of maleic anhydride onto polypropylene. Journal of Polymer Science Part A: Polymer Chemistry 2004, 42 (8), 1953-1962.
144. John, J.; Bhattacharya, M., Synthesis and properties of reactively compatibilized polyester and polyamide blends. Polymer international 2000, 49 (8), 860-866.
145. Zheng, X.; Zhang, J.; He, J., Compatibilization of nylon 6/liquid crystalline polymer blends with three types of compatibilizers. Journal of applied polymer science 2003, 87 (9), 1452-1461.
146. Chiou, K. C.; Chang, F. C., Reactive compatibilization of polyamide-6 (PA 6)/polybutylene terephthalate (PBT) blends by a multifunctional epoxy resin. Journal of Polymer Science Part B: Polymer Physics 2000, 38 (1), 23-33.
147. Huang, C.-C.; Chang, F.-C., Reactive compatibilization of polymer blends of poly (butylene terephthalate)(PBT) and polyamide-6, 6 (PA66): 1. Rheological and thermal properties. Polymer 1997, 38 (9), 2135-2141.
148. Huang, C.-C.; Chang, F.-C., Reactive compatibilization of polymer blends of poly (butylene terephthalate) and polyamide 6, 6: 2. Morphological and mechanical properties. Polymer 1997, 38 (17), 4287-4293.
149. Prattipati, V.; Hu, Y.; Bandi, S.; Schiraldi, D.; Hiltner, A.; Baer, E.; Mehta, S., Effect of compatibilization on the oxygen-barrier properties of poly (ethylene terephthalate)/poly (m-xylylene adipamide) blends. Journal of applied polymer science 2005, 97 (3), 1361-1370.
150. Özen, İ.; Bozoklu, G.; Dalgıçdir, C.; Yücel, O.; Ünsal, E.; Çakmak, M.; Menceloğlu, Y. Z., Improvement in gas permeability of biaxially stretched PET films blended with high barrier polymers: The role of chemistry and processing conditions. European Polymer Journal 2010, 46 (2), 226-237.
151. Iyer, S.; Schiraldi, D. A., Role of ionic interactions in the compatibility of polyester ionomers with poly (ethylene terephthalate) and nylon 6. Journal of Polymer Science Part B: Polymer Physics 2006, 44 (15), 2091-2103.
152. Lee, R.; Hutchinson, G.; Farha, S.; Tharmapuram, S., Compatibilized polyester/polyamide blends. Google Patents: 2003.
153. Rajagopalan, P.; Kim, J. S.; Brack, H. P.; Lu, X.; Eisenberg, A.; Weiss, R.; Risen, W. M., Molecular interpretation of miscibility in polyamide-6 blends with alkali ionomers of sulfonated polystyrene. Journal of Polymer Science Part B: Polymer Physics 1995, 33 (3), 495-503.
154. Boykin, T.; Moore, R., Extent of interchange reactions for blends of polyester ionomers with poly (ethylene therephthalate). Polymer Preprints(USA) 1998, 39 (1), 393-394.
155. Utraki, L. A., Polymer Alloys and Blends. Hanser Publishers: New York, 1990.
156. Majumdar, B.; Keskkula, H.; Paul, D., Morphology of nylon 6/ABS blends compatibilized by a styrene/maleic anhydride copolymer. Polymer 1994, 35 (15), 3164-3172.
157. Li, S.; Tang, R.; Jing, B.; Dai, W.; Zou, X., Phase morphology and interfacial characteristics of polycarbonate/acrylonitrile-ethylene-propylene-diene-styrene blends compatibilized by styrene-maleic anhydride copolymers. Journal of Applied Polymer Science 2015, 132 (24).

158. Tan, Z.; Xu, X.; Sun, S.; Zhou, C.; Ao, Y.; Zhang, H.; Han, Y., Influence of rubber content in ABS in wide range on the mechanical properties and morphology of PC/ABS blends with different composition. Polymer Engineering & Science 2006, 46 (10), 1476-1484.
159. Eguiburu, J. L.; Iruin, J. J.; Fernandez-Berridi, M. J.; San Roman, J., Blends of amorphous and crystalline polylactides with poly(methyl methacrylate) and poly(methyl acrylate): a miscibility study. Polymer 1998, 39 (26), 6891-6897.
160. Nijenhuis, A. J.; Colstee, E.; Grijpma, D. W.; Pennings, A. J., High molecular weight poly(L-lactide) and poly(ethylene oxide) blends: thermal characterization and physical properties. Polymer 1996, 37 (26), 5849-5857.
161. Iannace, S.; Ambrosio, L.; Huang, S. J.; Nicolais, L., Poly(3-hydroxybutyrate)-co-(3-hydroxyvalerate)/Poly-L-Lactide Blends: Thermal and Mechanical Properties. J. Appl. Polym. Sci. 1994, 54, 1525-1536.
162. Woo, E. M.; Yau, S. N., Morphology and glass transition behavior of polycarbonate-phenoxy system: Effects of trans-reactions in domain interface regions. J. Polym. Sci.: Part A: Polym. Chem. 1997, 35, 97-103.
163. Yang, J. M.; Chen, H. L.; You, J. W.; Hwang, J. C., Miscibility and crystallization of poly(L-lactide)/poly(ethylene glycol) and poly(L-lactide)/poly(e-caprolactone) blends. Polym. Jour. 1997, 29 (8), 657-662.
164. Register, R. A.; Tomita, H., Miscibility of Polystyrene-Based Ionomers with Poly(2,6-dimethyl-1,4-penylene oxide). Macromolecules 1993, 26, 2796-2801.
165. Pan, Y.; Huang, Y.; Liao, B.; Chen, M.; Cong, G.; Leong, L. M., Studies on miscibility of poly(phenylene oxide)-based ionomer/polystyrene-based ionomer blends. J. Appl. Polym. Sci. 1997, 65, 341-346.
166. Eisenberg, A.; Hara, M., Miscibility Enhancement via Ion-Dipole Interactions. 1. Polystyrene Ionomer/Poly(alkylene oxide) Systems. Macromolecules 1984, 17, 1335-1340.
167. Rostami, S., Polymer 1991, 31, 899-904.
168. Rim, P. B.; Runt, J. P., Melting point depression in crystalline/compatible polymer blends. Macromolecules 1984, 17 (8), 1520-1526.
169. Huo, P. P.; Cebe, P., Melting point depression in poly (butylene terephthalate)/polyarylate blends. Macromolecules 1993, 26 (12), 3127-3130.
170. Weiss, R. A., Compatibilizer for polymer blends and the polymer blends derived therefrom. Google Patents: 1995.
171. Feng, Y.; Schmidt, A.; Weiss, R., Compatibilization of polymer blends by complexation. 1. Spectroscopic characterization of ion-amide interactions in ionomer/polyamide blends. Macromolecules 1996, 29 (11), 3909-3917.

Chapter 3. Synthesis and Characterization of Phosphonated Poly(ethylene terephthalate) Ionomers

(Published in *Polymer* **2018**, *151*, 154-163)

Lin Ju,[a,c] Juan Pretelt,[b,c] Tianran Chen,[b,c] Joseph M. Dennis,[a,c] Katherine V. Heifferon,[a,c] Donald G. Baird,[b,c] Timothy E. Long,[a,c] and Robert B. Moore[a,c,*]

[a]Department of Chemistry, Virginia Polytechnic Institute and State University, Blacksburg, VA 24061, United States

[b]Department of Chemical Engineering, Virginia Polytechnic Institute and State University, Blacksburg, VA 24060, United States

[c]Macromolecules Innovation Institute, Virginia Polytechnic Institute and State University, Blacksburg, VA 24061, United States

3.1 Abstract

A more efficient route for the synthesis of phosphonated dimethyl isophthalate, disodium salt is shown to provide a significantly higher yield (42%), in contrast to a previously reported yield (15%). This higher yield enabled the synthesis of phosphonated poly(ethylene terephthalate) (PPET) ionomers using conventional melt polycondensation with ethylene glycol and dimethyl terephthalate. The physical properties of these phosphonated PET ionomers (Na^+-PPET) were characterized using differential scanning calorimetry (DSC), melt rheology, and tensile testing. DSC analysis showed that the crystalline melting temperatures, crystallization temperatures, degrees of crystallinity, and crystallization rates decreased with increasing ionic content. Melt rheology

confirmed the existence of physical crosslinks in Na^+-PPET ionomers, as indicated by a crossover of the storage and loss moduli, attributed to strong electrostatic associations between phosphonated units on the polymer chains. Tensile tests of the Na^+-PPET samples showed enhanced Young's modulus and yield stress compared to pure PET.

3.2 Introduction

Ionomers are charged polymers containing minor amounts of covalently attached ionic functionalities, typically less than 15 mol%, incorporated into or pendant to the polymer backbones.[1-3] Generally, the polar ionic groups, surrounded by a less polar matrix, tend to form nanometer-sized ionic aggregates due to attractive Coulombic interactions between the ionic-pairs.[4] These ionic aggregates, acting as physical crosslinks, decrease the mobility of polymer chains, and are known to exert a profound effect on the thermo-mechanical and rheological properties of polymers.[5-7] Compared to nonionic analogues, semi-crystalline ionomers have been shown to exhibit a higher modulus, higher melt viscosity, and a significant decrease in the overall rate of crystallization.[8-10] The ability to control thermo-mechanical and rheological properties by choice of ion type and content provides the opportunity for ionomers to be applied in a wide variety of technologies, such as coatings,[11-12] adhesives,[13-14] dyeable textile materials,[15-16] polymer blend and nanocomposite compatibilization,[17-18] shape memory polymers,[19-20] and self-healing materials.[21-22]

The valence of charged monomer units in ionomers can vary with the type of ionic species attached to the ionomer chains and the type of neutralizing counterions. For the purposes of the following discussion, the ionic groups that are covalently attached to

the ionomer backbone will be referred to as *pendant ions*, whereas the free ions that electrostatically neutralize the pendant ions will be referred to as *counterions*. Ionomers containing anionic pendant ions are usually called *anionic ionomers*, while those bearing cationic pendant ions are named *cationic ionomers*. A relatively wide range of both monovalent (e.g., carboxylates, sulfonates) and multivalent (e.g., phosphonates, dicarboxylates) pendant anions have been utilized for the preparation of anionic ionomers.[23-28] Both monovalent counterions (e.g., the alkali metal ions, organic alkyl ammonium ions (e.g., ammonium, pyridiniums) and multivalent counterions (e.g., the alkaline earth ions, transition metal ions) can be used to neutralize anionic pendant ions. Cationic ionomers containing monovalent (e.g., quaternary ammoniums, pyridiniums, imidizoliums) and multivalent pendant cations (e.g., 1,4-diazabicyclo[2.2.2]octane (DABCO) double ammoniums salt) have also been described in the literature.[29-31] Monovalent anions (e.g., the halides, tosylate anions) have been utilized to neutralize these pendant cations.

Ionomers bearing multivalent counterions have attracted significant attention because they offer a greater range of Coulombic interactions, and thus physical properties, as compared to ionomers containing both monovalent pendant ions and counterions.[32-38] Typically, monovalent pendant ions are used to coordinate with only monovalent counterions to generate a physical crosslink *via* an dipole-dipole interactions between two or more ion pairs. In contrast, multivalent counterions can form an ionic bond between two monovalent pendant anions, which establishes a fundamentally stronger physical crosslink in satisfying the requirement for local charge neutrality.[37] For example, compared to sulfonated poly(ethylene terephthalate) (SPET) ionomers

containing monovalent counterions (Na^+, and Li^+), SPET ionomers with divalent counterions, such as alkaline earth (Ca^{2+}) and divalent transition metal cations (Co^{2+}, Ni^{2+}, Cu^{2+}, and Zn^{2+}), display longer crystallization half times due to restricted mobility of the polymer chains. In addition, SPET/poly(ethyl acrylate-*co*-4-vinylpyridine) (EAVP) blends containing divalent counterion exhibit enhanced modulus and tensile strength.[32-35] However, aside from the widely applied Surlyn® ionomers, few other ionomers with multivalent counterions are commercially applicable due to the difficulty of conversion to multivalent counterions by neutralization of the acid groups or by ion exchange of monovalent counterions.[39-40]

Recently, ionomers containing multivalent pendant ions have emerged as interesting candidates for the design of new ionomers with enhanced properties governed by multivalency. The multivalent pendant ion generates multiple dipole-diploe interactions per functional group between two ion pairs that provides a stronger physical crosslink due to the increased charge density compared to monovalent analogues. Direct polymerization of ionic monomers bearing multivalent pendant ions generally provides better tunability regarding ion type, concentration, and distribution within the polymer chain. However, only a few reports describe ionic monomers that contain multivalent pendant ions. Kim *et. al*[27] synthesized poly(styrene-*co*-itaconate) ionomers that have two ion pairs in the same ionic repeat unit, and found that the cluster T_g of the itaconate ionomers is much higher than that of monovalent methacrylate ionomers. Zhang *et. al*[31] synthesized a cationic ionomer containing the divalent 1,4-diazabicyclo[2.2.2]octane (DABCO) salt, which displays superior thermomechanical properties and promotes more well-defined microphase-separation compared to analogous ionomers bearing singly-

charged pendant groups. Other reports of polymers containing multivalent pendant groups have focused on the acid form of phosphonated polymers (e.g., polysulfone, poly(ether ether ketone)) or phosphonated polyelectrolytes (e.g., phosphonated poly(*m*-phenylene)).[41-43] Little information exists, however, regarding the properties of ionomers bearing multivalent pendant ions with monovalent counterions.

Sulfonated poly(ethylene terephthalate) ionomers in Na^+-form (Na^+-SPET) are one of the most widely studied polyester ionomers, and was originally commercialized by DuPont as textile fibers with improved dyeability to basic dyes compared to pure PET.[44-45] While the introduction of sulfonate groups onto PET has been shown to enhance mechanical properties, the strong ionic interactions are also known to slow the rate of crystallization and adversely affect processability due to a high melt viscosity.[46-49] Due to the advantage of specific interactions of sulfonate groups with a wide range of polar materials, SPET ionomers are often applied in compatibilizing polyester/polyamide blends by generating attractive interactions between the sulfonate salt functionalities and the amide units of the polyamide. In these inherently immiscible blends, the specific interactions lower the interfacial tension leading to a reduction in phase dimensions.[50-54]

Despite the well-studied effect of monovalent sulfonate pendant ions on the properties of SPET ionomers, no systematic studies have been focused on the investigation of PET ionomers bearing multivalent pendant ions, such as phosphonate salts. To date, only one patent reference of limited scope from 1962 refers to a phosphonated PET ionomer in Na^+-form (Na^+-PPET).[55] This patent described that melt polycondensation with ethylene glycol, dimethyl terephthalate, and the phosphonate ionic monomer yielded Na^+-PPET ionomers that could be processed into textile fibers with an

affinity for basic type dyes, such as colored cationic organic substances containing sulfonium, oxonium, or quaternary ammonium functional groups. No other detail regarding thermal, rheological, or mechanical properties of the resulting Na^+-PPET ionomers were reported. Nevertheless, the yield of the essential phosphonated isophthalate monomer was reported to be only 15%, which apparently limited subsequent comprehensive structure-property investigations. Moreover, the Na^+-PPET ionomers synthesized in this patent exhibited substantial insolubility in solvents commonly used to dissolve linear polyesters, but they remained melt-processable. Not surprisingly, this very low yield limited industrial applicability of Na^+-PPET ionomer, and no further reports of PPET have surfaced.

To expand our fundamental understanding of PET-based ionomers, this work focuses on an improved synthetic route for Na^+-PPET ionomers and a detailed characterization regarding their thermal, mechanical, and rheological properties. With a substantially modified synthetic scheme that achieves a significantly higher yield of the phosphonated monomer, we have generated PPET with various ionic contents to probe the effects of multivalent pendant ions on the physical properties of this potentially valuable class of polyester ionomers. Physical characterization, including thermal, rheological, and mechanical analyses, are correlated to establish valuable structure-property relationships for these PET ionomers containing pendant phosphonate groups.

3.3 Experimental Section

Materials. All reagents were used as received without further purification. Dimethyl 5-aminoisophthalate (DMAIP, 98%), sodium nitrite ($NaNO_2$, ≥97.0%), sodium tetrafluoroborate ($NaBF_4$, 98%), copper(I) bromide (CuBr, 98%), phosphorus trichloride

(PCl_3, 99%), sodium methoxide (NaOMe, 95%), sodium hydroxide (NaOH, ≥98%), Chelex® 100 sodium form (50-100 mesh), dimethyl terephthalate (DMT, ≥99%), ethylene glycol (EG, anhydrous, 99.8%), sodium acetate (NaOAc, >99%, anhydrous), manganese(II) acetate tetrahydrate ($Mn(OAc)_2 \cdot 4H_2O$, 99.99%), and *n*-butanol (99%) were purchased from Sigma-Aldrich. $Ti(OiPr)_4$ was diluted to 10.18 mg/mL in *n*-butanol, and $Mn(OAc)_2 \cdot 4H_2O$ was diluted to 21.5 mg/mL in ethylene glycol. All deuterated solvents were purchased from Cambridge Isotope Laboratories, Inc.

Synthesis of Dimethyl 5-Phosphoisophthalate Disodium Salt. Dimethyl 5-phosphoisophthalate disodium salt was synthesized following a four step procedure, as shown in **Scheme 3.1**. In the first step, dimethyl 5-aminoisophthalate (10.0 g, 47.9 mmol), sodium tetrafluoroborate (8.94 g, 81.4 mmol), hydrochloric acid (11.65 M, 6.7 mL), and distilled water (19.0 mL) were added to a 250-mL, round-bottomed flask equipped with a magnetic stir bar. The flask was placed into an ice bath with constant stirring. A saturated sodium nitrite (3.3 g, 47.9 mmol) solution in H_2O was then added into the mixture dropwise, and allowed to stir for 1 h. A yellow precipitate was formed and removed from the solution using vacuum filtration. The precipitate was washed with cold saturated sodium tetrafluoroborate solution (2 × 5 mL) and cold diethyl ether (2 × 5 mL) in a filter funnel. The resulting light yellow solid was dried *in vacuo* at room temperature for about 10 h (13.6 g, 92% yield). Structure and purity of the obtained 3,5-dicarbomethoxyphenyldiazonium tetrafluoroborate intermediate were confirmed using NMR spectroscopy. ^{1}H NMR (400 MHz, DMSO-d_6): δ 9.46 (m, 2H), 8.95 (m, 1H), 4.00 (s, 6H).

In the second step, 3,5-dicarbomethoxyphenyldiazonium tetrafluoroborate (13.6 g, 44.1 mmol), CuBr (0.889 g, 6.2 mmol), and anhydrous ethyl acetate were added into a 250-mL, round-bottom flask equipped with a magnetic stir bar. Phosphorus trichloride (7.7 mL, 88.2 mmol) was added into the suspension dropwise. During the addition of PCl_3, rapid evolution of N_2 gas was observed. Following the complete addition of PCl_3, the N_2 evolution subsided, and the suspension transformed to a dark brown solution. The resulting solution was allowed to stir at room temperature for 3 h, followed by dropwise addition of distilled water (11.0 mL). This reaction mixture was then stirred for additional 3 h. The crude product was concentrated using a rotatory evaporator, and the resulting brown oil was used without further purification for the following step.

In the third step, the crude brown oil was dissolved in methanol (40mL), and then sodium methoxide (7.15 g, 132.3 mmol) was added to the solution and allowed to stir for 1 h. This step generated a light green precipitate, which was then collected using vacuum filtration, washed with ethyl acetate (2 × 10 mL) and methanol (1 × 5 mL), and then dried *in vacuo* at room temperature for about 2 h. The resulting light green solid was dissolved in 300 mL of water, followed by the addition of 25 g of Chelex® 100 resin in sodium form. The solution was allowed to stir overnight, filtered to removed the Chelex® 100 resin, rotatory evaporated to remove water, and re-crystallized from an acetone/water (3:1, v/v) solvent system. The resulting white crystals were dried *in vacuo* at 40 °C overnight (5.9 g, 45.6% yield). ^{1}H NMR (400 MHz, D_2O): δ 8.58 (m, 1H), 8.50 (d, 1H), 8.47 (d, 1H), 3.96 (s, 6H); ^{31}P NMR (400 MHz, D_2O): δ 9.56. HRMS (ES+): *m/z* calculated for $[M\text{-}Na+2H]^+$ 275.0062 g mol^{-1}; found 275.0320 g mol^{-1}.

In the fourth step, dimethyl 5-phosphoisophthalate monosodium salt (5.9 g, 20 mmol) was dissolved in water (100 mL), and titrated with an aqueous 0.87 mol/L NaOH solution (standardized with benzoic acid) to the equivalence point, as monitored using a Mettler Toledo SevenMulti^{TM} pH meter. Water was removed under reduced pressure (40 mtorr) using a rotatory evaporator, and the resulting white solid was dried *in vacuo* overnight (6.3 g, 99% yield). ^{1}H NMR (400 MHz, D_2O): δ 8.55 (m, 1H), 8.53 (d, 1H), 8.50 (d, 1H), 3.94 (s, 6H); ^{31}P NMR (400 MHz, D_2O): δ 9.52. HRMS (ES+): *m/z* calculated for $[M-2Na+3H]^+$ 274.9881 g mol^{-1}; found 275.0136 g mol^{-1}.

Synthesis of the Phosphonated Poly(Ethylene Terephthalate) Ionomers (Na^+-PPET). Na^+-PPET ionomers were fabricated by melt polycondensation as described in **Scheme 3.2**. DMT (10.0630 g, 51.8 mmol), dimethyl 5-phosphoisophthalate disodium salt (0.0828 g, 260 mmol), EG (6.4656 g, 104.2 mmol), and NaOAc (4.3 mg, 0.052 mmol) were charged to a dry, 100-mL, round-bottom flask. Sb_2O_3 (7.6 mg, 456 ppm) and $Mn(OAc)_2$ in *n*-butanol (0.08 mL, 21.5 mg/mL) were added to facilitate transesterfication. The flask was then equipped with an overhead stir rod, nitrogen inlet, condensing tube, and collection flask, and the contents were sequentially degassed under vacuum and then purged with nitrogen three times. Under a constant nitrogen purge, the reaction vessel was sequentially stepped to and held at 180 °C, 200 °C, 220 °C, and 240 °C for 1h, respectively. The reaction progress was monitored continuously by collection of the methanol distillate in a dry ice-cooled round-bottom flask. Finally, the reaction temperature was elevated to 275 ºC, the pressure was subsequently reduced to 20-30 mtorr, and the polymerization was allowed to proceed at 275 °C for an additional 2 h. The resulting polymer was removed from the stir rod by freeze-fracturing in liquid N_2,

and then used directly without further purification. A control sample of pure PET (without the phosphonated monomer) and four PPET ionomers with various ionic contents of 0.5, 1.0, 2.0 and 4.0 mol% were synthesized using this procedure.

Preparation of Compression-Molded Films. The polymer samples recovered from the polymerization were ground into coarse particles (diameter equal to ca. 3 mm), and dried *in vacuo* at 60 ºC overnight. Film samples were prepared by compression molding the polymer particles between Kapton sheets at 270 ℃, using a Carver laboratory press. The Kapton-enveloped films were quenched from 270 ºC into ice water to generate freestanding, amorphous films. The thicknesses of these melt-pressed samples were approximately 150 to 180 μm.

Differential Scanning Calorimetry. Thermal properties and crystallization kinetics of Na-PPET ionomers were studied using differential scanning calorimetry (DSC). A TA Instruments Q2000 DSC was used to probe the thermal behavior of Na^+-PPET, with a nitrogen purge. Compression-molded film samples were analyzed. These film samples were die cut and placed within aluminum DSC pans. The weight for each sample was maintained between 6 and 10 mg. The glass transitions, T_g, and melting temperatures, T_m, were determined from the second DSC heating scan after erasing the thermal history, and crystallization temperatures, T_c, were investigated from the subsequent cooling scans, using the TA instruments Universal Analysis Software.

Isothermal crystallization was carried out for Na-PPET ionomers. TA Instruments Universal Analysis software was used to analyze the resulting DSC traces. The crystallization half-time, $t_{1/2}$, the time at which the material reaches 50% of its maximum crystallinity, was obtained from isothermal scans at various temperatures, and was used

as a measure of the bulk crystallization rates of Na^+-PPET ionomers. Isothermal crystallization data were analyzed using the Avrami equation,[56]

$$\ln\left[-\ln\left(1 - X_c(t)\right)\right] = lnK + n\ lnt \tag{3.1}$$

where K is the kinetic growth rate constant, n is the Avrami exponent, and $X_c(t)$ is the relative extent of crystallization at time t. From the DSC data, $X_c(t)$ is defined as:

$$X_c(t) = \frac{\int_0^t \left(\frac{dH}{dt}\right) dt}{\int_0^\infty \left(\frac{dH}{dt}\right) dt} \tag{3.2}$$

where (dH/dt) is the heat evolution during crystallization as a function of time, relative to the total heat of crystallization.

Rheological Analysis. An ARES G2 Rheometer from TA instruments, utilizing 25 mm cone and plate fixtures, was used to measure the melt rheological properties of all samples. The use of a dry nitrogen atmosphere in the oven prevented the resins from absorbing ambient moisture. Strain sweeps were conducted to confirm the linear viscoelastic region (0.1-10% oscillatory strain) to be used for all rheological measurements for these samples. Frequency sweeps at temperatures of 280 °C (5% oscillatory strain, 0.1-100 rad/s) provided information on relevant viscoelastic properties, such as complex viscosity and storage and loss shear moduli over a broad range of frequencies.

Tensile Test. Dumbbell-shaped specimens were cut from melt-pressed films. The specimens were clamped in the tensile fixture with a distance between grips of 26.54 mm, and the width of narrow section of 3.32 mm. The thicknesses of these specimens were approximately 150 to 180 μm, and accurately measured for each sample using a calibrated caliper. Tensile testing was performed on a 5500R Instron universal testing

instrument at cross-head speed of 5 mm/min. The yield stress and Young's moduli are reported on an average of ten specimens.

Spectroscopic Methods. ^{1}H NMR spectra of monomers and intermediates were collected in DMSO-d_6 and deuterium oxide on an Agilent U4-DD2 spectrometer operating at 400 MHz at 23 °C. High resolution TOF mass spectroscopy (HRMS) of the monomers and intermediates was conducted using an Agilent 6220 mass spectrometer with a TOF analyzer in positive ion mode.

3.4 Results and Discussion

3.4.1 Synthesis of the Ionic Monomer. Diazonium salts with the general formula of R-N≡N^{+}X^{-} (R=alkyl or aryl) are important intermediates in organic synthesis, especially when R is an aryl group.[57] In the synthetic procedure for dimethyl 5-phosphoisophthalate disodium-salt, C-P bonds were created using a Cu-catalyzed C-P cross-coupling reaction from an aryl diazonium salt and a phosphorus nucleophile (PCl_3), which released N_2.[58] **Scheme 3.1** illustrates the synthesis of the phosphonated isophthalate monomer through a four-step sequence: 1) diazotisation of aniline; 2) Cu-catalyzed C-P cross-coupling, and subsequent hydrolysis to an aromatic phosphoric acid; 3) neutralization of phosphoric acid to the monosodium salt; 4) base titration to form the disodium-salt. Diazotisation of dimethyl 5-aminoisophthalate with nitrous acid (generated from $NaNO_2$ and conc. HCl), under standard conditions, produced the aryl diazonium salt in 92% yield. Phosphoric acid was generated by CuBr-catalyzed one-pot treatment of the diazonium salt with PCl_3 in EtOAc, followed by addition of H_2O. It should be noted that aryl phosphoric acid cannot be purified by flash column

chromatography due to the highly polar and strongly acidic phosphoric groups. Since most organophosphoric acids are extremely soluble, not only in water, but also in many organic solvents at room temperature, the isolation of the organophosphoric acids via recrystallization is considerably difficult. Thus, the efficient isolation of organophosphoric acids becomes the key to this new synthetic strategy.

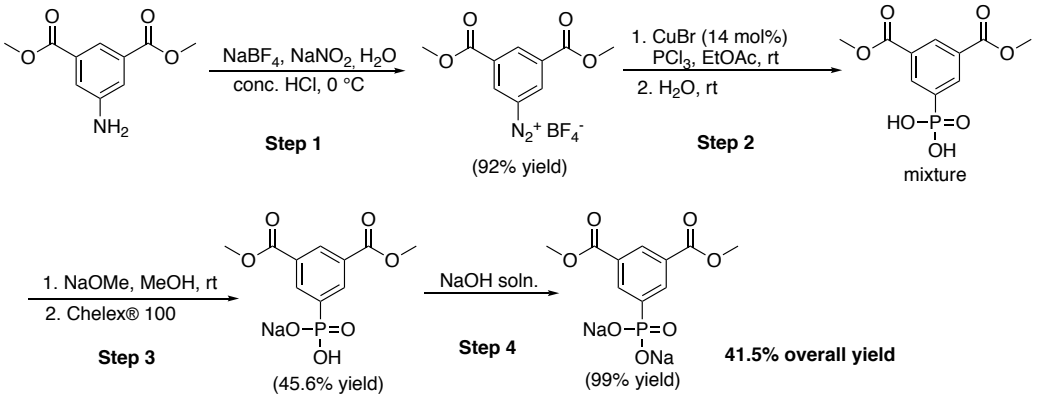

Scheme 3.1. Synthesis of dimethyl 5-phosphoisophthalate disodium salt

Freedman and coworkers demonstrated hemi-sodium phosphonate salts were less soluble than the free acids, which can be used to facilitate isolation.[58] Thus, we turned our attention to the isolation of hemi-sodium salts. After the addition of NaOMe, hemi-sodium salts precipitated immediately from the mixture solution (**Step 3-1**). The mixture was then cooled, and the salts were removed by filtration. The collected salts displayed a light-green color, indicative of copper ion coordination to the oxygen atoms of the hemi-sodium salt. For step-growth polymerization, a high degree of monomer purity is necessary to achieve a stoichiometric equivalence of functional groups to obtain the necessary high degree of polymerization (DOP) for a desired high molecular weight of the polymer product. Therefore, extreme care was taken to achieve a high purity of the ionic monomer. In order to remove all traces of the copper ion, we applied the Chelex®

chelating ion exchange resin, which had high selectivity for copper, iron, and other heavy metals over monovalent cations such as sodium and potassium. The Chelex® purification protocol produced white crystals after removing solvent, and further re-crystallization from water/acetone system generated the desired hemi-sodium salt in 45.6% yield (**Step 2 and Step 3**). Finally, titration with NaOH solution converted hemi-sodium salt to disodium salt (99% yield, **Step 4**). This entire synthetic procedure of dimethyl 5-phosphoisophthalate disodium-salt led to a 42% overall yield.

Compared with a 15% yield reported in the 1962 DuPont patent,[55] our improved synthetic route provided a much more efficient way to synthesize the arylphosphonate salt, thus increasing the isolation yield by 300%. The crucial difference between the previous work and our method is the purification of the organophosphorous compounds. From the previous patent, arylphosphonic acid was obtained by re-crystallization from dilute hydrochloric acid solution. Due to the considerably high solubility of organophosphonic acid in aqueous solution, and the strong coordination between copper ions and the phosphonate groups, it is extremely difficult to achieve a high yield of arylphosphonic acid by recrystallization from water without the removal of copper ions. In our synthetic method, we isolated hemi-sodium salt from acetone/water system and removed the copper ions by the Chelex® purification protocol. The poor solubility of hemi-sodium salt in organic solvents facilitated the isolation from an organic/aqueous system, benefiting the highly improved yield of the phosphonated ionic monomer.

3.4.2 Synthesis of Phosphonated Poly(ethylene terephthalate) Ionomers (Na^+-PPET). As highlighted in **Scheme 3.2**, the synthesis of Na^+-PPET was conducted by melt polycondensation with both manganese (II) acetate and antimony trioxide as

transesterification and polycondensation catalysts, respectively. NaOAc, as commonly employed in the earlier literature,[49] was used to maintain the ionic monomer in the sodium salt form. Excess of diol facilitates transesterification of the dimethyl ester. Following the completion of methanol generation, a combination of higher temperatures and reduced pressure was applied to remove excess diol and to drive the reaction to high conversion (>99.9%). The reaction was completed when the melt viscosity increased substantially and remained constant (as inferred by a constant stirring torque). Methanol generation and diol boiling points determined the reaction times and designated the final reaction temperature. Transesterification of dimethyl phthalate with ethylene glycol was completed within 4 h from 180 °C to 240 °C, and overall reaction times did not exceed 7 h. Polymerization resulted in pale yellow products.

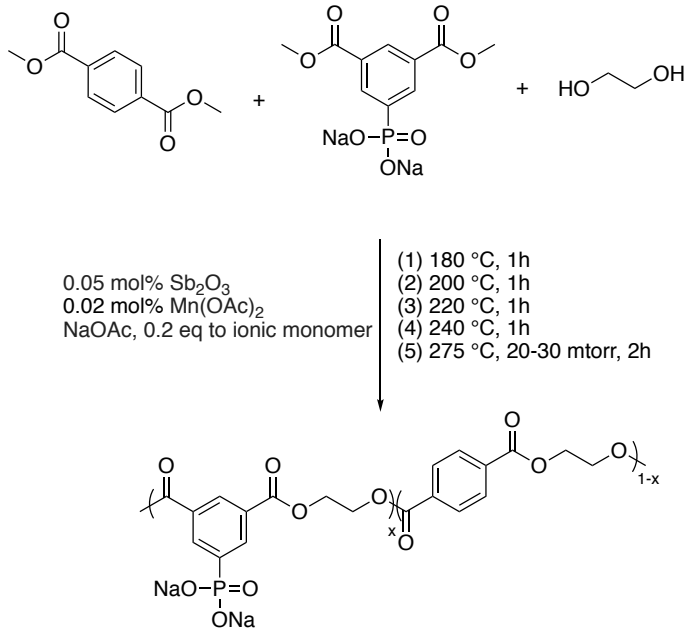

Scheme 3.2. Synthesis of phosphonated poly(ethylene terephthalate) ionomers in the Na^+-form (Na^+-PPET)

In order to determine the molecular weight for Na^+-PPET ionomers, several organic solvents and organic acids at various temperatures and dissolving times were examined to achieve a homogeneous solution of Na^+-PPET ionomers (**Table 3.1**). Unfortunately, only the 0.5 mol% Na^+-PPET ionomer was able to be dissolved in hexafluoro-2-propanol (HFIP) at 50 °C after stirring for 24 hours, while the other Na^+-PPET ionomers with higher mol% of ionic contents remained insoluble in the studied solvents at elevated temperatures. This behavior may be attributed to the strong physical crosslinks generated from divalent anionic pendant groups, which restricts chain mobility and leads to a poor solubility. Nevertheless, it is important to note that all samples were melt-processable, and the compression-molded films were transparent, tough, and flexible, consistent with achievement of a high molecular weight of the Na^+-PPET ionomers (**Figure 3.1**).

Table 3.1. Solubility tests of 1.0 mol% and 4.0 mol% Na^+-PPET ionomers.

Solvent	Temp	Time	Additive	Results	Solubility
HFIP	RT/50°C	24h	-	Swell	×
	RT	24h	LiBr	Swell	×
	120°C	3days	LiBr	Swell	×
TFA/DCA	RT/120°C	24h	LiBr	Swell	×
NMP	RT/120°C	24h	LiBr	Didn't Swell	×
DMSO	RT/120°C	24h	LiBr	Didn't Swell	×
Phenol:1,1,2,2-tetrachloroethane=5:5 wt%	RT/120°C	24h	LiBr/$TBAPF_6$	Swell	×
HFIP:Water=5:5	RT/120°C	4days	LiBr	Swell	×
HFIP	RT/120°C	3days	TBACl/$TBAPF_6$	Swell	×

×: Unable to be dissolved.
HFIP: hexafluoro-2-propanol; TFA: trifluoroacetic acid; DCA: dichloroacetic acid; NMP: N-methyl-2-pyrrolidone; DMSO: dimethyl sulfoxide; $TBAPF_6$: Tetrabutylammonium hexafluorophosphate.

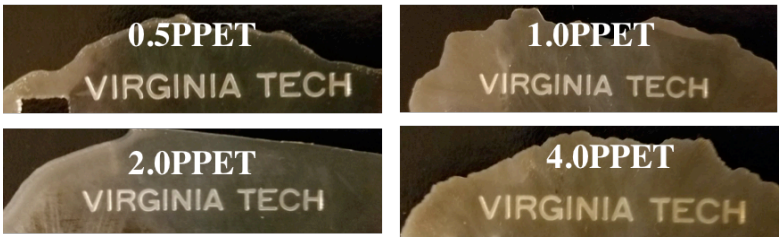

Figure 3.1. Compression-Molded Na^+-PPET films.

3.4.3 Thermal Analysis. Thermograms of melt-quenched PET and the Na^+-PPET ionomers containing different amounts of phosphonate groups are displayed in **Figure 3.2**. The heating scan of pure PET shows two enthalpic events: a glass-transition at 79 ºC, and then a prominent melting endotherm at 253 ºC. The absence of a crystallization exotherm in the neat PET thermogram indicates that the unfunctionalized PET crystallized completely during the quenching cycle (-180 ºC/min). Thermal behaviors of Na^+-PPET samples with 0.5-2.0 mol% of ionic groups were similar to that of pure PET. In contrast, the observation of a crystallization exotherm in the thermogram of the 4.0 mol% Na^+-PPET sample indicated that crystallization was incomplete during the time period of quenching, thus a significant degree of crystallization occurred during the subsequent heating scan. The appearance of a crystallization exotherm for 4.0 mol% Na^+-PPET ionomer suggests that the covalently-attached phosphonate groups act as interactive defects[8, 10] along the chains, which reduces the rate of crystallization. At 4 mol%, the concentration of these defects, and their ability to interact strongly (by dipole-dipole interactions), yielded a dynamic, electrostatically-crosslinked network in the melt that restricted the mobility of crystallizable chain segments. The combined effects of a relatively high concentration of defects and restricted chain mobility are attributed to the observed slow rate of crystallization.

Table 3.2 lists the thermal data for PET and Na^+-PPET samples shown in **Figures 3.2** and **3.3**. As a result of the low content of phosphonate groups, glass transition temperatures varied only slightly with increasing ionic content. However, the melting temperatures of Na^+-PPET were depressed from 253 °C (melting temperature for PET homopolymer) to a temperature range of 240 to 250 °C for Na^+-PPET ionomers containing 0.5-2.0 mol% of phosphonate functionality. Both melting temperature and the degree of crystallinity decreased significantly with increasing ionic content, as commonly seen in other semicrystalline ionomers.[10, 59] The reduced melting temperature with increasing ionic functionality indicates that the phosphonated monomer units along the chains are acting as structural defects that are excluded from the crystalline domains. With an increasing defect content, the statistical average length of crystallizable segments decreases, thus limiting the lamellar thickness and consequently the melting temperature.

From the thermal data in **Figure 3.3** and **Table 3.2**, it is interesting to note that subsequent cooling scans clearly show that the crystallization temperatures for the PPET ionomers decreased from 223 to 182 °C as the phosphonate group concentration increased from 0 to 4.0 mol%. The systematic decrease in crystallization temperatures with increasing ionic content is indicative of a decrease in the rate of crystallization during these non-isothermal scans. Upon cooling from the melt, as the polymer chains attempt to pack into crystalline structures, phosphonate groups act as interactive defects that are rejected from the growing crystalline interface. Again, the interactions between the defects restrict mobility during the time scale of the cooling cycle, which retards the crystallization phenomenon to lower temperatures.

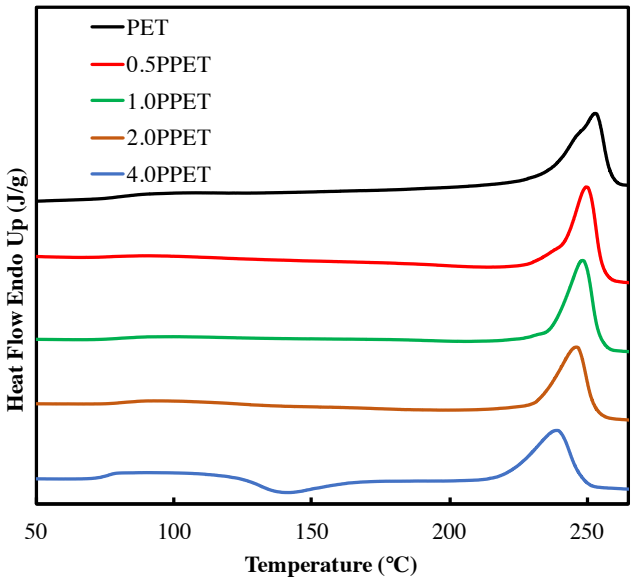

Figure 3.2. Relative heat flow versus temperature of Na^+-PPET ionomers. Second heat reported with a heating rate of 10 °C/min after quench cooling (-180 °C/min) from 270 °C.

Table 3.2. Summary of DSC Results for Na^+-PPET Ionomers.

Sample	T_g (°C)	T_{cc} (°C)	H_{cc} (J/g)	T_m (°C)	ΔH_f (J/g)	%[a] crystallinity	T_c (°C)	ΔH_c (J/g)
PET	79	-	-	253	44	31.0	223	50
0.5PPET	77	-	-	250	42	30.0	213, 218	48
1.0PPET	79	-	-	249	41	29.3	211	43
2.0PPET	76	-	-	246	36	25.7	196	37
4.0PPET	76	140	16	240	34	24.3	182	24

[a] The weight percent crystallinity is based on the theoretical heat of fusion computed for PET of 100% crystallinity (i.e. ΔH_f° = 140 J/g).[60]

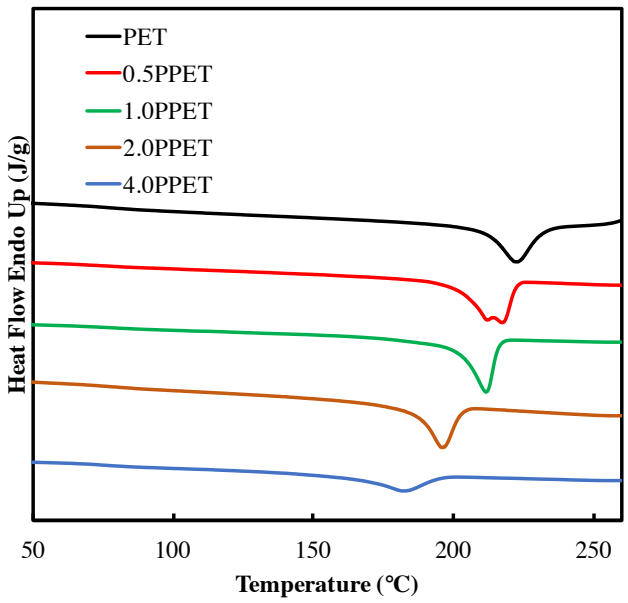

Figure 3.3. Relative cooling flow versus temperature of Na^+-PPET ionomers. Subsequent cooling scan reported with a cooling rate of -10 °C/min after heating to 270 °C.

3.4.4 Crystallization Kinetics. The effect of ionic interaction on the crystallization behavior of Na^+-PPET ionomers was further evaluated using DSC isothermal crystallization experiments over a range of controlled crystallization temperatures (**Figure 3.4**). Note that crystallization half-time, $t_{1/2}$, is inversely related to the overall rate of crystallization, such that a higher $t_{1/2}$, corresponds to a slower rate of crystallization. **Figure 3.4** shows the dependence of crystallization half-times on the crystallization temperature of Na^+-PPET ionomers with various ion contents ranging from 0 to 4.0 mol%. A complete Avrami analysis of crystallization isotherms is provided in the **Supporting Information**, included in **Table S3.1** as well as **Figure S3.1**. It is clear that the crystallization rate observed for neat PET is much faster than that observed for any of the Na^+-PPET ionomers. At the same crystallization temperature, higher ionic contents resulted in longer crystallization half-times (i.e., decreased crystallization rates).

As the crystallization temperature increased, the difference of $t_{1/2}$ values between each Na^+-PPET composition became greater. In this nucleation-controlled regime, it is not surprising that the rate of nucleation (i.e., the rate of crystallizable stem attachment to the growing crystal face) is diminished with increasing defect concentration (i.e., defective stems must be rejected). However, at these relatively low ion contents, it is likely that the effect of structural defects alone is not sufficient to account for the profound decrease in the rate of crystallization. For example, the rate of crystallization for PET containing a small content of isophthalate units (i.e., simple, non-interactive defects) is significantly faster than that observed for these ionomers containing a small content of interactive defects.[61-63] Consequently, in agreement with the behavior of model semicrystalline ionomers,[8, 10] diffusive effects are also operative when strong interactions between the functionalized chains are present. Thus, the profound decrease in the rate of crystallization with increasing ion content is attributed to the combined effect of interactive defects, which slow the rate of crystallization by the time required for the rejection of defective stems and restricted mobility of chains in the melt.

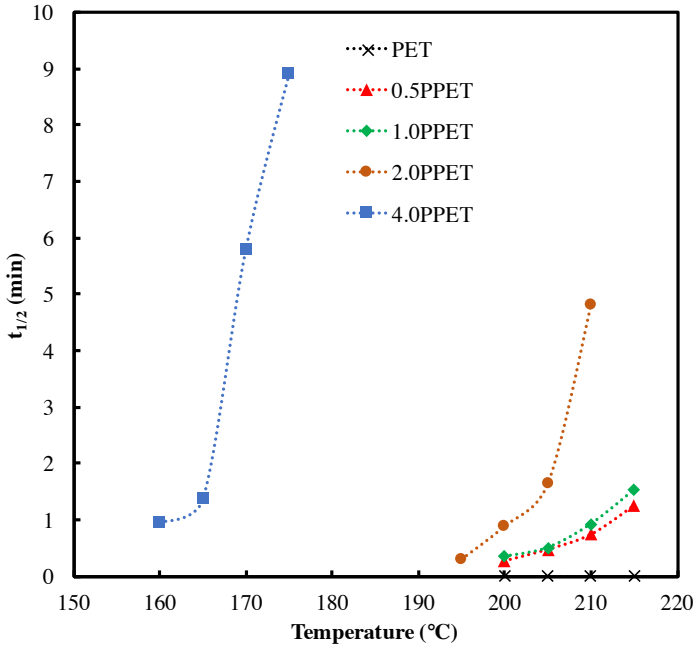

Figure 3.4. Crystallization half-time versus crystallization temperature for Na^+-PPET ionomers.

3.4.5 Rheological Characterization. The polar ionic groups of ionomers typically associate with each other, or with polar groups bearing partial charges, leading to physical crosslinks that delay the structural relaxation times, and thus dominate the melt rheological behavior.[4, 6-7, 47] As evident from the crystallization behavior (above), the contribution of restricted mobility in the melt to the reduced rates of crystallization in these relatively low ion content ionomers provides motivation to study the fundamental effects of these multivalent ionic associations on melt rheology. In addition, the lack of solubility while still melt-processable suggests a complex ionic association in these ionomers as opposed to some sort of chemical covalent crosslinking during the polymerization. Thus, an in-depth understanding of the effect of phosphonate pendant

ionic group on the rheological behavior of Na^+-PPET ionomers is crucial to evaluate their potential applicability as melt-processed materials.

Rheological analysis of PET and Na^+-PPET ionomers was performed in the melt at 280 °C. **Figure 3.5** compares the complex viscosities (η^*) of Na^+-PPET ionomers and the PET control over a wide range of frequencies from 0.1-100 rad/s. Consistent with the behavior of other ionomer systems,[47, 64-65] the complex viscosities of the Na^+-PPET ionomers were significantly higher than the non-ionic, pure PET, and η^* increased significantly with increasing ionic content. This common rheological behavior of ionomers is attributed to the interchain associations between the phosphonated units that leads to physical crosslinks in the melt. Due to the strong dipole-dipole interactions, these physical crosslinks persist at elevated temperatures, but it is important to note that these physical associations are in fact dynamic. At high temperatures (above the melting point of PET), the ionic groups can transfer from one site of association to another by a thermally-activated process known as "ion hopping".[66-68] For the Na^+-PPET ionomers studied here, we reserve the term "site of association" to include the local, instantaneous site of interactions between at least two separate phosphonate groups (i.e., interchain or intrachain dipole-dipole associations that constitute the physical crosslink). In contrast to conventional ionomers (e.g., sulfonated polystyrene[9, 69]), where ion-hopping occurs within an electrostatic network containing nanoscale multiplets of ion-pairs, our small angle X-ray scattering (SAXS) analysis of these ionomers (consisting of a relatively polar polyester matrix) reveals featureless scattering profiles suggesting the absence of well-developed multiplets (see **Supplemental Information**, **Figure S3.2**). Nevertheless, the ion-pairs in these ionomers clearly associate and dominate the rheological behavior.

The dynamic phenomenon of ion-hopping is governed by the lifetime of ionic associations and allows for diffusive flow of ionomers at elevated temperatures, even in the presence of an electrostatically-crosslinked physical network. Under conditions of melt flow, where the center of mass of a given chain diffuses through the viscous matrix, the long-range dynamics of the ionomer chains is not only governed by considerations of reptation in the entangled melt, but the diffusive motions are also hindered by the activation energy required to break associations between ion pairs.[68] Consequently, the melt viscosities of ionomers typically increase by orders of magnitude with the incorporation of low mole % of ionic groups along the chains.[65, 69-70] This general behavior is clearly evident in the data shown in **Figure 3.5**. In addition, the zero-shear viscosity (η_0) was calculated by fitting the Carreau-Yasuda model[71] to the η^*-ω data and extrapolating to $\omega \rightarrow 0$. The η_0 values *vs* ionic content are summarized in **Table 3.3**. Given the fact that ionic associations increase the longest relaxation time of the ionomers,[68] it is not surprising that the zero shear viscosities of the ionomers increase by orders of magnitude with increasing ionic content.

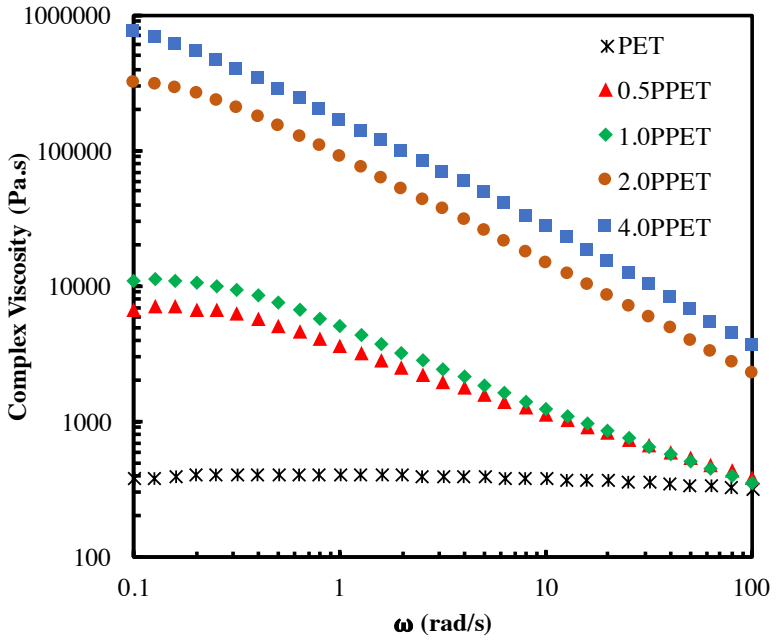

Figure 3.5. Complex viscosity-frequency mastercurves for Na^+-PPET ionomers at T = 280 °C.

Table 3.3. Zero-shear viscosities and *G' = G''* crossover frequencies of PET and Na^+-PPET ionomers at 280 °C.

	Log(η_0) (Pa·s)	**Crossover Frequency (rad/s)**
PET	2.6	NA
0.5PPET	3.8	0.787
1.0PPET	4.0	0.285
2.0PPET	5.6	0.234
4.0PPET	6.8	0.144

In addition to the profound increase in viscosity for the ionomers relative to pure PET, the frequency dependent data in **Figure 3.5** also show that the ionomers are much more shear sensitive than the non-ionic PET. All of the ionomers exhibit pronounced shear thinning behavior, while the pure PET sample is essentially Newtonian over the range of frequencies studied. This behavior is again linked to the dynamic electrostatic

network. According to the Leibler-Rubinstein-Colby (LRC) theory,[72] the reputation time of chains constrained by ionic associations, t_d, should scale as:

$$t_d \sim n^2\tau \tag{3.3}$$

where n is number of ionic groups per chain, and τ is life-time of an ionic association. When the shear rate exceeds $1/t_d$ (i.e., the relaxation rate of the ionomer chain), the electrostatic constraints upon diffusive motions diminish, and the viscosity begins to decrease in a power-law fashion with increasing shear rate. Given the dependence of t_d on the number of ionic groups per chain, the onset of shear-thinning is expected to decrease (in frequency) with increasing ionic content. Thus, the behavior of the Na^+-PPET ionomers (**Figure 3.5**), which show a decrease in frequency for the onset of shear-thinning with increasing ionic content, is in agreement with the LRC theory.

The viscoelastic behavior of the Na^+-PPET ionomers are further characterized by comparing the storage moduli (G') and loss moduli (G'') mastercurves shown in **Figure 3.6**. At high frequencies, the magnitude of the storage modulus (G') significantly exceeds that of the loss modulus (G") for the 2.0PPET and 4.0PPET ionomers. In contrast, G'and G" are quite similar for the 0.5PPET and 1.0PPET ionomers. This behavior is attributed to the physical integrity of the electrostatic network, which yields elastic character that increases with ionic content. As the frequency decreases, however, the storage modulus decreases below that of the loss modulus, revealing a dominant behavior of a viscous fluid. The crossover frequencies for each of the ionomers is highlighted with arrows and listed in **Table 3.3**. Consistent with the behavior of dynamic (transient) networks, these characteristic crossovers confirm the presence of a physical network in these ionomers attributed to the ionic associations. Moreover, in agreement

with the observed melt processability shown above, these data refute the existence of stable covalent crosslinks.

The crossover frequencies for the ionomers are also observed to decrease in frequency with increasing ionic content. Again, in agreement with the LRC theory, this behavior indicates that ionomer chain mobility decreases due to ionic associations (relaxation time, t_d, increases), and the effect is enhanced with increasing ionic content. In contrast to the viscoelastic behavior of the ionomers, the PET control does not exhibit a crossover within the observed range of frequencies, and the loss modulus is always greater than that of the storage modulus. This, of course, is expected for the fluid melt of the pure (non-ionic) PET sample.

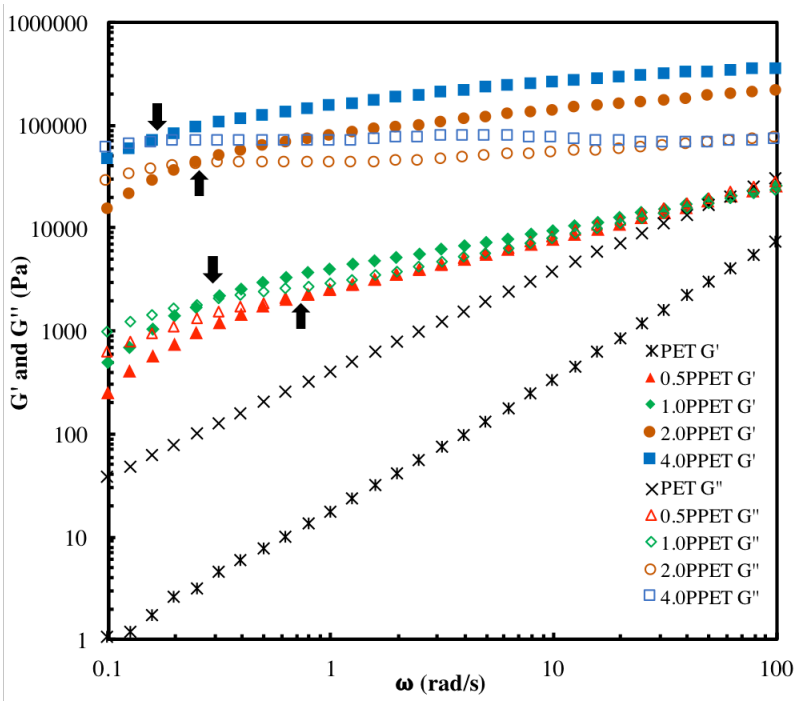

Figure 3.6. Storage and loss moduli-frequency mastercurves for Na^+-PPET ionomers at T = 280 °C.

3.4.6 Tensile Properties. Table 3.4 summarizes tensile properties, including Young's modulus and yield stress, of PET and the Na^+-PPET ionomers. The Young's moduli of the Na^+-PPET ionomers are significantly greater than that of the PET control, and the modulus is observed to increase with ionic content. The enhanced moduli of the ionomers are attributed to the ionic associations, which restrict the mobility (increase stiffness) of chain segments in the vicinity of these ionic associations and effectively increase the density of elastically active strands. As the ionic content is increased, a larger fraction of the pendant ions is likely participating in ionic associations, which increases the density of load-bearing strands and further increases the modulus.

The yield stress of ionomers is associated with the mechanical stability of the electrostatic network.[73-74] Chain slippage associated with the yield point in ionomers is affected by the lifetime and strength of dipole-dipole interactions of the associating ion-pairs. Compared to non-ionic polymers, more mechanical energy must be imparted to dissociate interacting ion-pairs, thus freeing the strands to slip past one another. For the Na^+-PPET ionomers, the yield stress is significantly higher than that for the pure PET (**Table 3.4**); however, the yield stress remains relatively constant over this relatively narrow range of ion contents.

Table 3.4. Tensile properties of compression-molded Na^+-PPET films.

	Young's Modulus (MPa)	Yield Stress (MPa)
PET	1884 ± 10	42.2 ± 2.2
0.5PPET	2135 ± 35	49.0 ± 1.3
1.0PPET	2134 ± 30	49.0 ± 0.6
2.0PPET	2360 ± 21	51.0 ± 0.6
4.0PPET	2473 ± 55	49.2 ± 0.8

3.5 Conclusions

We have synthesized Na^+-PPET ionomers with various ionic contents (0.5 mol% - 4.0 mol%), and characterized the effects of the divalent pendant ions on the thermal, rheological, and mechanical properties. By modifying the route for the synthesis of phosphonated dimethyl isophthalate, disodium salt, we demonstrated the isolation of hemi-sodium salt and the application of the Chelex® purification protocol greatly improved the isolation yield by 300% compared with the very low yield reported in the 1962 patent.[45] The Na^+-PPET ionomers were synthesized using typical melt polycondensation catalyzed by $Mn(OAc)_2$ and Sb_2O_3. Due to the combined effects of structural defects and restricted chain mobility attributed to ionic associations, crystalline melting temperatures, crystallization temperatures, degree of crystallinity, and crystallization rates decreased with increasing ionic content. In rheological studies, the Na^+-PPET ionomers exhibited increased complex viscosity as a result of increased ionic content. All of the Na^+-PPET ionomers demonstrated pronounced shear thinning behavior, while the pure PET sample was essentially Newtonian over the range of frequencies studied (0.1-100 rad/s). The Na^+-PPET ionomers showed a decrease in frequency for the onset of shear-thinning with increasing ionic content, attributed to the increased relaxation time of the ionomers. A crossover of G' and G'' was observed for the Na^+-PPET ionomer, and the crossover frequency shifted to lower shear rate with increasing ionic content, indicative of an enhanced effect of the physical network. Tensile tests demonstrated superior yield stress and Young's modulus for the Na^+-PPET ionomers compared to pure PET. An increase in Young's modulus was observed with increasing ionic content and attributed to the effect of ionic associations on chain stiffness and the density of elastically active strands. Future systematic investigation will

compare the different influences of divalent phosphonate and monovalent sulfonate pendant ions on the physical properties of PET ionomers. Moreover, PPET ionomers bearing divalent anionic pendant ions will be evaluated as alternative compatibilizers for polyester/polyamide blends.

3.6 Acknowledgements

The authors gratefully acknowledge the Institute for Advanced Learning and Research for providing funds to support the efforts of this project.

3.7 References

1. Tant, M. R.; Mauritz, K. A.; Wilkes, G. L., Ionomers: synthesis, structure, properties and applications. Springer Science & Business Media: 2012.
2. Lundberg, R. D., 12 Elastomers and fluid applications. Ionomers: Synthesis, structure, properties and applications 1997, 477.
3. Zhang, L.; Brostowitz, N. R.; Cavicchi, K. A.; Weiss, R., Perspective: ionomer research and applications. Macromol. React. Eng. 2014, 8 (2), 81-99.
4. Eisenberg, A.; Hird, B.; Moore, R., A new multiplet-cluster model for the morphology of random ionomers. Macromolecules 1990, 23 (18), 4098-4107.
5. Eisenberg, A., Ion-containing polymers: physical properties and structure. Elsevier: 2012; Vol. 2.
6. MacKnight, W.; Earnest, T., The structure and properties of ionomers. J. Polymer Sci. Macromol. Rev. 1981, 16 (1), 41-122.
7. Tant, M. R.; Wilkes, G. L., An overview of the viscous and viscoelastic behavior of ionomers in bulk and solution. Polymer Rev. 1988, 28 (1), 1-63.
8. Orler, E. B.; Calhoun, B. H.; Moore, R. B., Crystallization kinetics as a probe of the dynamic network in lightly sulfonated syndiotactic polystyrene ionomers. Macromolecules 1996, 29 (18), 5965-5971.
9. Orler, E. B.; Moore, R. B., Influence of ionic interactions on the crystallization of lightly sulfonated syndiotactic polystyrene ionomers. Macromolecules 1994, 27 (17), 4774-4780.
10. Orler, E. B.; Yontz, D. J.; Moore, R. B., Sulfonation of syndiotactic polystyrene for model semicrystalline ionomer investigations. Macromolecules 1993, 26 (19), 5157-5160.
11. Huang, C.; Young, N. P.; Grant, P. S., Spray processing of TiO 2 nanoparticle/ionomer coatings on carbon nanotube scaffolds for solid-state supercapacitors. J. Mater. Chem. A 2014, 2 (29), 11022-11028.

12. Ugo, P.; Moretto, L. M.; Vezza, F., Ionomer-Coated Electrodes and Nanoelectrode Ensembles as Electrochemical Environmental Sensors: Recent Advances and Prospects. ChemPhysChem 2002, 3 (11), 917-925.
13. Hamama, H.; Burrow, M.; Yiu, C., Effect of dentine conditioning on adhesion of resin-modified glass ionomer adhesives. Aust Dent J. 2014, 59 (2), 193-200.
14. Sezinando, A.; Linares Serrano, M.; Morales Pérez, V.; García Muñoz, R. A.; Ceballos, L.; Perdigão, J., Chemical Adhesion of Polyalkenoate-based Adhesives to Hydroxyapatite. J. Adhes Dent. 2016, 18 (3).
15. Hsiao, K. J.; Lee, S. P.; Kong, D. C.; Chen, F. L., Thermal and mechanical properties of poly (trimethylene terephthalate)(PTT)/cationic dyeable poly (trimethylene terephthalate)(CD-PTT) polyblended fibers. J. Appl. Polym. Sci 2006, 102 (2), 1008-1013.
16. Sheth, P. J.; Kolm, R. R., Dyeable polyolefin compositions and dyeing polyolefin compositions. US Patent 5,468,259.
17. Gao, Z.; Molnar, A.; Eisenberg, A., Blend compatibilization. In Ionomers, Springer: 1997; pp 390-443.
18. Longworth, R.; Nagel, H., Packaging. In Ionomers, Springer: 1997; pp 365-389.
19. Kim, B. K.; Lee, S. Y.; Lee, J. S.; Baek, S. H.; Choi, Y. J.; Lee, J. O.; Xu, M., Polyurethane ionomers having shape memory effects. Polymer 1998, 39 (13), 2803-2808.
20. Xie, T., Tunable polymer multi-shape memory effect. Nature 2010, 464 (7286), 267.
21. Ghosh, S. K., Self-healing materials: fundamentals, design strategies, and applications. John Wiley & Sons: 2009.
22. Varley, R. J.; van der Zwaag, S., Towards an understanding of thermally activated self-healing of an ionomer system during ballistic penetration. Acta Mater 2008, 56 (19), 5737-5750.
23. Dolog, R.; Weiss, R., Shape memory behavior of a polyethylene-based carboxylate ionomer. Macromolecules 2013, 46 (19), 7845-7852.
24. Fahs, G. B.; Benson, S. D.; Moore, R. B., Blocky Sulfonation of Syndiotactic Polystyrene: A Facile Route toward Tailored Ionomer Architecture via Postpolymerization Functionalization in the Gel State. Macromolecules 2017, 50 (6), 2387-2396.
25. Kakati, D.; Gosain, R.; George, M., New polyurethane ionomers containing phosphonate groups. Polymer 1994, 35 (2), 398-402.
26. Luqman, M.; Kim, J.-S., Effects of the cation valence on the mechanical properties of sulfonated polystyrene ionomers containing dicarboxylate salts. Polym Bull 2012, 69 (7), 861-871.
27. Kim, J.-S.; Hong, M.-C.; Nah, Y. H., Effects of two ionic groups in an ionic repeat unit on the properties of styrene ionomers. Macromolecules 2002, 35 (1), 155-160.
28. Kim, S.-H.; Kim, J.-S., Effects of low matrix glass transition temperature on the cluster formation of ionomers having two ion pairs per ionic repeat unit. Macromolecules 2003, 36 (6), 1870-1875.

29. Chen, D.; Hickner, M. A., Ion clustering in quaternary ammonium functionalized benzylmethyl containing poly (arylene ether ketone) s. Macromolecules 2013, 46 (23), 9270-9278.
30. Gauthier, S.; Duchesne, D.; Eisenberg, A., Vinylpyridinium ionomers. 1. Influence of the structure of the ion on the state of aggregation in random styrene-based systems. Macromolecules 1987, 20 (4), 753-759.
31. Zhang, K.; Drummey, K. J.; Moon, N. G.; Chiang, W. D.; Long, T. E., Styrenic DABCO salt-containing monomers for the synthesis of novel charged polymers. Polymer Chemistry 2016, 7 (20), 3370-3374.
32. Ng, C.-W. A.; Lindway, M. J.; MacKnight, W. J., Ionomeric blends of poly (ethyl acrylate-co-4-vinylpyridine) with zinc-neutralized sulfonated poly (ethylene terephthalate). 1. Effect of specific interactions upon the amorphous phase. Macromolecules 1994, 27 (11), 3027-3032.
33. Ng, C.-W. A.; MacKnight, W. J., Ionomeric blends of poly (ethyl acrylate-co-4-vinylpyridine) with zinc-neutralized sulfonated poly (ethylene terephthalate). 2. Effect of specific interactions upon the crystalline phase. Macromolecules 1994, 27 (11), 3033-3038.
34. Ng, C.-W. A.; MacKnight, W. J., Ionomeric Blends of Poly (ethyl acrylate-co-4-vinylpyridine) with Metal-Neutralized Sulfonated Poly (ethylene terephthalate). 4. Effects of Counterions. Macromolecules 1996, 29 (7), 2421-2429.
35. Ng, C.-W. A.; MacKnight, W. J., Ionomeric blends of poly (ethyl acrylate-co-4-vinylpyridine) with zinc-neutralized sulfonated poly (ethylene terephthalate). 3. Effects of functionalization level. Macromolecules 1996, 29 (7), 2412-2420.
36. Pekkanen, A. M.; Zawaski, C.; Stevenson Jr, A. T.; Dickerman, R.; Whittington, A. R.; Williams, C. B.; Long, T. E., Poly (ether ester) Ionomers as Water-Soluble Polymers for Material Extrusion Additive Manufacturing Processes. ACS Appl. Mater. Interfaces 2017, 9 (14), 12324-12331.
37. Shi, Y.; Weiss, R., Sulfonated Poly (ether ether ketone) Ionomers and Their High Temperature Shape Memory Behavior. Macromolecules 2014, 47 (5), 1732-1740.
38. Shi, Y.; Yoonessi, M.; Weiss, R., High temperature shape memory polymers. Macromolecules 2013, 46 (10), 4160-4167.
39. Bagrodia, S.; Wilkes, G. L., Comments on the effect of cation, type on ionomer properties. Polym Bull 1984, 12 (5), 389-392.
40. Tierney, N. K.; Register, R. A., The Role of Excess Acid Groups in the Dynamics of Ethylene− Methacrylic Acid Ionomer Melts. Macromolecules 2002, 35 (16), 6284-6290.
41. Abu-Thabit, N. Y.; Ali, S. A.; Zaidi, S. J.; Mezghani, K., Novel sulfonated poly (ether ether ketone)/phosphonated polysulfone polymer blends for proton conducting membranes. J. Mater. Res. 2012, 27 (15), 1958-1968.
42. Rager, T.; Schuster, M.; Steininger, H.; Kreuer, K. D., Poly (1, 3-phenylene-5-phosphonic Acid), a Fully Aromatic Polyelectrolyte with High Ion Exchange Capacity. Adv. Mater. 2007, 19 (20), 3317-3321.
43. Shukla, D.; Negi, Y. S.; Kumar, V., Modification of Poly (ether ether ketone) Polymer for Fuel Cell Application. J. Appl. Chem. 2013, 2013.
44. Horn, C. F., Acyloxymetallosulfophthalate containing dyeable polyesters. US Patent 3,185,671.

45. Malcolm, G. J.; Roscoe, R. W., Sulfonate containing polyesters dyeable with basic dyes. US Patent 5,607,765.
46. Chen, Y. M.; Zhao, D.; Wang, L. Y.; Wu, Q. C. In Synthesis and Characterization of Branched Poly (Ethylene Terephthalate), Advanced Materials Research, Trans Tech Publ: 2013; pp 738-741.
47. Greener, J.; Gillmor, J.; Daly, R., Melt rheology of a class of polyester ionomers. Macromolecules 1993, 26 (24), 6416-6424.
48. Wang, Y.-Z.; Chen, X.-T.; Tang, X.-D.; Du, X.-H., A new approach for the simultaneous improvement of fire retardancy, tensile strength and melt dripping of poly (ethylene terephthalate). J. Mater. Chem. 2003, 13 (6), 1248-1249.
49. Kang, H.; Lin, Q.; Armentrout, R. S.; Long, T. E., Synthesis and characterization of telechelic poly (ethylene terephthalate) sodiosulfonate ionomers. Macromolecules 2002, 35 (23), 8738-8744.
50. Gemeinhardt, G. C.; Moore, A. A.; Moore, R. B., Influence of ionomeric compatibilizers on the morphology and properties of amorphous polyester/polyamide blends. Polym. Eng. Sci 2004, 44 (9), 1721-1731.
51. Hu, Y.; Prattipati, V.; Mehta, S.; Schiraldi, D.; Hiltner, A.; Baer, E., Improving gas barrier of PET by blending with aromatic polyamides. Polymer 2005, 46 (8), 2685-2698.
52. Iyer, S.; Schiraldi, D. A., Role of ionic interactions in the compatibility of polyester ionomers with poly (ethylene terephthalate) and nylon 6. J. Polym. Sci., Polym. Phys. 2006, 44 (15), 2091-2103.
53. Özen, İ.; Bozoklu, G.; Dalgıçdir, C.; Yücel, O.; Ünsal, E.; Çakmak, M.; Menceloğlu, Y. Z., Improvement in gas permeability of biaxially stretched PET films blended with high barrier polymers: The role of chemistry and processing conditions. Eur Polym J. 2010, 46 (2), 226-237.
54. Prattipati, V.; Hu, Y.; Bandi, S.; Schiraldi, D.; Hiltner, A.; Baer, E.; Mehta, S., Effect of compatibilization on the oxygen-barrier properties of poly (ethylene terephthalate)/poly (m-xylylene adipamide) blends. J. Appl. Polym. Sci. 2005, 97 (3), 1361-1370.
55. Iannicelli, J., Metallic phosphonate containing polyester. US Patent 3,052,653.
56. Avrami, M., Kinetics of phase change. I General theory. J. Chem. Phys. 1939, 7 (12), 1103-1112.
57. Mo, F.; Dong, G.; Zhang, Y.; Wang, J., Recent applications of arene diazonium salts in organic synthesis. Org. Biomol. Chem. 2013, 11 (10), 1582-1593.
58. Doak, G.; Freedman, L. D., The Synthesis of Arylphosphonic and Diarylphosphinic Acids by the Diazo Reaction1. J. Am. Chem. Soc. 1951, 73 (12), 5658-5660.
59. Marx, C. L.; Cooper, S. L., The crystallinity of ionomers. J. Macromol Sci, Part B: Phys 1974, 9 (1), 19-33.
60. Wunderlich, B., Thermal analysis of polymeric materials. Springer Science & Business Media: 2005.
61. Lee, S.; Ree, M.; Park, C.; Jung, Y.; Park, C.-S.; Jin, Y.; Bae, D., Synthesis and non-isothermal crystallization behaviors of poly (ethylene isophthalate-co-terephthalate) s. Polymer 1999, 40 (25), 7137-7146.

62. Ostrowska-Gumkowska, B.; Ostrowska-Czubenko, J.; Gużynski, P., Crystallization of Lightly Sulfonated Poly (ethylene terephthalate) Ionomer. I. Isothermal Crystallization from the Melt. J. Macromol Sci, Part B: Phys 2008, 47 (4), 675-688.
63. Wu, T. M.; Chang, C. C.; Yu, T. L., Crystallization of poly (ethylene terephthalate–co–isophthalate). J. Polym Sci. Part B: Polym Phys 2000, 38 (19), 2515-2524.
64. Spencer, M.; Wetzel, M.; Troeltzsch, C.; Paul, D., Effects of acid neutralization on the properties of K+ and Na+ poly (ethylene-co-methacrylic acid) ionomers. Polymer 2012, 53 (2), 569-580.
65. Weiss, R.; Yu, W.-C., Viscoelastic behavior of very lightly sulfonated polystyrene ionomers. Macromolecules 2007, 40 (10), 3640-3643.
66. Cooper, W., Copolymers of butadiene and unsaturated acids: crosslinking by metal oxides. Journal of Polymer Science Part A: Polymer Chemistry 1958, 28 (116), 195-206.
67. Ling, G. H.; Wang, Y.; Weiss, R., Linear viscoelastic and uniaxial extensional rheology of alkali metal neutralized sulfonated oligostyrene ionomer melts. Macromolecules 2011, 45 (1), 481-490.
68. Register, R. A.; Prud'homme, R. K., Melt rheology. In Ionomers: Synthesis, structure, properties and applications, Tant, M. R.; Mauritz, K. A.; Wilkes, G. L., Eds. Springer Netherlands: Dordrecht, 1997; pp 208-260.
69. Weiss, R.; Zhao, H., Rheological behavior of oligomeric ionomers. J. Rheol. 2009, 53 (1), 191-213.
70. Huang, C.; Chen, Q.; Weiss, R., Rheological Behavior of Partially Neutralized Oligomeric Sulfonated Polystyrene Ionomers. Macromolecules 2016, 50 (1), 424-431.
71. Bird, R. B., Dynamics of polymeric liquids. Wiley: 1977.
72. Leibler, L.; Rubinstein, M.; Colby, R. H., Dynamics of reversible networks. Macromolecules 1991, 24 (16), 4701-4707.
73. Liu, D.; Kyriakides, S.; Case, S. W.; Lesko, J. J.; Li, Y.; McGrath, J. E., Tensile behavior of Nafion and sulfonated poly (arylene ether sulfone) copolymer membranes and its morphological correlations. J. Polym. Sci. Part B: Polym. Phys. 2006, 44 (10), 1453-1465.
74. Visser, S. A.; Cooper, S. L., Comparison of the physical properties of carboxylated and sulfonated model polyurethane ionomers. Macromolecules 1991, 24 (9), 2576-2583.

3.8 Supporting Information

Table S3.1. Kinetic parameters at various temperatures for Na^+-PPET ionomers

Na^+-PPET Kinetic Parameter				
0.5 mol% Na^+-PPET	200 °C	205 °C	210 °C	215 °C
$t_{1/2}$ (min)	0.27	0.47	0.74	1.26
n	2.29	2.47	2.57	2.85
K (min^{-1})	13.84	4.33	1.49	0.35
1.0 mol% Na^+-PPET	200 °C	205 °C	210 °C	215 °C
$t_{1/2}$ (min)	0.36	0.51	0.93	1.67
n	2.54	2.28	2.19	2.60
K (min^{-1})	9.65	3.17	0.81	0.18
2.0 mol% Na^+-PPET	195 °C	200 °C	205 °C	210 °C
$t_{1/2}$ (min)	0.31	0.93	1.65	4.93
n	2.36	2.09	2.21	2.34
K (min^{-1})	10.83	0.81	0.23	0.017
4.0 mol% Na^+-PPET	160 °C	165 °C	170 °C	175 °C
$t_{1/2}$ (min)	0.96	1.36	5.81	8.92
n	2.41	2.24	1.95	2.47
K (min^{-1})	0.76	0.34	0.023	0.0031

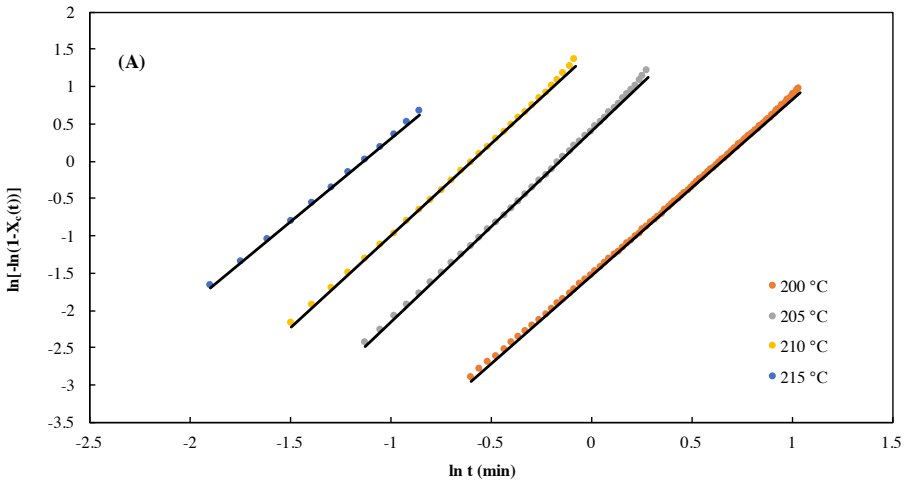
(A)
ln[-ln(1-Xc(t))]
ln t (min)
200 °C
205 °C
210 °C
215 °C

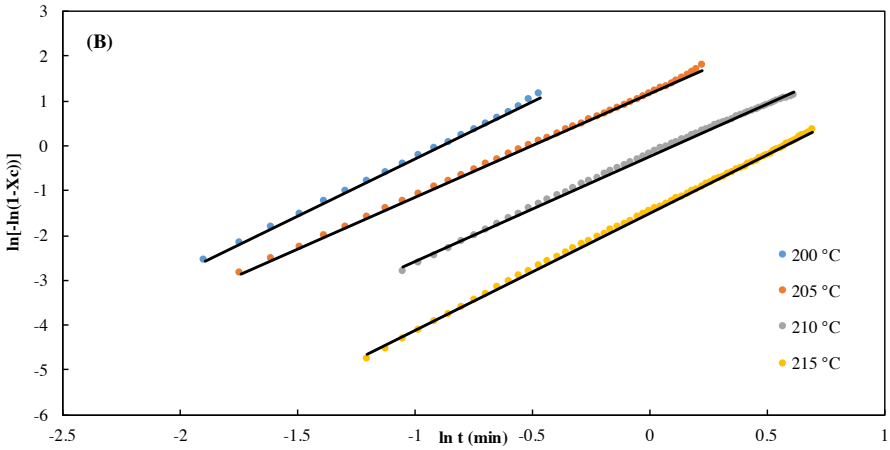
(B)
ln[-ln(1-Xc))]
ln t (min)
200 °C
205 °C
210 °C
215 °C

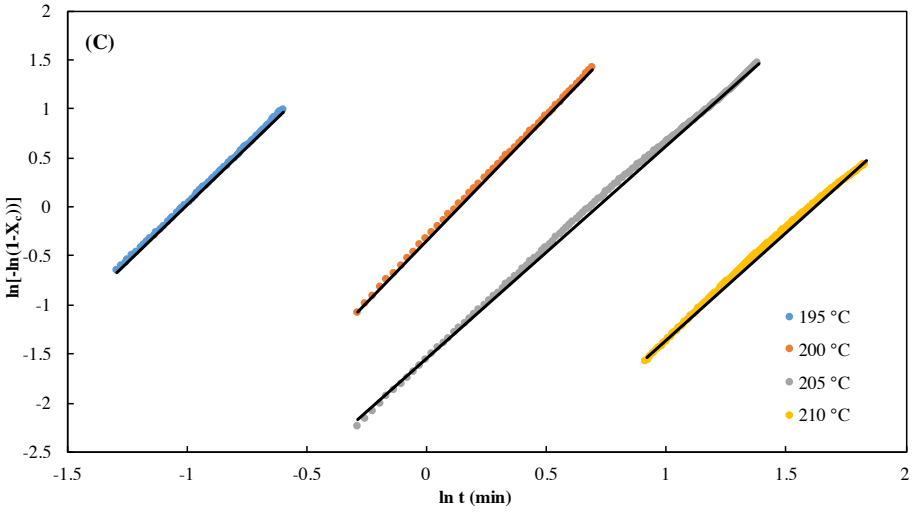
(C)
ln[-ln(1-Xc))]
ln t (min)
195 °C
200 °C
205 °C
210 °C

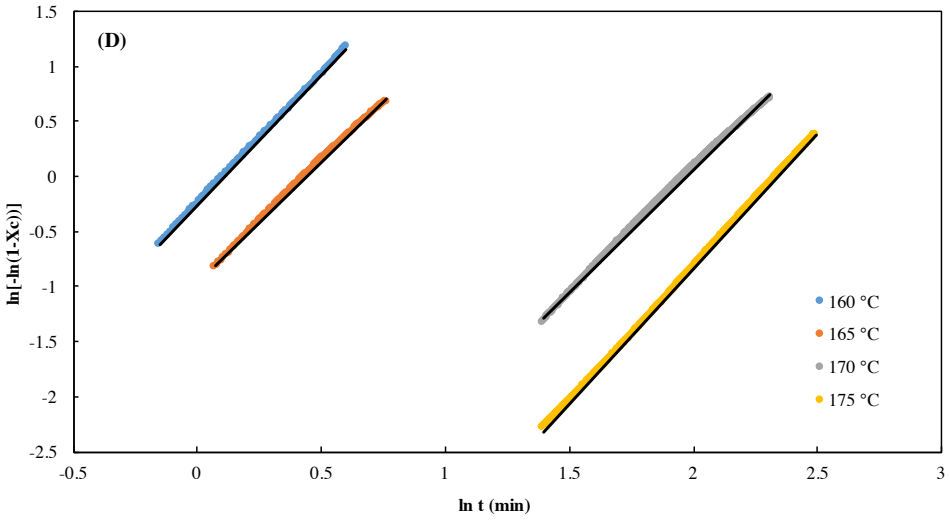

Figure S3.1. ln[-ln(1-Xc(t))] versus ln t at various temperatures for (A) 0.5 mol% Na^+-PPET, (B) 1.0 mol% Na^+-PPET, (C) 2.0 mol% Na^+-PPET, and (D) 4.0 mol% Na^+-PPET. Fit lines are shown in black used to determine the Avrami parameters shown in **Table S1**.

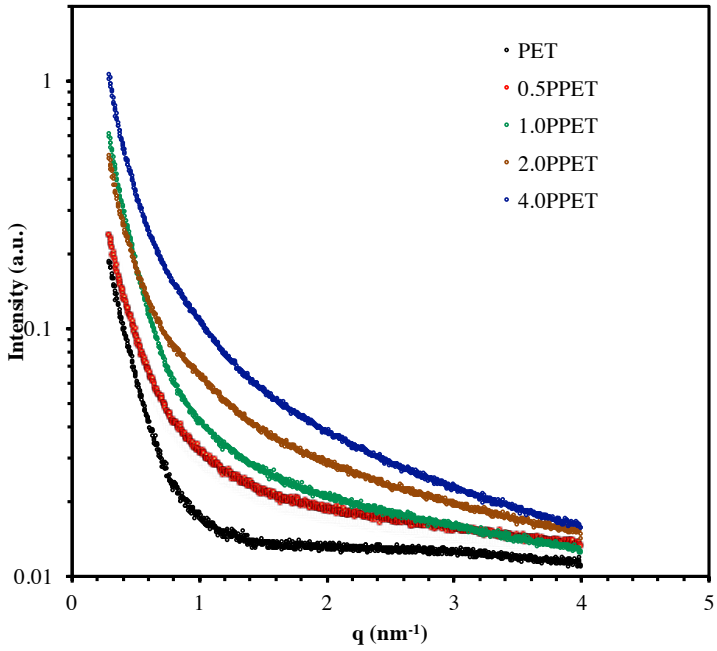

Figure S3.2. Small angle X-ray scattering (SAXS) profiles for compression-molded films of PET and the Na^+-PPET ionomers.

Chapter 4. A Comparison of Sulfonated and Phosphonated Poly(ethylene terephthalate) Ionomers: Thermal and Linear Viscoelastic Properties

(Manuscript in Preparation)

Lin Ju,[a,c] Tianran Chen,[b,c] Donald G. Baird,[b,c] and Robert B. Moore [a,c,*]

[a]Department of Chemistry, Virginia Polytechnic Institute and State University, Blacksburg, VA 24061, United States

[b]Department of Chemical Engineering, Virginia Polytechnic Institute and State University, Blacksburg, VA 24060, United States

[c]Macromolecules Innovation Institute, Virginia Polytechnic Institute and State University, Blacksburg, VA 24061, United States

4.1 Abstract

The effects of monovalent sulfonate and divalent phosphonate pendant ions on the thermal and linear viscoelastic properties of poly(ethylene terephthalate) (PET) ionomers were evaluated in this work. Both sulfonated and phosphonated PET ionomers (SPET and PPET) with small amounts of ionic functionalities (0.5-4.0 mol%) were synthesized by melt polycondensation reaction. The thermal transitions and crystallization kinetics were examined using differential scanning calorimetry (DSC). At the same ionic monomer concentrations, PPET ionomers exhibited higher crystallizability and faster crystallization kinetics than SPET ionomers. The effect of sulfonate and phosphonate functionalities on the flow behavior of PET ionomers was investigated via melt rheology

analysis. Time-temperature superposition (TTS) revealed significantly higher zero-shear viscosity (η_0) and longer reptation time (τ_{rep}) for PPET ionomers as compared to SPET analogues, suggesting the divalent phosphonate pendant ions were able to generate stronger physical crosslinks than monovalent sulfonate pendant ions.

4.2 Introduction

Ionomers are charged polymers that contain minor amounts (typically < 15 mol%) of covalently attached ionic functionalities incorporated into or pendant to the polymer backbones.[1-3] Generally, the polar ionic groups, surrounded by a less polar matrix, tend to form nanometer-sized ionic aggregates due to the attractive Coulombic interactions between the ionic pairs.[4] These ionic aggregates, acting as physical crosslinks, decrease the mobility of polymer chains, and are known to exert a profound effect on the thermal and rheological properties of polymers.[2, 5-17] Compared to nonionic analogues, semi-crystalline ionomers have been shown to exhibit lower melting temperatures (T_m), lower degrees of crystallinity (X_c), and a significantly decreased crystallizability.[5, 7, 9-13] Additionally, the incorporation of small amount of ionic functionalities altered the linear viscoelastic behavior of polymers, mainly a large increase in melt viscosity and an extended rubbery plateau.[3, 8, 9, 14, 17]

Carboxylated and sulfonated ionomers are the most widely studied ionomers in the literature.[3, 4, 10, 11, 16-22] The type of anionic pendant ion plays an important role on the physical crosslink generated between ion pairs via dipole-dipole interactions, and consequently affecting their physical properties.[9, 19, 20, 22] Polymers modified with sulfonate groups exhibit more dramatic changes in thermal, viscoelastic, rheological

properties than those modified with the carboxylate groups.[19, 20] For example, Lundberg and Makowski[20] compared carboxylated and sulfonated polystyrene ionomers containing 0.3-5.0 mol% ionic functionalities, and found sulfonated polystyrene ionomers exhibit higher glass transition temperatures and significantly increased melt viscosities than those of the carboxylated analogues. These results were attributed to the stronger dipole-dipole interactions formed between sulfonate ion pairs, thereby providing stronger physical crosslinks in sulfonated polystyrene ionomers.[20]

Compared to the widely studied ionomers with monovalent carboxylate and sulfonate ionic groups, relatively little research has been done on ionomers bearing divalent phosphonate ionic groups. Zhang and coworkers synthesized two types of PET ionomers: one is terminated with mono-functional phosphonate ionic groups incorporated on the backbone,[23] and the other one is derived from a small amount of mono-functional phosphonate monomers.[24] These phosphonate-containing PET ionomers displayed an improved crystallizability as compared to pure PET control as evidenced by a faster crystallization rate and an improved crystallinity. Additionally, Weiss and coworkers successfully synthesized poly(styrene-*co*-vinylphosphonate) (SVP) ionomers,[17, 25] and compared their viscoelastic properties to sulfonated polystyrene (SPS) ionomers.[17] Surprisingly, although phosphonic acid (pK_{a1} ~ 2-3; pK_{a2} ~7) is a weaker acid than sulfonic acid (pK_a ~ 1), the strength and persistence of the physical crosslinks produced by the SVP ionomers were greater than for SPS ionomers as indicated by the longer rubbery plateau region and higher plateau moduli for SVP ionomers. Despite of the substantial effects of the divalent phosphonate groups on the viscoelastic properties of phosphonated ionomers, this conclusion was restricted to the different polymer

backbones for these two specific ionomers. For SVP ionomers, the phosphonate groups were attached directly to an aliphatic part of the polymer chains, while the sulfonate functionalities were attached to aromatic monomer units (styrene). Furthermore, recently, we successfully synthesized phosphonated PET ionomers in the Na^+ form,[9] and evaluated the ability of the monovalent sulfonate and the divalent phosphonate pendant ions in PET ionomers to compatibilize amorphous polyester/poly(*m*-xylylene adipamide) (PETG/MXD6) blends.[26] This comparison showed that the phosphonated PET (PPET) ionomer-compatibilized PETG/MXD6 blends required 6 times fewer ionic monomers to achieve phase-separated domain dimension less than 1 μm as compared to sulfonated PET (SPET)/PETG/MXD6 blends. This finding demonstrated the divalent phosphonate pendant ions in PPET were more effective at compatibilizing PETG/MXD6 blends compared to the monovalent sulfonate pendant ions as a consequence of the stronger specific interactions generated per functional monomer unit. However, the evaluation of the effects of monovalent sulfonate and divalent phosphonate groups on the physical properties of ionomers bearing the same polymer backbones have not been reported yet.

In this work, we reported the first investigation of the monovalent sulfonate and divalent phosphonate ionic groups on the thermal and viscoelastic properties of PET ionomers by comparing the structure-property relationships for SPET and PPET at low ionic monomer concentration (0.5-4.0 mol%). Differential scanning calorimetry (DSC) was used to probe the crystallizability and crystallization kinetics of these two series of PET ionomers, and time-temperature superposition (TTS) was used as a technique to evaluate their linear viscoelastic behavior by analyzing storage and loss moduli along with melt viscosity at various mol% of ionic monomer units. The broad scope of this

work is to use SPET and PPET as templates to provide a deep insight into the effect of the types of anionic pendant ions on the physical properties of polyester ionomers.

4.3 Experimental Section

Materials. Dimethyl 5-sulfoisophthalate sodium salt (98%) was purchased from Sigma-Aldrich and used as received. Dimethyl 5-phosphoisophthalate disodium salt was synthesized by the procedure as described in our recent publication.[9] Sulfonated and phosphonated poly(ethylene terephthalate) ionomers (SPET and PPET) with 0.5, 1.0, 2.0, and 4.0 mol% ionic monomer units randomly distributed along the polymer chain were synthesized by melt polycondensation reaction as described in our recent publication.[9] A control sample of pure PET (without ionic monomer) was synthesized using the same procedure.

Differential Scanning Calorimetry. A TA instruments Q2000 differential scanning calorimetry (DSC) was used to determine the thermal properties and crystallization behavior of SPET and PPET ionomers. Compression-molded film samples (between Kapton sheets at 270 °C using a PHI hydraulic press) were die cut and placed within aluminum DSC pans. Under a nitrogen atmosphere, the samples (~5-8 mg) were heated from ambient temperature to 270 °C at 10 °C/min, quench cooled to 0 °C at -60 °C/min, reheated from 0 °C to 270 °C at 10 °C/min, and then cooled to 0 °C at -10 °C/min. The glass transition temperature (T_g), cold crystallization temperature (T_{cc}), enthalpy of cold crystallization (ΔH_{cc}), melting temperature (T_m), enthalpy of melting (ΔH_m), and degree of crystallinity (X_c) were determined from the second heating scan after erasing the thermal history; the crystallization temperature (T_c) and enthalpy of

crystallization (ΔH_c) were investigated from the subsequent cooling scan by using the TA Instruments Universal Analysis software. X_c was determined using the following relationship:

$$X_c = \frac{\Delta H_m}{\Delta H_m^\circ} \tag{4.1}$$

where ΔH_m is the enthalpy of melting determined from integration of the melting endotherm and ΔH_m° is the theoretical enthalpy of melting of 100% crystalline PET (140 J/g).[27]

Isothermal crystallization was carried out for SPET and PPET ionomers. TA Instruments Universal Analysis software was used to analyze the resulting DSC traces. The crystallization half-time, $t_{1/2}$, the time at which the material reaches 50% of its maximum crystallinity, was obtained from isothermal scans at various temperatures, and was used as a measure of the bulk crystallization rates of PET ionomers. Isothermal crystallization data were analyzed using the Avrami equation,[28]

$$\ln\left[-\ln\left(1 - X_c(t)\right)\right] = lnK + n\, lnt \tag{4.2}$$

where K is the kinetic growth rate constant, n is the Avrami exponent, and $X_c(t)$ is the relative extent of crystallization at time t. From the DSC data, $X_c(t)$ is defined as:

$$X_c(t) = \frac{\int_0^t \left(\frac{dH}{dt}\right) dt}{\int_0^\infty \left(\frac{dH}{dt}\right) dt} \tag{4.3}$$

where (dH/dt) is the heat evolution during crystallization as a function of time, relative to the total heat of crystallization.

Rheological Analysis. Rheological analysis of all samples was performed on an ARES-G2 Rheometer from TA instruments utilizing 25 mm parallel plates. A dry nitrogen atmosphere in the oven was utilized to prevent the samples from absorbing

ambient moisture. Strain sweeps were conducted to confirm the linear viscoelastic (LVE) region, i.e., 0.1 %-24 % oscillatory strain. Dynamic frequency sweeps (0.1-500 rad/s) and temperature step (10 °C/step) were performed over a temperature range of 240-280 °C using a 5 % oscillatory strain within the LVE region to provide storage and loss moduli and viscosity responses over a wide range of frequency. Time-temperature superposition (TTS) master curves for each sample were constructed at the same reference temperature T_r = 250 °C using the TA Instruments TRIOS software.

4.4 Results and Discussion

4.4.1 Thermal Properties. DSC heating thermograms of the SPET and PPET ionomers after rapid cooling from the melt to 0 °C at -60 °C/min are shown in **Figure 4.1**, and the corresponding thermal data are summarized in **Table 4.1**. The heating trace of pure PET displays two endothermic events, a glass transition (T_g) at 79 °C and an intense melting endotherm (T_m) at 253 °C. While an increase in T_g with ionic content is commonly observed in amorphous ionomers due to a reduction in chain mobility from the physical cross-links formed by aggregation of the polar ionic groups, T_g of both SPET and PPET ionomers vary only slightly with increasing ionic content due to the low content of ionic groups. In addition, both T_m and the degree of crystallinity (X_c) decrease significantly with increasing ionic content, as commonly seen in other semi-crystalline ionomers.[5, 7, 12, 13] The ionic groups attached to the crystallizable PET ionomers can act as physical defects along the polymer chains, limiting crystallizability and lamellar thickness. It is not surprising then that both sulfonated and phosphonated PET ionomers

exhibit T_m and X_c depression with increasing ionic functionality as a consequence of shorter crystallizable chain segments and thus thinner crystallites.[29-32]

SPET and PPET ionomers exhibit similar melting behaviors, but significantly different crystallizability (**Figure 4.1**). SPET ionomers start to display an exothermic event (ascribed to cold crystallization, T_{cc}) during heating scans when the ionic functionality is 1.0 mol%, while a cold crystallization is observed for PPET ionomers at a higher ionic functionality, i.e., 4.0 mol%, under the same thermal conditions as SPET ionomers. Cold crystallization during the heating scan following a rapid cool is attributed to a reduction in the rate of crystallization, indicative of an incomplete crystallization during the quenching cycle (-60 °C/min). The appearance of cold crystallization for SPET ionomers at a lower ionic functionality implies a lower crystallizability in comparison to PPET analogues.

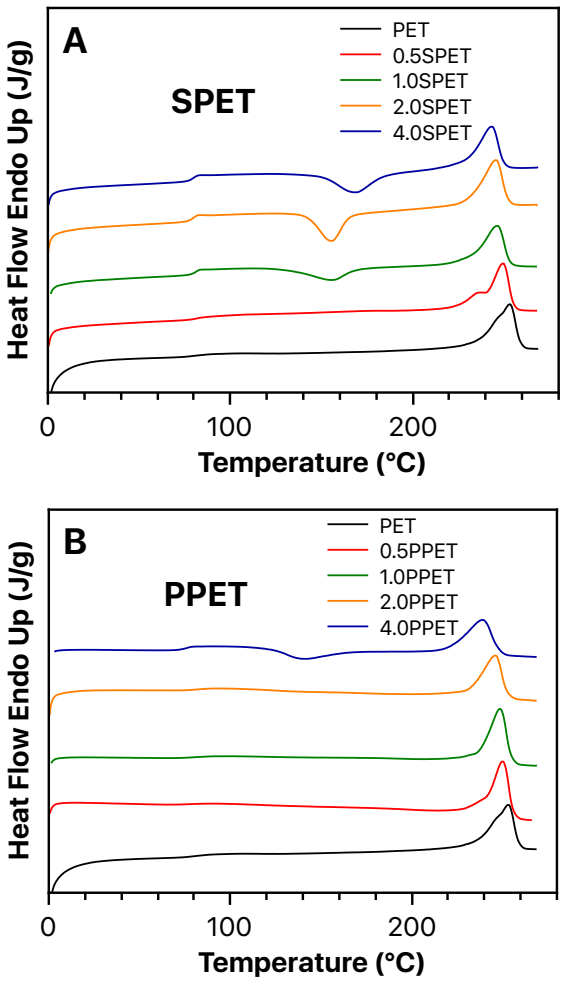

Figure 4.1. DSC heating scans of the (A) SPET and (B) PPET ionomers after rapid cooling from the melt (270 °C) at -60 °C /min. Heating rate: 10 °C/min.

During conditions of slow cooling (-10 °C/min), the crystallization exotherm, T_c, decreases in temperature and intensity with increasing mol% of ionic functionality, which also reflects a reduction in the rate of crystallization (**Figure 4.2**). Upon cooling from the melt, as the polymer chains attempt to pack into crystalline structures, ionic groups act as interactive defects that are rejected from the growing crystalline surface.[11, 13] The electrostatic interactions between the defects restrict mobility during the time scale of the

cooling cycle, which retards the crystallization phenomenon to lower temperatures.[5, 9] Furthermore, our previous work revealed that PPET ionomers lead to a more effective compatibilization in polyester/polyamide blends compared to SPET ionomers at the same mol% of ionic monomer units. This is attributed to the stronger specific interactions generated between the divalent phosphonate ionic groups and the amide linkages of polyamide than that of monovalent sulfonate groups. Thus, compared to the monovalent sulfonate groups, the same amount of divalent phosphonate functionalities is expected to yield stronger electrostatic networks, leading to a higher extent of restricted chain mobility, and thereby a lower crystallization rate for PPET ionomers. Surprisingly, PPET ionomers exhibit a less profound decrease in T_c than the SPET analogues with increasing ionic content. For example, at 4.0 mol% ionic monomer concentration, T_c of SPET decreases to 171 °C from 223 °C (i.e., T_c of pure PET), while 4.0PPET exhibits a much higher T_c (i.e., 182 °C), as shown in **Table 4.1**. This contradicts the expected results that, for the same mol% of ionic monomer, PPET would have a lower T_c than SPET. In agreement with the higher mol% of ionic functionalities whereby a cold crystallization appears for PPET ionomers, this less profound T_c depression for PPET further suggests the stronger crystallizability in comparison to SPET ionomers at the same ionic monomer concentration.

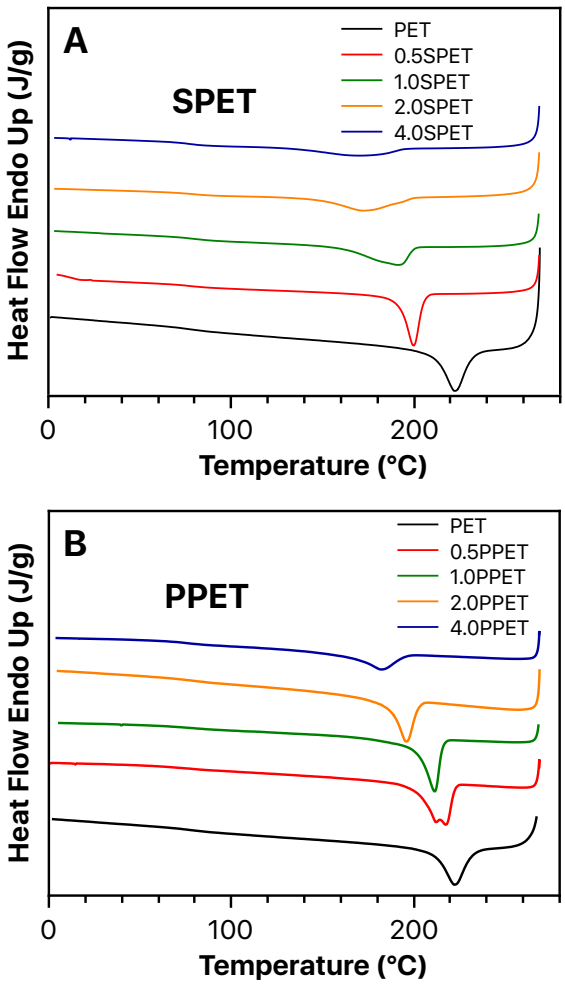

Figure 4.2. DSC slow cooling scans (-10 °C/min) for (A) SPET and (B) PPET ionomers.

Table 4.1. Summary of DSC Results for SPET and PPET Ionomers.

Sample	T_g (°C)	T_{cc} (°C)	H_{cc} (J/g)	T_m (°C)	ΔH_m (J/g)	% crystallinity	T_c (°C)	ΔH_c (J/g)
PET	79	-	-	253	44	31.0	223	50
0.5SPET	81	-	-	250	37	26.4	200	30
1.0SPET	81	155	13	246	33	23.6	191	30
2.0SPET	79	156	22	245	33	23.6	173	24
4.0SPET	80	168	22	243	32	22.9	171	15
0.5PPET	77	-	-	250	42	30.0	213, 218	48
1.0PPET	79	-	-	249	41	29.3	211	43
2.0PPET	76	-	-	246	36	25.7	196	37
4.0PPET	76	140	16	240	34	24.3	182	24

4.4.2 Isothermal Crystallization Kinetics. To further elucidate the effect of sulfonate and phosphonate ionic groups on the crystallizability of PET ionomers, DSC isothermal crystallization experiments were performed over a range of controlled crystallization temperatures below T_m. The crystallization kinetics of SPET and PPET ionomers were evaluated by quantifying the crystallization half-time, $t_{1/2}$, as shown in **Figure 4.3**. In addition, a full Avrami analysis of the results is shown in the **Supporting Information** (**Table S4.1**). Note that $t_{1/2}$ is inversely related to the overall rate of crystallization, such that a higher $t_{1/2}$, corresponds to a slower rate of crystallization. Based on the plot of $t_{1/2}$ versus crystallization temperatures (**Figure 4.3**), it is clear that the crystallization rate observed for neat PET is much higher than that for each PET ionomer, and at the same crystallization temperature, higher ionic contents result in longer $t_{1/2}$, indicative of lower crystallization rate. In addition, as the crystallization temperature increases, the difference of $t_{1/2}$ values between each SPET or PPET composition becomes greater. In this nucleation-controlled crystallization regime, the growth of crystallites is dependent on the ability of the crystallizanle chain segments to establish and grow upon a crystal surface. More importantly, especially for ionomers, the diffusion of chain segments within the melt also plays a significant role due to the presence of electrostatic interactions between the interactive defects that restrict polymer chain mobility through ionic association. Thus, this retarded crystallization kinetics for these PET ionomers are attributed to the combined effect of interactive defects, which slow the crystallization rate by the time required for the rejection of defective stems and the diffusion of the ionomer chain segments in the melt.[5, 9, 11, 12, 33]

Comparing the crystallization kinetics of SPET and PPET ionomers, SPET ionomers crystallize much slower than PPET analogues at the same mol% ionic functionality and crystallization temperature, and the difference becomes even more distinct at higher mol% of ionic functionalities. For example, at 215 °C, the $t_{1/2}$ for 1.0SPET is more than 3 times longer than the $t_{1/2}$ for 1.0PPET (i.e., 1.3 min versus 4.1 min). For 2.0SPET, the $t_{1/2}$ is about 5.3 min, which is more than 17 times longer than that for 2.0PPET (i.e., 0.3 min). As the degree of ionic functionality is increased to 4.0 mol%, the difference between the $t_{1/2}$ of sulfonated and phosphonated PET ionomers are even more pronounced. 4.0PPET is capable of crystallizing rapidly at temperatures from 160 °C to 175 °C ($t_{1/2}$ < 10 min). In contrast, a much longer crystallization time is needed for 4.0SPET ($t_{1/2}$ > 10 min). Consistent with the more profound T_c depression observed for SPET from the non-isothermal cooling scans, it is evident that PPET ionomers containing divalent phosphonate ionic groups display a higher crystallizability as compared to SPET analogues at the same ionic monomer contents.

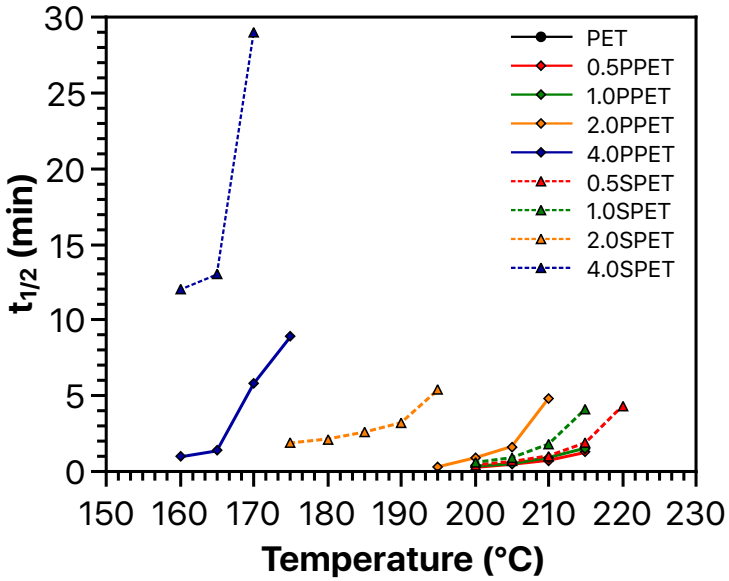

Figure 4.3. Crystallization half-time ($t_{1/2}$) versus temperature profiles for SPET (dash line with triangle symbols) and PPET (solid line with square symbols) ionomers.

Wang and coworkers[34] investigated crystallization behaviors of a segmented poly(ester urethane) ionomer (PESI) containing low ionic contents, i.e., 1 mol% and 3 mol% diethanolamine hydrochloride (DEAH) units. Avrami analysis of PESI indicated that, at the same crystallization temperature, $t_{1/2}$ value highly decreased with increasing mol% of the incorporated DEAH units, indicating an improved crystallizability. Polarized light microscopy was performed to characterize the spherulites growth at the same isothermal crystallization temperature. The results indicated higher mol% of ionic functionalities yielded a higher nucleation density for PESI ionomers, while no significant difference was observed in the crystal growth rates among all the compositions. This finding demonstrated that the increase in bulk crystallization rates of PESI ionomers was attributed to the improved nucleation density, and was independent

of the crystal growth rate. Therefore, in agreement with the higher T_c observed for phosphorus-containing PET ionomers[23, 24] (e.g., derived from monofunctional phosphinate ionic monomers) at low ionic functionalities (< 3 mol%) as compared to near PET, the higher crystallizability for PPET ionomers than that for SPET is presumably due to the higher nucleation density resulted from the phosphonate groups as compared to sulfonate groups. Future work will focus on a systematic study of spherulite growth to probe the in-depth origins of this substantially different crystallizability for these two types of PET ionomers.

4.4.3 Linear Viscoelastic Properties. An in-depth understanding of the viscoelastic behavior for SPET and PPET ionomers is crucial in evaluating their potential applicability in polymer processing field, e.g., melt spinning, injection molding, or extrusion.[35-38] The linear viscoelastic measurements were carried out at different temperatures from 240 °C to 280 °C, above the crystallization temperatures of these polyesters. The normal degradation issue for polyesters at high temperatures and the semi-crystalline morphology of these PET ionomers prohibited a detailed rheological analysis over a wider temperature range (higher than 280 °C or lower than 240 °C). Based on the time-temperature superposition (TTS) principle, the measurements at different temperatures were superposed to the reference temperature of 250 °C by means of horizontal shift factors to produce the master curves. **Figure 4.4** depicts a representative plot of both storage (*G'*) and loss (*G''*) moduli master curves, and viscosity profiles are displayed in **Figure 4.5**. A well-behaved frequency range from 1 to 10^3 rad/s reveals predictable viscoelastic behavior for various processing techniques, such as thermoforming, extrusion, and blow/injection molding.[39-42]

The *G'* and *G''* of SPET and PPET ionomers are compared in **Figure 4.4**. Neat PET and SPET ionomers reach the terminal zone at the low frequency end around 0.1 rad/s with the characteristic slope of *G'* and *G''* to be 2 and 1 (typical for polymer melts), respectively.[2] The TTS was not obeyed in the *G'* for SPET ionomers in the terminal region, suggesting a thermorheological complex as commonly seen in other ionomers.[43-45] This failed superposition for *G'* is attributed to the nanophase separation resulted from the formation of ionic aggregates.[2, 46] The relaxation times for the two phases were so far apart that only one mechanism was accessed in a single experiment.[46] In contrast, PPET ionomers fail to reach terminal behavior even at a lower frequency of 0.01 rad/s, and an remarkable enhancement for PPET ionomers is observed in the magnitude of moduli as compared to SPET analogues. In addition, PPET ionomers exhibit a plateau in *G'*, which is characteristic of the formation of a crosslinked network.[2, 16, 47, 48] With increasing mol% of phosphonated functionalities, the plateau becomes more profound and the plateau moduli increase systematically. Consistent with the theory of rubber elasticity, which states that the plateau modulus is proportional to the cross-link density generated from interchain or intrachain dipole-dipole associations, the increased phosphonation level leads to stronger physical crosslinks, which produces a higher plateau modulus.[16, 47] This significant difference between the moduli of sulfonated and phosphonated PET ionomers suggests that the phosphonate ionic groups are able to generate stronger physical crosslinks than those for sulfonate groups, thus leading to a delayed terminal relaxation to lower frequencies and imparting elastomeric behavior to these PPET ionomers.[46, 49]

A crossover between *G'* and *G''* curves is found for each PPET ionomer. This crossover is characteristic of the reptation time of the associated chain (τ_{rep}).[2] TTS

measurements for SPET ionomers were unable to generate the crossover of *G'* and *G''* due to the crystallization of semi-crystalline polymers at lower temperatures. In this case for the series of SPET ionomers, the crossover frequency was determined by fitting the Maxwell model to the moduli-ω data.[40, 50] **Table 4.2** illustrates the influence of the types of ionic functionality on the crossover frequency and τ_{rep}. According to the Leibler-Rubinstein-Colby (LRC) theory,[51] the τ_{rep} of polymer chains constrained by ionic associations is in proportional to $n^2\tau$, where n is number of ionic groups per chain, and τ is life-time of an ionic association. With increasing ionic content, it is not surprising that the crossover for these two series of PET ionomers shifts to a lower frequency region, and the corresponding τ_{rep} increases. Furthermore, compared to SPET ionomers at the same mol% of ionic functionalities, the crossover frequencies for PPET ionomers are significantly lower than those for SPET ionomers by about 3 orders of magnitudes, and consequently, the τ_{rep} for PPET ionomers were greatly longer than those for SPET analogues. This significantly higher τ_{rep} for PPET ionomers suggests a longer life-time of the ionic association derived from the phosphonate ionic groups, indicating the physical crosslinking network formed by phosphonate ionic groups is more extensive and more persistent in PPET ionomers.

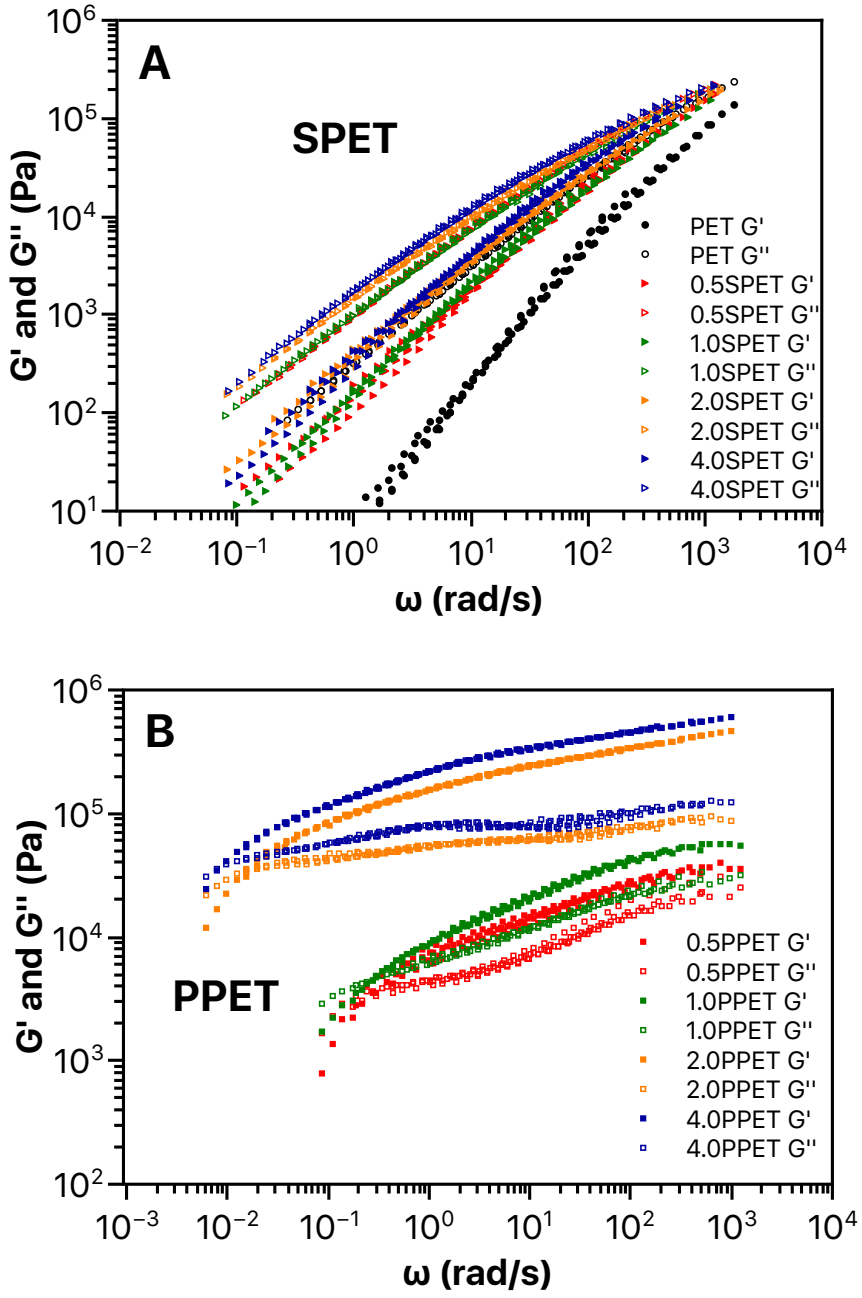

Figure 4.4. Storage and loss moduli master curves for (A) SPET and (B) PPET ionomers at T_r = 250 °C.

Figure 4.5 compares the melt viscosity (η) of sulfonated and phosphonated PET ionomers. Below τ_{rep} frequencies, the η becomes independent of frequency, and the

polymer melt behaves as a Newtonian fluid.[48, 52] Higher frequencies result in shear thinning as the experimental time exceeds the chain reptation relaxation time. The zero-shear viscosity (η_0) and parameter n (representing the degree of shear thinning) were calculated by fitting the η curve with the Careau-Yasuda model,[53] and corresponding values are listed in **Table 4.2**. It is apparent that the ion incorporation dramatically enhances η_0 as compared to pure PET control. The longest relaxation time increases as a consequence of hindered self-diffusion of the chains by ionic associations.[48] It is not surprising that the η_0 of PET ionomers can climb by orders of magnitude upon incorporation only a few mole percent of ionic units. Moreover, PPET ionomers exhibit a higher η_0 than SPET ionomers at the same mol% of ionic monomers. For example, the η_0 values of SPET ionomers are around 10^3 Pa, while the η_0 for PPET ionomers are 2-3 orders of magnitude higher than SPET analogues. Consistent with the higher τ_{rep} for PPET ionomers, the apparently higher η_0 for PPET further imply the stronger ionic associations offered by divalent phosphonate functionalities.

Adding ionic groups to PET decreases the n values, and PPET ionomers exhibit much lower n values as compared to those for SPET at the same mol% of ionic monomer units (**Table 4.2**). For example, the n values for SPET ionomers are around 0.8, while greatly decreased n values around 0.3 are observed for PPET ionomers at 0.5 mol% and 1.0 mol% phosphonation levels and 4.0PPET exhibits the lowest n value (< 0.1). Given that the higher the degree of shear thinning and the smaller the exponent n vaule,[52] this result illustrates that PPET ionomers exhibit a higher degree of shear-thinning than SPET ionomers. Additionally, the onset of shear thinning occurs at lower frequencies in PPET than in SPET, indicating PPET ionomers are more shear sensitive.

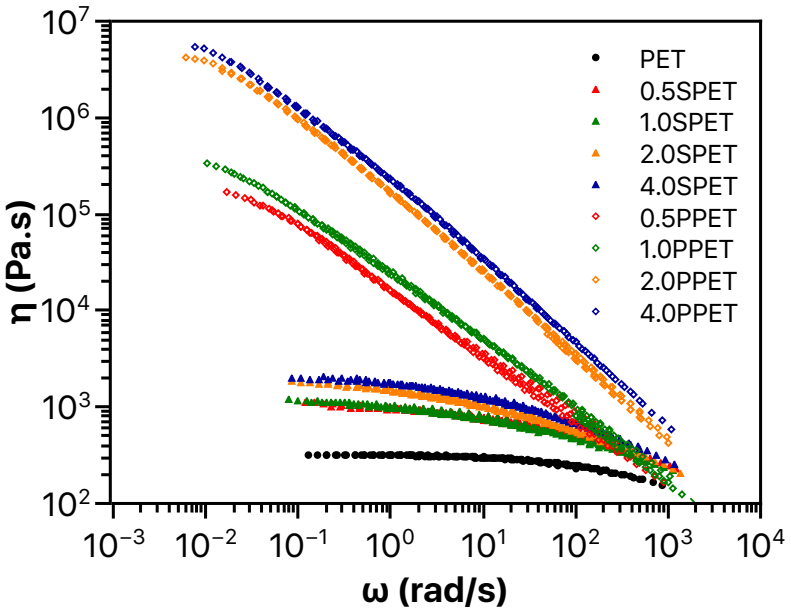

Figure 4.5. Melt viscosity master curves of SPET (triangle symbols) and PPET (square symbols) ionomer at T_r = 250 °C.

Table 4.2. Zero-Shear Viscosity, Parameter n, τ_{rep} Frequency, and τ_{rep} for SPET and PPET Ionomers.

	Log(η_0) (Pa·s)	n	**τ_{rep} Frequency (rad/s)**	**τ_{rep} (s)**
PET	2.70	0.933	2089	0.0030
0.5SPET	3.34	0.864	1819	0.0035
1.0SPET	3.38	0.849	1698	0.0039
2.0SPET	3.64	0.804	1479	0.0042
4.0SPET	3.69	0.791	1288	0.0049
0.5PPET	5.76	0.326	0.318	19.75
1.0PPET	6.22	0.310	0.244	25.79
2.0PPET	7.04	0.153	0.0121	518.58
4.0PPET	7.92	0.0665	0.00963	651.86

4.5 Conclusions

In this work, we investigated the effects of monovalent sulfonate and divalent phosphonate pendant ions on the thermal and linear viscoelastic properties of PET ionomers with small amounts of ionic functionalities (0.5-4.0 mol%). PPET ionomers have been shown to exhibit a higher crystallizability as compared to SPET at the same mol% of ionic monomers. DSC analysis revealed less profound T_c depression for PPET upon slow cooling from the melt state, and crystallization kinetics study indicated a higher crystallization rate for PPET at the same isothermal temperatures as compared to SPET analogues. In addition, PPET displayed a shift of terminal relaxations to lower frequencies, higher zero-shear viscosity, and significantly longer reptation time in comparison to SPET. This confirmed the divalent phosphonate pendant ions generated stronger physical crosslinks than monovalent sulfonate pendant ions. Overall, compared to the SPET ionomers, this study demonstrated the higher crystallizability and stronger physical crosslinks for PPET with the incorporation of small amounts of divalent phosphonate functionalities.

4.6 Acknowledgements

The authors gratefully acknowledge the Institute for Advanced Learning and Research for providing funds (449414) to support the efforts of this project.

4.7 References

1. Lundberg, R. D., Elastomers and fluid applications. In Ionomers: Synthesis, structure, properties and applications, Tant, M. R.; Mauritz, K. A.; Wilkes, G. L., Eds. Springer Netherlands: Dordrecht, 1997; pp 477-501.

2. Tant, M. R.; Mauritz, K. A.; Wilkes, G. L., Ionomers: synthesis, structure, properties and applications. Springer Science & Business Media: 2012.
3. Zhang, L.; Brostowitz, N. R.; Cavicchi, K. A.; Weiss, R., Perspective: Ionomer research and applications. Macromolecular Reaction Engineering 2014, 8 (2), 81-99.
4. Eisenberg, A.; Hird, B.; Moore, R., A new multiplet-cluster model for the morphology of random ionomers. Macromolecules 1990, 23 (18), 4098-4107.
5. Anderson, L. J.; Yuan, X.; Fahs, G. B.; Moore, R. B., Blocky Ionomers via Sulfonation of Poly (ether ether ketone) in the Semicrystalline Gel State. Macromolecules 2018, 51 (16), 6226-6237.
6. Eisenberg, A., Ion-containing polymers: physical properties and structure. Elsevier: 2012; Vol. 2.
7. Fahs, G. B.; Benson, S. D.; Moore, R. B., Blocky sulfonation of syndiotactic polystyrene: a facile route toward tailored ionomer architecture via postpolymerization functionalization in the gel state. Macromolecules 2017, 50 (6), 2387-2396.
8. Huang, C.; Chen, Q.; Weiss, R., Rheological behavior of partially neutralized oligomeric sulfonated polystyrene ionomers. Macromolecules 2016, 50 (1), 424-431.
9. Ju, L.; Pretelt, J.; Chen, T.; Dennis, J. M.; Heifferon, K. V.; Baird, D. G.; Long, T. E.; Moore, R. B., Synthesis and characterization of phosphonated Poly (ethylene terephthalate) ionomers. Polymer 2018, 151, 154-163.
10. Kang, H.; Lin, Q.; Armentrout, R. S.; Long, T. E., Synthesis and characterization of telechelic poly (ethylene terephthalate) sodiosulfonate ionomers. Macromolecules 2002, 35 (23), 8738-8744.
11. Orler, E. B.; Calhoun, B. H.; Moore, R. B., Crystallization kinetics as a probe of the dynamic network in lightly sulfonated syndiotactic polystyrene ionomers. Macromolecules 1996, 29 (18), 5965-5971.
12. Orler, E. B.; Moore, R. B., Influence of ionic interactions on the crystallization of lightly sulfonated syndiotactic polystyrene ionomers. Macromolecules 1994, 27 (17), 4774-4780.
13. Orler, E. B.; Yontz, D. J.; Moore, R. B., Sulfonation of syndiotactic polystyrene for model semicrystalline ionomer investigations. Macromolecules 1993, 26 (19), 5157-5160.
14. Qiao, X.; Wang, X.; Wang, C.; Weiss, R., Effect of zinc stearate on the properties of a sulfonated polystyrene ionomer. Journal of Rheology 2018, 62 (4), 821-830.
15. Tant, M. R.; Wilkes, G. L., An overview of the viscous and viscoelastic behavior of ionomers in bulk and solution. Polymer Reviews 1988, 28 (1), 1-63.
16. Weiss, R.; Yu, W.-C., Viscoelastic behavior of very lightly sulfonated polystyrene ionomers. Macromolecules 2007, 40 (10), 3640-3643.
17. Wu, Q.; Weiss, R., Viscoelastic properties of poly (styrene-co-vinylphosphonate) ionomers. Polymer 2007, 48 (26), 7558-7566.
18. Dolog, R.; Weiss, R., Shape memory behavior of a polyethylene-based carboxylate ionomer. Macromolecules 2013, 46 (19), 7845-7852.

19. Hird, B.; Eisenberg, A., Sizes and stabilities of multiplets and clusters in carboxylated and sulfonated styrene ionomers. Macromolecules 1992, 25 (24), 6466-6474.
20. Lundberg, R.; Makowski, H., A comparison of sulfonate and carboxylate ionomers. ACS Publications: 1980.
21. Nakano, Y.; MacKnight, W. J., Dynamic mechanical properties of perfluorocarboxylate ionomers. Macromolecules 1984, 17 (8), 1585-1591.
22. Rees, R.; Vaughan, D., Physical structure of ionomers. Polymer preprints. American Chemical Society. Division of Polymer Chemistry 1965, 6, 287.
23. Ge, X. G.; Wang, C.; Hu, Z.; Xiang, X.; Wang, J. S.; Wang, D. Y.; Liu, C. P.; Wang, Y. Z., Phosphorus-containing telechelic polyester-based ionomer: Facile synthesis and antidripping effects. Journal of Polymer Science Part A: Polymer Chemistry 2008, 46 (9), 2994-3006.
24. Zhang, Y.; Chen, L.; Zhao, J.-J.; Chen, H.-B.; He, M.-X.; Ni, Y.-P.; Zhai, J.-Q.; Wang, X.-L.; Wang, Y.-Z., A phosphorus-containing PET ionomer: from ionic aggregates to flame retardance and restricted melt-dripping. Polymer Chemistry 2014, 5 (6), 1982-1991.
25. Wu, Q.; Weiss, R., Synthesis and characterization of poly (styrene-co-vinyl phosphonate) ionomers. Journal of Polymer Science Part B: Polymer Physics 2004, 42 (19), 3628-3641.
26. Ju, L.; Dennis, J. M.; Heifferon, K. V.; Long, T. E.; Moore, R. B., Compatibilization of Polyester/Polyamide Blends with a Phosphonated Poly (ethylene terephthalate) Ionomer: Comparison of Monovalent and Divalent Pendant Ions. ACS Applied Polymer Materials 2019, 1 (5), 1071-1080.
27. Wunderlich, B., Thermal analysis of polymeric materials. Springer Science & Business Media: 2005.
28. Avrami, M., Kinetics of phase change. I General theory. The Journal of chemical physics 1939, 7 (12), 1103-1112.
29. Annunziata, L.; Sarazin, Y.; Duc, M.; Carpentier, J. F., Well-defined Syndiotactic Polystyrene-b-Atactic Polystyrene Stereoblock Polymers. Macromolecular rapid communications 2011, 32 (9-10), 751-757.
30. Gao, Y.; Li, H. M., Synthesis and characterization of acetylated syndiotactic polystyrene. Polymer international 2004, 53 (10), 1436-1441.
31. Noble, K. F.; Noble, A. M.; Talley, S. J.; Moore, R. B., Blocky bromination of syndiotactic polystyrene via post-polymerization functionalization in the heterogeneous gel state. Polymer Chemistry 2018, 9 (41), 5095-5106.
32. Shin, J.; Chang, Y.; Nguyen, T. L. T.; Noh, S. K.; Bae, C., Hydrophilic functionalization of syndiotactic polystyrene via a combination of electrophilic bromination and Suzuki–Miyaura reaction. Journal of Polymer Science Part A: Polymer Chemistry 2010, 48 (19), 4335-4343.
33. Flory, P. J., Thermodynamics of Crystallization in High Polymers II. Simplified Derivation of Melting-Point Relationships. The Journal of Chemical Physics 1947, 15 (9), 684-684.
34. Zeng, J.-B.; Wu, F.; Huang, C.-L.; He, Y.-S.; Wang, Y.-Z., Urethane ionic groups induced rapid crystallization of biodegradable poly (ethylene succinate). ACS Macro Letters 2012, 1 (8), 965-968.

35. Dennis, J. M.; Enokida, J. S.; Long, T. E., Synthesis and characterization of decahydronaphthalene-containing polyesters. Macromolecules 2015, 48 (24), 8733-8737.
36. Mondschein, R. J.; Dennis, J. M.; Liu, H.; Ramakrishnan, R. K.; Nazarenko, S.; Turner, S. R.; Long, T. E., Synthesis and characterization of amorphous bibenzoate (co) polyesters: permeability and rheological performance. Macromolecules 2017, 50 (19), 7603-7610.
37. Pang, K.; Kotek, R.; Tonelli, A., Review of conventional and novel polymerization processes for polyesters. Progress in polymer science 2006, 31 (11), 1009-1037.
38. Scheirs, J.; Long, T. E., Modern polyesters: chemistry and technology of polyesters and copolyesters. John Wiley & Sons: 2005.
39. Franck, A., Understanding rheology of thermoplastic polymers. TA Instruments 2004, 118, 1-8.
40. Baird, D. G.; Collias, D. I., Polymer processing: principles and design. John Wiley & Sons: 2014.
41. Blizard, K. G.; Baird, D. G., The morphology and rheology of polymer blends containing a liquid crystalline copolyester. Polymer Engineering & Science 1987, 27 (9), 653-662.
42. Gotsis, A. D.; Baird, D. G., Rheological properties of liquid crystalline copolyester melts. II. Comparison of capillary and rotary rheometer results. Journal of Rheology 1985, 29 (5), 539-556.
43. Noroozi, N.; Thomson, J. A.; Noroozi, N.; Schafer, L. L.; Hatzikiriakos, S. G., Viscoelastic behaviour and flow instabilities of biodegradable poly (ε-caprolactone) polyesters. Rheologica acta 2012, 51 (2), 179-192.
44. Xiang, P.; Ye, Z., Hyperbranched polyethylene ionomers containing cationic tetralkylammonium ions synthesized by Pd–diimine-catalyzed direct ethylene copolymerization with ionic liquid comonomers. Macromolecules 2015, 48 (17), 6096-6107.
45. Zhang, Z.; Chen, Q.; Colby, R. H., Dynamics of associative polymers. Soft Matter 2018, 14 (16), 2961-2977.
46. Weiss, R.; Zhao, H., Rheological behavior of oligomeric ionomers. Journal of Rheology 2009, 53 (1), 191-213.
47. Weiss, R.; Fitzgerald, J.; Kim, D., Viscoelastic behavior of lightly sulfonated polystyrene ionomers. Macromolecules 1991, 24 (5), 1071-1076.
48. Register, R. A.; Prud'homme, R. K., Melt rheology. In Ionomers: Synthesis, structure, properties and applications, Tant, M. R.; Mauritz, K. A.; Wilkes, G. L., Eds. Springer Netherlands: Dordrecht, 1997; pp 208-260.
49. Ling, G. H.; Wang, Y.; Weiss, R., Linear viscoelastic and uniaxial extensional rheology of alkali metal neutralized sulfonated oligostyrene ionomer melts. Macromolecules 2011, 45 (1), 481-490.
50. Ferry, J. D., Viscoelastic properties of polymers. John Wiley & Sons: 1980.
51. Leibler, L.; Rubinstein, M.; Colby, R. H., Dynamics of reversible networks. Macromolecules 1991, 24 (16), 4701-4707.
52. Dealy, J. M.; Wissbrun, K. F., Melt rheology and its role in plastics processing: theory and applications. Springer Science & Business Media: 2012.

53. Bird, R. B.; Armstrong, R. C.; Hassager, O., Dynamics of polymeric liquids. Vol. 1: Fluid mechanics. 1987.

4.8 Supporting Information

Table S4.1. Kinetic Parameters Determined from the Avrami Analysis of PPET and SPET Ionomers.

PPET Kinetic Parameter				
0.5 mol% PPET	200 °C	205 °C	210 °C	215 °C
$t_{1/2}$ (min)	0.27	0.47	0.74	1.26
n	2.29	2.47	2.57	2.85
K (min^{-1})	13.84	4.33	1.49	0.35
1.0 mol% PPET	200 °C	205 °C	210 °C	215 °C
$t_{1/2}$ (min)	0.36	0.51	0.93	1.67
n	2.54	2.28	2.19	2.60
K (min^{-1})	9.65	3.17	0.81	0.18
2.0 mol% PPET	195 °C	200 °C	205 °C	210 °C
$t_{1/2}$ (min)	0.31	0.93	1.65	4.93
n	2.36	2.09	2.21	2.34
K (min^{-1})	10.83	0.81	0.23	0.017
4.0 mol% PPET	160 °C	165 °C	170 °C	175 °C
$t_{1/2}$ (min)	0.96	1.36	5.81	8.92
n	2.41	2.24	1.95	2.47
K (min^{-1})	0.76	0.34	0.023	0.0031
SPET Kinetic Parameter				
0.5 mol% SPET	200 °C	205 °C	210 °C	215 °C
$t_{1/2}$ (min)	0.44	0.66	1.01	1.90
n	2.32	2.18	2.83	2.02
K (min^{-1})	4.56	1.75	0.63	0.19
1.0 mol% SPET	200 °C	205 °C	210 °C	215 °C
$t_{1/2}$ (min)	0.60	0.91	1.81	4.13
n	1.96	1.98	2.35	1.83
K (min^{-1})	1.80	0.34	0.17	0.079
2.0 mol% SPET	175 °C	180 °C	185 °C	190 °C
$t_{1/2}$ (min)	1.89	2.15	2.60	3.22
n	2.46	2.50	1.98	2.56
K (min^{-1})	0.15	0.10	0.96	0.043
4.0 mol% SPET	160 °C	165 °C	170 °C	
$t_{1/2}$ (min)	12.23	13.48	28.86	
n	2.45	2.16	1.92	
K (min^{-1})	0.0014	0.0025	0.00096	

Chapter 5. Influence of Sulfonate and Phosphonate Pendant Ions on Morphological and Rheological Properties of Polystyrene Ionomers

(Manuscript in Preparation)

Lin Ju,[a,c] Tianran Chen,[b,c] Glenn A. Spiering,[a,c] Donald G. Baird,[b,c] and Robert B. Moore [a,c,*]

[a]Department of Chemistry, Virginia Polytechnic Institute and State University, Blacksburg, VA 24061, United States

[b]Department of Chemical Engineering, Virginia Polytechnic Institute and State University, Blacksburg, VA 24060, United States

[c]Macromolecules Innovation Institute, Virginia Polytechnic Institute and State University, Blacksburg, VA 24061, United States

5.1 Abstract

The effects of monovalent sulfonated and divalent phosphonated pendant ions on the thermal, morphological, and linear viscoelastic behaviors of atactic polystyrene ionomers were investigated in this work. The glass transitions were examined using differential scanning calorimetry (DSC), and phosphonated polystyrene (PPS) ionomers exhibited significantly higher glass transition temperatures (T_g) than sulfonated analogues. Small angle X-ray scattering (SAXS) and solid-state ^{23}Na NMR provided insight into the microphase-separated morphology, and the results indicated the divalent phosphonate pendant ions formed larger ionic aggregates with higher charge density in PPS ionomers as compared to SPS ionomers at the same ionic monomer content. In

addition, oligomeric SPS and PPS ionomers with no chain entanglements (molecular weight below chain entangle molecular weight of polystyrene) were synthesized in order to evaluate the effects of ionic associations on the dynamic melt rheology of PS ionomers. At the same mol% of ionic monomers, PPS ionomers exhibited wider frequency range of the plateau in storage modulus (*G'*), longer terminal relaxation time, and higher zero-shear viscosity compared to SPS analogues. These analyses demonstrated the divalent phosphonate pendant ions generated stronger ionic associations, thus providing a stronger physically crosslinked network in PPS ionomers compared to the monovalent sulfonate groups in SPS ionomers.

5.2 Introduction

Ionomers are charged polymers that contain minor amounts (typically < 15 mol%) of covalently attached ionic functionalities incorporated into or pendant to the polymer backbones.[1-3] Due to the attractive Coulombic interactions between the ionic-pairs, the polar ionic groups, surrounded by a less polar matrix, tend to form nanometer-sized ionic aggregates.[4] These aggregates, acting as physical crosslinks, decrease the mobility of polymer chains, consequently providing a profound effect on the thermal, morphological, and rheological properties of polymers. [3, 5-14]

Ionomers containing anionic pendant ions are usually called anionic ionomers.[2] The type of anionic pendant ions plays an important role on the physical properties of ionomers. Ionomers bearing carboxylate and sulfonate pendant ions are the most widely studied ionomers in the literatures.[3, 4, 8, 11, 12, 15-20] Polymers modified with sulfonate pendant ions exhibited more profound effects in the thermal, viscoelastic, rheological

properties than those bearing carboxylate groups.[16, 17, 21] For example, Lundberg and Makowski[17] compared carboxylated and sulfonated polystyrene ionomers containing 0.3-5.0 mol% ionic functionalities, and found that sulfonated polystyrene (SPS) ionomers exhibited higher glass transition temperatures and higher melt viscosities than those of the carboxylated analogues. Winey and coworkers[21] studied the microphase-separated morphology of SPS ionomers in the Cu^{2+} form and a poly(styrene-*co*-methacrylate) (P(S-MAA)) ionomers with carboxylate pendant ions in the same cation form using small angle X-ray scattering (SAXS). Sulfonated polystyrene ionomers possess stronger ionic aggregates as compared to P(S-MAA) with carboxylates due to a higher fraction of ionic species in the aggregates generated from the sulfonate groups.

Despite of the widely studied ionomers with monovalent pendant ions, relatively fewer reports have focused on ionomers with divalent phosphonate pendant ions. Recently, we evaluated the compatibilization effects of sulfonated and phosphonated poly(ethylene terephthalate) (SPET and PPET) ionomers on the phase behavior of amorphous polyester/poly(*m*-xylylene adipamide) (PETG/MXD6) blends.[22] PPET ionomer-compatibilized PETG/MXD6 blends required 6 times fewer ionic monomers to achieve phase-separated domain dimension less than 1 μm as compared to PETG/MXD6 blends containing SPET ionomers. This finding demonstrated the divalent phosphonate pendant ions was able to generate stronger specific interactions per functional monomer unit, thereby more effective at compatibilizing PETG/MXD6 blends in comparison to the monovalent sulfonate pendant ions. Furthermore, Weiss and coworkers[8, 23] investigated the viscoelastic properties of poly(styrene-*co*-vinylphosphonate) (SVP) ionomers in comparison to sulfonated polystyrene ionomers. Although phosphonic acid (pK_{a1} ~ 2-3;

pK_{a2} ~7) is a weaker acid than sulfonic acid (pK_a ~ 1), the strength and persistence of the physical crosslinks in SVP ionomers produced by the phosphonate ionic groups were greater than those for SPS ionomers as indicated by the higher extent of the rubbery plateau region and higher plateau moduli. However, this conclusion was restricted to the different polymer backbones for these two two types of ionomers. For SVP ionomers, the phosphonate groups were attached directly to an aliphatic part of the polymer chains, while the sulfonate functionalities were attached to aromatic monomer units (styrene). The evaluation of the effects of monovalent sulfonate and divalent phosphonate groups on the properties of ionomers bearing the same polymer backbones have not been reported yet.

In this work, we report the first, systematic investigation of monovalent sulfonate and divalent phosphonate pendant ions on the thermal, morphological, and rheological behaviors of atactic polystyrene ionomers. Both sulfonated and phosphonated polystyrene (SPS and PPS) ionomers in Na^+-form were obtained by radical polymerization to generate the copolymers in the ester form and the conversion of the ester form to the Na^+ form. Differential scanning calorimetry (DSC) was used to probe the glass transitions of these ionomers. Small angle X-ray scattering (SAXS) and solid-state ^{23}Na NMR were performed to evaluate the microphase-separated morphology. Oligomeric polystyrene ionomers with no chain entanglements were synthesized and utilized to study the influence of ionic associations on linear viscoelastic behaviors of polystyrene ionomers.

5.3 Experimental Section

Materials. 4-Styrenesulfonic acid sodium salt hydrate, silver nitrate ($AgNO_3$, ≥ 99.0%), bromoethane (EtBr, ≥ 99%), 4-vinylphenylboronic acid (≥ 95%), diethyl phosphite (98%), copper(I) oxide (Cu_2O, ≥ 99.99%), 1,10-phenanthroline (≥ 99%), triethylamine (Et_3N, ≥ 99%), and dimethylacetamide (DMAc, anhydrous, 99.8%) were purchased from Sigma-Aldrich, and were used as received. Sodium methoxide (NaOMe, anhydrous powder, ≥ 97%) was purchased from Acros Organics, and was used as received. 2,2'-azobis(2-methylpropionitrile) (AIBN, 98%) was purchased from Sigma-Aldrich, and was recrystallized from ethanol at 50 °C prior to use. Styrene (≥ 99%) was purchased from Sigma-Aldrich, and was passed through a neutral alumina column prior to use.

Synthesis of Sulfonated and Phosphonated Monomers in the Ester Form. Ethyl 4-vinylbenzenesulfonate monomers were synthesized by the procedure as described in the literature.[24] Diethyl 4-vinylbenzenephosphonate monomers were synthesized by copper-catalyzed cross-coupling of H-phosphonate diester (diethyl phosphite) with arylboronic acid (4-vinylphenylboronic acid) by the procedure as reported in the literature.[25] Both sulfonated and phosphonated monomers were purified by column chromatography on silica gel 300-400 mesh. Structure and purity of the obtained monomers were confirmed using NMR spectroscopy based on the literature. The resulting monomers were dried under vacuum at room temperature for about 5 h prior to use.

Synthesis of Sulfonated and Phosphonated Polystyrene Copolymers in the Ester Form. Sulfonated and phosphonated polystyrene copolymers in the ester form, i.e., poly(styrene-*co*-ethyl 4-styrenesulfonate) and poly(styrene-*co*-diethyl 4-

styrenephosphonate), were prepared by free-radical polymerization of styrene and functionalized monomers in DMAc at 60 °C using AIBN as an initiator. The concentration of monomers was 60% w/v in DMAc. The reaction mixture was bubbled using Argon for about 30 min prior to the start of the reaction. The reaction was quenched after 24 h by precipitating into methanol, and the resulted white products were then dried in a vacuum oven at 40 °C for 8 h prior to the next step.

Two types of polystyrene copolymers were prepared with M_n around 100K g/mol and 8K-9K g/mol, respectively. Polystyrene copolymers with M_n ~ 100K g/mol were obtained by applying 0.01 mol% AIBN to the moles of monomers, and 3 mol% AIBN was utilized to generate the oligomeric polystyrene copolymer with M_n ~ 8K-9K g/mol g/mol. Three compositions with functionalized monomer units from 3 mol% to 9 mol% (**Table 5.1**) were synthesized for polystyrene copolymers with M_n ~ 100K g/mol, and the composition was confirmed by using ^{1}H NMR ($CDCl_3$, ambient conditions, 400 Hz) based on the integration of protons on the functionalized aromatic rings and the integration of $–CH_2-$ protons on the ethyl groups of ethyl sulfonate or diethyl phosphonate. For oligomeric polystyrene copolymers, three compositions with low ionic contents, from 0.5 mol% to 1.5 mol%, were synthesized (**Table S5.1**). Control samples of pure polystyrene with M_n = 105K and 8.8K g/mol were prepared using the same procedure.

Table 5.1. Summary of Compositional and SEC Analysis of Sulfonated and Phosphonated Polystyrene Copolymers (M_n ~ 100K g/mol) in the Ester Form.

Sample	Functionalized Styrene : Styrene (mol%)		M_n (g/mol)	Đ	M_w (g/mol)
	feed (x:y)	obsd ^{1}H NMR			
PS	0:100	0:100	105000	1.50	157500
3SPS	3:97	3:97	100300	1.46	146400
5SPS	6:94	5:95	100300	1.51	151500
9SPS	9:91	8:92	100100	1.47	147100
3PPS	3:97	3:97	100400	1.46	146600
6PPS	6:94	6:94	100100	1.48	148100
9PPS	9:91	9:91	104900	1.48	155300

Size Exclusion Chromatography (SEC). The synthesized polystyrene copolymers in the ester form were analyzed by size exclusion chromatography to determine molecular weight. SEC was carried out in tetrahydrofuran (THF) at 1 mL/min at 30 °C on two Agilent PLgel 10 μm MIXED-B columns connected in series with a Wyatt Dawn Heleos 2 light scattering detector and a Wyatt Optilab Rex refractive index detector. No calibration standards were used, and the literature value of 0.185 for d*n*/dc of polystyrene was used.[26] M_n, M_w and the polydispersity index (Đ) for these samples were listed in **Table 5.1** (M_n ~ 100K g/mol) and **Table S5.1** (M_n ~ 8K-9K g/mol).

Conversion of the Ester Form of Sulfonated and Phosphonated Polystyrene Copolymers to the Na^+ Form. The Na^+ form of sulfonated and phosphonated polystyrene ionomers were achieved by reacting the ester groups with NaOMe. Sulfonated and phosphonated polystyrene copolymers in the ester form were dissolved in a solution mixture of toluene/methanol (9:1 v/v). 1 eq of NaOMe to the moles of ester groups were added to the polystyrene copolymer solution, and the generated mixture was

allowed to stir at 80 °C for about 24 h until all ester groups were converted to the Na^+ form. ^1H NMR was utilized to confirm the conversion of the reaction, and a 100% conversion was evidenced by the disappearance of the ethyl groups in ^1H NMR spectrum.

Preparation of Polystyrene Ionomer Samples for Properties Characterization. Polystyrene ionomers with M_n ~ 100K g/mol were obtained in the film form by casting the above solution mixture onto Kapton® film at room temperature using a doctor blade set to 0.075 inch. The wet films were allowed to first dry at room temperature for 24 h and then at 80 °C for 12 h. The generated films were used for thermal and morphological analysis. It is important to note that these films are brittle due to the relatively low molecular weight.

Polystyrene ionomers with M_n ~ 8K-9K g/mol were obtained as white products by precipitating the solution mixture into methanol. The collected white products were dried in vacuum at 50 °C for 24 h. The film samples were obtained by melting the white products under vacuum at 170 °C for 2 h, and were utilized for melt rheology characterization.

Differential Scanning Calorimetry (DSC). Film samples (M_n ~ 100K g/mol) after vacuum drying were utilized for DSC measurement. A TA instruments Q2000 differential scanning calorimetry (DSC) was used to determine the glass transitions of these polystyrene ionomers along with neat polystyrene. Under a nitrogen atmosphere, the samples (~ 5-8 mg) prepared in aluminum Tzero pans were heated from ambient temperature to 200 °C at 10 °C/min, quench cooled to 0 °C at -60 °C/min, and then reheated from 0 °C to 200 °C at 10 °C/min. The glass transition temperature (T_g) was

determined from the second heating scan after erasing the thermal history by using the TA Instruments Universal Analysis software.

Solid-State ^{23}Na NMR. Polystyrene ionomers with M_n ~ 100K g/mol were grinded into fined powders and the resulting powders were then dried in vacuum at 40 °C for 24 h prior to solid state ^{23}Na NMR characterization. Room temperature solid-state ^{23}Na NMR experiments were acquired at a Larmor frequency of 79.38 MHz on a Bruker Avance III wide bore 300-MHz spectrometer. A standard 4-mm Bruker triple-resonance MAS probe was used to collect all spectra with a magic angle spinning frequency of 6.5 KHz. Spectra were referenced to NaCl (crystalline solid) at a chemical shift of 7.1 ppm. Samples were run using single pulse direct excitation with no decoupling using a 90 degree pulse width (2.4 us) and a 50 us delay (d1) averaging 16K scans.

Rheological Analysis. Polystyrene ionomers with M_n ~ 8K-9K g/mol were utilized for melt rheology characterization. An ARES-G2 Rheometer from TA instruments was used to measure the melt rheological properties of all samples utilizing 25 mm parallel plates. A dry nitrogen atmosphere in the oven was utilized to prevent the samples from absorbing ambient moisture. Strain sweeps were conducted to confirm the linear viscoelastic (LVE) region, i.e., 0.1%-25% oscillatory strain. Dynamic frequency sweeps (0.1-200 rad/s) and temperature step (10 °C/step) were performed over a temperature range of 130-250 °C using a 1 % oscillatory strain within the LVE region to provide storage and loss moduli and viscosity responses over a wide range of frequency. Time-temperature superposition (TTS) master curves for each sample were constructed at the same reference temperature (T_r = 150 °C) using the TA Instruments TRIOS software.

5.4 Results and Discussion

5.4.1 Thermal Properties. DSC was performed on the sulfonated and phosphonated PS ionomers to determine the influence of pendant ions on thermal transitions. **Figure S5.1** displays the second heating thermograms after removal of thermal history, and the corresponding glass transition temperatures (T_g) are summarized in **Table S5.2**. Pure PS exhibits a T_g of 108 °C, which is lower than all PS ionomers. With increasing ionic content, an increased T_g is observed for both SPS and PPS ionomers. In addition, all ionomers exhibit broader glass transitions as compared to pure PS. The higher T_g and broader glass transitions, as commonly seen in other ionomers,[8-10, 12, 20] are attributed to a reduction in chain mobility from the physical crosslinks formed by the dipole-dipole interactions between ion pairs. **Figure 5.1** shows the comparison of T_g between SPS and PPS ionomers with respects to ionic monomer content. At low ionic content, i.e., 3 mol%, both SPS and PPS exhibit similar T_g. When the ionic monomer concentration increases to 6 mol% and 9 mol%, it is evident that the T_g of PPS ionomers are higher than SPS analogues, and the glass transitions are much broader. This significantly higher T_g suggests the divalent phosphonate pendant ions are capable of generating a stronger electrostatically-crosslinked network as compared to the monovalent sulfonate groups, thus leading to a more profound effect on the glass transitions of PPS ionomer.

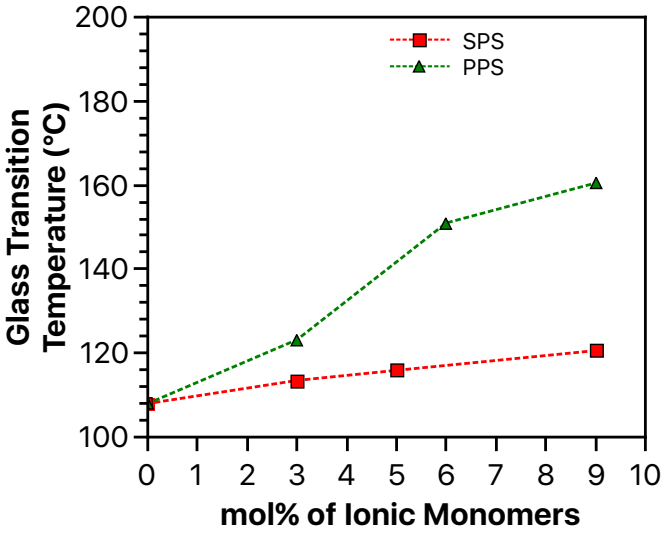

Figure 5.1. Glass transition temperature versus mol% of ionic monomers of sulfonated (red square symbols connected with red dash line) and phosphonated (green triangle symbols connected with green dash line) PS ionomers (M_n ~ 100K g/mol).

5.4.2 Small Angle X-ray Scattering (SAXS) Analysis. Morphological characterization of sulfonated and phosphonated PS ionomers was performed using SAXS as shown in **Figure 5.2**. SAXS experiments were conducted on the dried, as-cast films. The SAXS profiles of PS ionomers exhibit distinct ionic peaks with the position of peak maximum (q_{max}) from 1 nm^{-1} to 2 nm^{-1}. The presence of this ionic peak is characteristic of many ionomers containing multiplets,[13, 27-32] indicating that the strong Coulombic interactions between the ionic groups yield aggregates, as commonly seen in other ionomers.[13] To further elucidate the morphological features of the ionic domains, the SAXS curves were fit using a liquid-like hard sphere model according to Kinning and Thomas.[33] These fits provided quantitative insight concerning the center-to-center distance between ionic domains and the size of ionic aggregates. The liquid-like hard sphere model describes collections of aggregates with respect to three principle spatial

parameters: the radius of the spherical aggregate (R_1), the radius of closet approach (R_{ca}), and the average center-to-center aggregate separation ($2R_{is}$). The fitting data are summarized in **Table 5.2**.

As the ionic monomer concentration increases from 3 mol% to 9 mol%, the q_{max}-value for either SPS ionomers or PPS ionomers increases and the ionic peaks become sharper The fitting data for these PS ionomers indicate that both aggregate size R_1 and average interpartical separation R_{is} decrease with increasing ion content, consistent with the observed ionic peak shift to higher q_{max}-value. These observations suggest that PS ionomers tend to form a larger number of smaller aggregates that are closer together with higher ionic content. In addition, 9 mol% phosphonated PS ionomer exhibits a slightly increased R_1 as compared to the composition containing 6 mol% phosphonated ionic monomers. This phenomenon is attributed to the fact that more phosphonate ions are associated in one aggregate as a result of higher ionic content.[34]

PPS ionomers with divalent phosphonate pendant ions exhibit significant higher q_{max} values in comparison to SPS ionomers containing monovalent sulfonate pendant ions. This observation is consistent with the fitting data showing larger aggregate size (R_1) and significantly shorter average interaggregate separation (R_{is}) for PPS compared to SPS analogues. The comparison between SPS and PPS ionomers reveals that the divalent phosphonate ionic groups tend to form larger aggregates in PPS ionomers, which is possibly due to the larger size of the phosphonate pendant ions.[34] Given the higher T_g observed from thermal analysis and the significantly higher zero viscosity and longer terminal relaxation time from melt rheology study for PPS (will be discussed below), it is reasonably to postulate that the larger aggregates generated from associated phosphonate

pendant ions imparts a stronger physically crosslinked network in PPS ionomers as compared to SPS. In addition, the scattering peaks for PPS ionomers are sharper than SPS analogues at the ionic monomer content and exhibit higher intensity, indicating a more profound microphase separation.[30, 35]

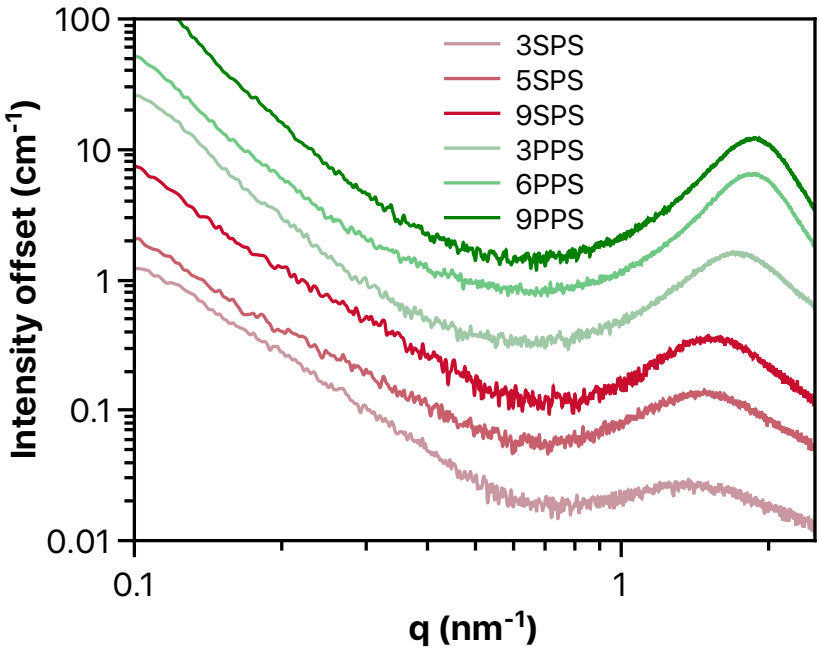

Figure 5.2. SAXS profiles of dried, as-cast films of the SPS and PPS ionomers (M_n ~ 100K g/mol). Scattering profiles have been vertically shifted for ease of viewing.

Table 5.2. Fitting Parameters from the Kinning and Thomas Model for SAXS Profiles of SPS and PPS Ionomers (M_n ~ 100K g/mol).[a]

Sample	R_1 (nm)	R_{ca} (nm)	R_{is} (nm)
3SPS	0.76 ± 0.06	1.92 ± 0.06	6.94 ± 0.58
5SPS	0.7 ± 0.2	1.94 ± 0.02	3.50 ± 0.09
9SPS	0.5 ± 0.1	1.910 ± 0.005	3.24 ± 0.04
3PPS	0.94 ± 0.03	1.730 ± 0.005	2.68 ± 0.01
6PPS	0.905 ± 0.009	1.660 ± 0.001	2.441 ± 0.003
9PPS	0.98 ± 0.01	1.640 ± 0.002	2.412 ± 0.004

[a]R_1 represents the radius of the spherical aggregate, R_{ca} represents the radius of closest approach, and $2R_{is}$ pertains to the average center-to-center aggregate separation.

5.4.3 Solid-State ^{23}Na NMR. Solid-state ^{23}Na NMR was performed at room temperature to further investigate the influence of sulfonate and phosphonate pendant ions on the morphology of polystyrene ionomers. The corresponding NMR spectra are displayed in **Figure 5.3**. A broad peak at -10 ppm to -20 ppm is observed for all samples, and is attributed to the sodium in aggregates.[36] For both SPS and PPS ionomers, the peak of aggregated sodium ions becomes sharper and shifts gradually upfield with increasing ionic content, attributed to a higher value of the quadrupolar coupling constant (QCC).[36] Note that the QCC is related to the environment surrounding the sodium ion, e.g., the symmetry of the site, the number of atoms surrounding the sodium ion, and the distances between the sodium ions and the surrounding atoms.[36] The increased QCC is possibly attributed to an increased number of ions held in the aggregate, closer packing between atoms, less symmetrical packing of atoms, or a combination of these factors.[36] Thus, an upfield shift is observe with adding more sodium ions.

The peak at about 3 ppm for 3SPS and 9SPS is assigned to the isolated sodium ions dispersed throughout the polymer matrix,[36] and 5SPS exhibits a peak at 0 ppm, which corresponds to hydrated sodium ions in a symmetric tetrahedral environment when surrounded by water molecules as $Na(H_2O)_4^+$.[36-38] As the sulfonation level increases, fewer isolated ions are present. This is possibly due to the decreased distance between sulfonate groups at higher ionization levels, which is consistent with the more profound microphase-separated morphology at higher ionic contents as observed from SAXS characterization. In contrast, for the NMR spectra of PPS ionomers, no isolated ion peaks are observed in any composition. It should be noted that an aggregated sodium ion, as recognized by NMR, is any sodium ion that is not completely isolated from other sodium ions on the NMR length scale of ~ 10 Å.[36] The two sodium ions on a phosphonate group is close enough to each other, leading to an absence of isolated ion peak.

PPS ionomers exhibit an upfield shift for the peak of aggregated sodium ions at all ionic monomer contents as compared to SPS analogues. Despite of the higher charge density for phosphonate pendant ions than that for sulfonate groups, the significant shift to upfield is possibly attributed to a closer packing in the aggregates with associated phosphonate ionic groups.[30, 35, 36] In agreement with the SAXS results showing a more profound microphase separation for PPS ionomers, the NMR results here suggests ionic aggregates with higher charge density are achieved in PPS containing phosphonate ionic groups compared to SPS.

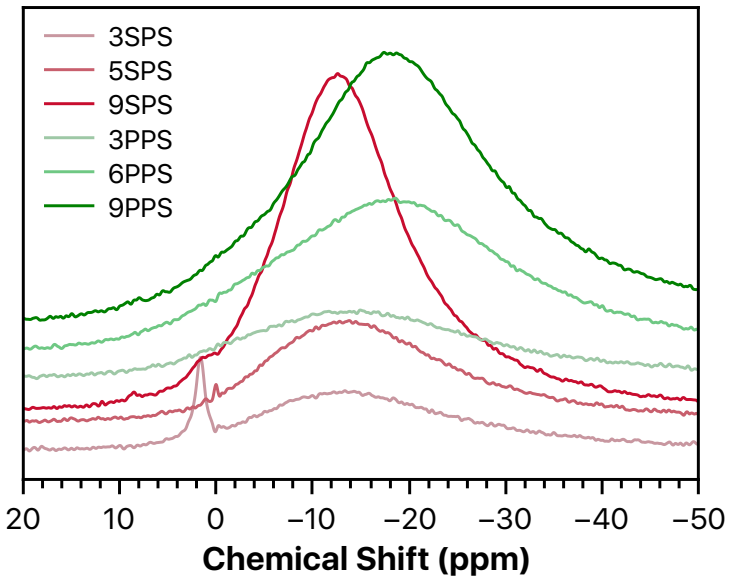

Figure 5.3. Solid-state ^{23}Na NMR spectra of SPS and PPS ionomers (M_n ~ 100K g/mol). Scattering profiles have been vertically shifted for ease of viewing.

5.4.4 Dynamic Melt Rheology. For random sulfonated polystyrene oligomer, the entangle molecular weight (MW), M_e, is 17000 g/mol.[5, 39, 40] Thus, for those PS ionomers studied above, the ionomer chains are highly entangled. One complication with studying entangled ionomers is the difficulty in separating the effects of entanglements, especially trapped entanglements, and the supramolecular ionic associations on the dynamics. This problem may be resolved by studying oligomeric ionomer with no chain entanglements.[5, 39, 40] In this section, oligomeric SPS and PPS ionomers (similar M_n ~ 8K-9K g/mol) with ionic content at 0.5 mol% - 1.5 mol% were synthesized in order to evaluate the effect of monovalent sulfonate and divalent phosphonate pendant ions on the rheological behaviors of oligomeric polystyrene ionomers. The linear viscoelastic measurements were carried out at different temperatures from 130 °C to 250 °C, and were superposed to the reference temperature (T_r) of 150 °C by means of horizontal shift factors to produce

the master curves based on the time-temperature superposition (TTS) principle. **Figure 5.4** depicts a representative plot of both storage (*G'*) and loss (*G''*) moduli master curves, and viscosity profiles are displayed in **Figure 5.5**.

Pure PS and all SPS ionomers exhibit terminal behavior as evidenced by $G'(\omega) \sim \omega^2$ and $G''(\omega) \sim \omega$ at lower frequencies. The experimental data of 0.5 mol% PPS ionomer fail to present the terminal flow due to the degradation issue at temperatures higher than the highest test temperature of 250 °C. The terminal flow region of 0.5PPS at low frequencies (lower than 0.000456 rad/s) was confirmed by fitting the Maxwell model[41, 42] to the moduli-ω data. For pure PS, *G'* and *G''* indicate Rouse-like behavior, where $G'(\omega) \sim G''(\omega) \sim \omega^{1/2}$ prior to the terminal relaxation. No plateau in the storage modulus is observed, indicating unentangled network. Increasing the mol% of sulfonate pendant ions to 0.5 mol% delays the terminal relaxation and expand the Rouse region to lower frequencies due to the stronger ionic associations as a consequence of higher ionic content. Further increasing the mol% sulfonate groups to 1.0 mol% leads to an apparent plateau in *G'*, and the plateau becomes more profound with increasing mol% of sulfonate groups to 1.5 mol%. In addition, the terminal relaxation shifts to lower frequencies and the terminal relaxation time (τ) becomes longer (**Table 5.3**) upon increasing mol% of sulfonated monomers, indicating stronger physically crosslinked network. Furthermore, a systematic increase in the plateau modulus, G_N, is observed for SPS ionomers as the sulfonated functionality increases (**Figure 5.4** and **Table 5.3**). Consistent with the theory of rubber elasticity that predicts G_N is proportional to the crosslink density, the higher G_N further confirms the stronger ionic associations as a result of added sulfonate ions.[40, 43]

0.5 mol% PPS ionomer indicates a more profound plateau in *G'* over a wider frequency range in comparison to all SPS ionomers. More importantly, the terminal relaxation time, τ, for 0.5PPS is 3 orders of magnitude longer than that for SPS ionomer at the same mol% of ionic monomers, and is one order of magnitude longer than 1.5 mol% SPS. These phenomena are in agreement with our previous work on sulfonated and phosphonated poly(ethylene terephthalate) (SPET and PPET) ionomers,[44] which demonstrated that PPET ionomers with divalent phosphonate pendant ions exhibited a much longer reptation time than SPET analogues. From the comparison between SPS and PPS ionomers, it is evident that the divalent phosphonate pendant ions are capable of generating stronger ionic associations as compared to the monovalent sulfonate pendant ions. In addition, it is interesting to note that the plateau modulus for 0.5PPS is lower than those for SPS ionomers. This phenomenon is not unique for PS ionomers, and has been found in our related work on SPET and PPET ionomers. Given that the plateau modulus is related to the crosslinked network of ionomers, this finding possibly suggests that sulfonate ionic groups generate a higher crosslinking density than phosphonate groups, but the stronger ionic associations in phosphonated ionomers lead to a longer relaxation time. A reversible gelation model has been developed and utilized to predict the linear viscoelastic behavior of neat ionomers.[5, 39] Future work will focus on a systematic investigation of the cross-linkable sites for phosphonate pendant ions and the cross-linked network for SPS and PPS ionomers at low ionic contents (e.g., < 1.5 mol%).

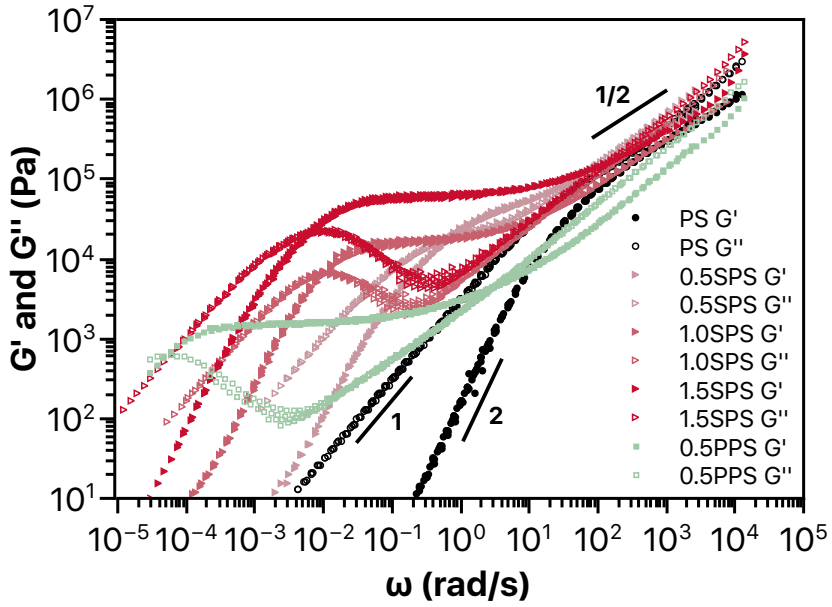

Figure 5.4. Frequency dependence of storage and loss moduli, *G'* and *G''*, master curves at T_r = 150 °C for sulfonated and phosphonated polystyrene ionomers (M_n ~ 8K-9K g/mol).

Table 5.3. η_0, $\boldsymbol{\tau}$ Frequency, $\boldsymbol{\tau}$, E_a, and G_N for SPS and PPS Ionomers (M_n ~ 8K-9K g/mol).

	Log(η_0) (Pa·s)	**τ (s)[b]**	**E_a (kJ/mol)**	**Log(G_N) (Pa)**
PS	3.50	0.29	131.4	-
0.5SPS	5.03	23.9	141.5	-
1.0SPS	6.24	560	155.0	4.23
1.5SPS	7.04	2501	160.9	4.80
0.5PPS	7.37[a]	99572	160.9	3.20

[a]Calculated by fitting the η curve with the Careau-Yasuda model.[45]

[b] $\tau = \lim_{\omega \to 0} [\frac{G'(\omega)}{\omega G''(\omega)}]$

Figure 5.5 compares the melt viscosity (η) of sulfonated and phosphonated polystyrene ionomers, and the corresponding zero-shear viscosity (η_0) values are summarized in **Table 5.3**. η_0 for 0.5PPS ionomer was obtained by fitting the η curve

with the Careau-Yasuda model. It is evident that η_0 for SPS ionomers increase with increasing sulfonation level, and the onset of shear thinning shifts to lower frequencies, suggesting higher longest relaxation time.[2] PPS ionomer with 0.5 mol% ionic monomers exhibits a significantly higher η_0 by 2 orders of magnitude as compared to 0.5 mol% SPS, and the η_0 for 0.5PPS is comparable to that of 1.5 mol% SPS ionomer. Furthermore, the activation energy, E_a, for these ionomers along with neat PS were calculated by fitting into Arrhenius equation from 200 °C to 250 °C with T_r = 200 °C. From the listed E_a in **Table 5.3**, the E_a for 0.5PPS ionomer is about 20 kJ/mol higher than that for 0.5SPS ionomer, and similar to that of 1.5SPS ionomer. In agreement with the significantly longer terminal relaxation time for 0.5PPS compared to SPS analogue, the higher η_0 for PPS ionomer further emphasizes the physically cross-linked network generated by divalent phosphonate ions in PPS is stronger than that in SPS analogues with monovalent sulfonate groups.

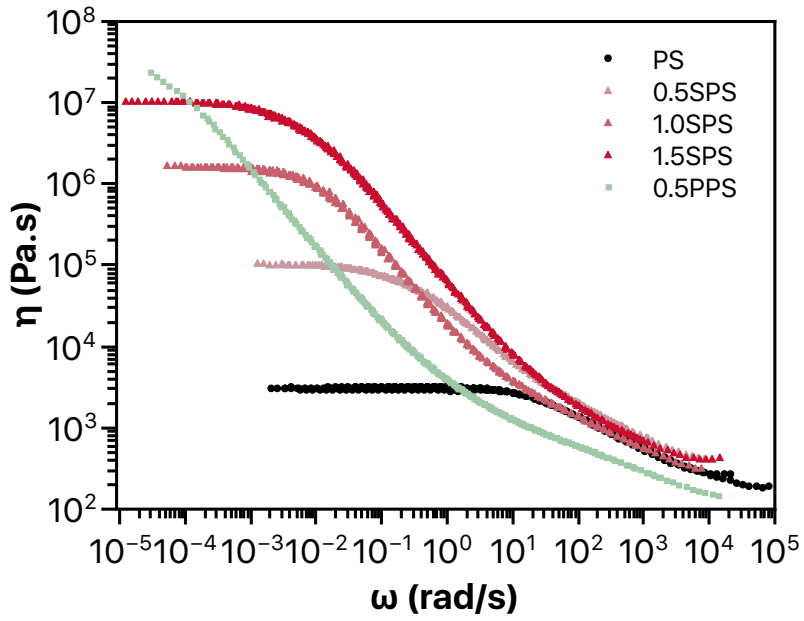

Figure 5.5. Melt viscosity master curves of sulfonated (triangle symbols) and phosphonated (square symbols) PS ionomers (M_n ~ 8K-9K g/mol) at T_r = 150 °C.

5.5 Conclusions

This work demonstrated that the divalent phosphonate pendent ions generated stronger ionic associations, and consequently provided a stronger physically crosslinked network in PPS ionomers as compared to SPS analogues. DSC analysis on the glass transitions of SPS and PPS ionomers indicated PPS ionomers exhibited higher T_g as compared to SPS ionomers. Dynamic melt rheology characterization of oligomeric SPS and PPS ionomers revealed 0.5 mol% PPS ionomer exhibited longer relaxation time, wider frequency range of the plateau in *G'*, and higher zero-shear viscosity than those for SPS ionomer containing the same mol% of ionic monomers. Furthermore, larger ionic aggregates with higher charge density were observed in PPS ionomers by SAXS and ^{23}Na NMR analysis. Overall, this work provides a deep insight into ionomers bearing divalent

phosphonate pendant ions, and confirms the more profound influence of phosphonate groups on the properties of polystyrene ionomers compared to the monovalent sulfonate pendant ions.

5.6 Acknowledgements

The authors gratefully acknowledge the Institute for Advanced Learning and Research for providing funds (449414) to support the efforts of this project. The authors thank Ryan J. Carrazzone and Prof. John B. Matson in the Department of Chemistry at Virginia Tech for SEC analysis help.

5.7 References

1. Lundberg, R. D., Elastomers and fluid applications. In Ionomers: Synthesis, structure, properties and applications, Tant, M. R.; Mauritz, K. A.; Wilkes, G. L., Eds. Springer Netherlands: Dordrecht, 1997; pp 477-501.
2. Tant, M. R.; Mauritz, K. A.; Wilkes, G. L., Ionomers: synthesis, structure, properties and applications. Springer Science & Business Media: 2012.
3. Zhang, L.; Brostowitz, N. R.; Cavicchi, K. A.; Weiss, R., Perspective: Ionomer research and applications. Macromolecular Reaction Engineering 2014, 8 (2), 81-99.
4. Eisenberg, A.; Hird, B.; Moore, R., A new multiplet-cluster model for the morphology of random ionomers. Macromolecules 1990, 23 (18), 4098-4107.
5. Huang, C.; Chen, Q.; Weiss, R., Rheological behavior of partially neutralized oligomeric sulfonated polystyrene ionomers. Macromolecules 2016, 50 (1), 424-431.
6. Ju, L.; Pretelt, J.; Chen, T.; Dennis, J. M.; Heifferon, K. V.; Baird, D. G.; Long, T. E.; Moore, R. B., Synthesis and characterization of phosphonated Poly (ethylene terephthalate) ionomers. Polymer 2018, 151, 154-163.
7. Qiao, X.; Wang, X.; Wang, C.; Weiss, R., Effect of zinc stearate on the properties of a sulfonated polystyrene ionomer. Journal of Rheology 2018, 62 (4), 821-830.
8. Wu, Q.; Weiss, R., Viscoelastic properties of poly (styrene-co-vinylphosphonate) ionomers. Polymer 2007, 48 (26), 7558-7566.
9. Anderson, L. J.; Yuan, X.; Fahs, G. B.; Moore, R. B., Blocky Ionomers via Sulfonation of Poly (ether ether ketone) in the Semicrystalline Gel State. Macromolecules 2018, 51 (16), 6226-6237.

10. Fahs, G. B.; Benson, S. D.; Moore, R. B., Blocky sulfonation of syndiotactic polystyrene: a facile route toward tailored ionomer architecture via postpolymerization functionalization in the gel state. Macromolecules 2017, 50 (6), 2387-2396.
11. Kang, H.; Lin, Q.; Armentrout, R. S.; Long, T. E., Synthesis and characterization of telechelic poly (ethylene terephthalate) sodiosulfonate ionomers. Macromolecules 2002, 35 (23), 8738-8744.
12. Orler, E. B.; Calhoun, B. H.; Moore, R. B., Crystallization kinetics as a probe of the dynamic network in lightly sulfonated syndiotactic polystyrene ionomers. Macromolecules 1996, 29 (18), 5965-5971.
13. Orler, E. B.; Moore, R. B., Influence of ionic interactions on the crystallization of lightly sulfonated syndiotactic polystyrene ionomers. Macromolecules 1994, 27 (17), 4774-4780.
14. Orler, E. B.; Yontz, D. J.; Moore, R. B., Sulfonation of syndiotactic polystyrene for model semicrystalline ionomer investigations. Macromolecules 1993, 26 (19), 5157-5160.
15. Dolog, R.; Weiss, R., Shape memory behavior of a polyethylene-based carboxylate ionomer. Macromolecules 2013, 46 (19), 7845-7852.
16. Hird, B.; Eisenberg, A., Sizes and stabilities of multiplets and clusters in carboxylated and sulfonated styrene ionomers. Macromolecules 1992, 25 (24), 6466-6474.
17. Lundberg, R.; Makowski, H., A comparison of sulfonate and carboxylate ionomers. ACS Publications: 1980.
18. Nakano, Y.; MacKnight, W. J., Dynamic mechanical properties of perfluorocarboxylate ionomers. Macromolecules 1984, 17 (8), 1585-1591.
19. Rees, R.; Vaughan, D., Physical structure of ionomers. Polymer preprints. American Chemical Society. Division of Polymer Chemistry 1965, 6, 287.
20. Weiss, R.; Yu, W.-C., Viscoelastic behavior of very lightly sulfonated polystyrene ionomers. Macromolecules 2007, 40 (10), 3640-3643.
21. Zhou, N. C.; Chan, C. D.; Winey, K. I., Reconciling STEM and X-ray scattering data to determine the nanoscale ionic aggregate morphology in sulfonated polystyrene ionomers. Macromolecules 2008, 41 (16), 6134-6140.
22. Ju, L.; Dennis, J. M.; Heifferon, K. V.; Long, T. E.; Moore, R. B., Compatibilization of Polyester/Polyamide Blends with a Phosphonated Poly (ethylene terephthalate) Ionomer: Comparison of Monovalent and Divalent Pendant Ions. ACS Applied Polymer Materials 2019, 1 (5), 1071-1080.
23. Wu, Q.; Weiss, R., Synthesis and characterization of poly (styrene-co-vinyl phosphonate) ionomers. Journal of Polymer Science Part B: Polymer Physics 2004, 42 (19), 3628-3641.
24. Sikkema, F. D.; Comellas-Aragones, M.; Fokkink, R. G.; Verduin, B. J.; Cornelissen, J. J.; Nolte, R. J., Monodisperse polymer–virus hybrid nanoparticles. Organic & biomolecular chemistry 2007, 5 (1), 54-57.
25. Zhuang, R.; Xu, J.; Cai, Z.; Tang, G.; Fang, M.; Zhao, Y., Copper-Catalyzed C− P Bond Construction via Direct Coupling of Phenylboronic Acids with H-Phosphonate Diesters. Organic letters 2011, 13 (8), 2110-2113.

26. Berger, K.; Brandrup, G.; Brandrup, J.; Immergut, E., Polymer handbook. Wiley & Sons, II/136, New York 1989.
27. Galambos, A.; Stockton, W.; Koberstein, J.; Sen, A.; Weiss, R.; Russell, T., Observation of cluster formation in an ionomer. Macromolecules 1987, 20 (12), 3091-3094.
28. Moore, R. B.; Bittencourt, D.; Gauthier, M.; Williams, C. E.; Eisenberg, A., Small-angle x-ray scattering investigations of ionomers with variable-length side chains. Macromolecules 1991, 24 (6), 1376-1382.
29. Moore, R. B.; Gauthier, M.; Williams, C. E.; Eisenberg, A., Heterogeneities in random ionomers. A small-angle x-ray scattering investigation of alkylated polystyrene-based materials. Macromolecules 1992, 25 (21), 5769-5773.
30. Weiss, R.; Lefelar, J., The influence of thermal history on the small-angle X-ray scattering of sulphonated polystyrene ionomers. Polymer 1986, 27 (1), 3-10.
31. Williams, C. E.; Russell, T. P.; Jerome, R.; Horrion, J., Ionic aggregation in model ionomers. Macromolecules 1986, 19 (11), 2877-2884.
32. Yarusso, D. J.; Cooper, S. L., Microstructure of ionomers: interpretation of small-angle x-ray scattering data. Macromolecules 1983, 16 (12), 1871-1880.
33. Kinning, D. J.; Thomas, E. L., Hard-sphere interactions between spherical domains in diblock copolymers. Macromolecules 1984, 17 (9), 1712-1718.
34. Zhang, K.; Fahs, G. B.; Drummey, K. J.; Moore, R. B.; Long, T. E., Doubly-Charged Ionomers with Enhanced Microphase-Separation. Macromolecules 2016, 49 (18), 6965-6972.
35. Peiffer, D.; Weiss, R.; Lundberg, R., Microphase separation in sulfonated polystyrene ionomers. Journal of Polymer Science: Polymer Physics Edition 1982, 20 (8), 1503-1509.
36. O'Connell, E. M.; Root, T. W.; Cooper, S. L., Morphological studies of lightly-sulfonated polystyrene using 23Na NMR. 1. Effects of sample composition. Macromolecules 1994, 27 (20), 5803-5810.
37. Jardetzky, O.; Wertz, J. E., Weak complexes of the sodium ion in aqueous solution studied by nuclear spin resonance. Journal of the American Chemical Society 1960, 82 (2), 318-323.
38. Maeda, M.; Ohtaki, H., An X-ray diffraction study of a concentrated aqueous sodium iodide solution. Bulletin of the Chemical Society of Japan 1975, 48 (12), 3755-3756.
39. Chen, Q.; Huang, C.; Weiss, R.; Colby, R. H., Viscoelasticity of reversible gelation for ionomers. Macromolecules 2015, 48 (4), 1221-1230.
40. Weiss, R.; Zhao, H., Rheological behavior of oligomeric ionomers. Journal of Rheology 2009, 53 (1), 191-213.
41. Baird, D. G.; Collias, D. I., Polymer processing: principles and design. John Wiley & Sons: 2014.
42. Ferry, J. D., Viscoelastic properties of polymers. John Wiley & Sons: 1980.
43. Weiss, R.; Fitzgerald, J.; Kim, D., Viscoelastic behavior of lightly sulfonated polystyrene ionomers. Macromolecules 1991, 24 (5), 1071-1076.
44. Lin Ju, T. C., Donald G. Baird, and Robert B. Moore*, A Comparison of Sulfonated and Phosphonated Poly(ethylene terephthalate) Ionomers: Thermal and Linear Viscoelastic Properties. Manuscript in preparation.

45. Bird, R. B.; Armstrong, R. C.; Hassager, O., Dynamics of polymeric liquids. Vol. 1: Fluid mechanics. 1987.

5.8 Supporting Information

Table S5.1. Summary of Compositional and SEC Analysis of Sulfonated and Phosphonated Polystyrene Copolymer (M_n ~ 8K-9K g/mol) in the Ester Form.

Sample	Functionalized Styrene : Styrene (mol%) feed (x:y)	M_n (g/mol)	PDI	M_w (g/mol)
PS	0:100	8.8K	1.63	14K
0.5SPS	0.5:99.5	8.7K	1.44	13K
1.0SPS	1.0:99.0	8.7K	1.52	13K
1.5SPS	1.5:98.5	8.4K	1.69	14K
0.5PPS	0.5:99.5	8.6K	1.50	13K

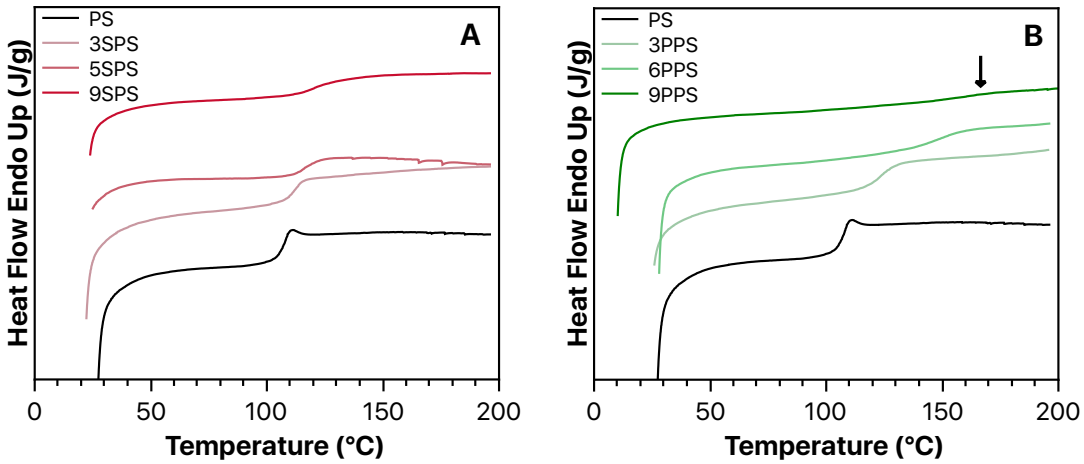

Figure S5.1. DSC heating scans of sulfonated and phosphonated polystyrene ionomers along with pure polystyrene after rapid cooling from the melt (200 °C) at -60 °C/min. Heating rate: 10 °C/min. (M_n ~ 100K g/mol).

Table S5.2. Summary of the Glass Transition Temperatures for Sulfonated and Phosphonated Polystyrene Ionomers (M_n ~ 100K g/mol) in the Na^+ Form.

Sample M_w ~ 150K g/mol	T_g (°C)
PS	108
3SPS	114
5SPS	116
9SPS	121
3PPS	123
6PPS	151
9PPS	161

Chapter 6. Compatibilization of Polyester/Polyamide Blends with a Phosphonated Poly(Ethylene Terephthalate) Ionomer: Comparison of Monovalent and Divalent Pendant Ions

(Published in *ACS Appl. Polym. Mater.* **2019**, *1*, 1071-1080)

Lin Ju, Joseph M. Dennis, Katherine V. Heifferon, Timothy E. Long, and Robert B. Moore*

Department of Chemistry, Macromolecules Innovation Institute, Virginia Polytechnic Institute and State University, Blacksburg, VA 24061, United States

6.1 Abstract

The successful compatibilization of immiscible amorphous polyester (PETG) and semicrystalline polyamide (poly(*m*-xylylene adipamide) (MXD6)) blends using a phosphonated poly(ethylene terephthalate) ionomer in the Na^+ form (Na^+-PPET) as a minor-component compatibilizer was demonstrated. The Na^+-PPET/PETG/MXD6 blends were prepared using a solution mixing method to enable thin film characterization. The phase morphology with respect to various phosphonated monomer concentrations was studied using phase contrast optical microscopy (PC-OM) and small angle laser light scattering (SALLS). The phase-separated, interdomain spacing decreased with increasing mol% phosphonated monomers, and was attributed to the specific interactions between the ionic phosphonate groups on the polyester ionomer and the amide linkages of polyamide. The ability of the divalent phosphonate pendant ions to compatibilize

PETG/MXD6 blends was also compared to a conventional sulfonated PET (SPET) compatibilizer. This comparison showed that the Na^+-PPET/PETG/MXD6 blends required 6 times fewer ionic monomers to achieve domain dimension less than 1 μm as compared to Na^+-SPET-containing PETG/MXD6 blends. Moreover, on a mol% of pendant ions basis, the divalent phosphonate pendant ions in PPET were found to be 3 times more effective at compatibilizing PETG/MXD6 blends compared to the monovalent sulfonate pendant ions in SPET.

6.2 Introduction

Polyester/polyamide blends attract attention in the area of food packaging due to the combination of the low oxygen and carbon dioxide permeability of the polyamide component with good toughness, clarity, and economics of the polyester matrix.[1-6] The broad application of polyester/polyamide blends in gas barrier packaging, however, is often limited by poor optical clarity due to the thermodynamic immiscibility between the two dissimilar polymers.[7-8] Therefore, efforts to enhance the polyester/polyamide compatibility in order to significantly reduce domain dimensions of the minor polyamide phase within the polyester matrix have remained a priority for many researchers.

Ionomers are charged polymers that contain minor amounts (typically less than 15 mol%) of covalently attached ionic functionalities incorporated into or pendant to the polymer backbones.[9-11] The functional polymers have proven to be attractive, interfacially-active compatibilizers for a number of blend systems because of specific interactions that may develop between the ionic groups and complementary functional groups on other polar polymers within the blend.[12-17] These specific interactions tend to

decrease the interfacial tension between the dissimilar polymers, leading to reduced phase dimensions and enhanced phase stability that inhibits coalescence during melt processing.[18-19] Several ionomers bearing pendant carboxylate or sulfonate ionic groups have been utilized as efficient compatibilizers in immiscible polyester/polyamide blends.[1, 3-4, 6, 12-13, 18, 20] For example, Kalfoglou et al.[20] employed Surlyn®, an acrylic-modified polyolefin type ionomer, to compatibilize a melt-mixed poly(ethylene terephthalate) (PET)/nylon 6 blend. Mechanical tests demonstrated effective compatibilization at ionomer loadings greater than 10 wt% as revealed by increased ductility and enhanced impact strength. Weiss et al.[13] reported the successful compatibilization of liquid crystalline polyester (LCP) with nylon 66 by the incorporation of a zinc-neutralized lightly sulfonated polystyrene (Zn^{2+}-SPS) ionomer. The addition of Zn^{2+}-SPS to LCP/nylon 66 blend reduced the dispersed-phase size, and the compatibilized blends exhibited significantly enhanced tensile modulus and tensile stress at break compared to the blends without the ionomer. In our earlier work, we proved the enhanced compatibility of an amorphous polyester/polyamide (PETG 6763/Durethan T40) blend with an added amorphous sulfonate polyester ionomer (Na^{+}-SPETG) as a compatibilizer using solution mixing and melt blending methods, as revealed by enhanced dispersion of the minor phase and a significant reduction in the dispersed-phase sizes.[18] Sulfonated poly(ethylene terephthalate) ionomers in Na^{+}-form (Na^{+}-SPET) have also been widely utilized as compatibilizers in melt-mixed polyester/polyamide blends, e.g., poly(ethylene terephthalate) (PET)/poly(*m*-xylylene adipamide) (MXD6), and PET/nylon 6.[1, 3-4, 6] Both specific interactions and transesterification reactions within SPET-compatibilized polyester/polyamide blends have been demonstrated to play a role

in the overall compatibilization process for melt-mixed polyester/polyamide blends.[12]

The ability of an ionomer to effectively compatibilize immiscible polymer blends strongly depends on the counterion type of the ionomer.[12, 21-24] Ionomers that are neutralized using divalent counterions can exhibit stronger effects on the compatibility of immiscible polymer blends compared to ionomers with monovalent counterions. For example, MacKnight et al.[21] studied the effect of counterion type on the binary blend system of a metal-neutralized SPET ionomer with poly(ethyl acrylate-*co*-4-vinylpyridine) (EAVP). In contrast to the blends containing monovalent Na^+ and Li^+ form SPET ionomers, SPET/EAVP blends containing divalent counterions, such as alkaline earth (Ca^{2+}) and divalent transition metals (Co^{2+}, Ni^{2+}, Cu^{2+}, and Zn^{2+}), exhibited enhanced modulus and tensile strength. Similarly, our previous investigation[12] focused on the evaluation of counterion type, e.g., Na^+, Mn^{2+}, and Zn^{2+}, of an amorphous polyester ionomer (AQ 55) on the degree of compatibility for AQ 55/nylon 66 blends. The blends with AQ ionomer in the divalent form showed superior compatibility (i.e., larger T_m depression and enhanced dispersion of the minor phase) in contrast to the monovalent analogs.

As alternative pendant groups, phosphonated monomer units have been relatively under represented in the ionomer literature. Weiss et al.[25] reported the viscoelastic properties of poly(styrene-*co*-vinylphosphonate) ionomers in a variety of counterion forms. In the field of polymer blends, Pearce and coworkers[26] found that polystyrene containing pendant phosphonic acid groups were immiscible with poly(*n*-butyl methacrylate). Despite the well-studied effect of polyester ionomer counterion type on the compatibility of immiscible polymer blends, no systematic studies have been focused

on an investigation of multivalent pendant ions in polyesters, such as the divalent phosphonate pendant ion. Recently, we synthesized phosphonated PET ionomers in the Na^+-form (Na^+-PPET) by melt polycondensation reaction, and reported their thermal, rheological, and mechanical properties.[27] As an alternative compatibilizer to the widely used Na^+-SPET ionomer, the Na^+-PPET ionomer bearing divalent pendant ions is potentially an attractive candidate for polyester/polyamide blends. Monovalent sulfonate ion pairs are known to interact strongly with the amide linkages,[22] thus establishing an interphase of specific interactions (**Figure 6.1A**).[15] It is postulated that the divalent phosphonate pendant ions are capable of generating stronger specific interactions per functional monomer unit (**Figure 6.1B**) that could provide a more effective mode of compatibilization in polyester/polyamide blends as compared to a polyester ionomer bearing monovalent sulfonate pendant ions. In this work, we report the first investigation of the compatibilization of polyester/polyamide blends with a Na^+-PPET ionomer, along with a direct comparison of monovalent sulfonate and divalent phosphonate pendant ions on the compatibilization of polyester/polyamide blends.

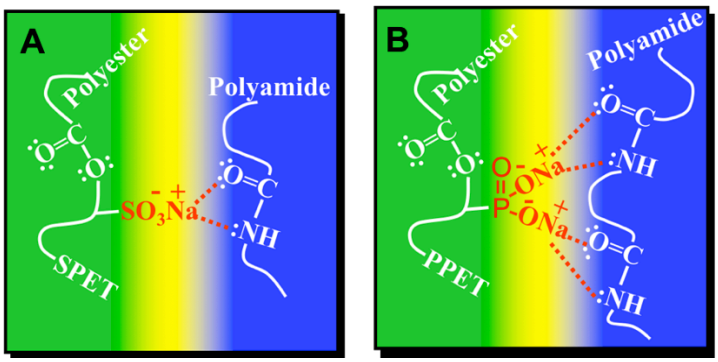

Figure 6.1. Schematic representations for the specific interactions between the pendant ions and amide linkages of the polyamide in polyester/polyamide blends. (A) Monovalent sulfonate pendant ion; (B) Postulated interactions with the divalent phosphonate pendant ion.

6.3 Experimental Section

Materials. 1,1,1,3,3,3-Hexafluoro-2-propanol (HFIP, ≥99.5%) was purchased from Acros Organics, and used as received. The amorphous polyester (PETG 6763) composed of terephthalic acid and ethylene glycol with a portion of the glycol units substituted with cyclohexanedimethanol was supplied by Eastman Chemical Company. Poly(*m*-xylylene adipamide) (MXD6) was supplied by Mitsubishi Gas Chemical Company and sulfonated poly(ethylene terephthalate) ionomers in Na^+-form (Na^+-SPET) with 1.80 mol% terephthalate replaced with sodium 5-sulfoisophthalate was obtained from Eastman Chemical Company. Phosphonated poly(ethylene terephthalate) ionomer in Na^+-form (Na^+-PPET) with 0.5 mol% 5-phosphoisophthalate units randomly distributed along the polymer chain was synthesized by melt polycondensation reaction as described in our recent publication.[27]

Preparation of Solution Blends. All blends were prepared as 1.5% (w/v) solutions in HFIP. To prepare the blends, Na^+-PPET ionomer was first dissolved in HFIP and the solution was allowed to stir for 48 h at 60 °C to ensure complete dissolution and mixing. PETG/MXD6 solutions were obtained by dissolving various ratios of PETG and MXD6 in 2 mL of HFIP at 60 °C after stirring for about 3 h. The Na^+-PPET/PETG/MXD6 solution blends were prepared by combining the appropriate Na^+-PPET and PETG/MXD6 solutions to achieve the desired blend compositions (specifically focusing on the mol% of ionic monomers) as listed in **Table 1**. The generated solution blends were allowed to stir at 60 °C for 24 h to ensure complete dissolution and mixing. The blend compositions were designated as wt% polyester matrix (mol% of phosphonated monomers in the polyester component)/wt% MXD6. Na^+-SPET/PETG/MXD6 blends with the same mol% of ionic monomers as in the Na^+-PPET/PETG/MXD6 blends were also prepared by the same procedure.

Table 6.1. PETG / Na^+-PPET /MXD6 Blend Compositions.

	Composition[a]	wt% PETG	wt% 0.5Na^+-PPET	wt% MXD6	mol% of Ionic Monomer[b]	Stoichiometry[c]
A	75(0.000)/25	75	0	25	0	0
B	75(0.00333)/25	74.5	0.5	25	0.00333	0.000064
C	75(0.00667)/25	74	1	25	0.00667	0.00013
D	75(0.0133)/25	73	2	25	0.0133	0.00026
E	75(0.0333)/25	70	5	25	0.0333	0.00064
F	75(0.0667)/25	65	10	25	0.0667	0.0013
G	75(0.100)/25	60	15	25	0.100	0.0019
H	75(0.167)/25	50	25	25	0.167	0.0032
I	75(0.233)/25	40	35	25	0.233	0.0045
J	75(0.240)/25	39	36	25	0.240	0.0046
K	75(0.247)/25	38	37	25	0.247	0.0058
L	75(0.300)/25	30	45	25	0.300	0.0077

[a] Blend compositions are designated as wt% polyester matrix (mol% of phosphonated monomers in the polyester component)/wt% MXD6;
[b] mol% of phosphonated monomers in the polyester component; and
[c] molar ratio of phosphonated monomers to amide units in the MXD6 component.

Solution Casting Method. To prepare thin film blend specimens, less than 10 μm thick, suitable for characterization by phase contrast optical microscopy (PC-OM) and small angle laser light scattering (SALLS), 0.05 mL of the solution blends as cast onto microscope slides at room temperature. Then, the wet film was covered using an inverted 20 mL glass vial and allowed to dry for about 15 min at room temperature to generate a uniform film (i.e., without observed defects or air bubbles). The same film casting process was utilized to prepare the Na^+-SPET/PETG/MXD6 solution blends.

Phase Contrast Optical Microscopy (PC-OM). The phase morphology of the solution-cast films was characterized using a Nikon Eclipse LV100 microscope equipped with a Linkam TMS 94 hot stage and a Linkam LNP temperature controller. A Nikon

Digital Camera (DXM1200) was utilized for image acquisition. The optical microscope was used in phase contrast mode with a 10X Ph1 objective and the polarizer removed. The as-cast film was heated to 240 °C (50 °C/min) and held at this temperature for 10s to allow for complete melting of the Na^+-PPET and MXD6 crystallites and possible liquid-liquid phase separation. The phase-separated morphology was observed after the film was rapidly cooled to room temperature. The interdomain spacing was measured using ImageJ. For each blend composition, the mean ± σ value was calculated from 200 measurements by fitting a histogram of the measurements to a Gaussian distribution.

Small Angle Laser Light Scattering (SALLS). The same heat-treated films analyzed by PC-OM were utilized in the small-angle laser light scattering (SALLS) experiment. The incident light was obtained from a 3 mW He-Ne laser (λ = 632.8 nm, Oriel Corp., model 6697). The scattered V_v (i.e., the polarizer in the incident beam and the analyzer in the scattered beam are in parallel orientations) pattern was projected onto a detector plane (i.e., a sheet of white paper) that was positioned at a set distance from the sample stage. The digital image on the detector plane was captured using a Photometrics SenSys 1401E CCD camera interfaced with a computer. The sample-to-detector distance (SDD) was 30 cm and the *q*-range, where *q* was the scattering vector, was calibrated using a 300 lines/mm diffraction grating. All SALLS data were analyzed using the Rigaku SAXSGUI software package to obtain radially integrated SALLS intensity versus scattering vector *q* profiles. The experimental interdomain spacing, *d*, was obtained at the maximum intensity and the corrected interdomain spacing, d', was calculated by compensating for the refractive indices of PETG and MXD6 according to **Equations 6.1** and **6.2**:[18, 28-29]

$$d = \frac{n_1 \lambda}{2 \sin(\theta/2)} \tag{6.1}$$

$$d' = \frac{1.025\lambda/n_2}{\pi \sin(\theta'/2)} \tag{6.2}$$

where n_1 is the order of reflection (n_1 = 1); λ is the wavelength of incident light (λ = 632.8 nm); θ and θ' are the experimentally observed and the corrected scattering angles at maximum intensity, respectively; and n_2 is the blend sample refractive index. The scattering angle was corrected for refraction at the sample surface by the formula $n_2 = \sin\theta / \sin\theta'$. The value of n_2 was calculated according to the relationship, $n_2 = n_{PETG} \times wt\%\ of\ polyester + n_{MXD6} \times wt\%\ of\ polyamide$, where n_{PETG} = 1.567 and n_{MXD6} = 1.577.[8, 30]

Fourier Transform Infrared Spectroscopy (FTIR). As a model study, four MXD6/ionic monomer blends with 40 mol% and 60 mol% sulfonated (i.e., sodium 5-sulfoisophthalate) and phosphonated ionic monomers (i.e., sodium 5-phosphoisophthalate) to amide monomer units of MXD6 were prepared as 1.2% (w/v) solutions in HFIP. To prepare the mixtures, MXD6 and ionic monomers were dissolved in HFIP and allowed to stir for 12 h at 60 °C to ensure complete dissolution and mixing. The MXD6/ionic monomer mixtures were obtained by removal of HFIP under ambient pressure (1 atm) at 50 °C and further vacuum drying for 12 h at 50 °C. FTIR was performed on the resulting solids using a Varian 670-IR spectrometer with a DTGS detector using the Pike Technologies GladiATR^{TM} attachment (diamond crystal). Spectra were collected as the average of 32 scans at 4 cm^{-1} resolution.

Differential Scanning Calorimetry (DSC). A TA Instruments Q2000 DSC was used to determine the thermal transitions and crystallization behavior of the Na^+-PPET/PETG/MXD6 blends, tabulated in the **Supporting Information**, **Table S6.1**. Samples were pre-dried at 50 °C for 12 h before DSC tests. Under a nitrogen atmosphere, the samples (~5-8 mg) were heated from 0 °C to 270 °C at 10 °C/min, quench cooled to 0 °C at -60 °C/min, reheated from 0 °C to 270 °C at 10 °C/min, and then cooled to 0 °C at -10 °C/min. The glass transition temperature (T_g), melting temperature (T_m), and enthalpy of melting (ΔH_m) were determined from the second heating scan after erasing the thermal history, and crystallization temperature (T_c) and enthalpy of crystallization (ΔH_c) were investigated from the subsequent cooling scan, using the TA Instruments Universal Analysis software.

6.4 Results and Discussion

6.4.1 Phase Morphology of the PETG/MXD6 Blend. Blends of PETG and MXD6 (composition A, without compatibilizer) are referred to as the base blend in this study. **Figure 6.2** shows images of the as-cast PETG/MXD6 blend film and the film after rapid cooling from the melt (240 °C held for 10s) to room temperature. When the blend of PETG and MXD6 was cast from solution, the resulting thin film was optically transparent (**Figure 6.2A**). Upon heating the blend film to 240 °C (i.e., above the melting temperature (T_m) of the MXD6 component of 236 °C), the film became visibly translucent, and this translucence remained after rapid cooling to room temperature (**Figure 6.2B**). As with most amorphous polymer blends, opacity is generally considered to be indicative of a phase-separated morphology and is attributed to light scattering from

the blend domains of dimensions comparable or greater than the wavelength of visible light having distinctly different refractive indices.[31] While MXD6 is crystallizable, and spherulitic development in a semi-crystalline polymer can also produce opacity, it is important to note that the opacity noted here was observed above the T_m of MXD6, and no spherulites were observed in the cooled samples. Therefore, this translucence is consistent with the expected immiscibility of the PETG/MXD6 blends.

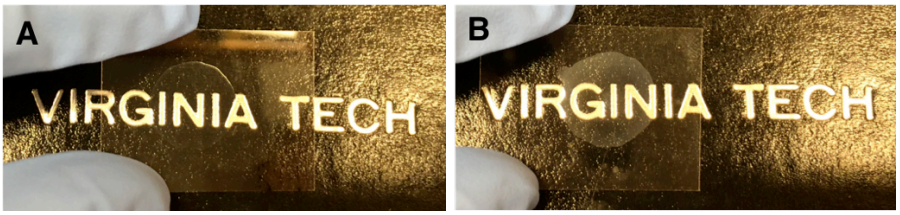

Figure 6.2. PETG/MXD6 base blend film on a microscope slide. (A) Transparent as-cast film at room temperature, and (B) translucent film after rapid cooling from the melt (240 °C held for 10s) to room temperature.

The phase morphology of the solution-cast PETG/MXD6 (75/25) base blend was initially investigated by phase contrast optical microscopy (PC-OM). The optical micrographs of the as-cast PETG/MXD6 base blend film at room temperature and after rapid cooling from 240 °C to room temperature are displayed in **Figure 6.3**. The featureless optical micrograph of the as-cast film (**Figure 6.3A**) is attributed to a kinetically-trapped, homogeneous state of excessive molecular mixing resulting from the relatively rapid solvent evaporation of the blend solution at a temperature well below the glass transition temperatures of the blend components.[32] As opposed to the featureless optical micrograph for the as-cast PETG/MXD6 blend, the film heated to 240 °C exhibits

a well-developed, domain morphology (**Figure 6.3B**) that is characteristic of thermally induced phase separation by spinodal decomposition.[33] This behavior strongly suggests that liquid-liquid phase separation has taken place above the T_m of MXD6. Moreover, the phase-separated structure persists upon rapidly cooling the film to room temperature (**Figure 6.3B**). Consistent with the translucence observed from the image of melt-treated film (**Figure 6.2B**), these data confirm that PETG is immiscible with MXD6, which yields phase-separated domains with dimensions on the order of micrometers.

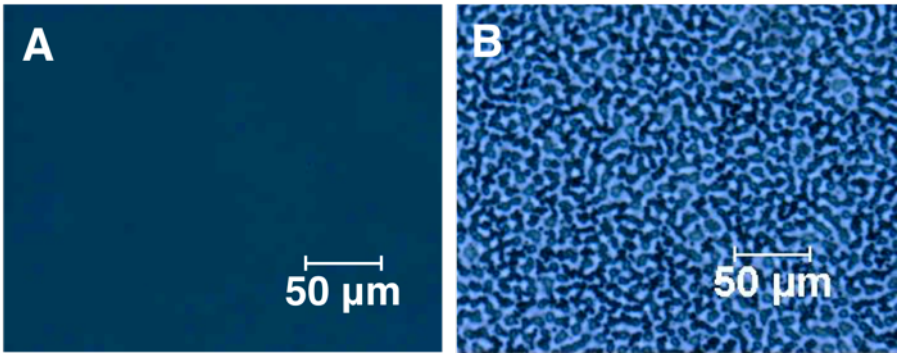

Figure 6.3. Phase contrast optical microscopy (PC-OM) images of the PETG/MXD6 (75/25) base blend. (A) As-cast film at room temperature, and (B) after rapid cooling from the melt (240 °C held for 10s) to room temperature.

While PC-OM provides a means for real space analysis of specific domain dimensions in a phase-separated blend (see below), small angle laser light scattering (SALLS) is a complementary technique to analyze the global dimensions of structural features in reciprocal space.[18, 33-35] The formation of phase-separated structures in a polymer blend is revealed as a scattering halo in the SALLS experiment. The size of the halo is inversely proportional to the global average center-to-center interdomain spacing of the phase-separated blend at a constant sample-to-detector distance (SDD). Thus,

SALLS is often utilized together with PC-OM to fully characterize the morphology and phase separation behavior of various blend systems.

Figure 6.4 shows the V_v scattering patterns for the as-cast and melt-treated PETG/MXD6 (75/25) blend film. In agreement with the PC-OM results (above), no scattering halo is observed in the SALLS patterns of the as-cast PETG/MXD6 blend film at room temperature, again attributed to the excessive mixing of the blend components during solvent casting (**Figure 6.4A**). In contrast, the melt-treated blend film shows a distinct scattering halo, which is attributed to the phase-separated morphology of the immiscible blend (**Figure 6.4B**). This behavior is consistent with the spinodal structure induced by the phase separation process.

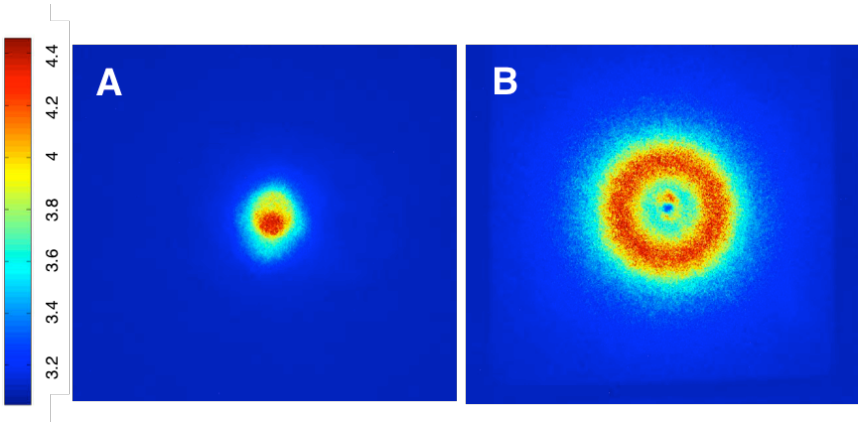

Figure 6.4. V_v small angle laser light scattering patterns of the PETG/MXD6 (75/25) base blend. (A) As-cast film at room temperature, and (B) after rapid cooling from the melt (240 °C held for 10s) to room temperature. The sample-to-detector distance (SDD) is 30 cm.

6.4.2 Investigation of Na^+-PPET Ionomer-Compatibilized PETG/MXD6 Blends by Phase Contrast Optical Microscopy (PC-OM). The compatibilization effect

of the phosphonate pendant ions in Na^+-PPET on the phase behavior of PETG/MXD6 blends was investigated using PC-OM. The optical micrographs for Na^+-PPET/PETG/MXD6 blends after rapid cooling from the melt (240 °C held for 10s) with various amounts of phosphonate groups are shown in **Figure 6.5**. The ternary Na^+-PPET/PETG/MXD6 blends (**Figure 6.5B-6.5J**) exhibit the same spinodal structure as the binary PETG/MXD6 control (base blend, **Figure 6.5A**). As the mol% of ionic phosphonated monomers increases, the dispersed-phase dimensions are reduced (see **Supporting Information**, **Figures S6.1 and S6.2**). For the blends with 0.247 mol% ionic phosphonated monomers and higher, phase-separated domains are not clearly observed within the contrast and resolution limits of this optical microscopy technique. The significant loss of contrast for the blends containing 0.247 mol% ionic phosphonated monomers and higher is indicative of nearly identical refractive indices of the small phases (if present), and is attributed to significant phase mixing between the polyester and polyamide components (**Figures 6.5K and 6.5L**).

As highlighted in **Figure 6.1B**, the phosphonate pendant ions are postulated to serve as sites of specific interactions with the polyamide component that decrease the interfacial tension between the PETG and MXD6 blend components and increase interfacial adhesion,[18-19, 36] thus leading to a reduction in the phase-separated domain sizes and an improved interphase mixing. To gain molecular-level insight into the nature of the compatibilization phenomenon, FTIR was used to spectroscopically probe the specific interactions between the pendant ions and amide groups. Since the ionic group content in these blends was extremely low (**Table 6.1**), a model study involving a mixture of MXD6 with the functional monomers at relatively high concentrations was

conducted (**Supporting Information**, **Figures S6.3-S6.5**). Consistent with previous studies of ionomer interactions with polyamides,[15] the phosphonate groups of PPET appear to interact with the amide functionalities of MXD6 causing a shift of the Amide II band to higher frequencies (**Figure S6.3**). In addition, consistent with the work of Lu and Weiss,[37] as well as Gemeinhardt et al.,[18] the phosphonate/amide interactions are observed to disrupt the H-bonding of the amide groups causing an appearance of a band attributed to free N-H units at 3550 cm^{-1} (**Figures S6.4 and S6.5**). Interestingly, this band at 3550 cm^{-1} is pronounced for the phosphonate system, while virtually absent for the sulfonate analog. This observation agrees with the recent findings of Pike et al.,[38] which showed that phosphonate anions are stronger hydrogen-bond acceptors than sulfonate anions. Thus, these results suggest that the phosphonate groups on the Na^{+}-PPET ionomer interact with the amide groups of MXD6 to yield an effective compatibilization of the PETG/MXD6 blend.

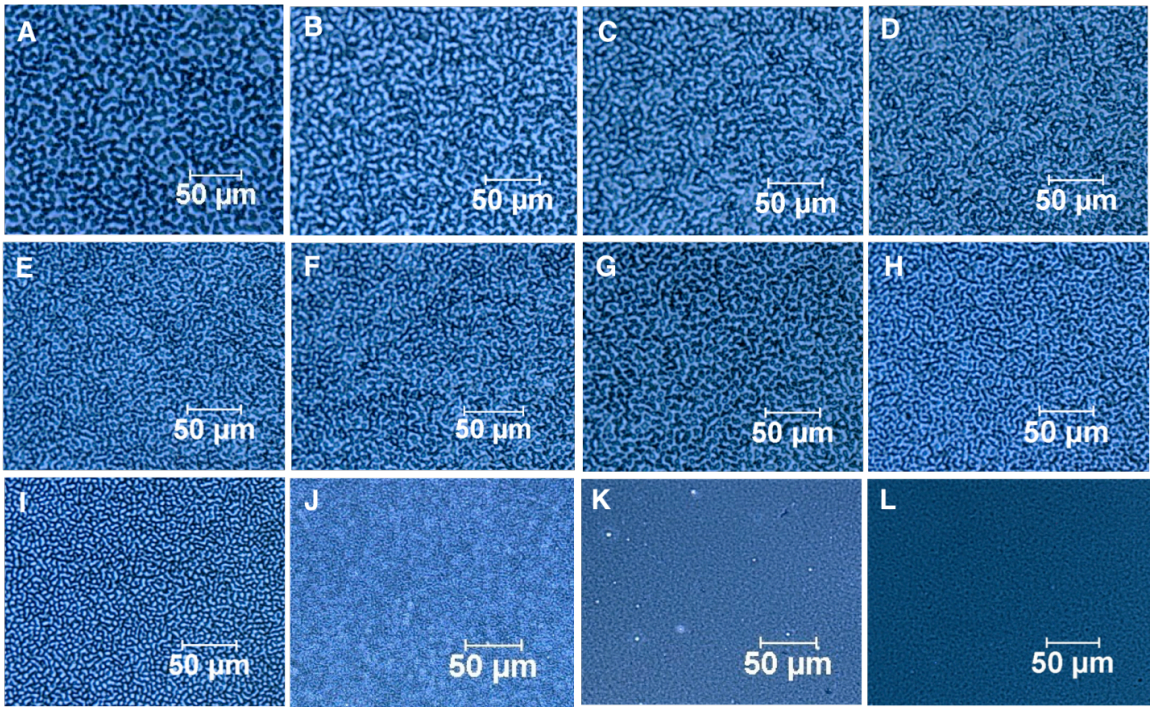

Figure 6.5. Phase contrast optical microscopy (PC-OM) images of the Na^+-PPET/PETG/MXD6 blends. (A) 75(0.000)/25; (B) 75(0.00333)/25; (C) 75(0.00667)/25; (D) 75(0.0133)/25; (E) 75(0.0333)/25; (F) 75(0.0667)/25; (G) 75(0.100)/25; (H) 75(0.167)/25; (I) 75(0.233)/25; (J) 75(0.240)/25; (K) 75(0.247)/25; (L) 75(0.300)/25. Scale bar = 50 µm.

While the decrease in phase dimensions with increasing phosphonate content and apparent phase mixing at relatively high Na^+-PPET contents is consistent with the concept of ionomer compatibilization in these blends, it should be noted that the phase dimensions observed in **Figure 6.5** are not necessilarily equilibrium morphologies. As shown in the **Supporting Information, Figure S6.6**, the phase dimensions of the base blends (without compatibilizer) and the Na^+-PPET (0.0667 mol%)-compatibilized blends remain constant over a period of 5 seconds to 4 minutes (i.e., a time frame consistent with

conventional melt-processing). Even at higher temperatures (e.g., up to 280 °C, **Figure S6.7**), only a minimal increase in phase dimensions of the base blend are observed. However, at longer times up to 5 hours, the dimensions of both systems tend to increase slightly with continued annealing (**Figures S6.8 and S6.9**, respectively); although, significantly diminshed for the Na^+-PPET-compatibilized blend. At relatively high Na^+-PPET contents (e.g., 0.233 mol%, **Figure S6.10**), the phase dimensions remain constant out to 5 hours, consistent with pinned morphologies[16, 39-40] attributed to ion-pair associations in the melt. Nevertheless, given the tendency for the easily oxidizable MXD6 to degrade at high temperatures (e.g., discoloration was observed at long annealing times), we have chosen in this study to compare phase dimensions at relatively short annealing times.

6.4.3 Investigation of Na^+-PPET Ionomer-Compatibilized PETG/MXD6 Blends by Small Angle Laser Light Scattering (SALLS). SALLS was utilized to provide further insight into the effect of Na^+-PPET ionomer on the phase behavior of PETG/MXD6 blends. **Figure 6.6** displays the V_v SALLS patterns for the set of Na^+-PPET/PETG/MXD6 blends. Note that these scattering patterns were acquired based on a constant SDD of 30 cm. At a phosphonated monomer concentration lower than 0.247 mol%, each blend film shows a halo scattering pattern, typical of phase separation in polymer blends. As the mol% of phosphonated monomers increases, the size of the scattering halo increases (i.e., the scattering halo shifts to larger scattering angles). As the size of the halo is inversely proportional to the interdomain spacing of the phase-separated blend at a constant SDD,[18] the larger halo size is evident of a shorter interdomain spacing. For the compositions with 0.247 mol% and 0.300 mol% of ionic

monomers, no detectable scattering halo is observed, even at lower SDDs. This undetectable scattering halo further confirms a profound interphase mixing (**Figures 6.6K** and **6.6L**). Moreover, for **Figures 6.6A-6.6J**, the scattered intensity diminishes with increased ionic monomer concentration, suggesting a diminishing contrast with increased phase mixing. As a compliment to the PC-OM results, these SALLS data reveal significant phase mixing with added sodium phosphonate content and further confirm the enhanced compatibility of PETG/MXD6 blends with the incorporation of the Na^+-PPET ionomer.

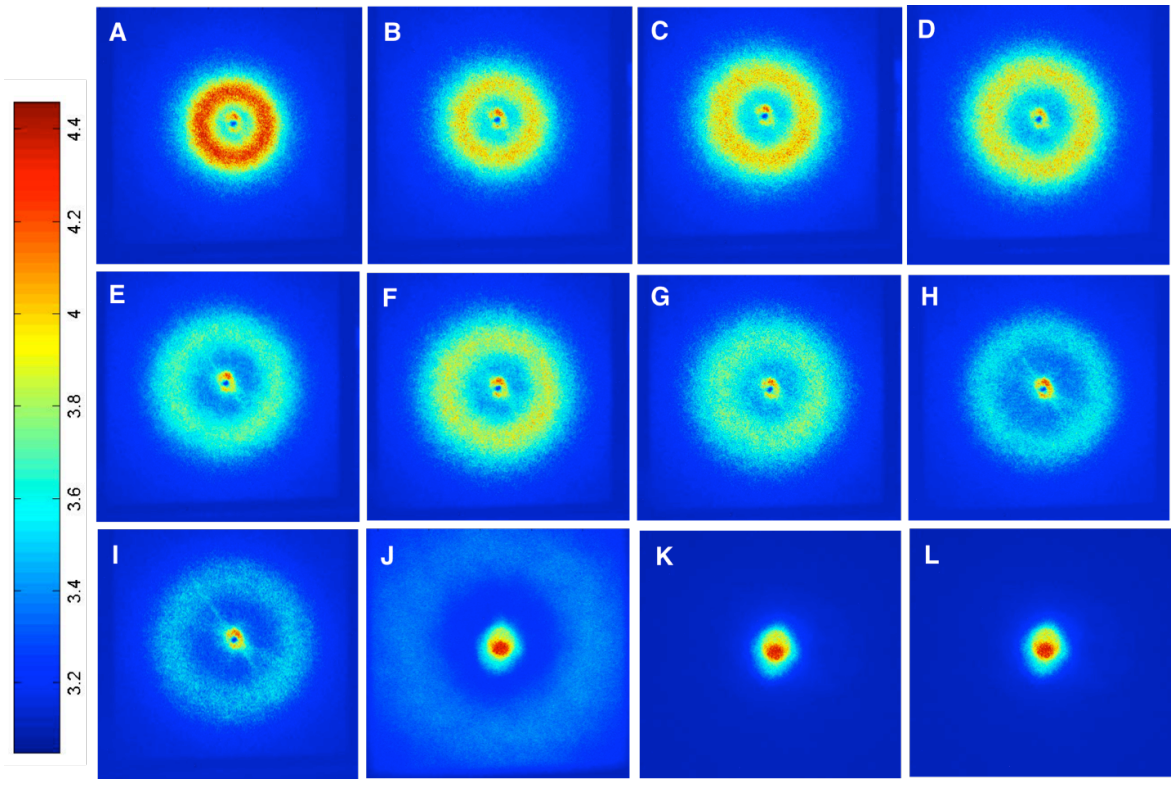

Figure 6.6. V_v small angle laser light scattering (SALLS) patterns of the Na^+-PPET/PETG/MXD6 blends. (A) 75(0.000)/25; (B) 75(0.00333)/25; (C) 75(0.00667)/25; (D) 75(0.0133)/25; (E) 75(0.0333)/25; (F) 75(0.0667)/25; (G) 75(0.100)/25; (H) 75(0.167)/25; (I) 75(0.233)/25; (J) 75(0.240)/25; (K) 75(0.247)/25; (L) 75(0.300)/25. The sample-to-detector distance (SDD) is 30 cm.

In order to quantify the phase-separated domain dimensions using SALLS, the experimental interdomain spacing for each Na^+-PPET/PETG/MXD6 blend was obtained by the procedure described in the **Experimental Section** and found to be in excellent agreement with the measured results from PC-OM (**Figure S6.2**). **Figure 6.7** shows the dependence of the average interdomain spacing on the phosphonated monomer concentration in the polyester component. The interdomain spacings may be divided into three distinct regions: an initial region at low phosphonated monomer concentration,

where interdomain spacing decreases greatly with increasing phosphonated monomer concentration (**Region I**), followed by a broad range of phosphonated monomer concentration between 0.0133 and 0.233 mol% (**Region II**), where interdomain spacing values remain relatively constant. Finally, at phosphonated monomer concentration above 0.233 mol% (**Region III**), a rapid decline in domain dimensions is observed, followed by the loss of a detectable phase morphology.

During the initial stage of increasing phosphonated monomer concentration, corresponding to **Region I** (i.e., below 0.0133 mol%), it is clear that very small amounts of ionic phosphonate groups incorporated to the polyester/polyamide blend system can significantly decrease the phase-separated domain dimensions. For example, with only 0.0133 mol% phosphonated monomers, the interdomain spacing has been reduced by 39% (i.e., from 9.26 μm to 5.66 μm). The plateau of relatively constant phase dimensions observed in **Region II** demonstrates that further increasing the mol% of phosphonated monomers has little effect on the interdomain spacing. In **Region III**, the plot begins a steep decline from 5.26 μm to 2.80 μm as the amount of phosphonated monomers increases from 0.233 mol% to 0.240 mol%. Above 0.240 mol% phosphonated monomer concentration, the domain dimensions suddenly drop below a 1 μm resolution limit such that the distinct domain structure is no longer observed by optical microscopy (**Figure 6.5K** and **6.5L**). From an applied perspective, this "cliff" in composition signifies a transition to a highly compatibilized blend capable of forming domains on a size scale comparable to the wavelength of visible light (e.g., dimensions needed to minimize haze from scattered light in packaging applications.) From a more fundamental perspective, the transitions between the three regions of composition may involve a complex interplay

between ionic aggregation (i.e., strong associations between ion-pairs, characteristic of ionomers[41]) and the ion-amide associations responsible for compatibilization. Clearly, further investigations will be required to confirm and discriminate the relative contributions of these competing interactions.

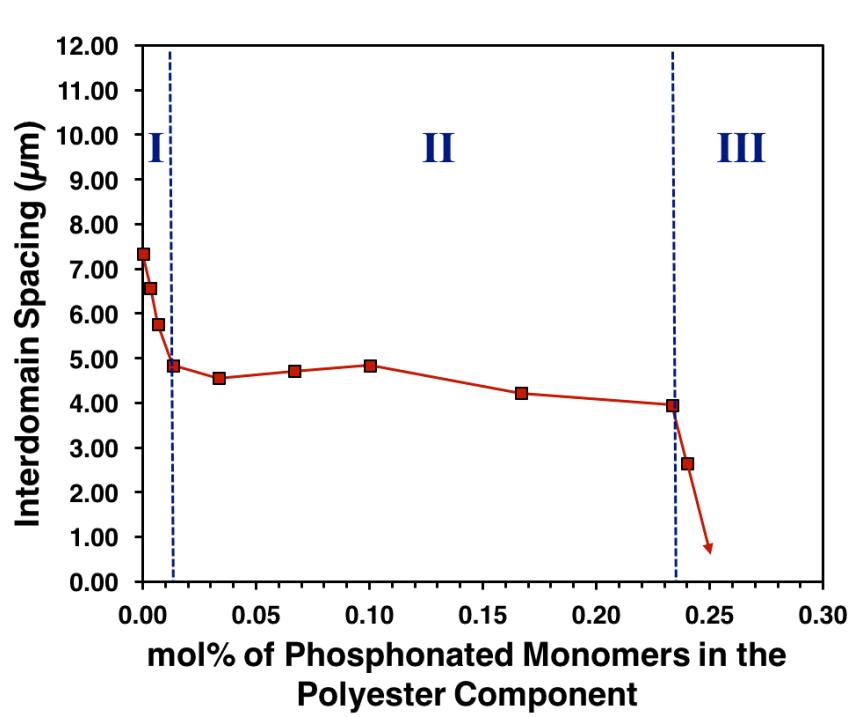

Figure 6.7. Average interdomain spacing of the Na^+-PPET/PETG/MXD6 blends calculated from small angle laser light scattering (SALLS) experiments as a function of phosphonated monomer concentration in the polyester component. Region I: below 0.0133 mol%, where domain size rapidly decreases; Region II: 0.0133 mol% - 0.233 mol%, where domain size remains relatively constant; Region III: above 0.233 mol%, where rapid loss of scattering is observed.

6.4.4 Comparison of the Monovalent Sulfonate and Divalent Phosphonate Pendant Ions. Given the widespread application of sulfonated PET (SPET) in polymer

blend compatibilization,[1, 4, 12, 18] it is of interest here to systematically compare the relative effectiveness of the monovalent sulfonate and divalent phosphonate pendant ions on the phase morphology of PETG/MXD6 blends. In this comparison, Na^+-SPET/PETG/MXD6 blends were prepared to contain the same mol% of ionic monomers in the polyester component as that of the Na^+-PPET/PETG/MXD6 blends. Given that the functionalized monomer in the PPET copolymer contains twice the number of pendant ions as that of the SPET comonomer, this analysis will show a comparison based on (1) the mol% of ionic monomers in the polyester component, as well as (2) a comparison based on the mol% of pendant ions in the blend.

The interdomain spacings obtained from PC-OM (**Figure 6.8A**) and SALLS (**Figure 6.8B**) for Na^+-SPET/PETG/MXD6 and Na^+-PPET/PETG/MXD6 blends are compared with respect to the mol% of ionic monomers. The PC-OM images, histograms with Gaussian distribution fits, and the SALLS patterns for Na^+-SPET/PETG/MXD6 blends are provided in the **Supporting Information Figures S6.11**, **S6.12**, and **S6.13**, respectively. Interestingly, the general interdomain spacing versus mol% ionic monomer plots of the Na^+-SPET/PETG/MXD6 blends follows a similar profile to that of the Na^+-PPET ionomer-compatibilized PETG/MXD6 blends, where three distinct regions of phase behavior are evident. This similar observation of the three-region behavior (described above), suggests that the ionic associations responsible for ionomer compatibilization is rather general, and not unique to PPET.

At low ionic monomer concentration, i.e., below 0.240 mol%, Na^+-PPET ionomer-compatibilized PETG/MXD6 blends exhibit comparable interdomain spacing to that of Na^+-SPET/PETG/MXD6 blends, indicating similar compatibilization effect on

PETG/MXD6 blends. In distinct contrast, however, the plateau region for Na^+-PPET/PETG/MXD6 blends, i.e., 0.0133-0.233 mol%, is 85% shorter than the very broad range of 0.167-1.62 mol% observed for Na^+-SPET/PETG/MXD6 blends. In the range of ionic monomer concentration higher than 0.240 mol%, no detectable spinodal structure is observed for Na^+-PPET/PETG/MXD6 blends, meanwhile Na^+-SPET ionomer-compatibilized blends still show phase-separated domains with interdomain spacing approximately ranging from 3.2 μm to 4.2 μm. The ionic monomer concentration where the steep decline occurs for Na^+-PPET ionomer-containing blends is 0.233 mol%, which is 86% lower than the 1.62 mol% for Na^+-SPET/PETG/MXD6 blends. This comparison reveals that the Na^+-PPET/PETG/MXD6 blends require 6 times fewer ionic monomers to achieve domain dimension less than 1 μm as compared to Na^+-SPET-containing PETG/MXD6 blends. Thus, it appears that the divalent phosphonate groups generate stronger specific interactions per functional monomer unit as compared to the monovalent sulfonate pendant ions, and consequently a more effective compatibilization in polyester/polyamide blends. From a practical perspective, the superior compatibilization with PPET requires less ionic monomers to achieve the same compatibility of polyester/polyamide blends than that of the conventional SPET-compatibilized blends.

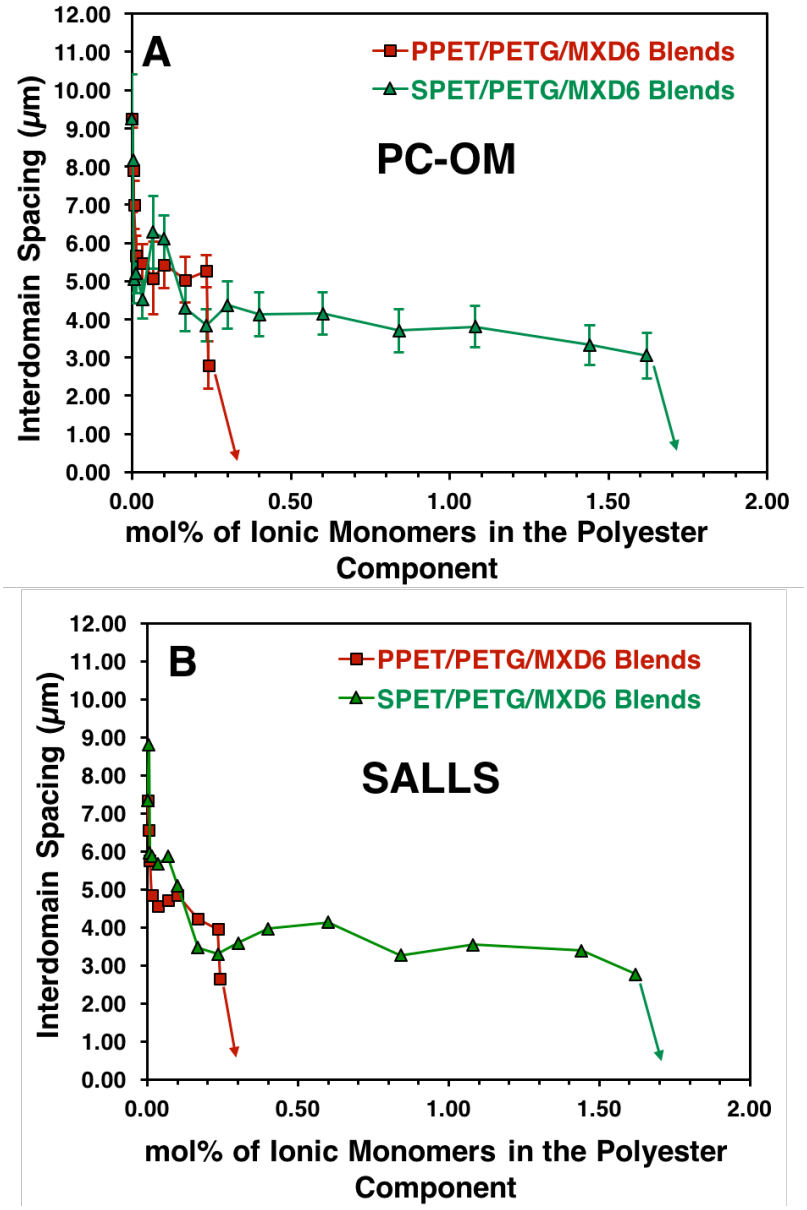

Figure 6.8. Interdomain spacing with respect to mol% of ionic monomers in the polyester component for the Na^+-SPET/PETG/MXD6 and Na^+-PPET/PETG/MXD6 blends based on (A) measured values from the phase contrast optical microscopy (PC-OM) images and (B) calculated values from small angle laser light scattering (SALLS).

The comparison of interdomain spacings for the Na^+-SPET/PETG/MXD6 blends and Na^+-PPET/PETG/MXD6 blends on mol% of pendant ions basis is shown in **Figure 6.9**. This comparison, while of course involving the same set of data as for **Figure 6.8**, highlights the fundamental difference between phosphonate and sulfonate ions, on a per ion basis. At low ion concentrations (less than 0.5 mol%), it appears that the sulfonate ions are slightly more effective at reducing phase dimensions compared to the phosphonate ions. Our recent viscoelastic investigation of the PPET ionomers indicate that these new ionomers have very strong ionic associations with long association lifetimes at low ionic concentrations.[27] Consequently, fewer phosphonate ions may be available to interact with the polyamide at concentrations below 0.5 mol%, as compared to the more weakly interacting sulfonate ions. Future rheological comparisons between PPET and SPET, on an equal mol% ion basis, will be required to confirm this consideration.

At concentrations approaching 0.5 mol% of pendant ions, it becomes apparent that the phosphonate ions are interacting more effectively with the polyamide, as compared to the sulfonate ions. The pendant ion concentration at the rapid decline in phase dimensions for Na^+-PPET/PETG/MXD6 blends is about 3 times smaller than that for Na^+-SPET ionomer-containing blends. This implies, at the same mol% of pendant ions, that the phosphonate ions are 3 times more effective at compatibilizing PETG/MXD6 blends compared to the sulfonate pendant ions. The specific interactions generated by phosphonate pendant ions are presumably much stronger than that for sulfonate pendant ions, thus phosphonate pendant ions are more effective in compatibilizing polyester/polyamide blends.

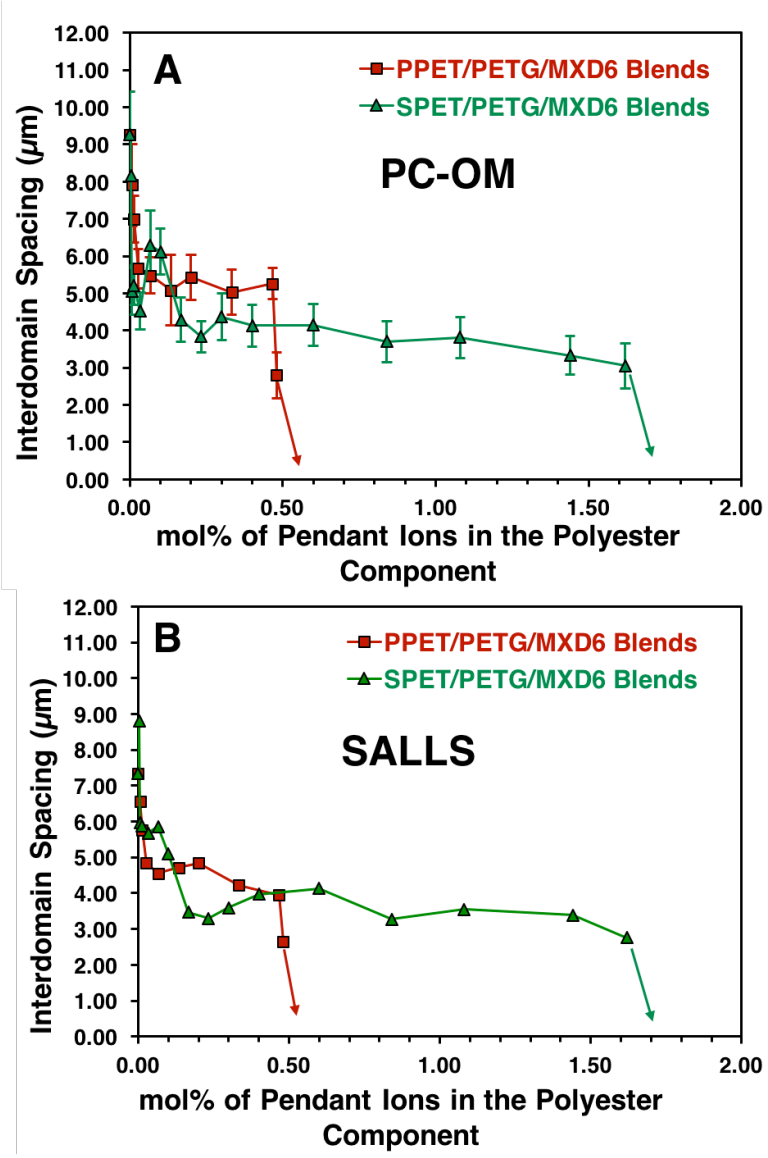

Figure 6.9. Interdomain spacing with respect to mol% of pendant ions in the polyester component for the Na^+-SPET/PETG/MXD6 and Na^+-PPET/PETG/MXD6 blends based on (A) measured values from the phase contrast optical microscopy (PC-OM) images and (B) calculated values from small angle laser light scattering (SALLS).

6.5 Conclusions

In this work, we have demonstrated the successful compatibilization of PETG/MXD6 blends using a new Na^+-PPET ionomer as a minor-component

compatibilizer, and confirmed that the divalent phosphonate pendant ion is more effective at compatibilizing polyester/polyamide blends in comparison to the monovalent sulfonate pendant ions. Melt-treated Na^+-PPET/PETG/MXD6 blend films show a phase-separated spinodal structure by PC-OM analysis, and a distinct scattering halo by SALLS characterization. The interdomain spacing has been characterized by measurement from the PC-OM images and calculation by SALLS. With respect to the mol% of phosphonated monomer, the interdomain spacing decreases greatly with increasing mol% of ionic monomer at low functional monomer concentration (i.e., below 0.0133 mol%), then reaches a plateau in the range of 0.0133-0.233 mol%, and finally undergoes a rapid decline above 0.233 mol%, followed by the loss of a detectable phase morphology. The compatibilization effect of monovalent sulfonate and divalent phosphonate pendant ions has been compared with respect to mol% of ionic monomers and mol% of pendant ions, respectively. The comparison on a mol% of ionic monomers basis demonstrates the Na^+-PPET/PETG/MXD6 blends require 6 times fewer ionic monomers to achieve the same compatibility of polyester/polyamide blends relative to blends compatibilized with the conventional SPET ionomer. On a per mol pendant ion basis, the phosphonate ions have been found to be 3 times more effective at compatibilizing polyester/polyamide blends relative to sulfonate ions. Given the superior compatibilization effect for the divalent phosphonate pendant ions, Na^+-PPET ionomer is an attractive compatibilizer for various polyester/polyamide blend systems. Future systematic investigations will be focused on the compatibilization of polyester/polyamide melt blends using Na^+-PPET ionomer for packaging applications.

6.6 Acknowledgements

The authors gratefully acknowledge the Institute for Advanced Learning and Research (IALR) for providing funds to support the efforts of this project. This material is based, in part, upon work supported by the National Science Foundation under Grant No. DMR-1809291.

6.7 References

1. Iyer, S.; Schiraldi, D. A. Role of Ionic Interactions in the Compatibility of Polyester Ionomers with Poly (ethylene terephthalate) and Nylon 6. J. Polym. Sci. Part B: Polym. Phys. 2006, 44, 2091-2103.
2. Lee, R.; Hutchinson, G.; Farha, S.; Tharmapuram, S. Compatibilized Polyester/Polyamide Blends. U.S. Patent Application No. 10/395,899.
3. Özen, İ.; Bozoklu, G.; Dalgıçdir, C.; Yücel, O.; Ünsal, E.; Çakmak, M.; Menceloğlu, Y. Z. Improvement in Gas Permeability of Biaxially Stretched PET Films Blended with High Barrier Polymers: The Role of Chemistry and Processing Conditions. Eur. Polym. J. 2010, 46, 226-237.
4. Prattipati, V.; Hu, Y.; Bandi, S.; Schiraldi, D.; Hiltner, A.; Baer, E.; Mehta, S. Effect of Compatibilization on the Oxygen-Barrier Properties of Poly (ethylene terephthalate)/Poly (m-xylylene adipamide) Blends. J. Appl. Polym. Sci 2005, 97, 1361-1370.
5. Turner, S. R.; Connell, G. W.; Stafford, S. L.; Hewa, J. D. Polyester-Polyamide Blends with Reduced Gas Permeability and Low Haze. U.S. Patent 6,444,283.
6. Hu, Y.; Prattipati, V.; Mehta, S.; Schiraldi, D.; Hiltner, A.; Baer, E. Improving Gas Barrier of PET by Blending with Aromatic Polyamides. Polymer 2005, 46, 2685-2698.
7. Bell, E. T.; Bradley, J. R.; Long, T. E.; Stafford, S. L. Polyester/Polyamide Blends with Improved Color. U.S. Patent 6,239,233.
8. Prattipati, V.; Hu, Y.; Bandi, S.; Mehta, S.; Schiraldi, D.; Hiltner, A.; Baer, E. Improving the Transparency of Stretched Poly (ethylene terephthalate)/Polyamide Blends. J. Appl. Polym. Sci 2006, 99, 225-235.
9. Lundberg, R. D. 12 Elastomers and Fluid Applications. Ionomers: Synthesis, Structure, Properties and Applications 1997, 477.
10. Tant, M. R.; Mauritz, K. A.; Wilkes, G. L. Ionomers: Synthesis, Structure, Properties and Applications. Springer Science & Business Media: 2012.
11. Zhang, L.; Brostowitz, N. R.; Cavicchi, K. A.; Weiss, R. Perspective: Ionomer Research and Applications. Macromol. React. Eng. 2014, 8, 81-99.
12. Boykin, T. L.; Moore, R. B. The Role of Specific Interactions and Transreactions on the Compatibility of Polyester Ionomers with Poly (ethylene terephthalate) and Nylon 6, 6. Polym. Eng. Sci 1998, 38, 1658-1665.

13. Dutta, D.; Weiss, R.; He, J. Compatibilization of Blends Containing Thermotropic Liquid Crystalline Polymers with Sulfonate Ionomers. Polymer 1996, 37, 429-435.
14. Eisenberg, A.; Hara, M. A Review of Miscibility Enhancement via Ion-Dipole Interactions. Polym. Eng. Sci 1984, 24, 1306-1311.
15. Rajagopalan, P.; Kim, J. S.; Brack, H. P.; Lu, X.; Eisenberg, A.; Weiss, R.; Risen Jr, W. M. Molecular Interpretation of Miscibility in Polyamide-6 Blends with Alkali Ionomers of Sulfonated Polystyrene. J. Polym. Sci. Part B: Polym. Phys. 1995, 33, 495-503.
16. Feng, Y.; Weiss, R.; Karim, A.; Han, C.; Ankner, J. F.; Kaiser, H.; Peiffer, D. G. Compatibilization of Polymer Blends by Complexation. 2. Kinetics of Interfacial Mixing. Macromolecules 1996, 29, 3918-3924.
17. Hara, M.; Eisenberg, A. Miscibility Enhancement via Ion-Dipole Interactions. 1. Polystyrene Ionomer/Poly (Alkylene Oxide) Systems. Macromolecules 1984, 17, 1335-1340.
18. Gemeinhardt, G. C.; Moore, A. A.; Moore, R. B. Influence of Ionomeric Compatibilizers on the Morphology and Properties of Amorphous Polyester/Polyamide Blends. Polym. Eng. Sci 2004, 44, 1721-1731.
19. Sullivan, M.; Weiss, R. Characterization of Blends of An Amorphous Polyamide with Lightly Sulfonated Polystyrene Ionomers. Polym. Eng. Sci 1992, 32, 517-523.
20. Samios, C. K.; Kalfoglou, N. K. Compatibilization of Poly (ethylene terephthalate)/Polyamide-6 Alloys: Mechanical, Thermal and Morphological Characterization. Polymer 1999, 40, 4811-4819.
21. Ng, C.-W. A.; MacKnight, W. J. Ionomeric Blends of Poly (ethyl acrylate-co-4-vinylpyridine) with Metal-Neutralized Sulfonated Poly (ethylene terephthalate). 4. Effects of Counterions. Macromolecules 1996, 29, 2421-2429.
22. Feng, Y.; Schmidt, A.; Weiss, R. Compatibilization of Polymer Blends by Complexation. 1. Spectroscopic Characterization of Ion−Amide Interactions in Ionomer/Polyamide Blends. Macromolecules 1996, 29, 3909-3917.
23. Goh, S.; Lee, S.; Zhou, X.; Tan, K. X-ray Photoelectron Spectroscopic Studies of Interactions between Poly (4-vinylpyridine) and Poly (styrenesulfonate) Salts. Macromolecules 1998, 31, 4260-4264.
24. Lu, X.; Weiss, R. Specific Interactions and Miscibility of Blends of Poly (ε-caprolactam) and Sulfonated PEEK Ionomer. J. Polym. Sci. Part B: Polym. Phys. 1996, 34, 1795-1807.
25. Wu, Q.; Weiss, R. Viscoelastic Properties of Poly (styrene-co-vinylphosphonate) Ionomers. Polymer 2007, 48, 7558-7566.
26. Zhuang, H.; Pearce, E. M.; Kwei, T. Self-association in Poly (styrene-co-4-vinylbenzenephosphonic acid) and Miscibility of its Blends. Polymer 1995, 36, 2237-2241.
27. Ju, L.; Pretelt, J.; Chen, T.; Dennis, J. M.; Heifferon, K. V.; Baird, D. G.; Long, T. E.; Moore, R. B. Synthesis and Characterization of Phosphonated Poly (ethylene terephthalate) Ionomers. Polymer 2018, 151, 154-163.

28. Orler, E. B.; Moore, R. B. Influence of Ionic Interactions on the Crystallization of Lightly Sulfonated Syndiotactic Polystyrene Ionomers. Macromolecules 1994, 27, 4774-4780.
29. Stein, R.; Misra, A. Morphological Studies on Polybutylene Terephthalate. J. Polym. Sci. Part B: Polym. Phys. 1980, 18, 327-342.
30. Hanes, M. D. Blends of Poly (ethylene terephthalate) and Monovinylarene/Conjugated Diene Block Copolymers. U.S. Patent 5,756,578.
31. Landis, F. A.; Moore, R. B. Blends of a Perfluorosulfonate Ionomer with Poly (vinylidene fluoride): Effect of Counterion Type on Phase Separation and Crystal Morphology. Macromolecules 2000, 33, 6031-6041.
32. Nishimoto, M.; Keskkula, H.; Paul, D. Role of Slow Phase Separation in Assessing the Equilibrium Phase Behaviour of PC-PMMA Blends. Polymer 1991, 32, 272-278.
33. Yang, J. C.; Kyu, T. Kinetics of Phase Separation of Nafion Perfluorinated Ionomer and Poly (vinylidene fluoride) Blends. Macromolecules 1990, 23, 182-186.
34. Kyu, T.; Yang, J. C. Miscibility Studies of Perfluorinated Nafion Ionomer and Poly (vinylidene fluoride) Blends. Macromolecules 1990, 23, 176-182.
35. Stein, R. S.; Rhodes, M. B. Photographic Light Scattering by Polyethylene Films. J. Appl. Phys. 1960, 31, 1873-1884.
36. Hashimoto, T.; Izumitani, T. Effect of A Block Copolymer on the Kinetics of Spinodal Decomposition of Polymer Blends. 1. Nonuniversality in Scaled Characteristic Quantities versus Reduced Time. Macromolecules 1993, 26, 3631-3638.
37. Lu, X.; Weiss, R. Development of Miscible Blends of Polyamide-6 and Manganese Sulfonated Polystyrene Using Specific Interactions. Macromolecules 1991, 24, 4381-4385.
38. Pike, S. J.; Hutchinson, J. J.; Hunter, C. A. H-Bond Acceptor Parameters for Anions. J. Am. Chem. Soc. 2017, 139, 6700-6706.
39. Feng, Y.; Weiss, R.; Han, C. Compatibilization of Polymer Blends by Complexation. 3. Structure Pinning during Phase Separation of Ionomer/Polyamide Blends. Macromolecules 1996, 29, 3925-3930.
40. Tucker, R.; Han, C. C.; Dobrynin, A. V.; Weiss, R. A. Small-Angle Neutron Scattering Analysis of Blends with Very Strong Intermolecular Interactions: Polyamide/Ionomer Blends. Macromolecules 2003, 36, 4404-4410.
41. Eisenberg, A.; Hird, B.; Moore, R. A New Multiplet-Cluster Model for the Morphology of Random Ionomers. Macromolecules 1990, 23, 4098-4107.

6.8 Supporting Information

Table S6.1. Summary of thermal properties for blends compositions, along with PETG, MXD6, and 0.5Na^+-PPET.

Materials and Compositions		Heating			Cooling	
		T_g (°C)	T_m(°C)	ΔH_m (J g^{-1})	T_c(°C)	ΔH_c (J g^{-1})
	PETG	84.0	-	-	-	-
	0.5Na^+-PPET	81.6	245.0	33.1	196.9	33.5
	MXD6	84.2	236.5	53.9	159.3	18.0
Blends	75(0.000)/25	84.5	234.0	12.9	147.5	7.0
	75(0.00333)/25	84.7	234.3	9.7	168.7	4.0
	75(0.00667)/25	84.5	233.8	13.5	175.1	8.8
	75(0.0133)/25	83.7	234.0	13.7	173.1	7.3
	75(0.0333)/25	85.0	234.1	11.7	160.7	5.7
	75(0.0667)/25	85.0	233.8	11.8	166.4	5.9
	75(0.100)/25	83.8	233.4, 245.1	16.6	176.6	1.2
	75(0.167)/25	83.4	233.5, 244.7	14.7	170.9	5.1
	75(0.233)/25	81.6	231.1, 244.7	19.9	168.8	9.8
	75(0.300)/25	84.2	233.8, 243.9	18.0	183.8	15.3
	75(0.400)/25	78.5, 87.3	243.2	22.7	176.8	18.2

Heating: Second heating with a hearting rate of 10 °C/min after quench cooling (-60 °C/min) from 270 °C. Cooling: Subsequent cooling with a cooling rate of -10 °C/min after heating to 270 °C. -: not applicable.

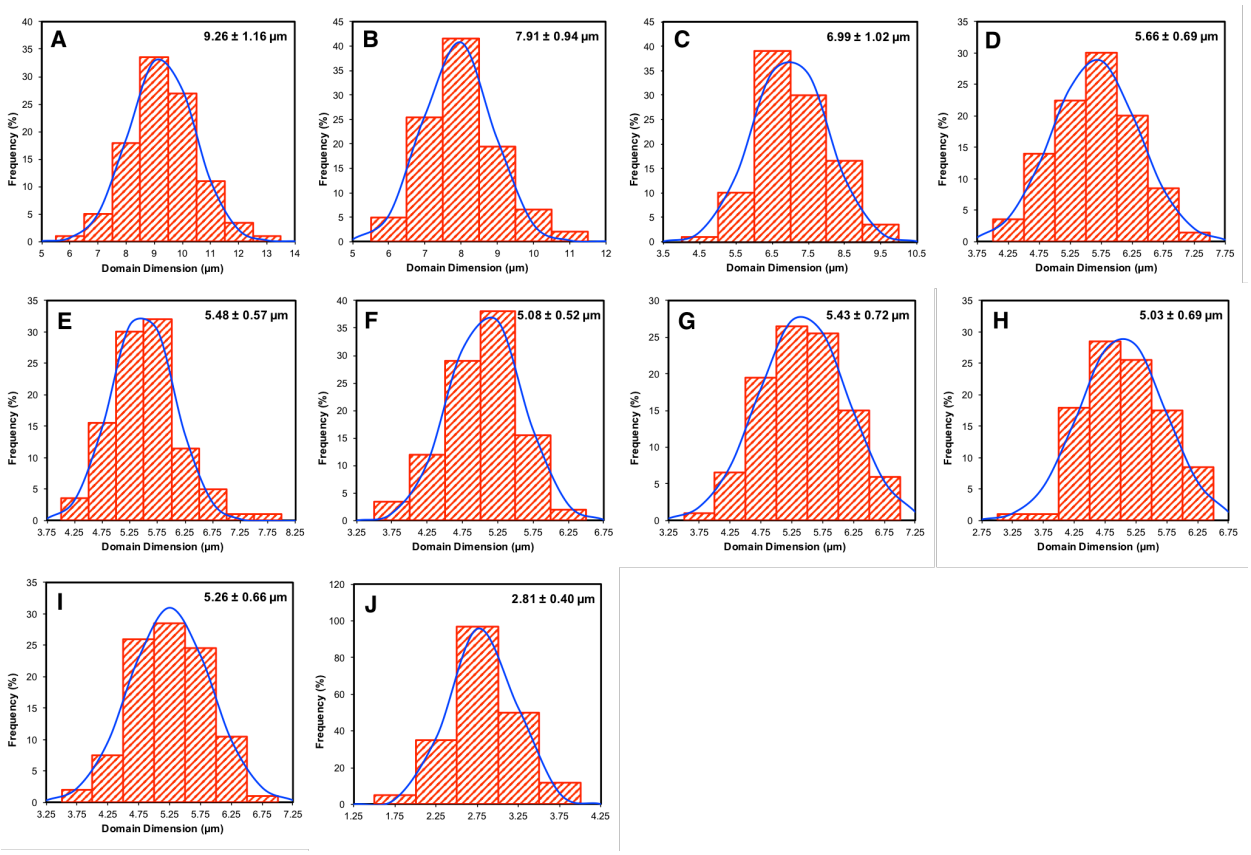

Figure S6.1. Interdomain spacing distribution (histogram and Gaussian fit) from phase contrast optical microscope (PC-OM) measurements for the Na^{+}-PPET/PETG/MXD6 blends. The mean ± σ values are indicated in each panel and are based on 200 measurements. (A) 75(0.000)/25; (B) 75(0.00333)/25; (C) 75(0.00667)/25; (D) 75(0.0133)/25; (E) 75(0.0333)/25; (F) 75(0.0667)/25; (G) 75(0.100)/25; (H) 75(0.167)/25; (I) 75(0.233)/25; (J) 75(0.240)/25.

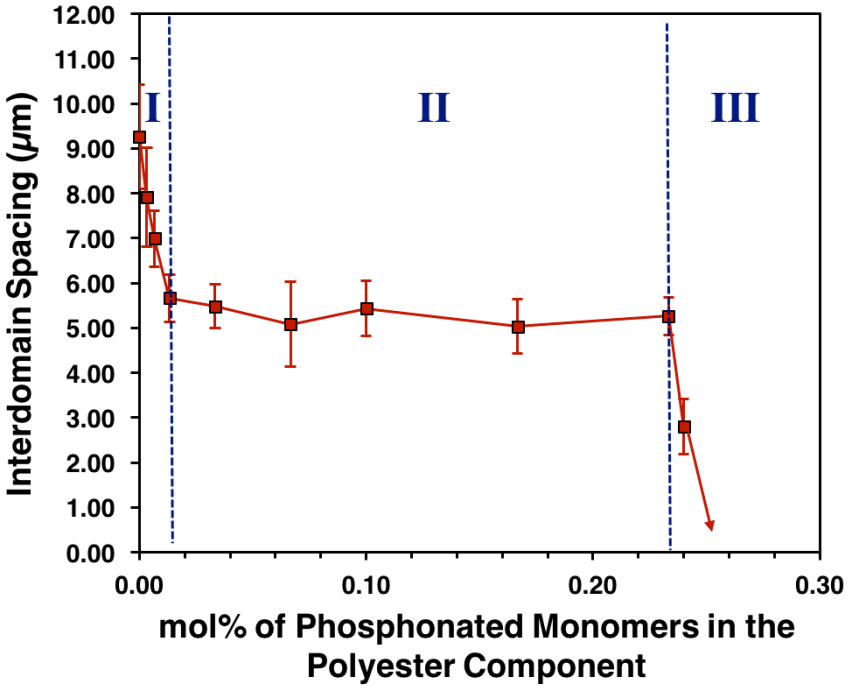

Figure S6.2. Average interdomain spacing of the Na^+-PPET/PETG/MXD6 blends measured from PC-OM images as a function of phosphonated monomer concentration in the polyester component. Region I: below 0.0133 mol%, where domain size rapidly decreases; Region II: 0.0133 mol% - 0.233 mol%, where domain size remains relatively constant; Region III: above 0.233 mol%, where rapid loss of scattering is observed.

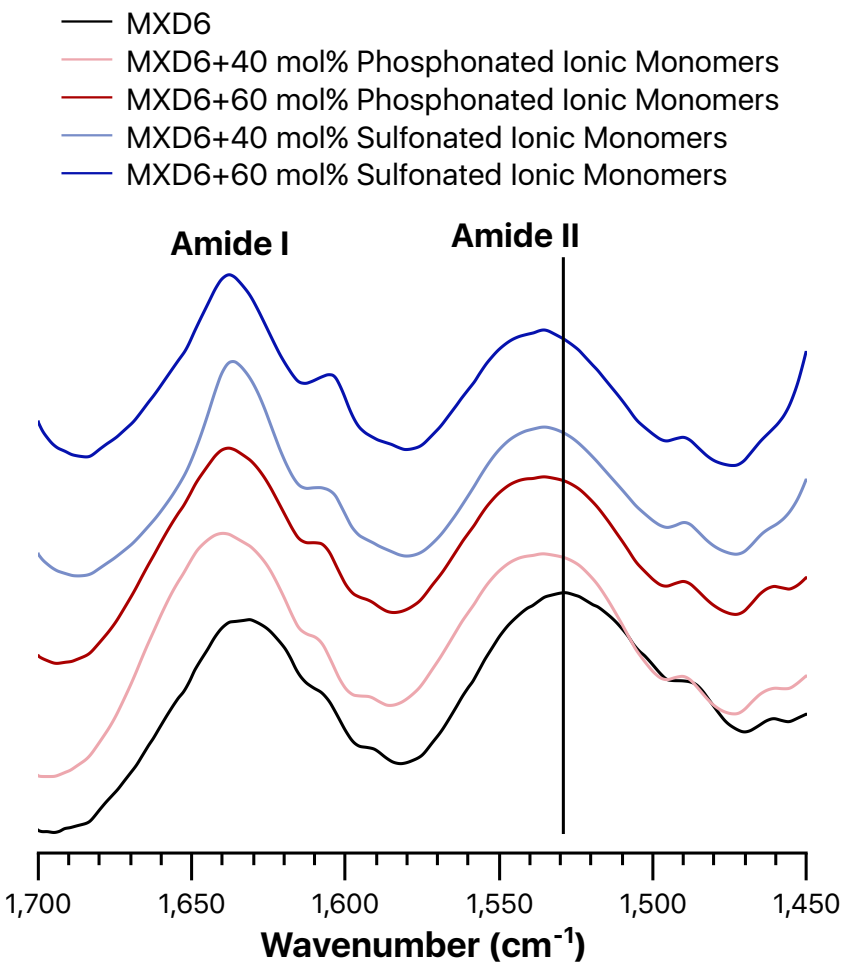

Figure S6.3. FTIR spectra of MXD6 (solid black), MXD6+40 mol% phosphonated ionic monomers (solid light red), MXD6+60 mol% phosphonated ionic monomers (solid red), MXD6+40 mol% sulfonated ionic monomers (solid light blue), MXD6+60 mol% sulfonated ionic monomers (solid blue). Test temperature: room temperature. "mol% of ionic monomers" are designated as mol% to amide monomer units.

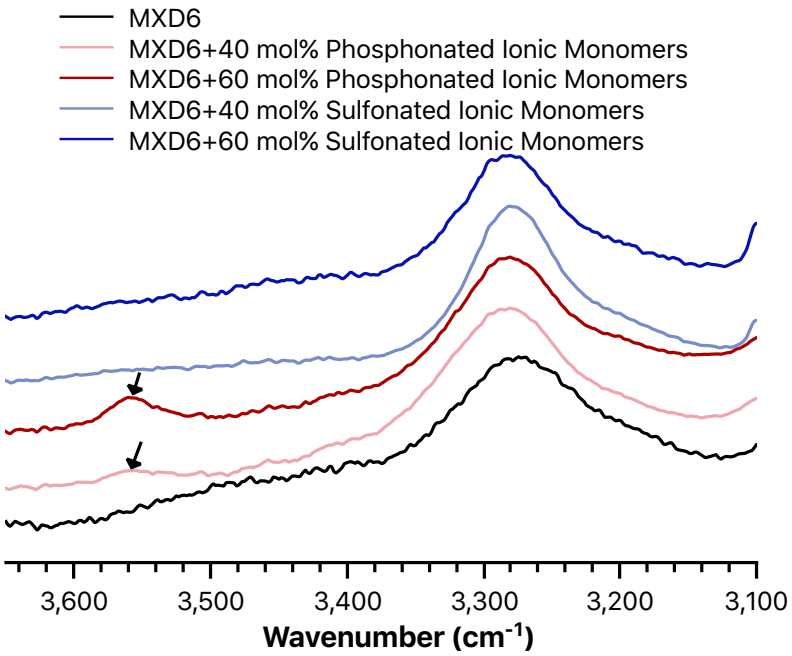

Figure S6.4. FTIR spectra of MXD6 (solid black), MXD6+40 mol% phosphonated ionic monomers (solid light red), MXD6+60 mol% phosphonated ionic monomers (solid red), MXD6+40 mol% sulfonated ionic monomers (solid light blue), MXD6+60 mol% sulfonated ionic monomers (solid blue). Test temperature: room temperature. "mol% of ionic monomers" are designated as mol% to amide monomer units.

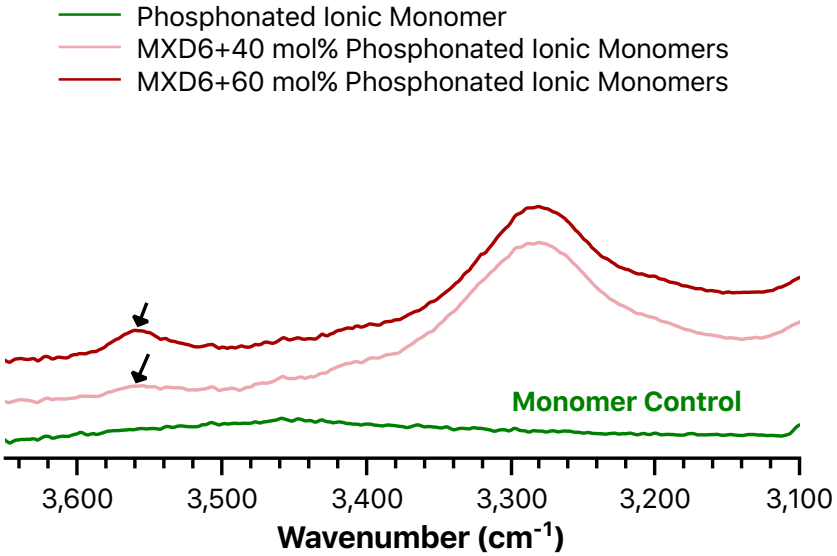

Figure S6.5. FTIR spectra of phosphonated ionic monomer (solid green), MXD6+40 mol% phosphonated ionic monomers (solid light red), MXD6+60 mol% phosphonated ionic monomers (solid red). Test temperature: room temperature. "mol% of ionic monomers" are designated as mol% to amide monomer units.

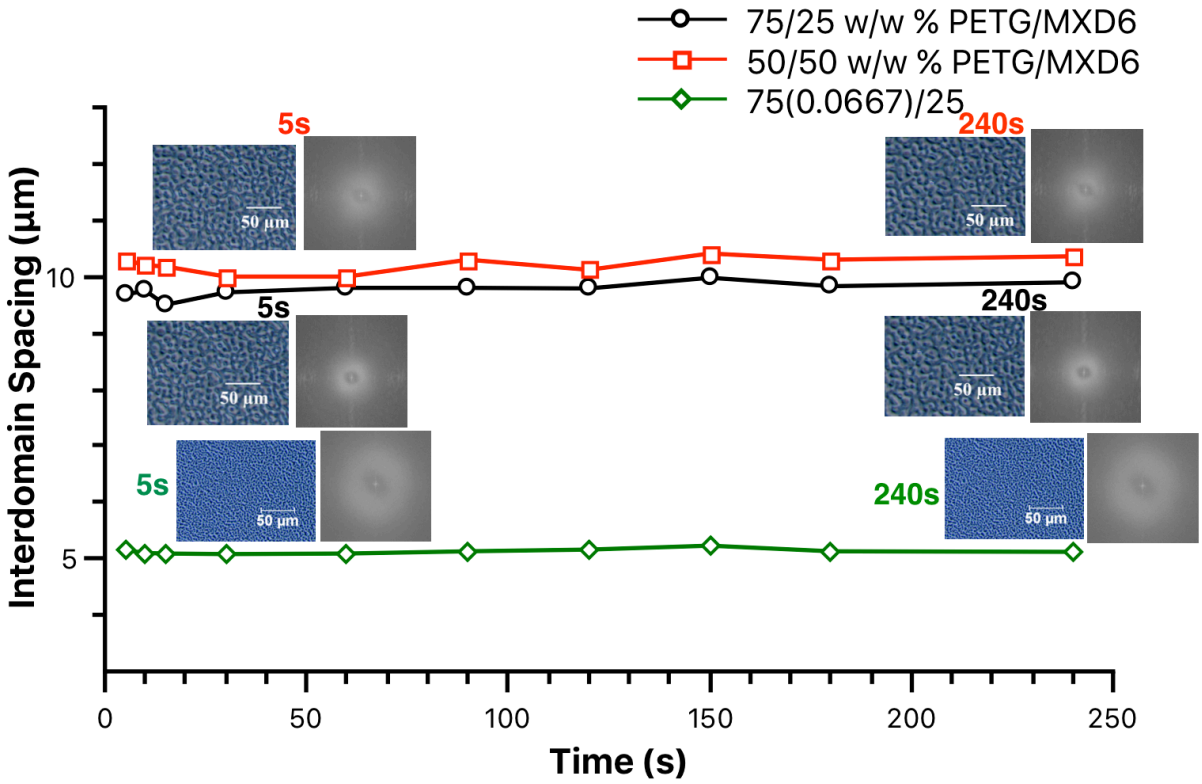

Figure S6.6. Interdomain spacing vs. time (from 5 s to 240 s) for base blends (uncompatibilized) of 75/25 (w/w %) PETG/MXD6 (black solid line with circular symbols), 50/50 (w/w %) PETG/MXD6 (red solid line with square symbols), and the compatibilized blend of 75(0.0667)/25 (green solid line with rhombus symbols) at 240 °C. Microscopic images were analyzed using 2D Fast Fourier Transform (FFT) from Image J. The corresponding 2D FFT power spectrum is shown on the right of microscopic image.

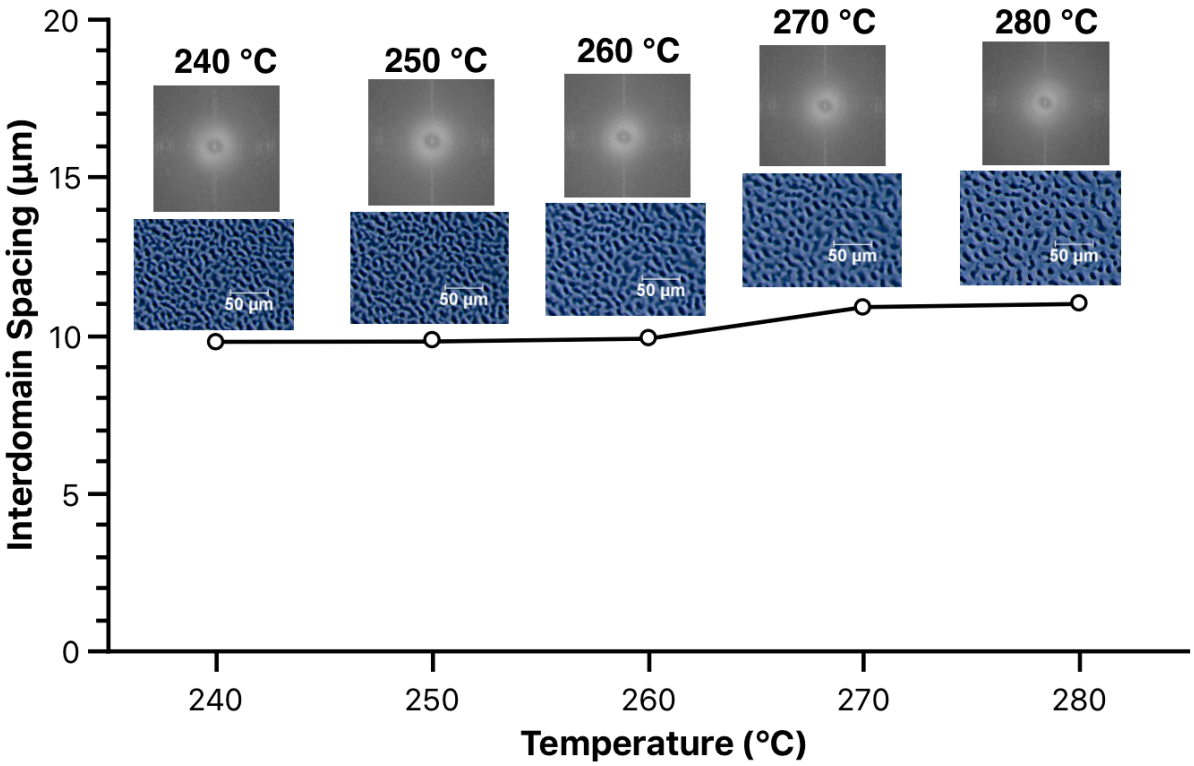

Figure S6.7. Interdomain spacing vs. temperature (from 240 °C to 280 °C) for the base blend (uncompatibilized) of 75/25 (w/w %) PETG/MXD6. Microscopic images were collected after equilibrating at each temperature for 2 min, and analyzed using 2D Fast Fourier Transform (FFT) from Image J. The corresponding 2D FFT power spectrum is shown near the microscopic image.

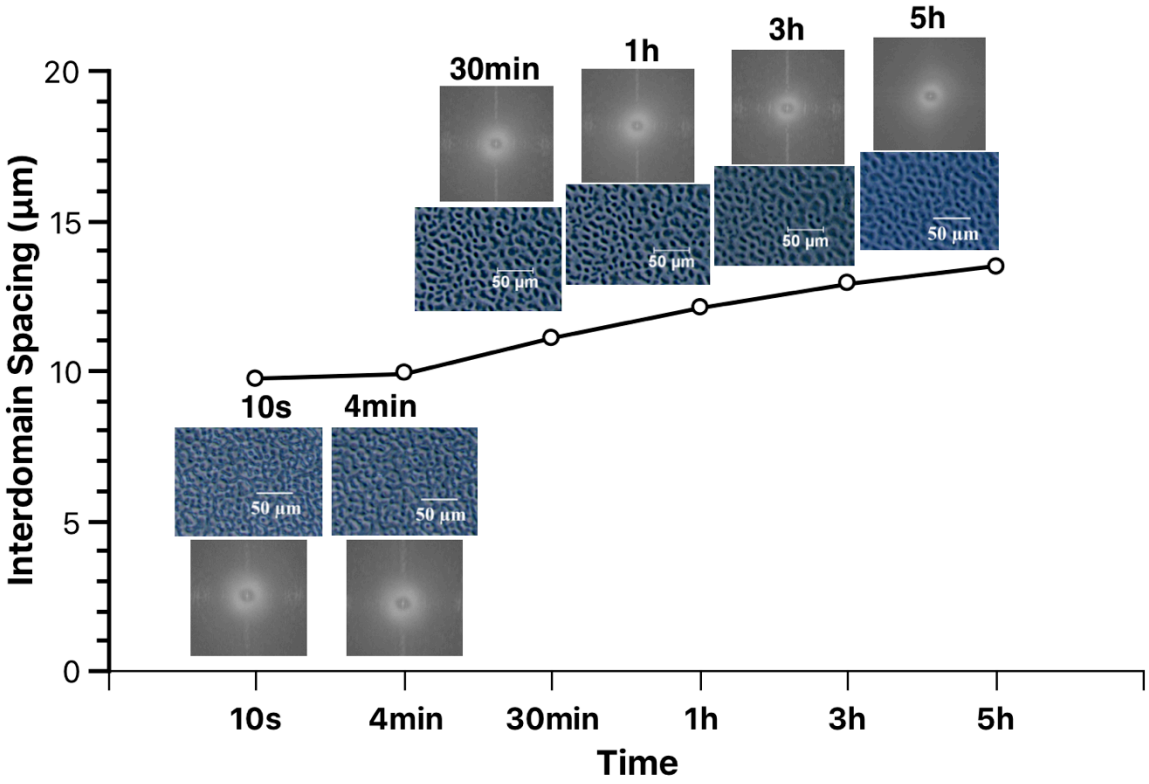

Figure S6.8. Interdomain spacing vs. time (from 10 s to 5 h) for the base blend (uncompatibilized) of 75/25 (w/w %) PETG/MXD6 at 240 °C. Microscopic images were analyzed using 2D Fast Fourier Transform (FFT) from Image J. The corresponding 2D FFT power spectrum is shown near the microscopic image.

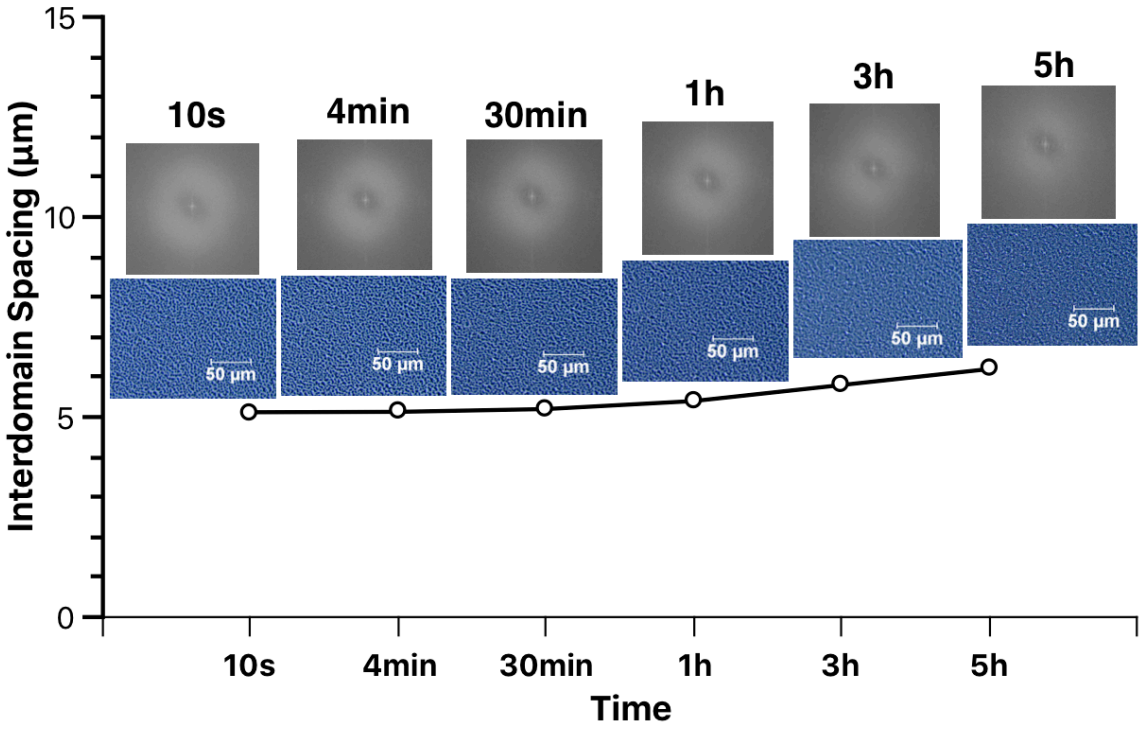

Figure S6.9. Interdomain spacing vs. time (from 10 s to 5 h) for the compatibilized blend of 75(0.0667)/25 at 240 °C. Microscopic images were analyzed using 2D Fast Fourier Transform (FFT) from Image J. The corresponding 2D FFT power spectrum is shown near the microscopic image.

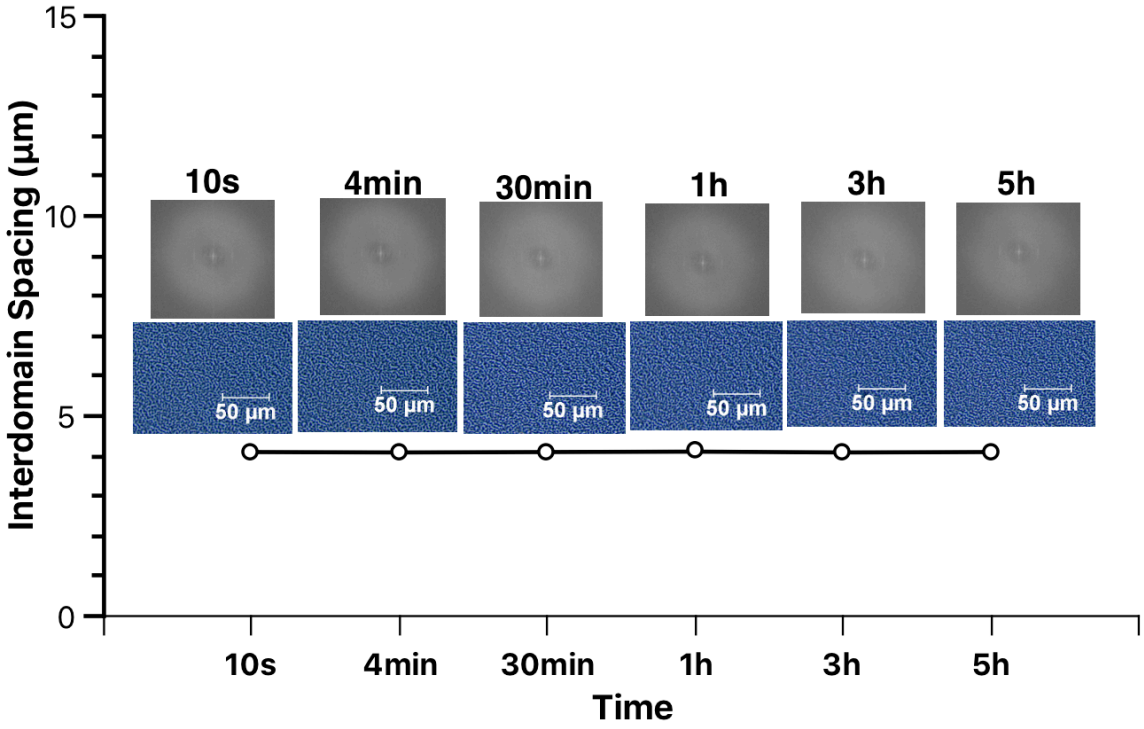

Figure S6.10. Interdomain spacing vs. time (from 10 s to 5 h) for the compatibilized blend of 75(0.233)/25 at 240 °C. Microscopic images were analyzed using 2D Fast Fourier Transform (FFT) from Image J. The corresponding 2D FFT power spectrum is shown near the microscopic image.

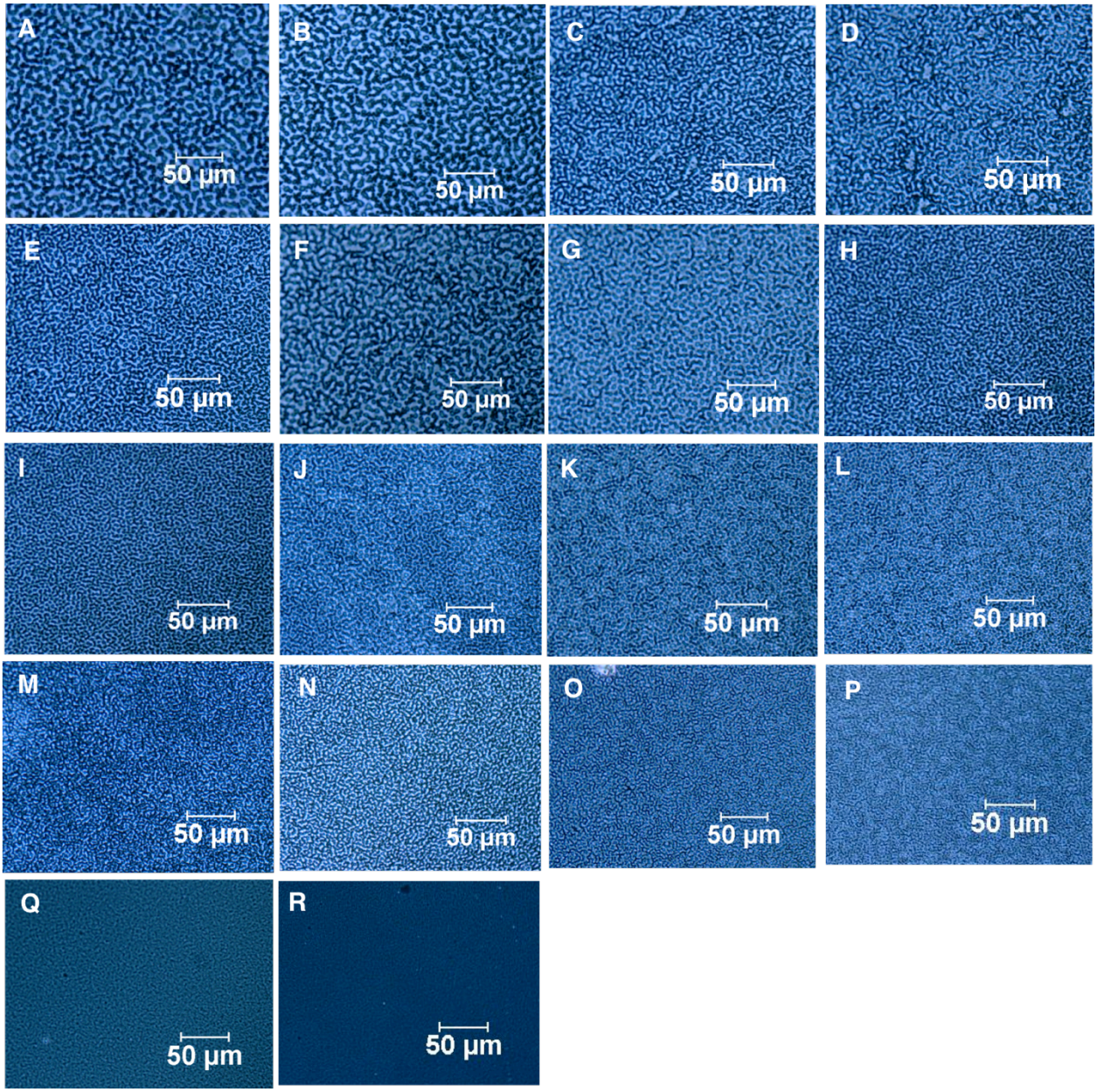

Figure S6.11. Phase contrast optical microscopy (PC-OM) images for the Na^+-SPET/PETG/MXD6 blends. (A) 75(0.000)/25; (B) 75(0.00333)/25; (C) 75(0.00667)/25; (D) 75(0.0133)/25; (E) 75(0.0333)/25; (F) 75(0.0667)/25; (G) 75(0.100)/25; (H) 75(0.167)/25; (I) 75(0.233)/25; (J) 75(0.300)/25; (K) 75(0.400)/25; (L) 75(0.600)/25; (M) 75(0.840)/25; (N) 75(1.08)/25; (O) 75(1.44)/25; (P) 75(1.62)/25; (Q) 75(1.680)/25; (R) 75(1.740)/25. Scale bar = 50 µm.

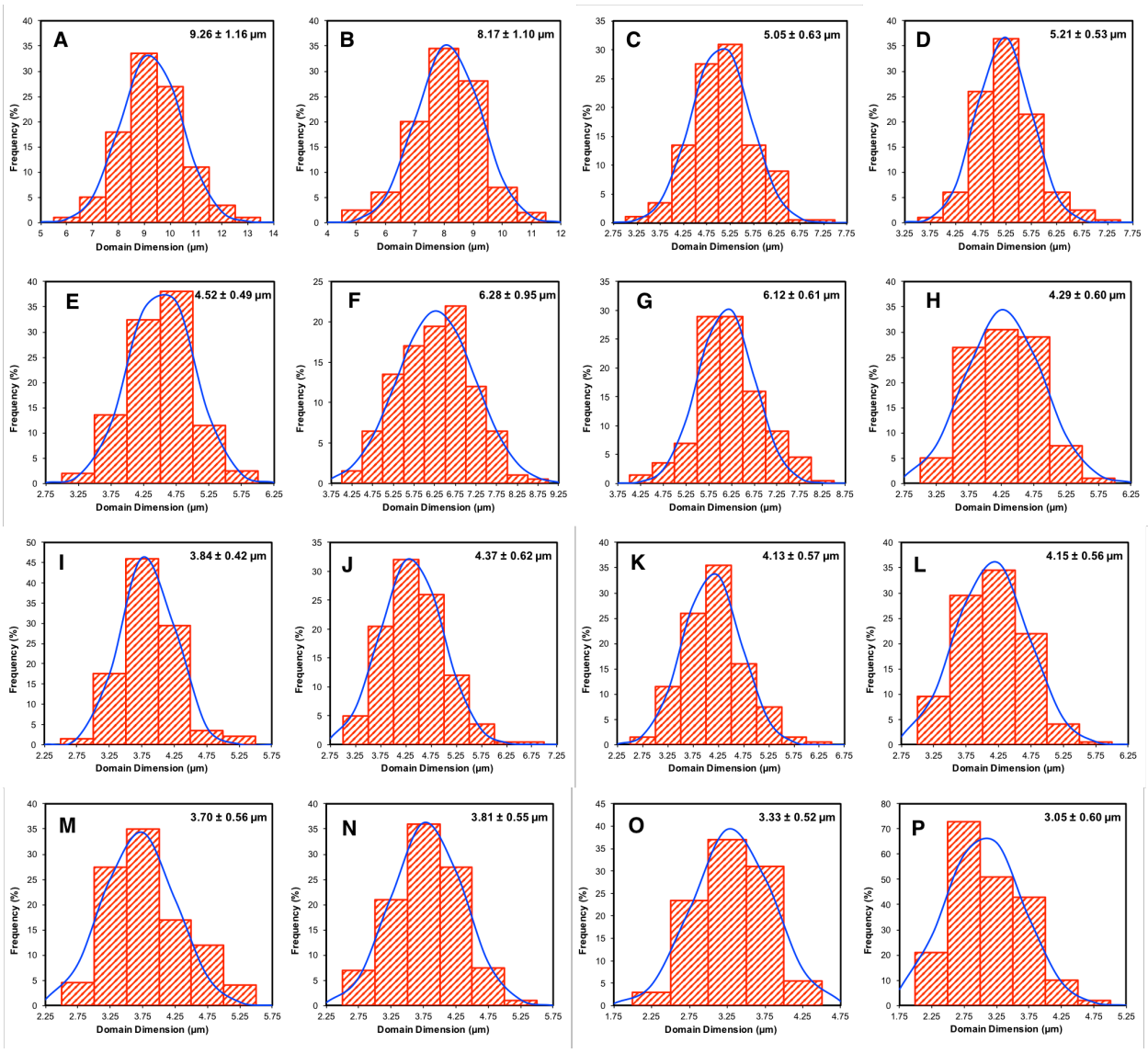

Figure S6.12. Interdomain spacing distribution (histogram and Gaussian fit) from phase contrast optical microscope (PC-OM) measurements for the Na^{+}-SPET/PETG/MXD6 blends. The mean ± σ values are indicated in each panel and are based on 200 measurements. (A) 75(0.000)/25; (B) 75(0.00333)/25; (C) 75(0.00667)/25; (D) 75(0.0133)/25; (E) 75(0.0333)/25; (F) 75(0.0667)/25; (G) 75(0.100)/25; (H) 75(0.167)/25; (I) 75(0.233)/25; (J) 75(0.300)/25; (K) 75(0.400)/25; (L) 75(0.600)/25; (M) 75(0.840)/25; (N) 75(1.08)/25; (O) 75(1.44)/25; (P) 75(1.62)/25.

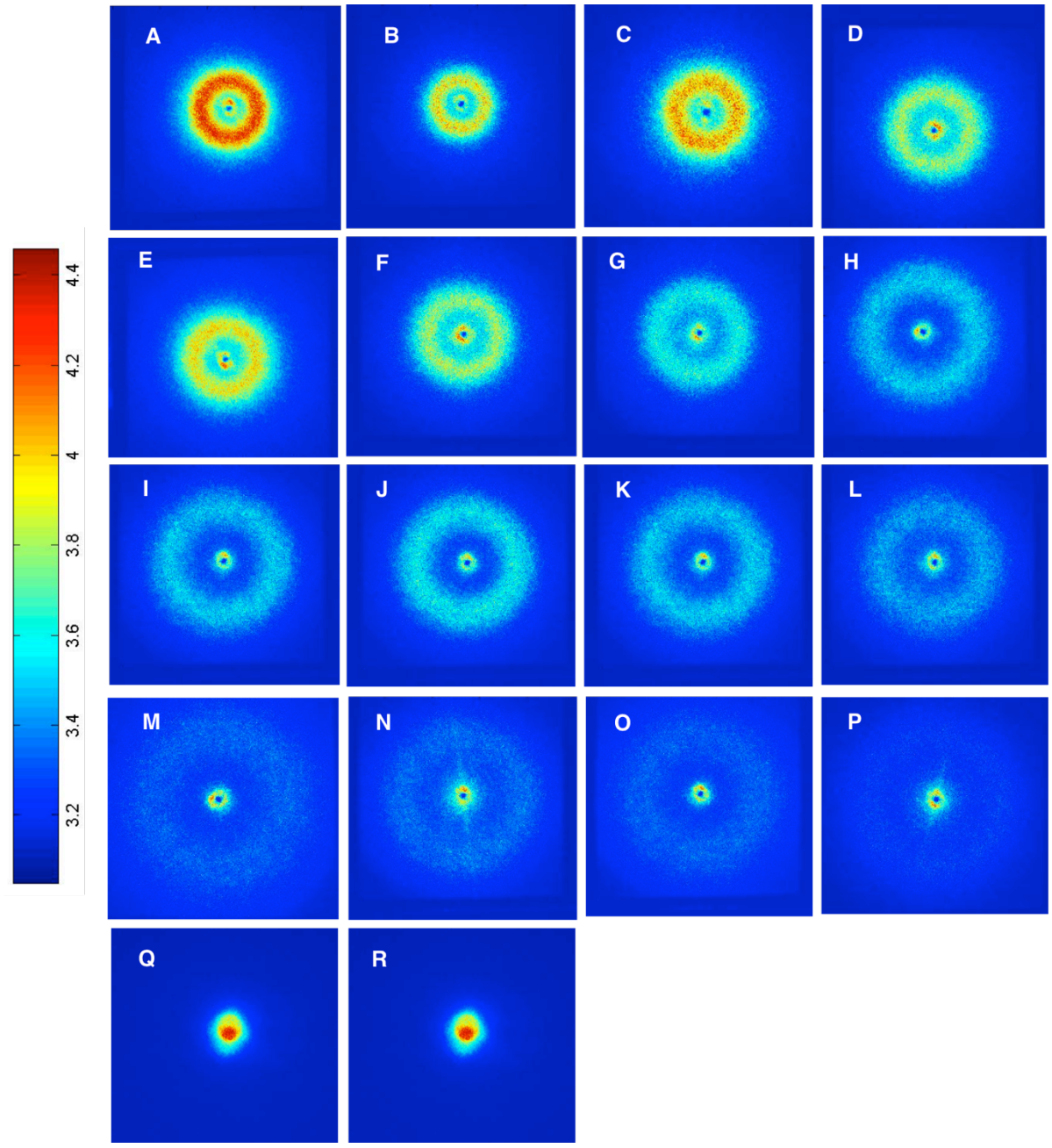

Figure S6.13. V_v small angle laser light scattering (SALLS) patterns of the Na^+-SPET/PETG/MXD6 blends. (A) 75(0.000)/25; (B) 75(0.00333)/25; (C) 75(0.00667)/25; (D) 75(0.0133)/25; (E) 75(0.0333)/25; (F) 75(0.0667)/25; (G) 75(0.100)/25; (H) 75(0.167)/25; (I) 75(0.233)/25; (J) 75(0.300)/25; (K) 75(0.400)/25; (L) 75(0.600)/25; (M) 75(0.840)/25; (N) 75(1.08)/25; (O) 75(1.44)/25; (P) 75(1.62)/25; (Q) 75(1.680)/25; (R) 75(1.740)/25. The sample-to-detector distance (SDD) is 30 cm.

Chapter 7. Phosphonated Poly(ethylene terephthalate) Ionomers as Compatibilizers in Poly(ethylene terephthalate)/Poly(*m*-xylylene adipamide) Blends for Packaging Applications

(Manuscript in Preparation for Publishing in *Polymer*)

Lin Ju,[a,b] Ryan J. Mondschein,[a,b] Johanna A. Vandenbrande,[a,b] Clay B. Arrington,[a,b] Timothy E. Long,[a,b] and Robert B. Moore [a,b,*]

[a]Department of Chemistry, Virginia Polytechnic Institute and State University, Blacksburg, VA 24061, United States

[b]Macromolecules Innovation Institute, Virginia Polytechnic Institute and State University, Blacksburg, VA 24061, United States

7.1 Abstract

Blends of poly(ethylene terephthalate) (PET) and poly(*m*-xylylene adipamide) (MXD6) were successfully compatabilized by using a phosphonated PET ionomer in the Na^+ form (Na^+-PPET) as a minor-component compatibilizer. The compatibilized PET/MXD6 blends containing various amounts of phosphonated ionic monomers in the polyester component were prepared by a melt blending method via a twin screw extruder. Scanning electron microscopy (SEM) revealed that the extruded blends contained spherical MXD6 domains dispersed in the PET matrix. The phase-separated MXD6 domain size decreased with increasing ionic monomer concentration, and the efficient compatibilization was attributed to specific interactions between the ionic phosphonate

groups on the Na^+-PPET ionomer and the amide linkages of MXD6. Thermal analysis suggested that the small MXD6 domains nucleated the crystallization of PET upon cooling as indicated by a shift of crystallization temperature of PET to higher temperatures. Furthermore, the specific interactions appeared to inhibit crystallization of MXD6. Biaxial orientation with a draw ratio of 3 × 3 transformed the spherical MXD6 domains into platelets with a high aspect ratio that were oriented in the plane of the film. Compared to the uncompatibilized base blends, optical property characterization on the oriented blends revealed a decreased haziness by 56% and an improved transparency by 35% with 0.22 mol% of phosphonated ionic monomers incorporated in the polyester component. Moreover, a 33% decrease of oxygen permeability was found for the oriented Na^+-PPET/PET/MXD6 blend composition containing 0.11 mol% of phosphonated monomers.

7.2 Introduction

Poly(ethylene terephthalate) (PET) is a widely used material in the packaging industry due to its desirable toughness, clarity, and cost.[1] The oxygen barrier properties of PET are acceptable for many food and beverage products (e.g., water, carbonated drinks, etc.), but do not meet the stringent requirements for packaging highly oxygen-sensitive products (e.g., beer, juices, fruit-based drinks, etc.).[2] Aromatic polyamides, such as poly(*m*-xylyene adipamide) (MXD6), show superior oxygen barrier properties, but a much higher cost compared to that of PET. Thus, blending PET with a small amount of MXD6 provides a route to effectively reduce the inherent oxygen permeability of the PET matrix.[3-11]

The broad application of polyester/polyamide blends in gas barrier packaging, however, is often limited by poor optical properties attributed to the thermodynamic immiscibility between the two dissimilar polymers.[6, 11-17] Unoriented PET/MXD6 blends have good transparency because the refractive indices of PET and MXD6 are closely matched.[13, 16] However, most PET packaging applications require oriented films, and the desirable gas barrier properties, attributed to a tortuous gas transport pathway, are only realized when the MXD6 phases are drawn and oriented in a planar geometry. Unfortunately, haze is generally observed when films of PET/MXD6 blends are oriented because stretching imparts greater refractive index anisotropy to PET than to MXD6, thereby resulting in a refractive index mismatch between PET and MXD6.[13] For example, blow-molded blends containing only 0.5 wt% MXD6 in a polyester consisting of terephthalic acid with 98-99 mol% ethylene glycol and 1-2 mol% 1,4-cyclohexanedimethanol have been reported to show an increase in haze by 71% (i.e., from 0.7% to 1.2%) compared to that of pure polyester.[17] Moreover, the haziness in immiscible polymer blends has been proven to depend on the size of the dispersed phase.[15] As the dispersed polyamide dimension increases, haze also increases. Therefore, efforts to compatibilize polyester/polyamide blends to significantly reduce the domain dimension of the minor polyamide phase within the polyester matrix have remained a priority in the field.

The incorporation of PET-based ionomers as minor-component compatibilizers in a number of immiscible polymer blend systems has attracted significant attention due to strong specific interactions that may develop between the ionic groups and complementary functional groups on the other polar polymers within the blends.[18-23]

These specific interactions tend to decrease the interfacial tension between the dissimilar polymers, leading to reduced phase dimensions.[24-26] Consequently, sulfonated poly(ethylene terephthalate) ionomers in the Na^+ form (Na^+-SPET) have been widely utilized as an efficient compatibilizer in melt-mixed immiscible polyester/polyamide blends.[3, 8, 10, 14, 24, 27, 28]

In PET/MXD6 blends, incorporation of a very small amount of sodium sulfoisophthalate ionic monomer into the PET matrix can effectively compatibilized the blend, leading to a significant reduction in MXD6 domain size. For example, Prattipati et al. showed that with only 0.13 mol% of sulfonated ionic monomer in a PET matrix, the MXD6 domain diameters in melt-extruded PET/MXD6 (90/10 w/w) blends diminished to approximately 0.1-0.7 μm, whereas the average domain diameter for base blends without compatibilizer was around 2 μm.[10] Özen et al. investigated the compatibilization of poly(ethylene terephthalate-*co*-isophthalate) copolymer/MXD6 (95/5 w/w) blends, and confirmed that only 0.47 wt% of the sulfonated ionic monomer in the blend was needed to significantly decreased the MXD6 domain diameter by 82% compared to the uncompatibilized blend.[27] Similarly, in our earlier work, we demonstrated the enhanced compatibilization of an amorphous polyester/polyamide (PETG 6763/Durethan T40) blend with an amorphous sulfonated polyester ionomer (Na^+-SPETG) as the compatibilizer using melt blending method. Enhanced dispersion of the minor phase (i.e., a much larger number of dispersed droplets) as well as a significant reduction in the dispersed-phase size have been achieved with small increases in the ionomer content.[24] Both specific interactions and transesterification reactions within SPET-compatibilized

polyester/polyamide blends have been demonstrated to play a role in the overall compatibilization process for melt-mixed polyester/polyamide blends.[18]

Compatibilization of PET/MXD6 blends using Na^+-SPET ionomers not only improves transparency, but is also capable of enhancing oxygen barrier properties of biaxially oriented blend films. Haziness depends upon the dispersed-phase dimension when the domain size is comparable or greater than the wavelength of visible light.[15] For biaxially oriented blend films, reduced haziness can be achieved in ionomer-compatibilized PET/MXD6 blends as a result of significantly decreased MXD6 domain dimensions, which adequately counters the refractive index mismatch upon orientation.[3, 16, 29] Biaxially oriented, Na^+-SPET ionomers-compatibilized blends have also been demonstrated to exhibit lower oxygen permeability in comparison to the uncompatibilized blend.[5, 8, 10, 27] For example, Prattipati et al. investigated the effect of a sulfonated PET compatibilizer on the oxygen barrier properties of biaxially oriented PET/MXD6 blends (90/10 w/w), and demonstrated that just 0.38 mol% of sulfonated ionic monomers incorporated into the PET matrix decreased oxygen permeability by 42% compared to the oriented, uncompatibilized blend.[10] Biaxial orientation transformed the relatively impermeable spherical MXD6 domains in unoriented films into platelets of a high aspect ratio that were oriented parallel to the direction of gas flux. This reduced permeability in the oriented, compatibilized was attributed to an increased tortuosity of the diffusion pathway due to an enhanced number of small impermeable MXD6 platelets with high surface area that act as passive gas barriers.

As an alternative to sulfonated PET, we recently synthesized phosphonated PET ionomers in the Na^+-form (Na^+-PPET) by a melt polycondensation reaction,[30] and

demonstrated the successful compatibilization of immiscible amorphous polyester (PETG 6763) and MXD6 in solution-mixed blends using the Na^+-PPET ionomers as compatibilizers.[25] By investigating the effectiveness of divalent phosphonate pendant ion versus monovalent sulfonate pendant ion on the compatibility of PETG/MXD6 blends, we confirmed that Na^+-PPET/PETG/MXD6 blends required 6 times fewer ionic monomers to achieve domain dimension <1 μm as compared to Na^+-SPET-containing PETG/MXD6 blends. This implies that the superior compatibilization with Na^+-PPET requires less ionic monomers to achieve the same compatibility of polyester/polyamide blends than that of the conventional Na^+-SPET-compatibilized blends. The divalent phosphonate groups generate stronger specific interactions per functional monomer unit as compared to the monovalent sulfonate pendant ions, and consequently a more effective compatibilization in polyester/polyamide blends. Given the superior compatibilization effect for the divalent phosphonate pedant ions, it is of great interest to expand the practical applications of this Na^+-PPET ionomer in PET/MXD6 blends using conventional melt-extrusion processing.

In this work, we report the first investigation of the compatibilization of PET/MXD6 blends using the Na^+-PPET ionomer as a minor-component compatibilizer via a melt-mixing method for packaging applications. The purpose of this research is to provide both fundamental and practical understandings of the compatibilization effect on the properties, including morphological, thermal, optical, and oxygen barrier properties, of the melt-blended PET/MXD6 blends, and to evaluate the potential of Na^+-PPET ionomer-compatibilized PET/MXD6 blends for future packaging applications. Scanning electron microscopy (SEM) was used to study the phase-separated morphology, and

differential scanning calorimetry (DSC) was used to probe the phase-separated MXD6 domain size on the crystallization behavior of these compatibilized PET/MXD6 blends. Since most PET bottles are manufactured by injection stretch blow molding, biaxial orientation was performed on unoriented blend films to mimic bottle blowing process. Haze, transmittance, and oxygen permeability were measured in order to investigate the compatibilization effect on the optical and oxygen barrier properties of PET/MXD6 blends.

7.3 Experimental Section

Materials. Poly(ethylene terephthalate) (PET) (Eastar^{TM} Polyester MN052) was obtained from Eastman Chemical Company and poly(*m*-xylylene adipamide) (MXD6) was supplied by Mitsubishi Gas Chemical Company. Phosphonated poly(ethylene terephthalate) ionomer in Na^+-form (Na^+-PPET) with 2.0 mol% 5-phosphoisophthalate units randomly distributed along the polymer chain (2.0PPET) was synthesized by melt polycondensation reaction as described in our recent publication.[30] The synthesized Na^+-PPET ionomer was grinded into pellets with similar size to PET and MXD6 pellets.

Blends Preparation. PET and Na^+-PPET ionomer were dried in vacuo at 60 °C for 24 h, and MXD6 pellets were dried in vacuo at 80 °C for 24 h to sufficiently remove the absorbed moisture. Pellets of PET, Na^+-PPET, and MXD6 were dry-mixed at the desired blend ratio before extrusion. All blends were prepared by using a co-rotating intermeshing twin screw extruder (Leistritz ZSE-18, L/D = 40, D = 18 mm). Temperature profile of the extruder is shown in **Figure S7.1**. The extrusion process was carried out with a screw rotation speed of 500 rpm and a feed rate of 3.0 kg/h. The residence time

distribution is between 50 s to 150 s. The molten blends were extruded through a 3 mm die, and pelletized after passing through a water bath. The collected pellets were then dried at 30 °C under vacuum for 24 h for further characterizations. The blend compositions were designated as wt% polyester matrix (mol% of phosphonated monomers in the polyester component)/wt% MXD6 (**Table 7.1**).

Table 7.1. Na^+-PPET/PET/MXD6 Blend Compositions.

	Composition[a]	wt% PET	wt% 2.0Na^+-PPET	wt% MXD6	mol% of Ionic Monomer[b]	Stoichiometry[c]
A	90(0.00)/10	90	0	10	0	0
B	90(0.035)/10	88.4	1.6	10	0.035	0.0020
C	90(0.075)/10	86.6	3.4	10	0.075	0.0043
D	90(0.11)/10	85.1	4.9	10	0.11	0.0063
E	90(0.22)/10	80.1	9.9	10	0.22	0.013

[a] Blend compositions are designated as wt% polyester matrix (mol% of phosphonated monomers in the polyester component)/wt% MXD6;
[b] mol% of phosphonated monomers in the polyester component; and
[c] molar ratio of phosphonated monomers to amide units in the MXD6 component.

Compression Molding. Unoriented film samples were prepared by compression molding the blends pellets between two aluminum plates layered with Kapton films using a PHI Q-203H manual hydraulic press. A stainless steel shim, 8 mil thick, was used to control film thickness, and a stepwise process was applied to remove air bubbles. Samples were heated (~3.5 min) at 270 °C before the top aluminum plate was added. After heating at 270 °C for an additional 2 min, four press-release-press cycles with the first two presses utilizing 5 tons of force and the last two presses utilizing 10 tons of force were applied to complete the film pressing procedure. After these four cycles, the plates

and film were removed from the press and quench cooled by immediate submersion in an ice bath to afford free-standing transparent films. The resulted films were dried under vacuum at room temperature overnight before use. The thickness of these films were approximately 140-160 μm.

Biaxial Orientation. Compression-molded films were utilized for biaxial orientation. 5 cm × 5 cm square specimens were marked with a grid pattern (1 cm × 1 cm for each unit). Biaxial orientation was performed on an Instron 5969 machine with a heating chamber. The film was first uniaxially stretched at 81 °C to a draw ratio of 3.5, then remounted in the grips at 90° to the first stretch and stretched again at the same temperature to achieve a balanced 3 × 3 draw ratio for the center unit. This resulted center unit with a dimension of 3 cm × 3 cm after stretching was utilized for oxygen permeability tests. Stretching was performed at a crosshead rate of 5 mm/min. After orientation, the film was rapidly cooled to room temperature.

Scanning Electron Microscopy (SEM). The phase morphology of cryogenically fractured surface for the extruded strands was examined using field-emission scanning electron microscopy (FE-SEM) performed on an LEO Zeiss 1550 at an accelerating voltage of 5 kV. Prior to SEM tests, all specimens were sputter-coated with an iridium coating (5 nm thickness) in a Cressington 208HR high-resolution sputter coater equipped with an MTM-20 thickness controller. Phase separated MXD6 domain diameter was measured using ImageJ. For each blend composition, the mean ± σ value was calculated from 200 measurements by fitting a histogram of the measurements to a Gaussian distribution.

Transmission Electron Microscopy (TEM). The phase morphology of biaxially oriented blend films were examined using TEM on a JEOL JEM-1400 transmission electron microscope with a side-mounted Gatan Orius SC1000 CCD camera. Biaxially oriented films were first sputter coated with gold, and then embedded in epoxy. Microtoming was performed at room temperature using a diamond knife to obtain thin samples about 120 nm thick. The microtomed samples were stained with a 2 wt% phosphotungstic acid (PTA) aqueous solution for 5 min before TEM tests.

Differential Scanning Calorimetry (DSC). A TA Instruments Q2000 DSC was used to determine the thermal transitions and crystallization behavior of Na^+-PPET/PET/MXD6 blends, along with pure PET and pure MXD6. Under a nitrogen atmosphere, samples (~5-8 mg) were subjected to a heat-cool cycle at a heating rate of 10 °C/min, a cooling rate of -10 °C/min, and a temperature range of 0 °C to 270 °C. The glass transition temperature (T_g), cold crystallization temperature (T_{cc}), enthalpy of cold crystallization (ΔH_{cc}), melting temperature (T_m), and enthalpy of melting (ΔH_m) were determined from the initial heating scan, and crystallization temperature (T_c) along with enthalpy of crystallization (ΔH_c) were investigated from the subsequent cooling scan, using the TA Instruments Universal Analysis software.

Haze Measurement. Haze and transmittance of both unoriented and biaxially oriented blend films were measured using BYK Gardner Haze-Gard i (4775) Haze Meter using visible light at room temperature. The presented haze and transmittance for each composition were the average value of five measurements. The thickness of unoriented films is 150 ± 5 μm, and thickness of biaxially oriented films is about 19 ± 1 μm.

Oxygen Permeability Measurement. A Systech Illinois 8001 oxygen permeation analyzer at 23 °C, 1 atm, and 0% relative humidity with an oxygen (purity: 99.993%) flow of 20 cm^3/min and a nitrogen (purity: 99.999%) flow of 10 cm^3/min was utilized to measure oxygen transmission rate (OTR). Permeability was calculated from the steady-state flux (J_0) according to **Equation 7.1**:[10]

$$P = (J_0 l)/p \tag{7.1}$$

where l is the film thickness, and p is the oxygen pressure. Only one measurement was performed on each unoriented blend film, and three films were tested for each biaxially oriented blend to obtain the average permeability.

Tensile Test. Tensile test was performed to determine the Young's modulus and yield stress of the unoriented Na^+-PPET/PET/MXD6 blends, displayed in **Figure S7.4 and Table S7.1**. Dumbbell-shaped specimens were cut from compression-molded films. The specimens were clamped in the tensile fixture with a distance between grips of 26.54 mm, and the width of narrow section of 3.32 mm. The thicknesses of these specimens were accurately measured for each sample using a calibrated caliper, and were approximately ranging from 140 μm to 160 μm. Tensile testing was performed on a 5500R Instron universal testing instrument at a crosshead speed of 5 mm/min. The Young's moduli and yield stress are reported on an average of ten specimens.

7.4 Results and Discussion

7.4.1 Morphological Analysis. The compatibilization effect of Na^+-PPET ionomers on the phase behavior of PET/MXD6 blends was investigated using scanning electron microscopy (SEM). The SEM micrographs of cryogenically fractured surface for

extruded Na^+-PPET/PET/MXD6 blends with various amounts of phosphonate groups in the polyester matrix are shown in **Figure 7.1**. The blend of PET and MXD6 without compatibilizer is termed the base blend in this study. The base blend, with MXD6 as the minor component (i.e., 10 wt%) and PET as the major component (i.e., 90 wt%), exhibits phase-separated morphology with spherical MXD6 domains dispersed in the continuous PET matrix (**Figure 7.1A**). This phase-separated morphology confirms that PET is immiscible with MXD6, which yields phase-separated MXD6 domains with dimensions on the order of micrometers. The ternary Na^+-PPET/PET/MXD6 blends reveal the same two-phase morphology as the binary PET/MXD6 blend (**Figure 7.1B-E**). As the mol% of ionic phosphonated monomers increases, the dispersed-MXD6 domain dimensions are reduced. This observation agrees with our recent findings, which showed that the phase-separated, interdomain spacing of immiscible amorphous polyester (PETG) and semicrystalline MXD6 blends decreased with increasing Na^+-PPET ionomer loadings.[25] The diminished MXD6 domain size is attributed to the specific interactions developed between the ionic groups on Na^+-PPET ionomer and the polar amide linkages of MXD6. These specific interactions tend to decrease the interfacial tension between the two dissimilar polymer components, leading to a reduced phase dimensions and enhanced phase stability that inhibits coalescence during melt processing, thus yielding an effective compatibilization of the PET/MXD6 blends.

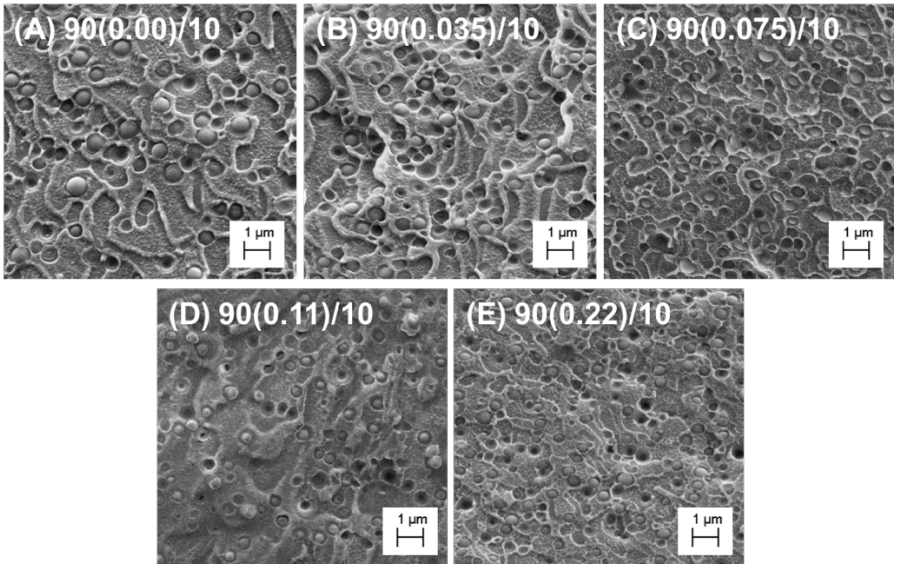

Figure 7.1. Scanning electron microscopy (SEM) images of cryogenically fractured surface for extruded Na^+-PPET/PET/MXD6 blends. Blend compositions: (A) 90(0.00)/10; (B) 90(0.035)/10; (C) 90(0.075)/10; (D) 90(0.11)/10; (E) 90(0.22)/10. Scale bar = 1 μm.

In order to quantify the phase-separated MXD6 domain size using SEM, domain diameter for each blend composition was measured using ImageJ, and the mean ± σ value was calculated by fitting a Gaussian distribution on a histogram based on 200 measurements (see **Supporting Information**, **Figure S7.2**). **Figure 7.2** shows the dependence of the average MXD6 domain diameter on the phosphonated monomer concentration in the polyester component. The base blend shows the largest MXD6 particle size of 0.54 μm among all the blend compositions. Addition of 0.035 mol% phosphonate ionic monomers to the PET phase reduced the MXD6 particle size to 0.43 μm. Consistent with our previous study on Na^+-PPET ionomer-compatibilized PETG/MXD6 blends prepared using a solution mixing method,[25] very small amounts of

ionic phosphonate groups incorporated to the polyester/polyamide blend system can significantly decrease the phase-separated domain dimension. Increasing phosphonated monomer concentration further to 0.22 mol% decreases the MXD6 domain size by 45% as compared to the base blend, and the 90(0.22)/10 blend shows the smallest particle size (i.e., 0.3 μm) among all blend samples. Clearly, the average MXD6 domain diameter reveals a significant decrease with increasing phosphonated monomer concentration, which further confirms the enhanced compatibility of PET/MXD6 blends with the incorporation of the Na^+-PPET ionomer.

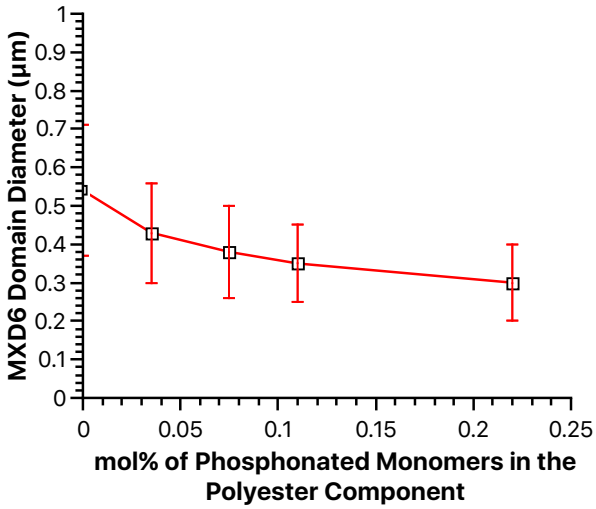

Figure 7.2. Phase-separated MXD6 domain diameter with respect to mol% of phosphonated monomer in the polyester component for Na^+-PPET/PET/MXD6 blends. The domain diameter was measured using ImageJ. The mean ± σ value was calculated from 200 measurements by fitting a histogram of the measurements to a Gaussian distribution.

7.4.2 Thermal Analysis. Differential scanning calorimetry (DSC) was utilized to provide further insight into the effect of the Na^+-PPET ionomer on the thermal properties

of PET/MXD6 blends. Heating thermograms of dry, extruded Na^+-PPET/PET/MXD6 blends with varying amounts of phosphonated ionic monomers, along with pure PET and pure MXD6, are compared in **Figure 7.3**, and the corresponding thermal data are summarized in **Table 7.2**. The heating thermograms for all the compositions display three enthalpic events: a glass transition (T_g), followed by a cold crystallization exotherm (T_{cc}), and finally a melting endotherm (T_m). T_gs of PET and MXD6 are 78 °C and 85 °C, respectively. Only one glass transition temperature, ranging from 69 °C to 76 °C, has been observed from the thermograms of both uncompatibilized and compatibilized PET/MXD6 blends. The appearance of only a single T_g is due to the low MXD6 content (i.e., 10 wt%) in the PET/MXD6 blends as well as the relatively small difference between T_gs of PET and MXD6. All PET/MXD6 blends exhibit significant lower T_{cc}s, approximate 30 °C decrease, than pure PET and pure MXD6. The spherical MXD6 particles dispersed in PET matrix nucleate the crystallization of PET phase and shift T_{cc} of PET to lower temperatures.[10] In addition, some scatter in T_{cc} among the various blends have been observed. Given the fact that small differences in the thermal history affect cold crystallization, the different T_{cc}s are presumably due to small variations in the quenching time of the extruded strands.[8, 10] Two melting endotherms have been observed for all the blend compositions, and are designated to the meltings of PET and MXD6, respectively. The small endotherm shoulder in heating thermograms of the blends at approximately 237 °C corresponds to the T_m of MXD6, and is attributed to the low content of MXD6.

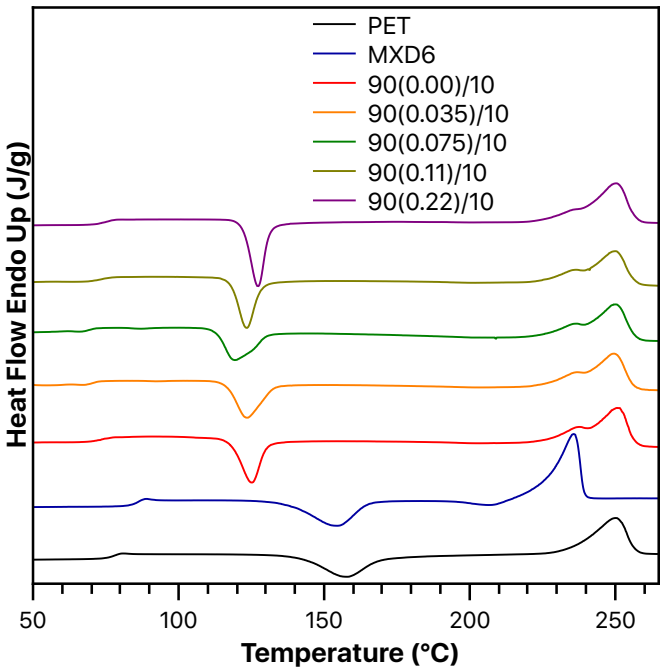

Figure 7.3. Differential scanning calorimetry (DSC) heating scans of PET, MXD6, and Na^+-PPET/PET/MXD6 blends. First heat reported with heating rate of 10 °C/min. All samples are dried extruded strands after quench cool directly into water bath from the extruder (280 °C).

Table 7.2. Summary of Thermal Properties for PET, MXD6, and Na^+-PPET/PET/MXD6 Blends.

	Heating[a]					**Cooling**[b]	
	T_g (°C)	T_{cc} (°C)	ΔH_{cc} (J g^{-1})	T_m (°C)	ΔH_m (J g^{-1})	T_c (°C)	ΔH_c (J g^{-1})
PET	78	158	30	250	38	182	32
MXD6	85	155	33	236	54	176	45
90(0.00)/10	74	125	26	238, 251	45	182, 190	40
90(0.035)/10	70	124	26	237, 250	43	180, 194	41
90(0.075)/10	69	119	25	237, 250	44	179, 199	3, 33
90(0.11)/10	74	123	26	237, 250	40	176, 196	2.6, 31
90(0.22)/10	76	127	30	237, 250	45	175, 197	1.4, 37

[a] Heating: First heating with a heating rate of 10 °C/min;
[b] Cooling: Subsequent cooling with a cooling rate of -10 °C/min after heating to 270 °C.

The subsequent cooling thermograms are shown in **Figure 7.4,** and the corresponding crystallization temperature (T_c) and enthalpy of crystallization (ΔH_c) are listed in **Table 7.2**. Cooling thermograms clearly reveal the nucleating effect of phase-separated MXD6 particles on the crystallization of PET from the melt. Crystallization of PET in the blends is accelerated as evidenced by an increase in T_c from 190 °C to 199 °C as the phosphonated ionic monomer content increases to 0.075 mol%. This increased T_c of PET in these cooling thermograms implies the nucleation effect of MXD6 particles on the crystallization behavior of the PET matrix.[8, 10] Decreased MXD6 domain size results higher MXD6 surface area, and thus increases the number of active heterogeneities responsible for the crystallization kinetics of PET in these blends. It appears that smaller MXD6 domains containing more active heterogeneities crystallize at a low supercooling, thus leading to a shift of PET T_c to a higher temperature. Further increasing the amount of phosphonated ionic monomers to 0.22 mol%, however, reverses the trend as indicated by a shift of T_c to slightly lower temperatures. The observed lower T_c at higher ionic monomer concentrations is possibly due to the fact that much smaller MXD6 particles may not have the required number of heterogeneities to further contribute to the nucleating effect on the crystallization of PET.[10]

A crystallization exotherm of MXD6 is clearly observed in the cooling scan of these blends directly after the T_c of PET. T_c of MXD6 gradually decreases from 182 °C to 175 °C, and the crystallization exotherm becomes broader and smaller with increasing the amount of ionic monomers to 0.22 mol%. Hindrance and inhibition of MXD6 crystallization are ascribed to fractionated crystallization behavior.[8, 10] It appears that the diminished MXD6 particle size results in less active heterogeneities responsible for the

crystallization of MXD6, thus nucleating the crystallization of MXD6 domains at a higher supercooling. Consequently, the cooling thermograms of these PET/MXD6 blends reveal a shift of MXD6 T_c to a lower temperature region. Furthermore, a greater range of specific interactions generated between phosphonated ionic groups and amide linkages of MXD6 with increasing mol% of ionic monomers retards the crystallization of MXD6, which also contributes to the decreased T_c of MXD6.[8] Similar behavior has been reported for sulfonated PET ionomers in the Na^+ form (Na^+-SPET)-compatibilized PET/MXD6 blends.[8, 10, 27] This crystallization behavior of MXD6 in these Na^+-PPETPET/MXD6 blends implies a significant interphase mixing with added sodium phosphonate content, and further confirms the effective compatibilization of PET/MXD6 blends with Na^+-PPET ionomer as a minor-component compatibilizer.

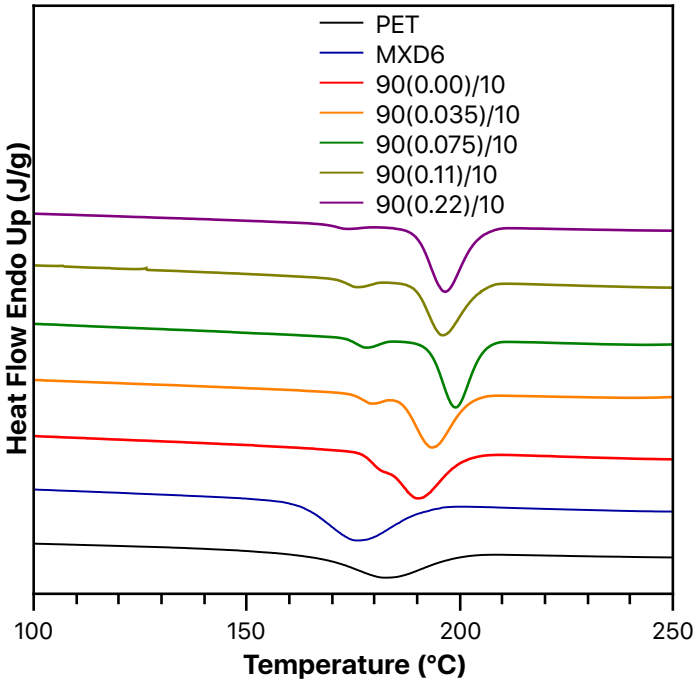

Figure 7.4. Differential scanning calorimetry (DSC) cooling scans of PET, MXD6, and Na^+-PPET/PET/MXD6 blends. Subsequent cooling reported with a cooling rate of -10 °C/min after heating to 270 °C. All samples are dried extruded strands after quench cool directly into water bath from the extruder (280 °C).

7.4.3 Biaxial Orientation. Plastic PET bottles are manufactured by injection stretch blow molding process. In order to mimic this blow molding process, compression-molded films were sequentially oriented to a draw ratio of 3 × 3 at a temperature (i.e., 81 °C) above the T_gs of these Na^+-PPET/PET/MXD6 blends by the procedure described in the **Experimental Section** to obtain biaxially oriented films. The phase morphology of the cross sections for biaxially oriented 90(0.00)/10, 90(0.11)/10, and 90(0.22)/10 blend films was investigated by using transmission electron microscopy (TEM), and the corresponding TEM micrographs are displayed in **Figure 7.5**. It is evident that the spherical MXD6 domains have been transformed into platelets with high aspect ratio

oriented in the plane of the film. Uniaxial stretching transforms spherical MXD6 particles into elongated ellipsoids, and biaxial stretching further deforms them into flat platelets. It is interesting to note that, as the mol% of phosphonated monomers increases, the average platelet dimension decreases (**Figure 7.5A-C**). Consistent with the decreased spherical MXD6 domain diameter investigated by using SEM, the reduced MXD6 platelet size further confirms the effective compatibilization in PET/MXD6 blends attributed to the specific interactions generated by phosphonate pendant ions and amide functionalities of MXD6.

To have an in-depth understanding of the MXD6 platelet dimension, the center thickness of the cross section for each MXD6 platelet was measured using ImageJ, and the mean ± σ value was calculated by fitting a Gaussian distribution on a histogram based on the measurements (see **Supporting Information**, **Figure S7.3**). Noting that microtoming was not performed straight through the center of each platelet, a large variation in the measured thickness has been observed for all these blend compositions (**Figure S7.3**). The base blend, i.e., 90(0.00)/10, reveals an average MXD6 platelet thickness at 139 nm (**Figure S7.3A**). The average platelet thickness for blends of 90(0.11)/10 (**Figure S7.3B**) and 90(0.22)/10 (**Figure S7.3C**) are 30 nm and 19 nm, respectively. Clearly, smaller MXD6 particles results in thinner platelets after biaxial orientation. The platelet-like MXD6 domains appeared to have a significant impact on the optical and gas barrier properties of biaxially oriented blend films.[5, 8, 10, 13, 16, 27] The compatibilization effect on optical properties and oxygen permeability of both unoriented and oriented blends will be evaluated in the following sections of this work.

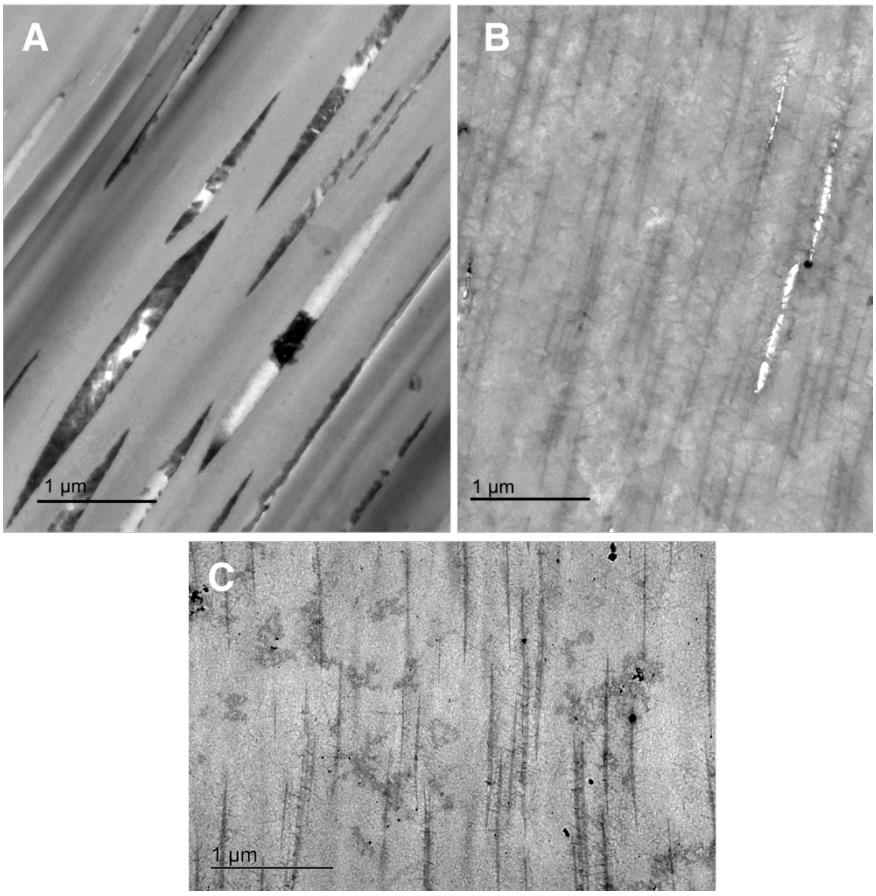

Figure 7.5. Transmission electron microscopy (TEM) images of cross sections for biaxially oriented Na^+-PPET/PET/MXD6 blends. Blend compositions: (A) 90(0.00)/10; (B) 90(0.11)/10; (C) 90(0.22)/10. Scale bar = 1 µm.

7.4.4 Optical Properties. Haze and transmittance are important optical properties for food and beverage packaging applications.[31] Low haze and high transmittance allow the consumer to clearly see the product inside of a bottle or a bag. Haze is defined as the percentage of light transmitted through a film that is deflected by > 2.5° from the direction of the incident beam, and usually utilized to quantify the turbid, cloudy appearance of film samples.[31] On the other hand, transmittance is defined as the ratio of light transmitted through the film.[31] Films of most immiscible amorphous polymer blends

are generally not clear due to light scattering from the phase-separated blend domains of dimensions comparable to or greater than the wavelength of visible light having distinctly different refractive indices.[13, 16] Due to the poor optical properties of most polymer blends, it is important to study the effect of compatibilization of PET/MXD6 blends by adding Na^+-PPET ionomer as a compatibilizer on the optical properties (e.g., haze and transmittance) of the blend films. Given the fact that PET bottles are manufactured by injection stretch blow molding, this analysis will focus on a comparison of haze and transmittance for both unoriented and biaxially oriented blends containing various mol% of ionic monomers in the polyester component.

Haze values of both unoriented and biaxially oriented films for Na^+-PPET/PET/MXD6 blends are compared with respect to the mol% of ionic monomers in the polyester component, along with pure PET and pure MXD6 films (**Figure 7.6 and Table 7.3**). For a polymer blend film, haze usually originates from Rayleigh scattering of the dispersed-phase particles smaller than the wavelength of visible light (i.e., 400 nm – 700 nm), or the difference in the refractive indices of the dispersed phase and the matrix polymer.[15] In the case of Na^+-PPET/PET/MXD6 blends discussed here, unoriented blends exhibit spherical MXD6 particles with average diameter ranging from 350 nm to 550 nm (**Figure 7.1 and 7.2**), and the diameter of MXD6 platelets in biaxially oriented blends is even larger (**Figure 7.5 and Figure S7.3**). Considering the MXD6 domain dimensions in both unoriented and oriented blends are larger than the wavelength of visible light, it is reasonable to ignore the effect of Rayleigh scattering on haze, and to use the concept of refractive index difference between the two dissimilar polymers to evaluate the haziness for these Na^+-PPET/PET/MXD6 blends. The refractive index of

MXD6 is 1.5773, which closely matches the PET refractive index of 1.5735.[13, 16] As a consequence of the similar refractive indices between PET and MXD6, haze values of compatibilized PET/MXD6 blends are almost as low as that of PET, about 6.6 – 9.4% compared to 4.66%. This implies that, if the refractive index match is maintained for all these blend compositions, the decreased MXD6 domain dimension with increasing phosphonated monomer concentration has no profound effect on the haze of unoriented blends.

Stretching the blend films to a draw ratio of 3 × 3 results in significantly higher haze for all the Na^+-PPET/PET/MXD6 blend compositions as compared to those unoriented blends (**Figure 7.6 and Table 7.3**). Hu et al. demonstrated that stretching imparted greater refractive index anisotropy to PET than to MXD6, leading to an increased refractive index mismatch between PET and MXD6.[13] Therefore, increased haziness has been observed after the blend films have been biaxially stretched. Biaxial orientation exhibits no significant effect on the haziness of pure PET and pure MXD6 as evidenced by similar haze values for both unoriented and oriented PET and MXD6 films. It is important to note that, for biaxially oriented Na^+-PPET/PET/MXD6 blend films, haze value greatly decreases with increasing mol% of phosphonated ionic monomers in the polyester component. Surprisingly, the incorporation of 0.22 mol% of phosphonate ionic monomers significantly reduces the haze of uncompatibilized PET/MXD6 blend from 50% to 22%. This suggests that, among all the blend compositions studied in this work, a 56% decrease in haziness has been achieved by adding 0.22 mol% phosphonate monomers in the polyester component. TEM study has confirmed the reduced MXD6

platelet dimension by adding phosphonate pendant ions (**Figure 7.5**), which contributes to the reduction in haze for biaxially oriented Na^+-PPET/PET/MXD6 blends.

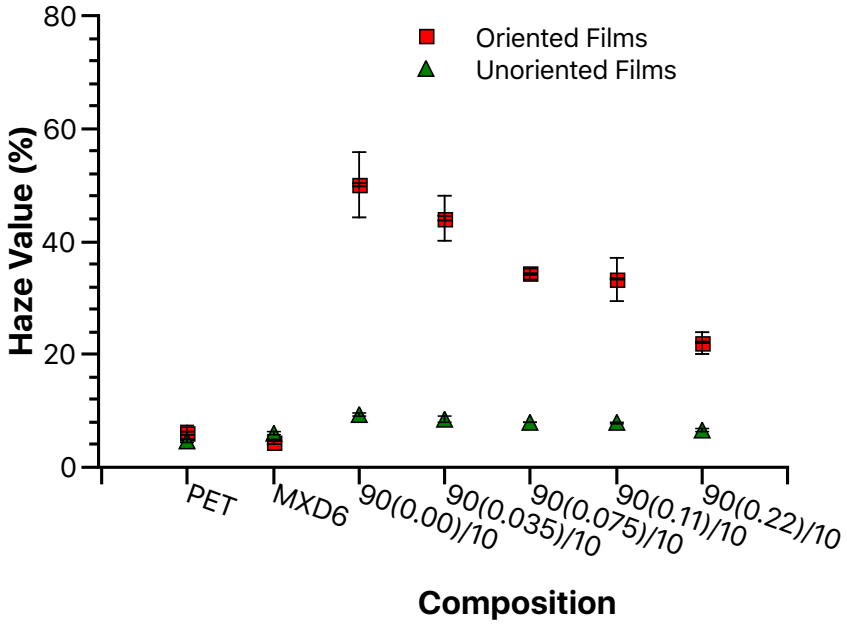

Figure 7.6. Haze value (%) of unoriented (green triangle) and oriented (red square) films for Na^+-PPET/PET/MXD6 blends with various mol% of phosphonated monomer in the polyester component, along with pure PET and pure MXD6 films. Unoriented films: compression-molded films. Oriented films: biaxially oriented films with draw a ratio of 3 × 3. Data reported on an average of 5 specimens with calculated standard deviations for each composition.

Table 7.3. Haze value and transmittance of unoriented and oriented PET, MXD6, and Na^+-PPET/PET/MXD6 blends films.

	Haze Value (%)		Transmittance (%)	
	Unoriented	**Oriented**	**Unoriented**	**Oriented**
PET	4.66 ± 0.26	6.12 ± 1.17	86.27 ± 1.70	85.33 ± 0.47
MXD6	5.98 ± 0.29	4.52 ± 0.47	85.40 ± 0.62	86.95 ± 0.21
90(0.00)/10	9.40 ± 0.29	50.00 ± 5.73	83.37 ± 0.81	55.00 ± 2.83
90(0.035)/10	8.60 ± 0.51	44.10 ± 3.96	84.00 ± 0.17	58.50 ± 2.83
90(0.075)/10	8.06 ± 0.04	34.23 ± 1.00	83.43 ± 0.81	67.23 ± 1.50
90(0.11)/10	7.92 ± 0.10	33.33 ± 3.80	85.60 ± 0.44	70.83 ± 4.49
90(0.22)/10	6.59 ± 0.16	22.03 ± 1.92	86.33 ± 0.59	74.40 ± 1.66

The comparison of transmittance for both unoriented and biaxially oriented Na^+-PPET/PET/MXD6 blend films with various amounts of phosphonated ionic monomers in the polyester matrix, along with pure PET and pure MXD6 films, is shown in **Figure 7.7,** and the transmittance data are summarized in **Table 7.3**. Before biaxial orientation, both uncompatibilized and compatibilized PET/MXD6 blends remain as transparent as pure PET and pure MXD6 films, attributed to the close refractive index match between PET and MXD6.[5, 13] Although the blend films become thinner after stretching, it is evident that the biaxial orientation of a blend film to a draw ratio of 3 × 3 highly decreases transmittance. Consistent with higher haze observed for Na^+-PPET/PET/MXD6 blends after orientation (**Figure 7.6**), the reduced transmittance is due to the increased refractive index mismatch of PET and MXD6. When comparing the oriented Na^+-PPET/PET/MXD6 blends containing various mol% of phosphonated monomers, an increased transmittance with increasing ionic monomer concentration has been observed. The incorporation of 0.22 mol% phosphonate ionic monomers into polyester matrix achieves an improvement on the transparency of base blend by 35%. This improved

transparency agrees well with the decreased haziness (**Figure 6**), again due to the smaller phase-separated MXD6 platelet size (**Figure 7.5**).

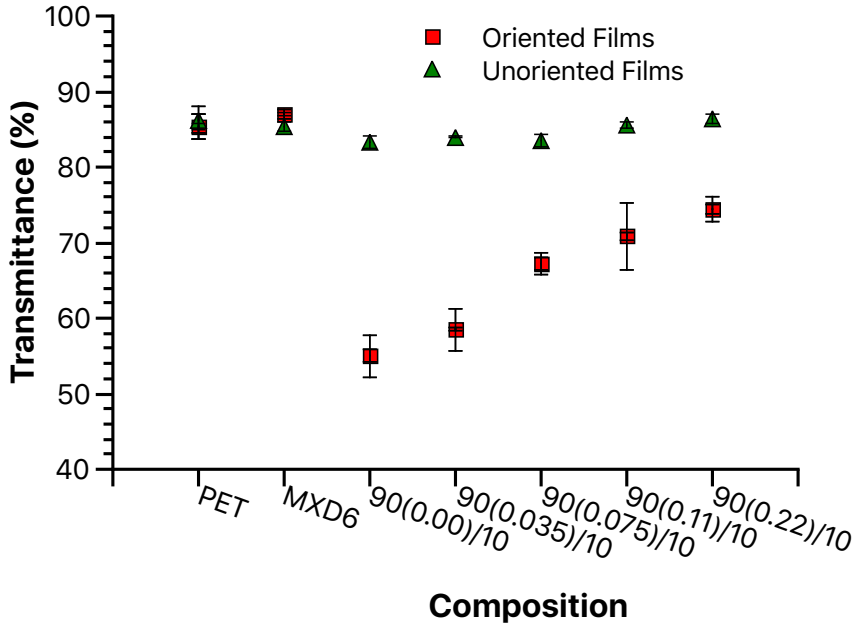

Figure 7.7. Transmittance (%) of unoriented (green triangle) and oriented (red square) films for Na^+-PPET/PET/MXD6 blends with various mol% of phosphonated monomer in the polyester component, along with pure PET and pure MXD6 films. Unoriented films: compression-molded films. Oriented films: biaxially oriented films with a draw ratio of 3 × 3. Data reported on an average of 5 specimens with calculated standard deviations for each composition.

7.4.5 Oxygen Barrier Properties. Given the widespread application of PET in food and beverage products packaging industry, it is of great interest here to systematically investigate the compatibilization effect of Na^+-PPET ionomer as a minor-component compatibilizer on the gas barrier property of PET/MXD6 blends. The oxygen

permeability measurements were performed on both unoriented and oriented Na^+-PPET/PET/MXD6 blend films at 0% relative humidity. **Figure 7.8** displays the corresponding oxygen permeability for these blends, along with pure PET and pure MXD6. The permeability data shown in **Figure 7.8** are also listed in **Table 7.4**. The compatibilization effect on oxygen barrier property will be evaluated for unoriented and oriented Na^+-PPET/PET/MXD6 blend films.

The oxygen permeability of unoriented films is indicated as green triangles shown in **Figure 7.8**. Apparently, the oxygen permeability of unoriented MXD6 is significantly lower than the unoriented PET (**Table 7.4**). Blending with 10 wt% MXD6 improves oxygen barrier of pure PET by about 30%. Comparing the unoriented Na^+-PPET/PET/MXD6 blends with different mol% of phosphonated monomers, no significant difference has been observed on their oxygen barrier property (**Figure 7.8 and Table 7.4**). Gas permeability (P) is defined as the product of solubility (S) and diffusivity (D), i.e., $P = S \times D$. In order to evaluate permeability, both solubility and diffusivity need to be considered. Solubility only depends on blend composition.[10] Since the Na^+-PPET/PET/MXD6 blends have the same composition with 10 wt% MXD6 in 90 wt% PET matrix, solubility remains unchanged for all these blends. Unlike solubility, diffusivity is known to strongly depend on the blend morphology.[8] Due to the much lower oxygen permeability of MXD6 compared to PET, the dispersed spherical MXD6 domains are considered as impermeable particles in the PET matrix. When an oxygen molecule diffuses through these unoriented blend films, it diffuses through the PET matrix (**Figure 7.9A**).[8, 10] Prattipati et al. demonstrated that, for Na^+-SPET ionomer-compatibilized PET/MXD6 blends, the diminished spherical MXD6 domain size with

increasing the Na^+-SPET compatibilizer content exhibited no significant effect on the oxygen diffusion pathway when the average diameter of spherical MXD6 particles is larger than 0.2 μm.[10] Thus, diffusivity remains almost constant for all the unoriented Na^+-PPET/PET/MXD6 blends. Given the constant solubility and diffusivity for these unoriented blends, compatibilization does not affect the oxygen barrier property of the unoriented blends.

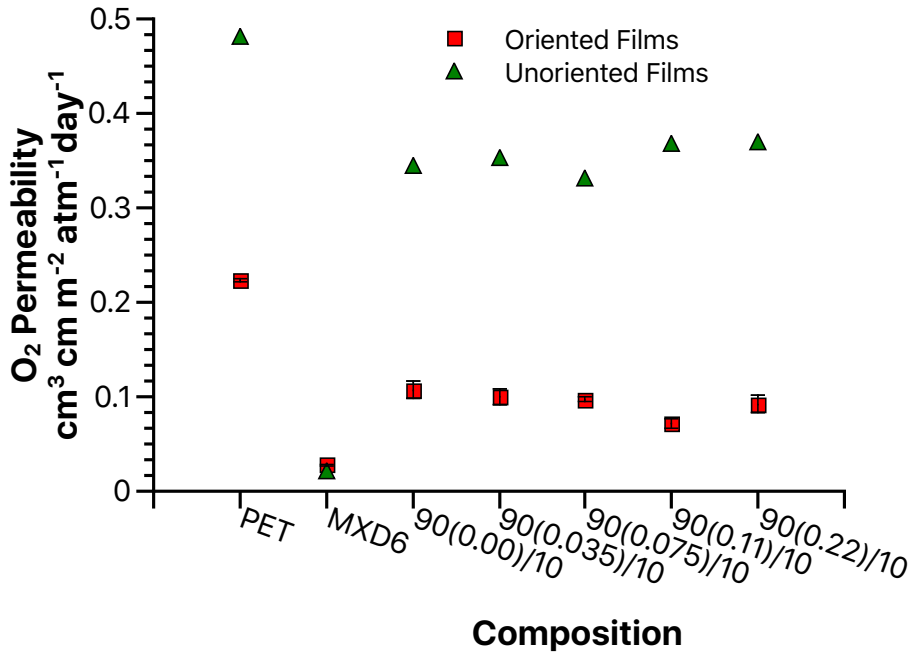

Figure 7.8. Oxygen permeability of unoriented (green triangle) and oriented (red square) films for Na^+-PPET/PET/MXD6 blends with various mol% of phosphonated monomer in the polyester component, along with pure PET and pure MXD6. Unoriented films: compression-molded films. Oriented films: biaxially oriented films with a draw ratio of 3 × 3. Data for oriented films reported on an average of 3 specimens with calculated standard deviations for each composition.

Table 7.4. Oxygen barrier properties of unoriented and oriented PET, MXD6, and Na^+-PPET/PET/MXD6 blends films.

	O_2 Permeability (cm^3 cm m^{-2} atm^{-1} day^{-1})		P/P_{PET}	
	Unoriented	**Oriented**	**Unoriented**	**Oriented**
PET	0.481	0.233 ± 0.002	-	-
MXD6	0.0210	0.028 ± 0.002	-	-
90(0.00)/10	0.345	0.107 ± 0.009	0.72	0.46
90(0.035)/10	0.353	0.102 ± 0.009	0.73	0.44
90(0.075)/10	0.332	0.097 ± 0.003	0.69	0.42
90(0.11)/10	0.368	0.072 ± 0.005	0.77	0.31
90(0.22)/10	0.370	0.092 ± 0.009	0.77	0.40

Biaxial orientation reduces the oxygen permeability of unoriented PET from 0.481 to 0.233 cm^3 cm m^{-2} atm^{-1} day^{-1}. The decreased permeability for oriented PET film is due to the strain-induced crystallization.[8, 10, 27, 32] As the PET film is extended, PET chains start to orient, and strain-induced crystallization occurs after a specific stretching ratio has been realized. Oxygen permeability is influenced by the crystallinity of the polymer because polymer crystals are considered virtually impermeable for gas transport.[33] As a consequence, the diffusion of oxygen is through a tortuous pathway in the amorphous region of the film due to the increased crystallinity. Therefore, biaxial orientation leads to a decrease on the oxygen permeability of PET. In contrast, stretching slightly increases the oxygen permeability of MXD6 from 0.0210 to 0.0276 cm^3 cm m^{-2} atm^{-1} day^{-1}. The higher oxygen permeability of biaxially unoriented MXD6 is possibly attributed to the hydrogen bonding interactions in the aromatic polyamide, which inhibit the conformational changes during stretching, and thereby cause a slightly increased free volume that is responsible for increased diffusivity.[10]

Compared to unoriented Na^+-PPET/PET/MXD6 blends, biaxial orientation dramatically reduces oxygen permeability by a factor of 3. For example, for the base blend without any compatibilizer, permeability is decreased to 0.107 from 0.345 cm^3 cm m^{-2} atm^{-1} day^{-1} after stretching (**Table 7.4**). P/P_{PET} is defined as the ratio of the permeability for a blend to the permeability for PET. P/P_{PET} is 0.69-0.77 for the unoriented blends, but decreases to 0.31-0.46 for the oriented blends. The profound decrease in P/P_{PET} for oriented blends compared to unoriented blends is attributed to the transformation of spherical MXD6 domains into platelets oriented perpendicular to the oxygen flux (**Figure 7.9B**). The resulted MXD6 platelets impart a tortuous diffusion pathway, which leads to a significant decrease in diffusivity; thus, a substantial decrease in permeability.

The compatibilization of PET/MXD6 blends reveals a strong effect on the oxygen barrier property of biaxially oriented Na^+-PPET/PET/MXD6 blends. It is evident that a reduction on oxygen permeability has been achieved with increasing mol% of phosphonated ionic monomers in the polyester matrix (**Figure 7.8**). The incorporation of 0.11 mol% phosphonated ionic monomers into the polyester matrix achieves the best oxygen barrier among all the compatibilized PET/MXD6 blends, as indicated by a higher than 33% decrease of permeability than that for the base blend. Lower permeability suggests that smaller MXD6 platelets in the compatibilized blends impart an increased tortuosity to the diffusion pathway (**Figure 7.9B**), thus leading to decreased permeability with reduced diffusivity. Interestingly, a higher phosphonated ionic monomer content, i.e., 0.22 mol%, results in slightly increased permeability. The average thickness of MXD6 platelets for 90(0.22)/10 blend is about 30 nm (**Figure S7.3B**), which is much

thinner compared to 19 nm for 90(0.11)/10 blend (**Figure S7.3C**). It is possible that the smaller MXD6 platelets in the blend containing a higher compatibilizer content are too thin after orientation, so that they are not completely impermeable to retain a tortuous oxygen diffusion pathway. Therefore, a slight increase of the oxygen permeability for 90(0.22)/10 blend has been observed (**Figure 7.9C**).

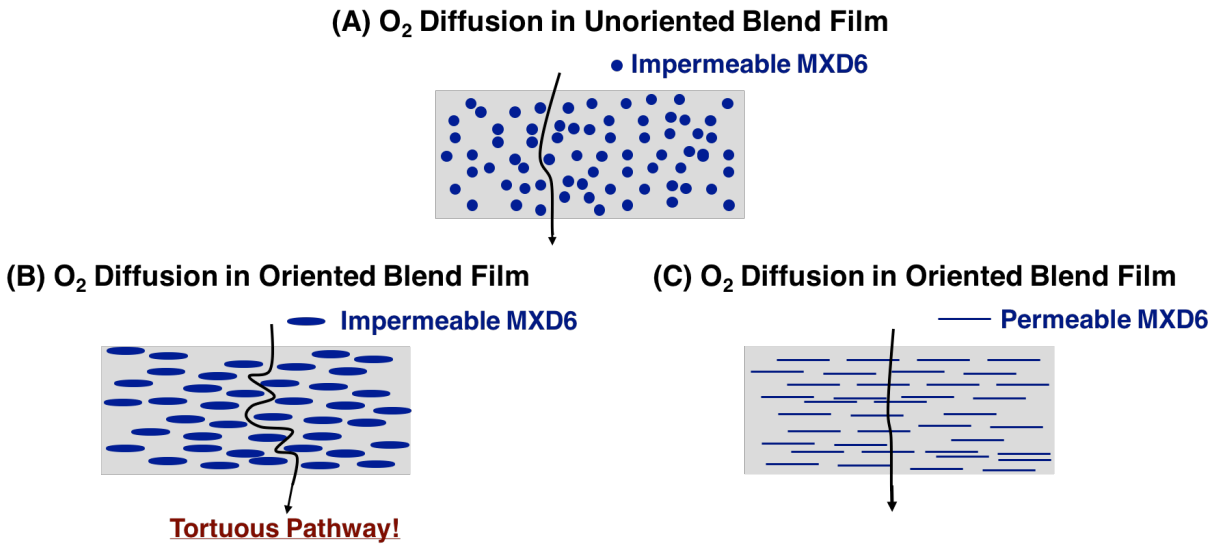

Figure 7.9. Pictorial representation of O_2 diffusion pathway in (A) unoriented blend film with impermeable, spherical MXD6 particles; (B) Oriented blend film with impermeable MXD6 platelets; and (C) oriented blend film with permeable MXD6 platelets.

7.5 Conclusions

In this work, the compatibilization of melt-mixed PET/MXD6 blends using Na^+-PPET ionomer as a minor-component compatibilizer was investigated. Evidence of the effective compatibilization is provided by the analysis of morphological and thermal properties of Na^+-PPET/PET/MXD6 blends with various mol% of phosphonated ionic

monomers in the polyester matrix. Increasing the amount of phosphonated pendant ions in the PET matrix reduces phase-separated MXD6 domain dimension, illustrating improved interphase mixing between the dissimilar PET and MXD6 components. The resulting smaller MXD6 domains were further confirmed by the nucleating effect on the crystallization behaviors of PET and MXD6, as evidenced by a shift of crystallization temperature of PET to higher temperatures as well as the inhibited crystallization of MXD6. The successful compatibilization of PET/MXD6 blends is attributed to specific interactions between the phosphonate pendant ions in Na^+-PPET and the amide units of MXD6, which lower the interfacial tension and lead to a reduction in the dispersed-phase dimensions.

Compatibilization of PET/MXD6 blends greatly improved optical properties for biaxially oriented blends. Biaxial orientation transforms the spherical MXD6 domains into platelets with higher aspect ratio oriented in the plane of the film. Since stretching imparts a greater refractive index anisotropy to PET than to MXD6, an increased haziness and a decreased transparency have been observed for oriented blends due to the refractive index mismatch between PET and MXD6 after stretching. With increasing the mol% of phosphonated ionic monomers in the polyester component, however, biaxially oriented Na^+-PPET-PET/MXD6 blends exhibited decreased haze and increased transmittance, attributed to the decreased MXD6 platelet size. Moreover, by adding 0.22 mol% of phosphonated ionic monomers into the PET matrix, haziness is reduced by 56%, and transparency is improved by 35%.

A significantly decrease on the oxygen permeability of biaxially oriented PET/MXD6 blends has been achieved. The smaller MXD6 platelets at higher

phosphonated monomer concentration increases tortuosity of oxygen diffusion pathway, leading to an increase in diffusivity, thus a reduced permeability. Furthermore, the oxygen barrier property of oriented Na^+-PPET/PET/MXD6 blends has been improved by 30% with the incorporation of 0.11 mol% phosphonated monomers. It is interesting to note that further increasing ionic monomer content, however, results in slightly increased permeability, possibly due to the fact that the platelet-like MXD6 domains are too thin and no longer considered completely impermeable to retain high tortuosity for the diffusion pathway when the MXD6 domains are small enough.

Overall, we have demonstrated the successful compatibilization of melt-blended PET/MXD6 blends using a new Na^+-PPET ionomer as a minor-component compatibilizer, and provided an understanding of the compatibilization effect on the properties of PET/MXD6 blends from fundamental and practical perspectives. By adding the Na^+-PPET ionomer as a minor-component compatibilizer in PET/MXD6 blends, both optical and oxygen barrier properties are highly improved. This work confirmed the potential applications of the Na^+-PPET ionomer as an effective compatibilizer in polyester/polyamide blends for plastic blown bottles in packaging industry.

7.6 Acknowledgements

The authors gratefully acknowledge the Institute for Advanced Learning and Research (IALR) for providing funds to support the efforts of this project. The authors thank Huachen Cui in the Department of Mechanical Engineering and Eric L. Gilmer in the Department of Chemical Engineering for biaxial orientation help.

7.7 References

1. Brooks, D. W.; Giles, G. A., PET packaging technology. Taylor & Francis US: 2002.
2. Robertson, G. L., Food packaging: principles and practice. CRC press: 2005.
3. Huenefeld, D.; Nichols, C., Polyamide-Polyester Polymer Blends and Methods of Making the Same. U.S. Pub. No.: US 2008/0009574 A1.
4. Kim, Y. J.; Germonprez, R., Barrier compositions and film made therefrom having improved optical and oxygen barrier properties. Google Patents: 1994.
5. Kim, Y. J.; Germonprez, R.; Kaas, R. L.; Mehta, A., Barrier compositions and articles made therefrom. U.S. Patent Pub. No.: US 2005/0106343 A1.
6. Mills, D. E.; Stafford, S. L., Polyester/polyamide blend having improved flavor retaining property and clarity. Google Patents: 1993.
7. Stafford, S. L.; Stewart, M. E.; Gamble, B. B., Polyester/polyamide blend having improved flavor retaining property and clarity. Google Patents: 2008.
8. Hu, Y.; Prattipati, V.; Mehta, S.; Schiraldi, D.; Hiltner, A.; Baer, E., Improving gas barrier of PET by blending with aromatic polyamides. Polymer 2005, 46 (8), 2685-2698.
9. Iyer, S.; Schiraldi, D. A., Role of ionic interactions in the compatibility of polyester ionomers with poly (ethylene terephthalate) and nylon 6. Journal of Polymer Science Part B: Polymer Physics 2006, 44 (15), 2091-2103.
10. Prattipati, V.; Hu, Y.; Bandi, S.; Schiraldi, D.; Hiltner, A.; Baer, E.; Mehta, S., Effect of compatibilization on the oxygen-barrier properties of poly (ethylene terephthalate)/poly (m-xylylene adipamide) blends. Journal of Applied Polymer Science 2005, 97 (3), 1361-1370.
11. Turner, S. R.; Connell, G. W.; Stafford, S. L.; Hewa, J. D., Polyester-polyamide blends with reduced gas permeability and low haze. Google Patents: 2002.
12. Bell, E. T.; Bradley, J. R.; Long, T. E.; Stafford, S. L., Polyester/polyamide blends with improved color. Google Patents: 2001.
13. Hu, Y.; Prattipati, V.; Hiltner, A.; Baer, E.; Mehta, S., Improving transparency of stretched PET/MXD6 blends by modifying PET with isophthalate. Polymer 2005, 46 (14), 5202-5210.
14. Liu, Z.; Mehta, S.; Huang, X.; Schiraldi, D. A., Method to make single-layer PET bottles with high barrier and improved clarity. Google Patents: 2011.
15. Maruhashi, Y.; Iida, S., Transparency of polymer blends. Polymer Engineering & Science 2001, 41 (11), 1987-1995.
16. Prattipati, V.; Hu, Y.; Bandi, S.; Mehta, S.; Schiraldi, D.; Hiltner, A.; Baer, E., Improving the transparency of stretched poly (ethylene terephthalate)/polyamide blends. Journal of applied polymer science 2006, 99 (1), 225-235.
17. Long, T. E.; Sprayberry, H. B.; Stafford, S. L.; Turner, S. R., Polyester/polyamide blend having improved flavor retaining property and clarity. Google Patents: 1997.
18. Boykin, T. L.; Moore, R. B., The role of specific interactions and transreactions on the compatibility of polyester ionomers with poly (ethylene terephthalate) and nylon 6, 6. Polymer Engineering & Science 1998, 38 (10), 1658-1665.

19. Dutta, D.; Weiss, R.; He, J., Compatibilization of blends containing thermotropic liquid crystalline polymers with sulfonate ionomers. Polymer 1996, 37 (3), 429-435.
20. Eisenberg, A.; Hara, M., A review of miscibility enhancement via ion-dipole interactions. Polymer Engineering & Science 1984, 24 (17), 1306-1311.
21. Feng, Y.; Weiss, R.; Karim, A.; Han, C.; Ankner, J. F.; Kaiser, H.; Peiffer, D. G., Compatibilization of polymer blends by complexation. 2. Kinetics of interfacial mixing. Macromolecules 1996, 29 (11), 3918-3924.
22. Hara, M.; Eisenberg, A., Miscibility enhancement via ion-dipole interactions. 1. Polystyrene ionomer/poly (alkylene oxide) systems. Macromolecules 1984, 17 (7), 1335-1340.
23. Rajagopalan, P.; Kim, J. S.; Brack, H. P.; Lu, X.; Eisenberg, A.; Weiss, R.; Risen Jr, W. M., Molecular interpretation of miscibility in polyamide-6 blends with alkali ionomers of sulfonated polystyrene. Journal of Polymer Science Part B: Polymer Physics 1995, 33 (3), 495-503.
24. Gemeinhardt, G. C.; Moore, A. A.; Moore, R. B., Influence of ionomeric compatibilizers on the morphology and properties of amorphous polyester/polyamide blends. Polymer Engineering & Science 2004, 44 (9), 1721-1731.
25. Ju, L.; Dennis, J. M.; Heifferon, K. V.; Long, T. E.; Moore, R. B., Compatibilization of Polyester/Polyamide Blends with a Phosphonated Poly(ethylene terephthalate) Ionomer: Comparison of Monovalent and Divalent Pendant Ions. ACS Applied Polymer Materials 2019, 1 (5), 1071-1080.
26. Sullivan, M.; Weiss, R., Characterization of blends of an amorphous polyamide with lightly sulfonated polystyrene ionomers. Polymer Engineering & Science 1992, 32 (8), 517-523.
27. Özen, İ.; Bozoklu, G.; Dalgıçdir, C.; Yücel, O.; Ünsal, E.; Çakmak, M.; Menceloğlu, Y. Z., Improvement in gas permeability of biaxially stretched PET films blended with high barrier polymers: The role of chemistry and processing conditions. European Polymer Journal 2010, 46 (2), 226-237.
28. Liu, Z., Colored oxygen scavenging polymers. US Patents: 2011.
29. Lee, R.; Hutchinson, G.; Farha, S.; Tharmapuram, S., Compatibilized polyester/polyamide blends. U.S. Patent Pub. No. : 2004.
30. Ju, L.; Pretelt, J.; Chen, T.; Dennis, J. M.; Heifferon, K. V.; Baird, D. G.; Long, T. E.; Moore, R. B., Synthesis and characterization of phosphonated Poly (ethylene terephthalate) ionomers. Polymer 2018, 151, 154-163.
31. Brown, N., Plastics in food patkaging: properties: design and fabrication. CRC Press: 1992; Vol. 5.
32. Doudou, B. B.; Dargent, E.; Grenet, J., Relationship between draw ratio and strain-Induced crystallinity in uniaxially hot-Drawn PET MXD6 films. Journal of Plastic Film & Sheeting 2005, 21 (3), 233-251.
33. Petropoulos, J., A comparative study of approaches applied to the permeability of binary composite polymeric materials. Journal of Polymer Science: Polymer Physics Edition 1985, 23 (7), 1309-1324.

7.8 Supporting Information

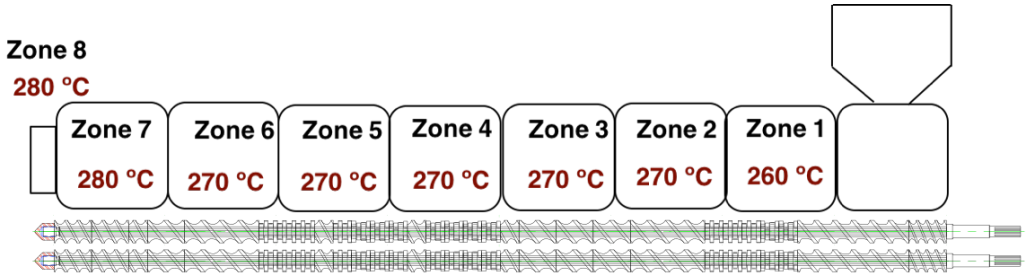

Figure S7.1. Temperature profile of the co-rotating intermeshing twin screw extruder (Leistritz ZSE-18, L/D = 40, D = 18 mm). Zone 8 represents the extruder die.

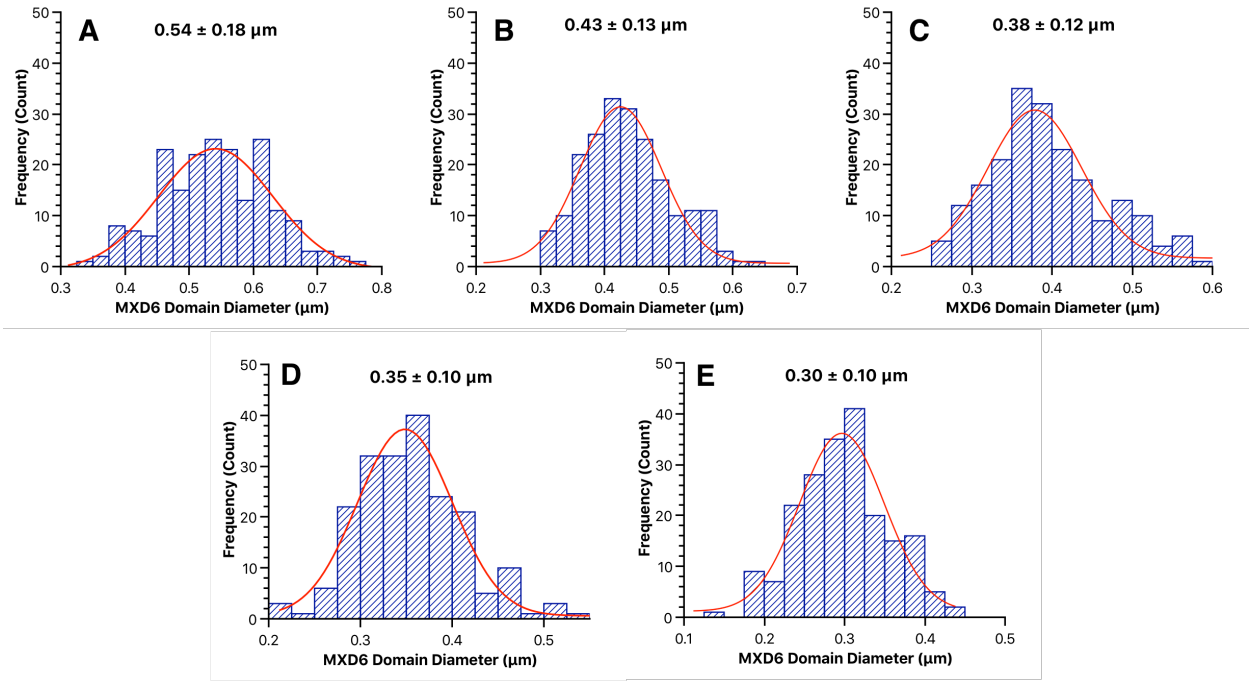

Figure S7.2. MXD6 domain diameter distribution (histogram and Gaussian fit) measured from scanning electron microscopy (SEM) images for the Na^+-PPET/PET/MXD6 blends. The mean ± σ values are indicated in each panel and are based on 200 measurements. (A) 90(0.00)/10; (B) 90(0.035)/10; (C) 90(0.075)/10; (D) 90(0.11)/10; (E) 90(0.22)/10.

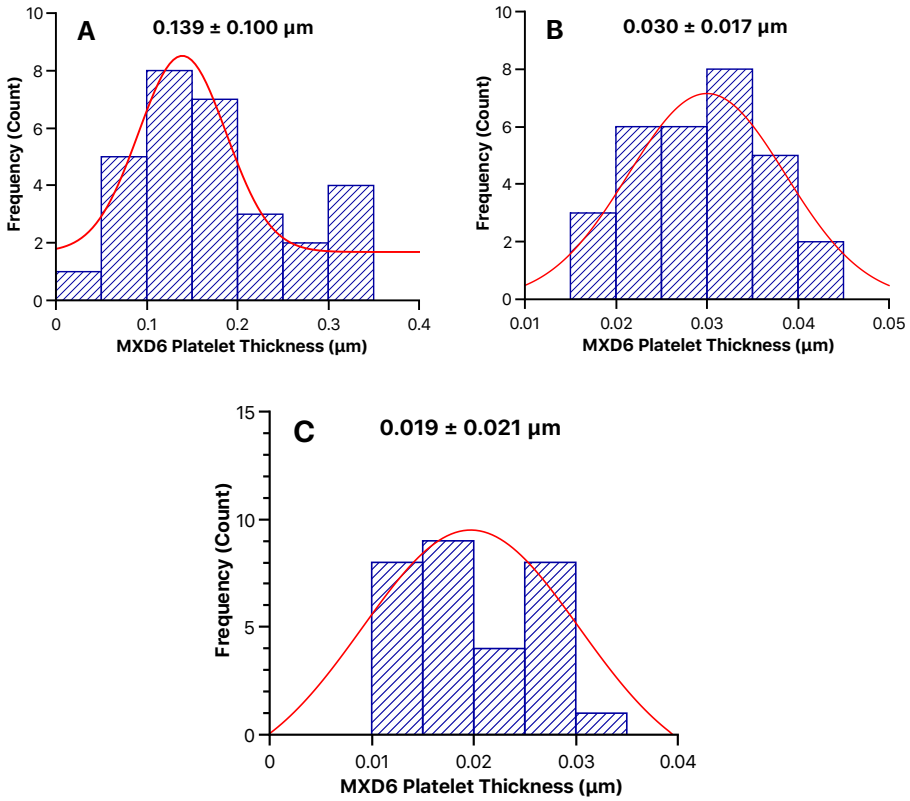

Figure S7.3. MXD6 platelet thickness distribution (histogram and Gaussian fit) measured from transmission electron microscopy (TEM) images for the Na^+-PPET/PET/MXD6 blends. The mean ± σ values are indicated in each panel and are based on 30 measurements. (A) 90(0.00)/10; (B) 90(0.11)/10; (C) 90(0.22)/10.

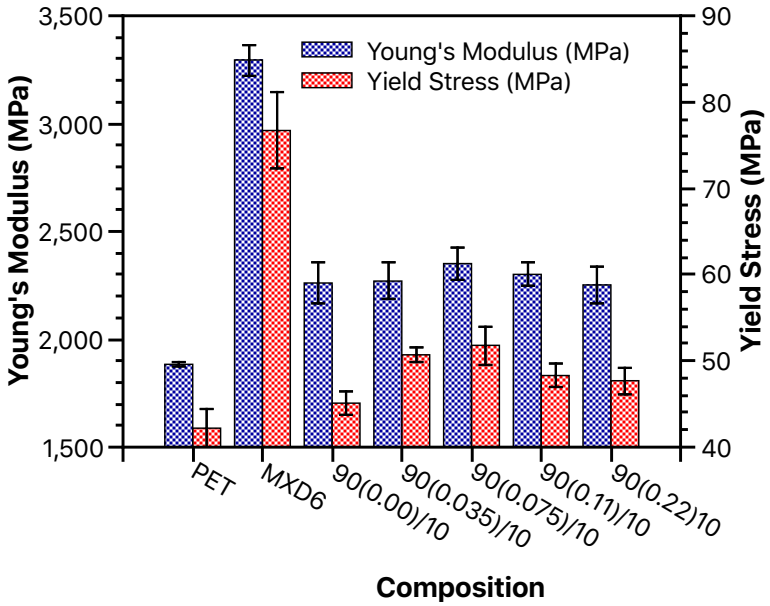

Figure S7.4. Young's modulus (blue) and yield stress (red) of Na^+-PPET/PET/MXD6 blends with various mol% of phosphonated monomer in the polyester component, along with pure PET and pure MXD6. Compression-molded films with thickness of 140-160 μm. Data reported on an average of 5 specimens with calculated standard deviations for each composition. Crosshead speed: 5 mm/min.

Table S7.1. Tensile properties of unoriented PET, MXD6, and Na^+-PPET/PET/MXD6 blend films.

	Young's Modulus (Mpa)	Yield Stress (Mpa)
PET	1884 ± 10	42 ± 2
MXD6	3295 ± 71	77 ± 4
90(0.00)/10	2261 ± 93	45 ± 2
90(0.035)/10	2270 ± 84	51 ± 1
90(0.075)/10	2351 ± 75	52 ± 2
90(0.11)/10	2301 ± 56	48 ± 1
90(0.22)/10	2252 ± 88	48 ± 2

Data reported on an average of 5 specimens with calculated standard deviations for each composition. Crosshead speed: 5 mm/min. Thickness: 140-160 μm.

Chapter 8. Comparison of Plasticization Effects of Deep Eutectic Solvent and Propylene Glycol on the Physical Properties of Poly(vinyl Alcohol) Films

(Manuscript in Preparation)

Lin Ju, Zahra Mansouri, Dong Guo, Guoliang Liu, and Robert B. Moore*

Department of Chemistry, Macromolecules Innovation Institute, Virginia Polytechnic Institute and State University, Blacksburg, VA 24061, United States

8.1 Abstract

This work demonstrated the successful plasticization of poly(vinyl alcohol) (PVOH) film using a deep eutectic solvent (DES) (choline chloride : malic acid (ChCl:MA)) as a plasticizer, and confirmed DES was more effective in plasticizing PVOH in comparison to propylene glycol (PG). Thermogravimetric analysis (TGA) indicated DES/PVOH blends exhibited higher thermal stability than PG/PVOH due to the low boiling point of PG. The thermal transitions and crystallization behaviors were examined using differential scanning calorimetry (DSC), and at the same wt% of plasticizer, DES-plasticized PVOH blends exhibited a greater glass transition temperature (T_g) depression, lower melting temperature (T_m), and lower crystallizability than PG analogues. Water absorption study investigated water uptake kinetics and equilibrium water uptake, and confirmed that DES/PVOH films were more moisture-sensitive and absorbed more moisture at higher plasticizer contents, while the water uptake of PG/PVOH films was independent of PG contents. Dynamic mechanical analysis (DMA)

revealed decreased T_g of DES/PVOH with increasing DES contents, which was in distinct contrast to the insignificant change in T_g of PG/PVOH films, suggesting DES afforded more chain mobility than PG. Tensile properties analysis implied rubber-like behavior for plasticized PVOH films. As compared to PG, DES leaded to lower Young's moduli and higher enhancement on elongation at break, confirming higher ductility for DES/PVOH films.

8.2 Introduction

Poly(vinyl alcohol) (PVOH) is one of the most popular water-soluble polymers produced by the polymerization of vinyl acetate monomer to form poly(vinyl acetate) (PVAc) followed by hydrolysis of the acetate groups.[1] PVOH exhibits excellent properties, such as high strength, high hydrophilicity, good barrier property, and good film-forming processability, and has been extensively applied in many fields including fibers, films, hydrogels, and adhesives.[1-4] PVOH usually displays a high crystallinity as well as a high melting temperature (T_m) due to the existence of a large number of strong inter- or intramolecular hydrogen bonding among the hydroxyl groups.[5] This high crystallinity affords very brittle PVOH films, and thermal processing of PVOH is limited since the T_m of PVOH is close to its thermal decomposition temperature (T_d).[6] Unlike most thermoplastic polymers, PVOH is processed mainly from an aqueous solution,[7] which limits the industrial applications in a large scale due to the time-consuming and uneconomical solution processing. Therefore, it is necessary to not only improve thermal processability of PVOH to expand it practical applications in manufacturing industries, but also enhance the ductility of PVOH films applied in the film packaging market.

Plasticization is a widely utilized technique for tailoring the thermal and mechanical properties of a given polymer by lowering crystallizability and increasing the mobility of polymer chains.[8, 9] Considerable efforts have focused on plasticizing PVOH by employing various types of plasticizers including water,[10-13] alcohols (e.g., ethylene glycol, propylene glycol, glycerol, sorbitol),[14-17] small organic compounds containing N-H and C=O functionalities (e.g., urea, caprolactam),[18, 19] low molecular weight poly(ethylene glycol),[20] ionic liquid,[21] and their proper combinations,[22] etc. O-H, N-H and C=O groups of these plasticizers could form stable hydrogen bonding with hydroxyl groups of PVOH, resulting in reduced degree of inter- or intramolecular interactions between PVOH chains, thereby diminishing the regularity and the rigidity of polymer chains.[14, 19] For example, PVOH blends consisting of plasticizers displayed decreased T_m and thus a wider thermal processing window compared to pure PVOH control.[14, 16, 17, 21] In addition, plasticized PVOH films have been demonstrated to exhibit rubber-like elasticity and increased elongation at break compared to unplasticized analogues attributed to the improved mobility of PVOH chains.[16, 17, 21] Practical processing of plasticized PVOH, however, is often limited due to partial evaporation, thermal decomposition, and instability of these plasticizers during extrusion process.[14, 15, 18]

Deep eutectic solvents (DES) have been reported to be the next generation solvents. A wide variety of compounds are known to form DES complexes, many of which are naturally occurring compounds. Naturally occurring DES are obtained upon mixing hydrogen donors, e.g., amino acids, organic acids, and sugars, and hydrogen acceptors, e.g., choline chloride derivatives.[23] DES exhibit negligible volatility (liquid state even far below 0 °C), high solubilization power strength for a wide range of

compounds, and high stabilization ability for some natural products.[24, 25] From an environmental and economic perspective, DES also offer many advantages including sustainability, low costs, simple preparation, and widespread material compatibility.[23, 26] All these properties make them of great interest for applications in a wide range of health-related product areas.[25-27]

More recently, Mano et al.[28] reported the application of choline chloride : citric acid (1:1 molar ratio) DES as a plasticizer in PVOH for the production of biopolymer fibers by electrospinning. Scanning electron microscopy (SEM) indicated smoother and more uniform fibers were achieved with the addition of DES as compared to pure PVOH control. Other applications of DES focused on the plasticization of other polymers,[29-31] e.g., corn starch and cellulose acetate, or on the compatibilization of biopolymer blends systems,[32, 33] e.g., blends of starch and polycaprolactone. However, to our knowledge, the plasticization effect of DES on the structure-property relationship of PVOH films has not been reported. Moreover, no systematic studies have been focused on an investigation of the effectiveness of DES versus other widely employed plasticizers in plasticizing PVOH.

In this work, we report the first investigation of the plasticization effect of choline chloride : malic acid (ChCl:MA, 1:1 molar ratio) DES on thermal, mechanical, and water absorption properties of PVOH by establishing the valuable structure-property relationship for DES/PVOH films. The plasticization effect of DES was also compared to propylene glycol (PG), one of the widely studied alcohol-type plasticizers for PVOH, on a mass basis in order to provide valuable insights to manufacturing and practical applications from industrial points of view. The purpose of this work is to evaluate the

commercial opportunities for these DES-plasticized PVOH films in future packaging applications.

8.3 Experimental Section

Materials. Poly(vinyl alcohol), 88% hydrolyzed, M_w = 85K-120K g/mol, was purchased from Acros Organics and was used as received. Choline chloride (>98%) was purchased from Alfa Aesar and was dried under vacuum overnight at 70 °C prior to use. DL-Malic acid (98%) and propylene glycol were purchased from Alfa Aesar and Sigma-Aldrich, respectively, and were used as received.

Preparation of Deep Eutectic Solvent (DES). A stoichiometric DES mixture of choline chloride (ChCl) and malic acid (MA) with 1:1 molar ratio was prepared. ChCl and MA were added to a round-bottomed flask equipped with a magnetic stir bar, and then the flask was placed into an oil bath at 90 °C with constant stirring. A clear liquid was obtained after stirring for about 0.5 h, and the generated clear DES mixture was allowed to stir for another 2.5 h at 90 °C to ensure complete mixing. The DES mixture remained in the clear liquid state after cooling to room temperature.

Preparation of Plasticizer/PVOH Solution Blends. All blends were prepared as 10 wt% solutions in deionized water (i.e., $\text{wt\%} = \frac{Mass_{PVOH} + Mass_{Plasticizer}}{Mass_{Solution\ Mixture}} \times 100\%$). To prepare the blends, PVOH was first dissolved in 40 mL deionized water at 90 °C, and the solution mixture was allowed to stir for about 5 h to ensure complete dissolution. The plasticizer solutions were obtained by dissolving plasticizer in 5 mL deionized water at room temperature after stirring for about 10 min. The plasticizer/PVOH solution blends were prepared by adding the plasticizer solution into the PVOH solution, and the

generated solution mixtures were allowed to stir at 90 °C overnight to ensure complete mixing. The blend compositions were designated as wt% plasticizer/wt% PVOH, and four plasticizer/PVOH blend compositions, i.e., 5/95, 10/90, 15/85 and 20/80 (w/w), were prepared. Both DES/PVOH and PG/PVOH solution blends were prepared by the same procedure, and a composition of pure PVOH (without plasticizer) as a control was also prepared.

Solution Casting Method. The generated solution blends were cast onto a glass substrate at room temperature using a doctor blade set to 0.075 inch. The wet films were allowed to first dry at room temperature for 48 h and then at 50 °C for about 2 h. The generated clear films were peeled off from glass substrate, and were further dried under vacuum at 30 °C for 48 h, resulting in a final thickness of 70-90 μm. Kimwipes were utilized to cover these films during drying in the vacuum oven.

Thermogravimetric Analysis (TGA). As-cast films after vacuum drying were utilized for thermal stability analysis. TGA of plasticizer/PVOH films was performed on a TA Instruments TGA Q500 with a heating ramp from ambient temperature to 550 °C at a heating rate of 10 °C/min under constant nitrogen purging. $T_{d,\,5\ wt\%}$ corresponded to the temperature at 5% weight loss of the initial sample weight, and was listed in **Table 8.1**.

Differential Scanning Calorimetry (DSC). As-cast films after vacuum drying were utilized for DSC measurement. A TA instruments Q2000 differential scanning calorimetry (DSC) was used to determine the thermal transitions and crystallization behavior of plasticized PVOH blends. Under a nitrogen atmosphere, the samples (~5-8 mg) prepared in aluminum Tzero hermetic pans were heated from ambient temperature to 190 °C (200 °C for PVOH control) at 10 °C/min, quench cooled to -50 °C at -60 °C/min,

reheated from -50 °C to 190 °C (200 °C for PVOH control) at 10 °C/min, and then cooled to 0 °C at -10 °C/min. The glass transition temperature (T_g), melting temperature (T_m), enthalpy of melting (ΔH_m), and degree of crystallinity (X_c) were determined from the second heating scan after erasing the thermal history; the crystallization temperature (T_c) and enthalpy of crystallization (ΔH_c) were investigated from the subsequent cooling scan by using the TA Instruments Universal Analysis software. X_c was determined using the following relationship:

$$X_c = \frac{\Delta H_m}{\Delta H_m^\circ} \tag{8.1}$$

where ΔH_m is the enthalpy of melting determined from integration of the melting endotherm and ΔH_m° is the theoretical enthalpy of melting of 100% crystalline PVOH (138.6 J/g).[34]

Water Uptake Measurement. The water uptake kinetics of PVOH films with various plasticizer contents were studied at a relative humidity of 50% at 30 °C, and the equilibrium water absorption was investigated at relative humidity of 30%, 50%, and 70% at 30 °C. The mass of the dry film (W_{dry}) was recorded prior to measurement, and the mass of the wet film (W_{wet}) was recorded as a function of time to determine the water sorption kinetics of PVOH blend films. The equilibrium water uptake for each film composition was determined by conditioning dry films in the humidity chamber for 6 h. The reported values are the average of 5 samples for each blend composition. The water uptake was calculated as:

$$\text{Water uptake} = \frac{W_{wet} - W_{dry}}{W_{dry}} \times 100\% \tag{2}$$

Dynamic Mechanical Analysis (DMA). The as-cast films after vacuum drying were conditioned in a 40% relative humidity atmosphere at 30 °C for 24 h before

measurements. A TA Instruments Q800 DMA in oscillatory tension mode was used to determine the mechanical properties of PVOH blend films as a function of temperature. Samples were ramped at 2 °C/min from -50 °C to 190 °C at a frequency of 1 Hz, an oscillatory amplitude of 15.0 μm, and a static force of 0.01 N to determine the effect of modulus versus temperature. The β and α relaxation were determined from the peaks in tanδ versus temperature.

Tensile Test. Dumbbell-shaped specimens were cut from the vacuum dried as-cast films, and were conditioned in a 40% relative humidity atmosphere at 30 °C for 24 h before measurements. Tensile testing was conducted at ambient relative humidity and room temperature. The specimens were clamped in the tensile fixture with a distance between grips of 26.54 mm, and the width of narrow section of 3.32 mm. The thicknesses of these specimens were accurately measured for each sample using a calibrated caliper, and were ranging from approximately 70 μm to 90 μm. Tensile testing was performed on a 5500R Instron universal testing instrument at a crosshead speed of 5 mm/min. The Young's moduli, elongation at break, and stress at break were reported on an average of five specimens, tabulated in **Table S8.2**.

8.4 Results and Discussion

8.4.1 Thermal Properties. Thermogravimetric analysis (TGA) was performed to evaluate the thermal stability of DES/PVOH and PG/PVOH blends, as shown in **Figure 8.1**. The thermal degradation temperatures (noted by the temperature at which 5 wt% weight loss is observed, $T_{d,\,5\ wt\%}$) of DES/PVOH and PG/PVOH blends, along with pure PVOH, are summarized in **Table 8.1** and compared in **Figure 8.2**. PVOH presents two

weight loss stages: the first stage starts near 260 °C, consistent with the elimination of the side groups of PVOH; and the second stage starts near 380 °C, corresponding to the breakdown of PVOH backbone.[35, 36] Pure PVOH itself shows a $T_{d,\ 5\ wt\%}$ of 278 °C. From the TGA thermograms shown in **Figure 8.1A**, it is clear that DES/PVOH blends display lower onsets of weight loss than that of pure PVOH, and $T_{d,\ 5\ wt\%}$ of DES/PVOH blends shifts to a lower temperature region with increasing DES incorporations. This decreased $T_{d,\ 5\ wt\%}$ of DES/PVOH blends indicates DES as a plasticizer fails to improve the thermal stability of PVOH due to DES ($T_{d,\ 5\ wt\%}$ of DES = 203 °C) degrading much earlier than pure PVOH ($T_{d,\ 5\ wt\%}$ of PVOH = 278 °C). By comparison, PG/PVOH blends exhibit much lower $T_{d,\ 5\ wt\%}$ at any plasticizer content than DES/PVOH blends (**Figure 8.2**). Considering the low boiling point of PG (i.e., 188 °C), the lower thermal stability of PG/PVOH blends is reasonably attributed to the volatility issue of PG. This comparison signifies the higher thermal stability of DES/PVOH blends than PG/PVOH analogs.

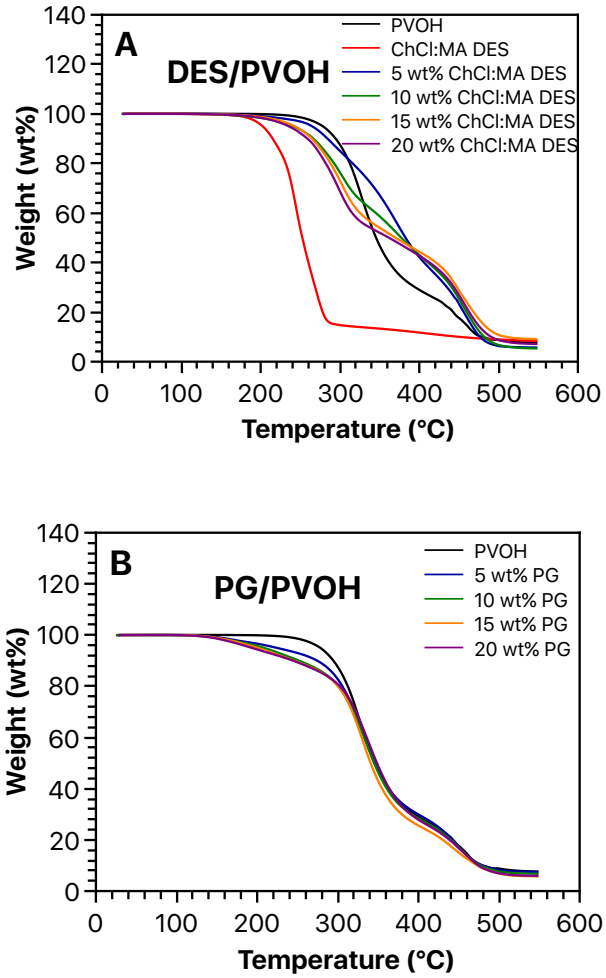

Figure 8.1. Thermogravimetric analysis (TGA) thermograms of (A) ChCl:MA (1:1 molar ratio) deep eutectic solvent (DES)/PVOH blends, along with ChCl:MA DES, and (B) propylene glycol (PG)/PVOH blends. TGA analysis was performed at 10 °C/min under nitrogen purge.

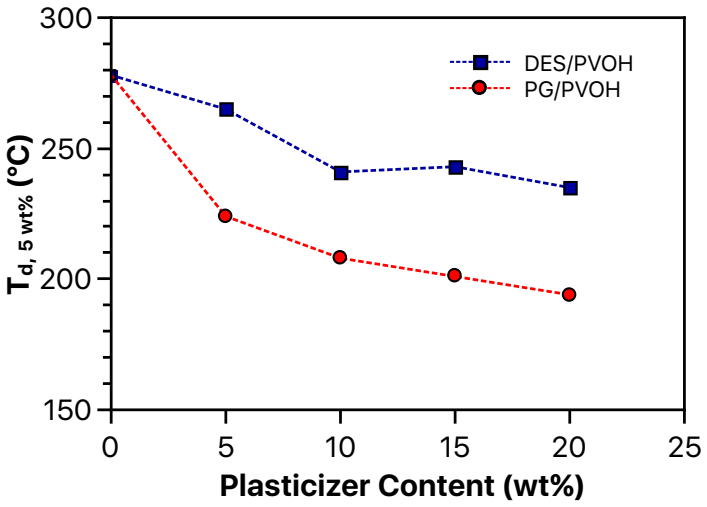

Figure 8.2. $T_{d,\ 5\ wt\%}$ (°C) of DES-plasticized (blue squares) and PG-plasticized (red circles) PVOH films as a function of plasticizer content (wt%). TGA analysis was performed at 10 °C/min under nitrogen purge.

Differential scanning calorimetry (DSC) was utilized to provide further insight into the plasticization effect of DES and PG on the thermal properties of PVOH blends. The samples were first heated into the melt and quench cooled to erase thermal history, and then heated into melt again followed by a slow cooling. The second heating thermograms and the subsequent slow cool thermograms of dry DES/PVOH and PG/PVOH blends with varying amounts of plasticizers are shown in **Figures 8.3-5**. The heating thermograms for all the blend compositions display two enthalpic events: a glass transition and a melting endotherm; and the subsequent cooling scans reveal a crystallization exotherm. The corresponding thermal data are summarized in **Table 8.1**, and the glass transition temperature (T_g), the melting temperature (T_m) and the

crystallization temperature (T_c) for DES/PVOH and PG/PVOH blends are compared separately in **Figure 8.6**.

The influence of DES and PG incorporations on the T_g of PVOH blends is presented in **Figure 8.3** and compared in **Figure 8.6A**. Based on the graph of T_g versus wt% of plasticizer, it is evident that DES leads to a greater T_g depression than PG across all plasticizer contents, implying DES is more effective at plasticizing PVOH. A linear decrease in T_g is observed with increasing DES content in DES/PVOH blends. Note that for pure PVOH, the hydroxyl groups contribute to the stiffness of the polymer chains via hydrogen bonding interaction.[13] DES form stable hydrogen bonding with the hydroxyl groups of PVOH, attenuating the hydrogen bonding interactions of PVOH, thus diminishing chain stiffness.[10] Consequently, with increasing DES content, DES/PVOH blends exhibit an increased degree of chain mobility, and hence, yielding a decreased T_g. In contrast, however, for PG/PVOH blends, there surprisingly appears to be a small effect on T_g with the addition of PG and a slight decrease in T_g with plasticizer concentration, which is in agreement with earlier study of solution-cast PG/PVOH films from Cho et al.[14] The more profound decrease in T_g of DES/PVOH blends implies DES is more effective in plasticizing PVOH possibly due to the presence of stronger H-bonding interactions generated between DES and PVOH in DES/PVOH blends as compared to PG-plasticized PVOH. Furthermore, the Fox equation[37] fits well to the experimental T_g of DES/PVOH blends, but fails to fit the T_g of PG-plasticized blends. For PVOH blends plasticized with 10-20 wt% of PG, the experimental T_g obtained from DSC analysis is higher than the predicted T_g from Fox equation. This behavior may be attributed to the

possible phase separation of PG within the polymer matrix[38, 39] or possible PG evaporation during drying process, which minimize the plasticization efficiency of PG.

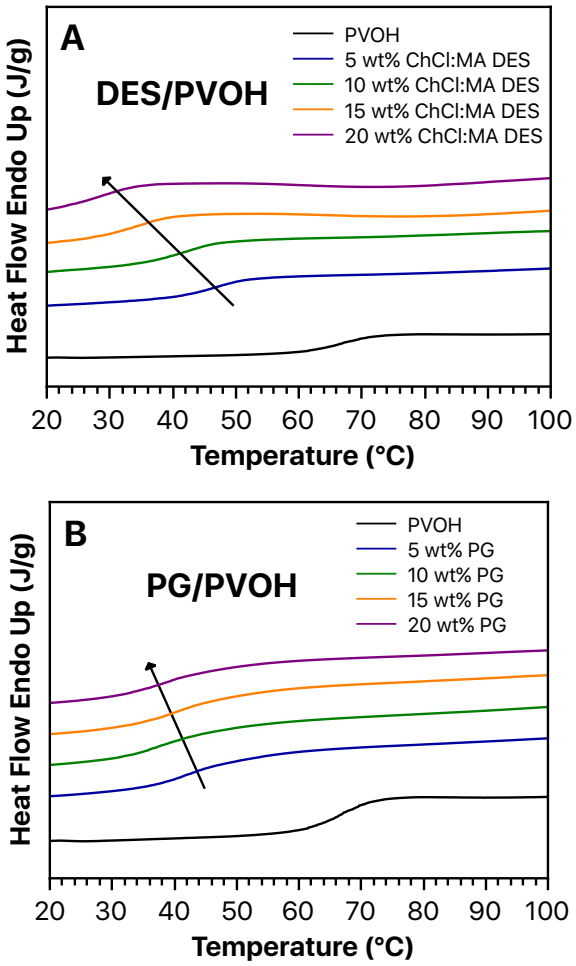

Figure 8.3. The glass transitions of (A) ChCl:MA DES-plasticized and (B) PG-plasticized PVOH blends. Second heat reported with a heating rate of 10 °C/min after quench cooling (-60 °C/min) from the 190 °C (200 °C for PVOH).

DSC was also utilized to investigate the plasticization effect of DES and PG on the crystallizability of PVOH blends, as displayed in **Figures 8.4** and **8.5**. As expected, both DES/PVOH and PG/PVOH exhibit decreased T_m and decreased degree of crystallinity (X_c) during heating, and a T_c depression during slow cooling with increasing

plasticizer content. The plasticizers hydrogen-bonded to the hydroxyl groups along the chains are presumably acting as physical defects that are excluded from the crystalline domains. With an increasing defect content, the statistical average length of crystallizable segment decreases, limiting the lamellar thickness.[40-43] Consequently, it is not surprising then that both DES- and PG-plasticized PVOH series show a T_m depression and a decreased X_c with increasing plasticizer content. Similarly, the systematic decrease in T_c reflects a reduction in the rate of crystallization during these non-isothermal scans. Upon cooling from the melt, as the polymer chains attempt to pack into crystalline structures, plasticizers act as interactive defects that are rejected from the growing crystalline interface, thus lowering crystallizability.[41, 43] Nonetheless, it is important to note that the effects on thermal properties of DES/PVOH blends occur to a much greater extent compared to the PVOH blends containing PG, despite of their analogous plasticizer contents.

At identical plasticizer content, DES/PVOH samples display significantly higher magnitude of the melting endotherms and crystallization exotherms than their PG-plasticized analogues (**Figures 8.4** and **8.5**). Furthermore, in comparison to PG/PVOH blends, DES-plasticized PVOH displays significantly greater T_c and T_m depression and a larger loss of crystallinity when referenced to pure PVOH. For example, the T_m of plasticized PVOH with 20 wt% DES (133 °C) is drastically depressed by 29% as compared to pure PVOH (187 °C), while PVOH with 20 wt% PG is only decreased by 11% to 166 °C. From a practical perspective, the more profound T_m depression of DES/PVOH suggests a higher thermal processability.[21, 44] This comparison reveals that the DES/PVOH blends require much lower plasticizer content to achieve the same

thermal processability as compared to PG-containing PVOH blends. Additionally, X_c of DES/PVOH decreases by 57% with the addition of 20 wt% DES, whereas a slight decrease (17%) in X_c is observed for PG/PVOH blends (**Table 8.1**). T_c of DES/PVOH blend at 15 wt% of DES decreases to 72 °C from 152 °C (pure PVOH), and at 20 wt% of DES, the DES/PVOH blend is not capable of crystallizing during the slow cooling. In contrast, however, only a slight depression in T_c is observed for PG/PVOH blends over a wide range of PG concentration (i.e., from 5 wt% to 20 wt%). Based on these different thermal behaviors, it is evident that DES/PVOH blends display a much lower crystallizability than PG-plasticized PVOH analogues. Given that the microstructure on the probability of encountering a defective stem affects crystallization behavior,[40] it is reasonable to postulate DES-plasticized PVOH has less crystallizable stems that minimize the time-consuming rejection/replacement process and thus limit crystallizability. This behavior also implies DES is presumably H-bonded to the hydroxyl groups of PVOH more effectively than PG, resulting in less crystallizable PVOH stems. Consistent with the greater depressed T_g for DES/PVOH blends, these differences in crystallizability between DES- and PG-plasticized PVOH blends further confirms the more profound plasticization effect achieved by adding DES.

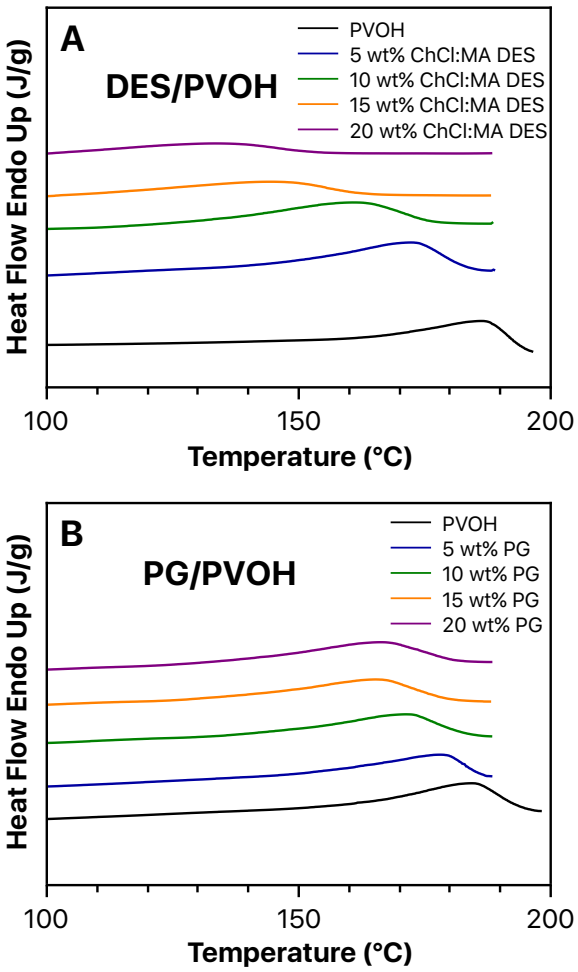

Figure 8.4. Melting endotherms of (A) ChCl:MA DES-plasticized and (B) PG-plasticized PVOH blends. Second heat reported with a heating rate of 10 °C/min after quench cooling (-60 °C/min) from the 190 °C (200 °C for PVOH).

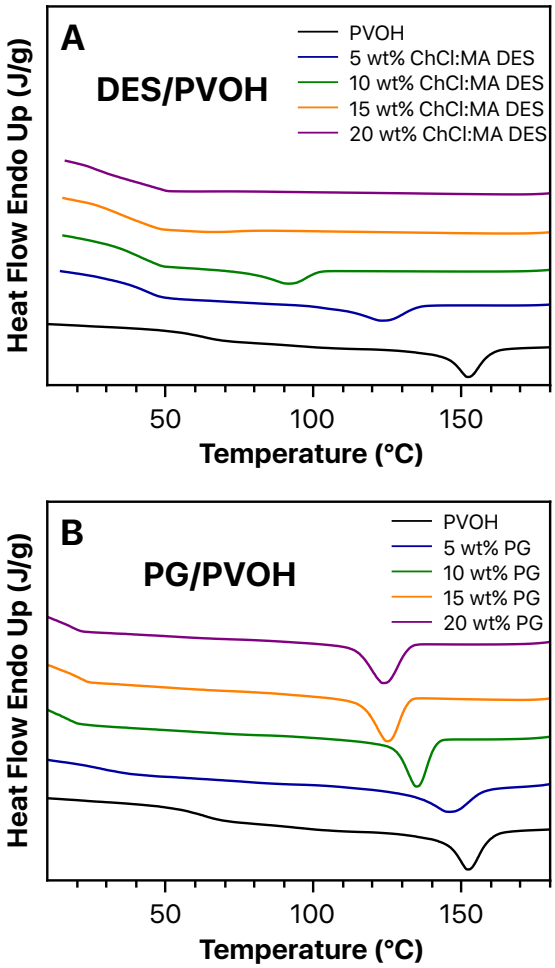

Figure 8.5. DSC cooling scans of (A) ChCl:MA DES-plasticized and (B) PG-plasticized PVOH blends. Subsequent cooling reported with a cooling rate of -10 °C/min after heating to 190 °C (200 °C for PVOH).

Table 8.1. Summary of DSC Results for DES/PVOH, PG/PVOH Blends.

Sample	$T_{d,\ 5\ wt\%}$ (°C)	T_g (°C)	T_m (°C)	ΔH_m (J/g)	% Crystallinity	T_c (°C)	ΔH_c (J/g)
PVOH	278	63	187	23	16.6	152	18
ChCl:MA DES	203	-	-	-	-	-	-
5wt% DES	265	47	173	21	15.2	112	17
10wt% DES	241	42	161	17	12.3	87	9
15wt% DES	243	36	144	14	10.1	72	4
20wt% DES	235	28	133	10	7.2	-	-
5wt% PG	224	42	177	19	13.7	142	12
10wt% PG	208	39	171	20	14.4	139	12
15wt% PG	201	39	165	19	13.7	141	13
20wt% PG	194	37	166	19	13.7	143	14

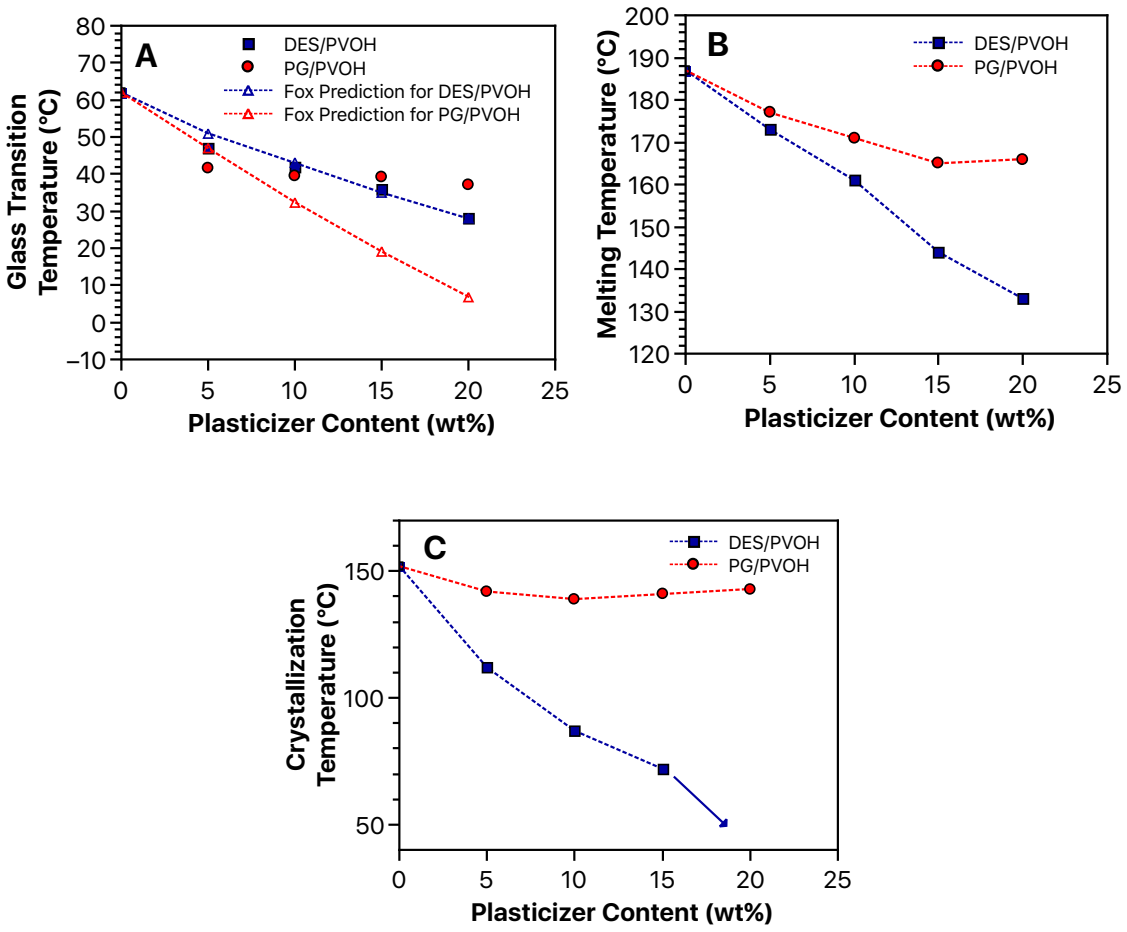

Figure 8.6. (A) Glass transition temperatures, (B) melting temperatures, and (C) crystallization temperatures of ChCl:MA DES-plasticized (blue squares) and PG-plasticized (red circles) PVOH blends versus plasticizer content (wt%). Predicted glass transition temperatures using Flory-Fox equation for ChCl:MA DES-plasticized (unfilled blue triangle) and PG-plasticized (unfilled red triangle) PVOH films are also shown in (A).

8.4.2 Water Absorption. PVOH films absorb moisture from the environment due to the hydrophilic nature resulting from the large amount of hydroxyl groups. Water uptake is an important parameter dictating not only the mechanical integrity but also the

gas barrier properties of the films.[13, 45] Thus, it is important to evaluate water absorption performance of PVOH blend films. Water absorption kinetics of the dried, as-cast PVOH blend films were investigated by conditioning the films in a 50% relative humidity atmosphere at 30 °C. **Figure 8.7** provides the water uptake of DES/PVOH and PG/PVOH films as a function of time. In each case, a rapid increase is observed at the beginning of the water absorption process, and thereafter water uptake curves level off for a range of time where it reaches an equilibrium after about 60-70 min. It is apparent that both water absorption rate and equilibrium water uptake of DES/PVOH films systematically increase with increasing the concentration of DES, which is in distinct contrast to the similar water absorption behavior among all PG/PVOH compositions. This behavior indicates that the increased DES concentration leads to enhanced water uptake performance for DES/PVOH films, while the water absorption of PG/PVOH films is independent of PG contents. Considering the ionic nature of DES as compared to nonionic PG, this enhanced water uptake for DES/PVOH films is reasonably attributed to the relatively greater hydrophilicity and the lower crystallinity with increasing DES content. Furthermore, DSC results reveal the presence of a greater chain mobility for DES/PVOH blends versus PG/PVOH blends as evidenced by a more profound T_g depression with increasing wt% of DES. Given that the greater chain mobility imparts a relatively higher free volume responsible for facilitating the diffusion of water in the films,[10, 22, 46-48] a higher water uptake rate is achieved for DES-plasticized PVOH films.

Additionally, the water uptake rate and equilibrium water uptake for DES-plasticized PVOH films at high plasticizer contents (i.e., 15 wt% and 20 wt%) are much higher compared to PG/PVOH analogues, but are lower than PG/PVOH films at low

plasticizer concentration (i.e., 5 wt%), as displayed in **Figure 8.7**. This behavior implies that DES/PVOH films are more moisture-sensitive and absorb more water at higher plasticizer concentrations. Consistent with the crystallinity determined from DSC analysis, the higher water uptake performance of DES/PVOH films is reasonably due to their lower crystallinity. Similarly, at 5 wt% plasticizer content, a higher crystallinity for DES/PVOH film (X_c = 15.2%) is observed as compared to PG/PVOH analogue (X_c = 13.7%), which explains the higher moisture resistance of DES/PVOH films at low wt% plasticizer.

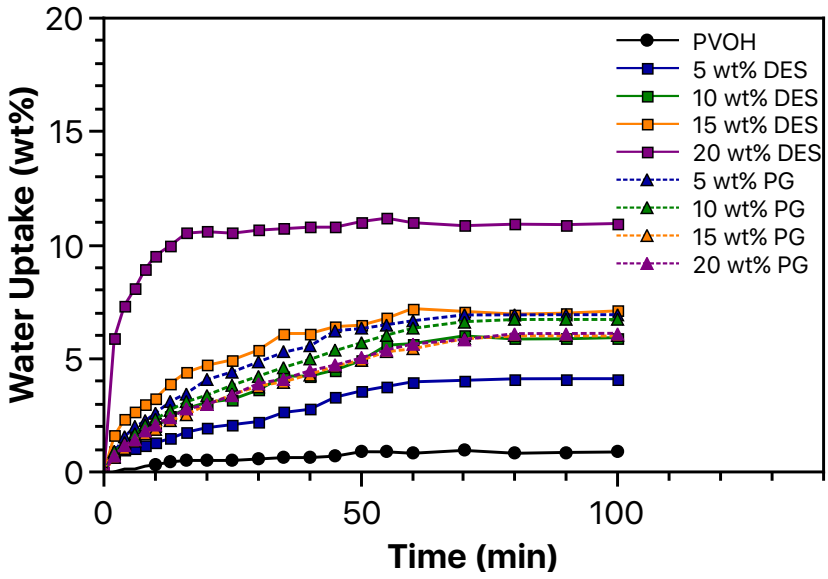

Figure 8.7. Water uptake of DES/PVOH (solid line) and PG/PVOH (dash line) films as a function of time in a 50% relative humidity atmosphere at 30 °C.

The water absorption performance of DES/PVOH and PG/PVOH blends is further investigated at different relative humidity (RH), i.e., 30% and 70%, and the corresponding equilibrium water uptake data are compared in **Figure 8.8**. Not surprisingly, higher relative humidity affords higher water uptake for both DES/PVOH

and PG/PVOH films. Additionally, it is clear that increased plasticizer content leads to significantly increased water uptake for DES-plasticized PVOH films. In contrast, however, no significant difference is observed for PG/PVOH blends at any wt% of PG. This different water update between DES/PVOH and PG/PVOH further emphasizes that water uptake of PG/PVOH films is independent of PG concentration, suggesting a similar polarity of PG compared to PVOH.

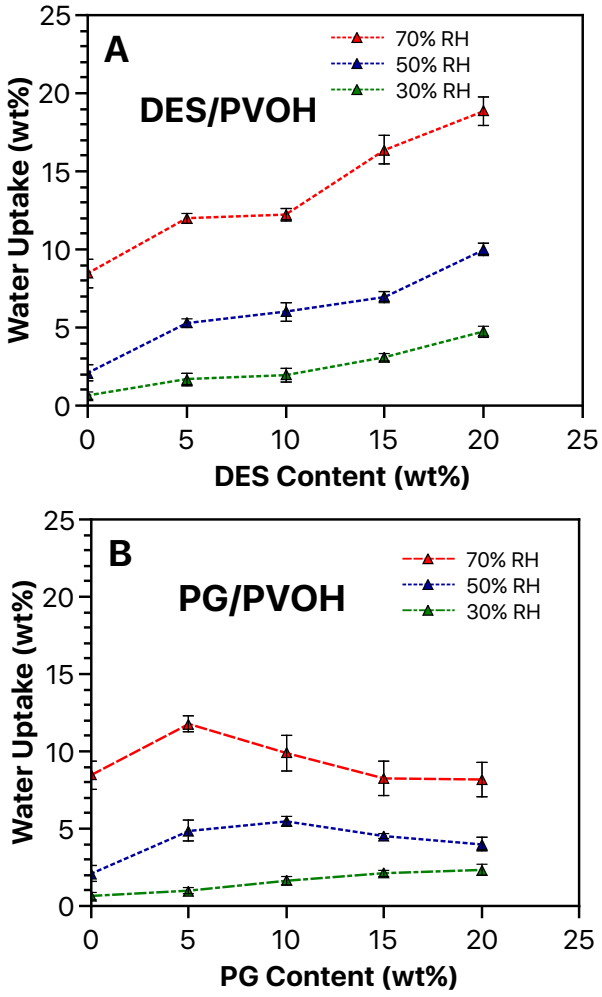

Figure 8.8. Equilibrium water uptake of (A) ChCl:MA DES-plasticized and (B) PG-plasticized PVOH films in relative humidity (RH) of 30%, 50% and 70%.

8.4.3 Dynamic Mechanical Analysis. Dynamic mechanical analysis (DMA) investigated the thermomechanical properties of DES/PVOH and PG/PVOH films from -50 °C to 190 °C (**Figure 8.9**). Given that PVOH is sensitive to moisture, it is important to consider storage conditions for film products when analyzing their mechanical properties. As-cast films were conditioned in a 40% relative humidity atmosphere at 30 °C for 24 h before measurements. Both DES/PVOH and PG/PVOH films exhibit similar moduli in the glassy region at low temperature, and then modulus curves start to drop, representing onset of the glass transition (i.e., from the glassy state to flowing). Following the glass transition, the crystalline phase maintains the mechanical integrity for these films, affording small plateau regimes approximately from 90 °C to 140 °C, and the plateau regimes become more distinguishable for PG/PVOH blend films. Finally, crystalline domains of all PVOH films served as reinforcing filler to preserve the modulus level with increasing temperature until the onset of melting, and the observed temperature agrees well with the T_m measured from DSC.

Increasing plasticizer content leads to earlier onset of flow, attributed to the decreased film stiffness as a result of disrupted H-bonding interaction of PVOH and the reduction in crystallinity. Further increasing wt% of DES gradually shifts onset of flow to a lower temperature region, while an insignificant effect is observed on the storage moduli of PG/PVOH films at various PG contents. This behavior is consistent with the decreased T_g and crystallinity as observed for DES/PVOH blends from DSC analysis, indicating DES yields a greater disruption of hydrogen bonding interaction of PVOH and affords a more flexible structure as compared to PG. This is further confirmed by the decreased plateau moduli with increasing DES contents, which differ significantly from

the similar plateau moduli for PG/PVOH films across all PG contents. Furthermore, given water is considered as a plasticizer for PVOH,[10-13] increased water uptake in DES/PVOH films with increasing DES content also contributes to the different moduli between these two series of PVOH films.

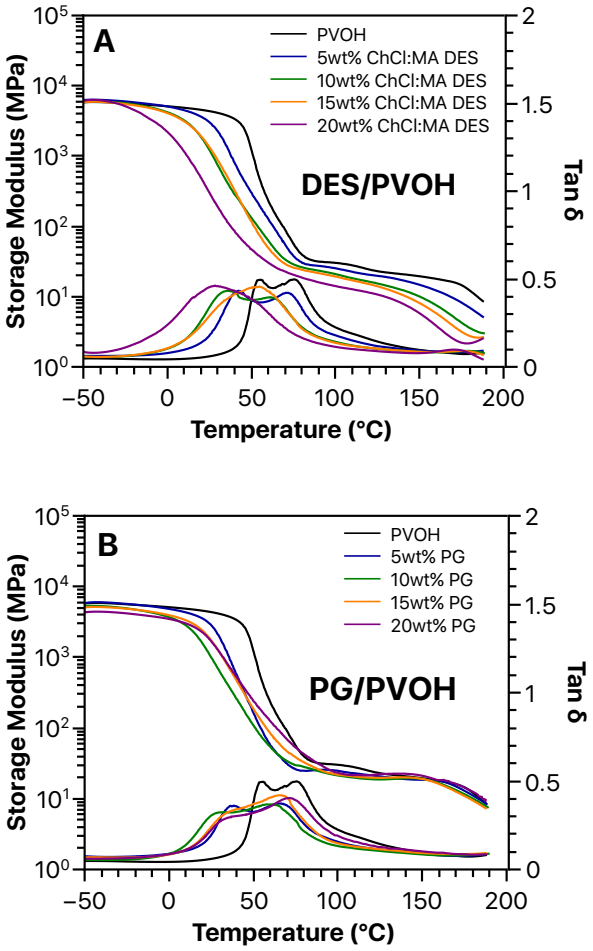

Figure 8.9. Dynamic mechanical temperature ramps of (A) ChCl:MA DES-plasticized and (B) PG-plasticized PVOH films at various plasticizer contents. 1 Hz, 2 °C/min, an oscillatory amplitude of 15.0 μm, and a static force of 0.01 N were employed. The films were conditioned in a 40% relative humidity atmosphere at 30 °C for 24 h before measurements.

Two mechanical relaxations corresponding to primary (α) and secondary (β) relaxations of PVOH[12, 13, 49] are shown in the tan δ versus temperature curves (**Figure 8.9**). The α relaxation, corresponding to the long-chain segmental motion in the amorphous region (i.e., the glass transition temperature),[12, 13, 49] takes place between 40 °C and 80 °C according to the water content and plasticizer concentration. The molecular mechanisms of the β relaxation of PVOH films are not well understood. The β relaxation has been related to the movement of polar groups on the polymer that are not hydrogen-bonded each other.[50] Therefore, the β relaxation of these PVOH films likely represents water-PVOH or plasticizer-PVOH complex units.

The α and β relaxations for DES- and PG-plasticized PVOH films derived from the tan δ versus temperature curves are summarized in **Table S8.1**, and compared in **Figure 8.10** with respect to the plasticizer concentration. The α relaxation of pure PVOH is 76 °C, and shifts to lower temperatures with increasing DES loading, indicating a decreased T_g. By comparison, DES/PVOH films display a slightly decreased T_g to 61 °C at 10 wt% PG and then an increase to 72 °C after further increasing PG content to 20 wt%. Note that T_g reflects the extent of the mobility of polymer chains.[10, 11] Consistent with the results from DSC analysis, the significant difference between T_g of DES/PVOH and PG/PVOH films further demonstrates DES affords more chain mobility than PG, again emphasizing the relatively higher effectiveness of DES in plasticizing PVOH. A similar trend is observed on the β relaxation of DES- and PG-plasticized PVOH films, which is consistent with the different equilibrium water uptake between DES/PVOH and PG/PVOH films.

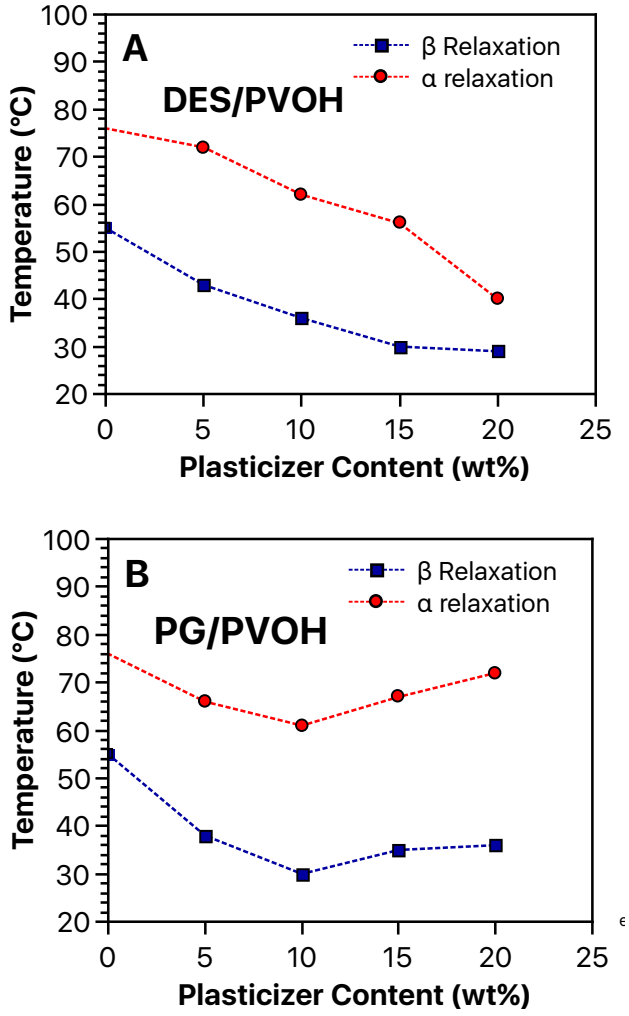

Figure 8.10. β relaxation (blue squares) and α relaxation (red circles) of (A) ChCl:MA DES-plasticized and (B) PG-plasticized PVOH films at various plasticizer contents. 1 Hz, 2 °C/min, an oscillatory amplitude of 15.0 µm, and a static force of 0.01 N were employed. The films were conditioned in a 40% relative humidity atmosphere at 30 °C for 24 h before measurements.

8.4.4 Tensile Properties. For use in packaging applications, plasticized PVOH films must have suitable mechanical strength to prevent film cracking during packaging and transportation. The plasticization effect of DES and PG concentration on the

mechanical properties of PVOH blends was investigated using tensile testing. Analysis was performed on as-cast films that were equilibrated at 40% relative humidity for 24 h. The representative engineering stress-strain curves of PVOH blends are displayed in **Figure 8.11**, and the corresponding tensile properties, including Young's modulus, elongation at break, and stress at break are summarized in **Table S8.2** and compared in **Figure 8.12**. The stress-strain curves of PVOH blend films display a continuous increase of strain with stress as well as an absence of yield point as compared to pure PVOH, suggesting rubber-like behavior. This reveals that the incorporation of plasticizer successfully overcomes the brittle film properties of pure PVOH and leads to an enhancement of film ductility.

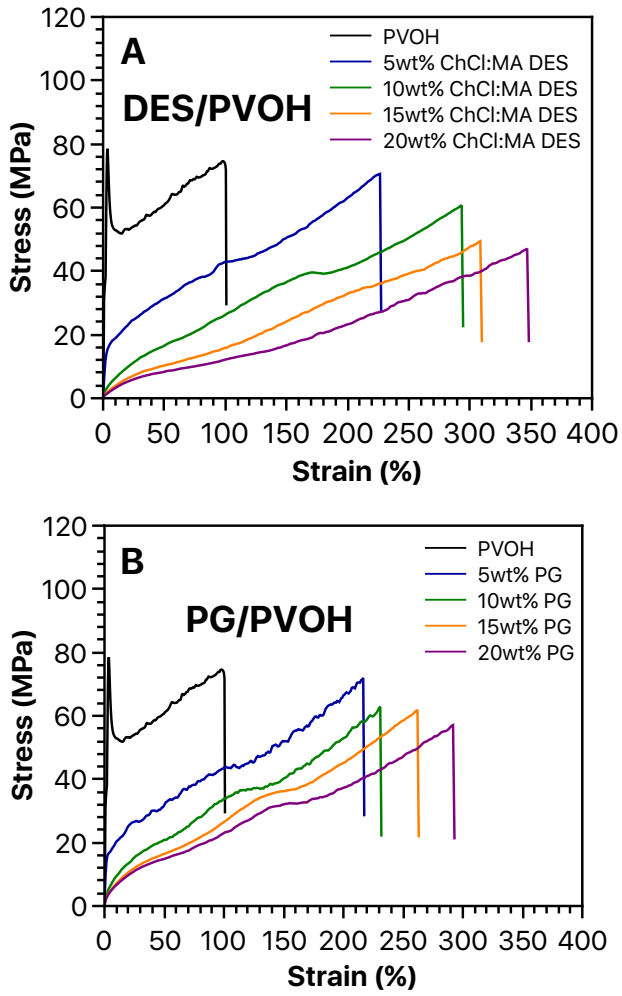

Figure 8.11. Stress-strain curves of (A) ChCl:MA DES-plasticized and (B) PG-plasticized PVOH films along with pure PVOH film. The films were conditioned in a 40% relative humidity atmosphere at 30 °C for 24 h before measurements. Samples were tested with a crosshead speed of 5 mm/min.

Young's modulus or elastic modulus is the fundamental measure of the film stiffness,[51] and is associated with the resistance of the film to elastic deformation.[52, 53] The lower the Young's modulus, the lower the stiffness of the films, thus the higher the film ductility. The effect of plasticizer concentration (0 wt% -20 wt%) on the Young's

moduli of DES- and PG-plasticized PVOH films is provided in **Figure 8.12A**. It is clear that the Young's moduli of PVOH blend films highly decrease with the addition of plasticizer, and continue decreasing with increasing plasticizer content. For example, the incorporation of only 5 wt% DES significantly decreases the Young's modulus of PVOH by almost 80%, and a 70% reduced Young's modulus is achieved for PG/PVOH blends at the same wt% plasticizer. Additionally, Young's moduli of DES/PVOH films gradually decrease from 701 MPa to 34 MPa as the DES wt% increases from 5 wt% to 20 wt%, and the same trend in Young's moduli is seen for PG/PVOH films. This significant decrease in Young's moduli suggests that PVOH films loss their stiffness and become more ductile with the addition of plasticizer. The H-bonding interactions between the plasticizer and the hydroxyl groups of PVOH disrupt the H-bonding interaction of pure PVOH, reducing the chain stiffness and improving the chain mobility, consequently resulting in more flexible networks. Thus, the plasticized PVOH films become less resistant to elastic deformation as evidenced by lower Young's moduli. Furthermore, PVOH films plasticized with DES reveal lower Young's moduli as compared to PG/PVOH films at the same plasticizer concentration. Consistent with the greater T_g depression of DES/PVOH blends in thermal properties analysis, this result further demonstrates that DES leads to a greater chain mobility as compared to PG.

The effect of plasticizer concentration on the elongation at break of DES- and PG-plasticized PVOH films is shown in **Figure 8.12B**. Increased plasticizer concentration from 0 wt% to 20 wt% leads to a significant improvement in the film elongation, i.e., about 3 times higher for both DES/PVOH and PG/PVOH films. In comparison to PVOH films containing PG, DES-plasticized PVOH films exhibit slightly higher elongation at

break values for each composition. Elongation at break is defined as the ability of film to deform before finally breaking, and is related to the chain mobility and film ductility.[51, 52] Consistent with the lower Young's moduli of DES/PVOH films, the incorporated DES leads to lower rigidity of PVOH chains and higher ductility of films by allowing more chain mobility, thus higher elongation at break than PG analogues.

Plasticized-PVOH films reveal lower stress at break compared to pure PVOH, and increasing plasticizer content causes a more significant reduction in the stress at break for DES/PVOH films as compared to PG/PVOH films (**Figure 8.12C**). This reduced stress at break for plasticized PVOH films is consistent with the observations reported by many researchers.[14, 21, 47, 51, 52, 54-56] Stress at break is the stress that a film can withstand being stretched before necking or failing.[47] The high film resistance under force for pure PVOH film is possibly attributed to the intermolecular H-bonding interaction between PVOH chains.[52, 56] The incorporated plasticizer leads to a large increase in the mobility of polymer chains, facilitating chain movements under force, therefore decreasing the stress at break as a result of reduced film resistance.[47] Additionally, in contrast to the small variation among all the compositions of PG/PVOH, the significant decrease in stress at break for DES/PVOH films again confirms DES imparts a higher chain mobility than PG.

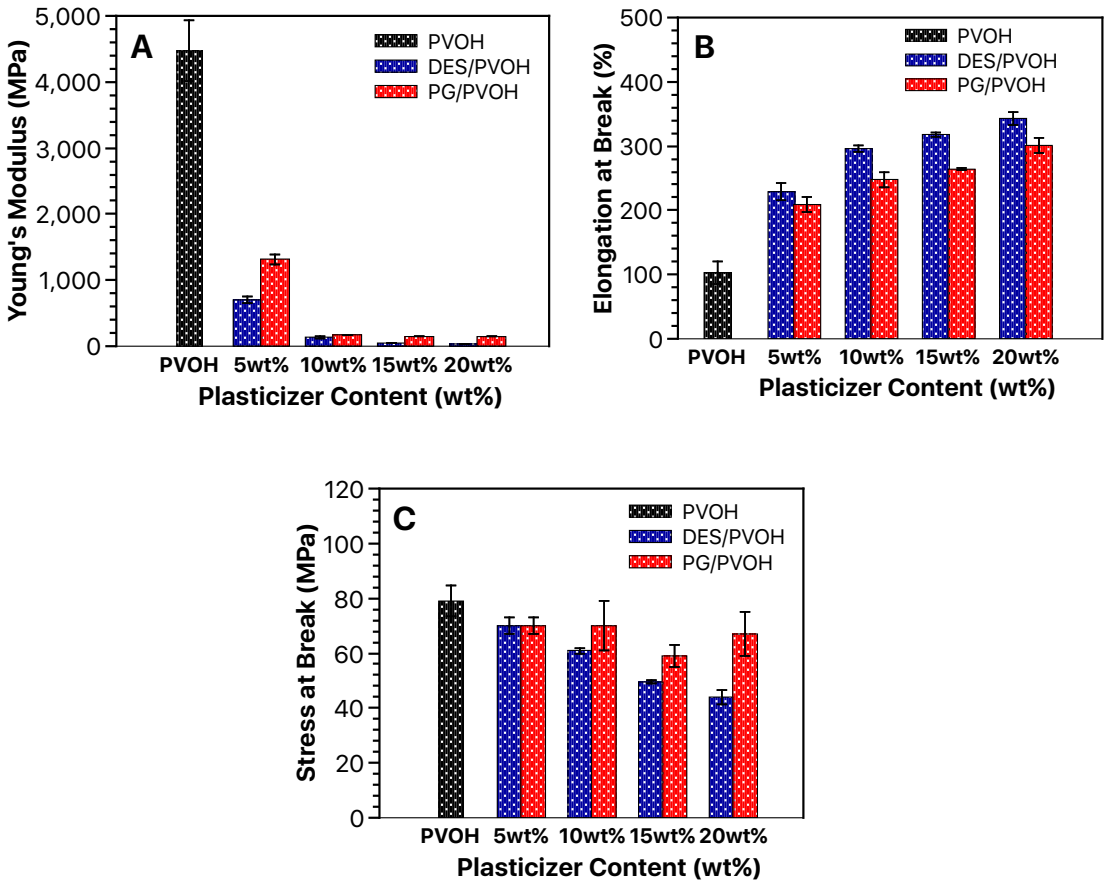

Figure 8.12. (A) Young's modulus, (B) elongation at break, and (C) stress at break of ChCl:MA DES-plasticized (blue) and PG-plasticized (red) PVOH films along with pure PVOH as a function of plasticizer content.

8.4.5 Explanation for the Different Plasticization Effect between DES and PG. Given the superior plasticization effect of DES as compared to PG, it is of interest here to provide further insights into the molecular-level interactions responsible for the relative effectiveness of DES and PG on the plasticization of PVOH. Note that ChCl:MA and PG have same functionalities (i.e., OH and C=O) as PVOH, thus, it is difficult to

systematically evaluate the H-bonding interactions between OH groups of PVOH and the functionalities of plasticizer in these two complicated plasticizer/PVOH systems. It has been demonstrated OH, C=O, and Cl^- can interact with OH of PVOH via neutral or ionic H-bonds.[14, 16, 18, 21, 22] Given that one ChCl molecule has one OH and one Cl^-, and one MA has three OH with two C=O, it is important to note that ChCl:MA (1:1 molar ratio) DES exhibit 25.6 mmols functionalities per gram, close to 26.3 mmols/g for PG. Despite comparing DES/PVOH and PG/PVOH series on a mass basis of the plasticizer, same wt% of DES and PG have similar moles of functional groups that can H-bond to the OH of PVOH. Therefore, the different plasticization effect between DES and PG is supposed to be addressed from the types of H-bonding interaction in DES/PVOH and PG/PVOH systems.

Since H-bond strength has been demonstrated as a factor to contribute to the plasticization effect on PVOH,[22] the different plasticization effectiveness between DES and PG are possibly due to the strength of the H-bonds afforded by a plasticizer. Ashworth et al.[57] examined the pairwise interactions of ChCl-urea (1:2 molar ratio) DES by a computational study, and found that (urea)NH···O=C(urea) H-bonds was stronger than (urea)NH···Cl(chloride) interaction, and the neutral (urea)NH···NH(urea) H-bond was the lowest as evidenced by decreased association energy. Thus, it is reasonable to postulate that (MA)O=C···OH(PVOH) and (chloride)Cl···OH(PVOH) H-bonds generated between PVOH and ChCl:MA DES are stronger than the neutral (PG)OH···OH(PVOH) interaction. Consequently, the stronger H-bonding interaction between DES and PVOH enables DES a more effective plasticizer as compared to PG. Further investigation will focus on a systematic model study to confirm the strength of

the H-bonds proposed between these functional groups of plasticizer and the OH groups of PVOH.

8.5 Conclusions

In this work, we have demonstrated the successful plasticization of PVOH using a ChCl:MA (1:1 molar ratio) DES as a plasticizer and confirmed that DES is more effective at plasticizing PVOH in comparison to PG, one of the widely studies alcohol-type plasticizer for PVOH. DES/PVOH films exhibit lower T_m and lower crystallizability compared to PG/PVOH blends across all plasticizer contents. By accounting for the volatile problem of PG, the highly decreased T_m of DES/PVOH blends implies a wider thermal processing window. Additionally, DES-plasticized PVOH films are more moisture sensitive than PG/PVOH films and exhibit a higher water content at the same plasticizer concentration. Furthermore, the addition of DES imparts a higher chain mobility than PG as evidenced by a greater T_g depression for DES/PVOH blends from DSC and DMA analysis. The increased chain mobility is further confirmed by lower Young's modulus and higher elongation at break as compared to PG/PVOH, signifying a greatly enhanced film ductility. Given the superior plasticization effect of DES, DES is a more attractive plasticizer than PG in plasticizing PVOH. From an applied perspective, DES-plasticized PVOH film is a promising candidate in the packaging market. Future work will focus on the investigation of molecular level interactions between DES and PVOH.

8.6 Acknowledgements

The authors gratefully acknowledge Proctor & Gamble Company for providing funds (460080) to support the efforts of this project.

8.7 References

1. Finch, C. A., Polyvinyl alcohol: properties and applications. Wiley London: 1973.
2. DeMerlis, C.; Schoneker, D., Review of the oral toxicity of polyvinyl alcohol (PVA). Food and chemical Toxicology 2003, 41 (3), 319-326.
3. Finch, C. A., Polyvinyl alcohol: developments. 1992.
4. Sakurada, I., Polyvinyl alcohol fibers. CRC Press: 1985; Vol. 6.
5. Assender, H. E.; Windle, A. H., Crystallinity in poly (vinyl alcohol). 1. An X-ray diffraction study of atactic PVOH. Polymer 1998, 39 (18), 4295-4302.
6. Bolto, B.; Tran, T.; Hoang, M.; Xie, Z., Crosslinked poly (vinyl alcohol) membranes. Progress in polymer science 2009, 34 (9), 969-981.
7. Goodship, V.; Jacobs, D., Polyvinyl alcohol: materials, processing and applications. Smithers Rapra Technology: 2009; Vol. 16.
8. Immergut, E. H.; Mark, H. F., Principles of plasticization. Plasticization and plasticizer processes 1965, 48, 1-26.
9. Platzer, N. A., Plasticization and plasticizer processes. ACS Publications: 1965.
10. Hodge, R.; Bastow, T.; Edward, G.; Simon, G.; Hill, A., Free volume and the mechanism of plasticization in water-swollen poly (vinyl alcohol). Macromolecules 1996, 29 (25), 8137-8143.
11. Hodge, R.; Edward, G. H.; Simon, G. P., Water absorption and states of water in semicrystalline poly (vinyl alcohol) films. Polymer 1996, 37 (8), 1371-1376.
12. Park, J. S.; Park, J. W.; Ruckenstein, E., A dynamic mechanical and thermal analysis of unplasticized and plasticized poly (vinyl alcohol)/methylcellulose blends. Journal of applied polymer science 2001, 80 (10), 1825-1834.
13. Park, J. S.; Park, J. W.; Ruckenstein, E., On the viscoelastic properties of poly (vinyl alcohol) and chemically crosslinked poly (vinyl alcohol). Journal of applied polymer science 2001, 82 (7), 1816-1823.
14. Cho, Y. H.; Kim, B. C.; Dan, K. S., Effects of propylene glycol on the physical properties of poly (vinyl alcohol) solutions and films. Macromolecular research 2009, 17 (8), 591-596.
15. Jiang, X.; Jiang, T.; Zhang, X.; Dai, H.; Zhang, X., Melt processing of poly (vinyl alcohol) through adding magnesium chloride hexahydrate and ethylene glycol as a complex plasticizer. Polymer Engineering & Science 2012, 52 (10), 2245-2252.
16. Mohsin, M.; Hossin, A.; Haik, Y., Thermal and mechanical properties of poly (vinyl alcohol) plasticized with glycerol. Journal of Applied Polymer Science 2011, 122 (5), 3102-3109.

17. Mohsin, M.; Hossin, A.; Haik, Y., Thermomechanical properties of poly (vinyl alcohol) plasticized with varying ratios of sorbitol. Materials Science and Engineering: A 2011, 528 (3), 925-930.
18. Hong, P.-D.; Chou, C.-M.; He, C.-H., Solvent effects on aggregation behavior of polyvinyl alcohol solutions. Polymer 2001, 42 (14), 6105-6112.
19. Ni, F.; Wang, G.; Zhao, H., The effects of urea and caprolactam on the molecular mechanisms and elastic modulus of polyvinyl alcohol (PVA): A molecular dynamics simulation study. Journal of the mechanical behavior of biomedical materials 2018, 87, 10-18.
20. Nies, C.; Messing, G. L., Effect of glass-transition temperature of polyethylene glycol-plasticized polyvinyl alcohol on granule compaction. Journal of the American Ceramic Society 1984, 67 (4), 301-304.
21. Chen, G.; Chen, N.; Li, L.; Wang, Q.; Duan, W., Ionic liquid modified poly (vinyl alcohol) with improved thermal processability and excellent electrical conductivity. Industrial & Engineering Chemistry Research 2018, 57 (15), 5472-5481.
22. Jiang, X.; Tan, B.; Zhang, X.; Ye, D.; Dai, H.; Zhang, X., Studies on the properties of poly (vinyl alcohol) film plasticized by urea/ethanolamine mixture. Journal of Applied Polymer Science 2012, 125 (1), 697-703.
23. Dai, Y.; van Spronsen, J.; Witkamp, G.-J.; Verpoorte, R.; Choi, Y. H., Natural deep eutectic solvents as new potential media for green technology. Analytica chimica acta 2013, 766, 61-68.
24. Choi, Y. H.; van Spronsen, J.; Dai, Y.; Verberne, M.; Hollmann, F.; Arends, I. W.; Witkamp, G.-J.; Verpoorte, R., Are natural deep eutectic solvents the missing link in understanding cellular metabolism and physiology? Plant physiology 2011, 156 (4), 1701-1705.
25. Dai, Y.; Verpoorte, R.; Choi, Y. H., Natural deep eutectic solvents providing enhanced stability of natural colorants from safflower (Carthamus tinctorius). Food chemistry 2014, 159, 116-121.
26. Mamajanov, I.; Engelhart, A. E.; Bean, H. D.; Hud, N. V., DNA and RNA in Anhydrous Media: Duplex, Triplex, and G-Quadruplex Secondary Structures in a Deep Eutectic Solvent. Angewandte Chemie International Edition 2010, 49 (36), 6310-6314.
27. Durand, E.; Lecomte, J.; Baréa, B.; Dubreucq, E.; Lortie, R.; Villeneuve, P., Evaluation of deep eutectic solvent–water binary mixtures for lipase-catalyzed lipophilization of phenolic acids. Green Chemistry 2013, 15 (8), 2275-2282.
28. Mano, F.; Aroso, I. M.; Barreiros, S.; Borges, J. o. P.; Reis, R. L.; Duarte, A. R. C.; Paiva, A., Production of poly (vinyl alcohol)(PVA) fibers with encapsulated natural deep eutectic solvent (NADES) using electrospinning. ACS Sustainable Chemistry & Engineering 2015, 3 (10), 2504-2509.
29. Ramesh, S.; Shanti, R.; Morris, E., Studies on the plasticization efficiency of deep eutectic solvent in suppressing the crystallinity of corn starch based polymer electrolytes. Carbohydrate polymers 2012, 87 (1), 701-706.
30. Zdanowicz, M.; Spychaj, T., Ionic liquids as starch plasticizers or solvents. Polimery 2011, 56.

31. Ramesh, S.; Shanti, R.; Morris, E., Discussion on the influence of DES content in CA-based polymer electrolytes. Journal of Materials Science 2012, 47 (4), 1787-1793.
32. Galvis-Sánchez, A. C.; Castro, M. C. R.; Biernacki, K.; Gonçalves, M. P.; Souza, H. K., Natural deep eutectic solvents as Green plasticizers for chitosan thermoplastic production with controlled/desired mechanical and barrier properties. Food Hydrocolloids 2018.
33. Martins, M.; Aroso, I. M.; Reis, R. L.; Duarte, A. R. C.; Craveiro, R.; Paiva, A., Enhanced performance of supercritical fluid foaming of natural-based polymers by deep eutectic solvents. AIChE Journal 2014, 60 (11), 3701-3706.
34. Peppas, N. A.; Hansen, P. J., Crystallization kinetics of poly (vinyl alcohol). Journal of Applied Polymer Science 1982, 27 (12), 4787-4797.
35. Ballistreri, A.; Foti, S.; Montaudo, G.; Scamporrino, E., Evolution of aromatic compounds in the thermal decomposition of vinyl polymers. Journal of Polymer Science: Polymer Chemistry Edition 1980, 18 (4), 1147-1153.
36. Holland, B.; Hay, J., The thermal degradation of poly (vinyl alcohol). Polymer 2001, 42 (16), 6775-6783.
37. Bucknall, C.; Paul, D., Polymer Blends, Formulation and Performance. John Wiley and Sons: New York, NY, USA: 2000.
38. Jang, J.; Lee, D. K., Plasticizer effect on the melting and crystallization behavior of polyvinyl alcohol. Polymer 2003, 44 (26), 8139-8146.
39. Sakellariou, P.; Rowe, R.; White, E., An evaluation of the interaction and plasticizing efficiency of the polyethylene glycols in ethyl cellulose and hydroxypropyl methylcellulose films using the torsional braid pendulum. International journal of pharmaceutics 1986, 31 (1-2), 55-64.
40. Noble, K. F.; Noble, A. M.; Talley, S. J.; Moore, R. B., Blocky bromination of syndiotactic polystyrene via post-polymerization functionalization in the heterogeneous gel state. Polymer Chemistry 2018, 9 (41), 5095-5106.
41. Ju, L.; Pretelt, J.; Chen, T.; Dennis, J. M.; Heifferon, K. V.; Baird, D. G.; Long, T. E.; Moore, R. B., Synthesis and characterization of phosphonated Poly (ethylene terephthalate) ionomers. Polymer 2018, 151, 154-163.
42. Fahs, G. B.; Benson, S. D.; Moore, R. B., Blocky sulfonation of syndiotactic polystyrene: a facile route toward tailored ionomer architecture via postpolymerization functionalization in the gel state. Macromolecules 2017, 50 (6), 2387-2396.
43. Anderson, L. J.; Yuan, X.; Fahs, G. B.; Moore, R. B., Blocky Ionomers via Sulfonation of Poly (ether ether ketone) in the Semicrystalline Gel State. Macromolecules 2018, 51 (16), 6226-6237.
44. Liu, Q.; Chen, N.; Bai, S.; Li, W., Effect of silver nitrate on the thermal processability of poly (vinyl alcohol) modified by water. RSC Advances 2018, 8 (5), 2804-2810.
45. Nyflött, Å.; Meriçer, Ç.; Minelli, M.; Moons, E.; Järnström, L.; Lestelius, M.; Baschetti, M. G., The influence of moisture content on the polymer structure of polyvinyl alcohol in dispersion barrier coatings and its effect on the mass transport of oxygen. Journal of Coatings Technology and Research 2017, 14 (6), 1345-1355.

46. Aharoni, S. M., Increased glass transition temperature in motionally constrained semicrystalline polymers. Polymers for Advanced Technologies 1998, 9 (3), 169-201.
47. Lim, H.; Hoag, S. W., Plasticizer effects on physical–mechanical properties of solvent cast Soluplus® films. Aaps Pharmscitech 2013, 14 (3), 903-910.
48. Pradhan, D. K.; Choudhary, R.; Samantaray, B.; Karan, N.; Katiyar, R., Effect of plasticizer on structural and electrical properties of polymer nanocompsoite electrolytes. Int. J. Electrochem. Sci 2007, 2, 861-871.
49. Nishio, Y.; Manley, R. J., Cellulose-poly (vinyl alcohol) blends prepared from solutions in N, N-dimethylacetamide-lithium chloride. Macromolecules 1988, 21 (5), 1270-1277.
50. Pramoda, K.; Liu, T., Effect of moisture on the dynamic mechanical relaxation of polyamide-6/clay nanocomposites. Journal of Polymer Science Part B: Polymer Physics 2004, 42 (10), 1823-1830.
51. McHugh, T. H.; Krochta, J. M., Sorbitol-vs glycerol-plasticized whey protein edible films: integrated oxygen permeability and tensile property evaluation. Journal of agricultural and food chemistry 1994, 42 (4), 841-845.
52. Jantrawut, P.; Chaiwarit, T.; Jantanasakulwong, K.; Brachais, C.; Chambin, O., Effect of plasticizer type on tensile property and in vitro indomethacin release of thin films based on low-methoxyl pectin. Polymers 2017, 9 (7), 289.
53. Roberts, R.; Rowe, R., The Young's modulus of pharmaceutical materials. International journal of pharmaceutics 1987, 37 (1-2), 15-18.
54. Audic, J.-L.; Chaufer, B., Influence of plasticizers and crosslinking on the properties of biodegradable films made from sodium caseinate. European Polymer Journal 2005, 41 (8), 1934-1942.
55. Pillin, I.; Montrelay, N.; Grohens, Y., Thermo-mechanical characterization of plasticized PLA: Is the miscibility the only significant factor? Polymer 2006, 47 (13), 4676-4682.
56. Sanyang, M.; Sapuan, S.; Jawaid, M.; Ishak, M.; Sahari, J., Effect of plasticizer type and concentration on tensile, thermal and barrier properties of biodegradable films based on sugar palm (Arenga pinnata) starch. Polymers 2015, 7 (6), 1106-1124.

57. Ashworth, C. R.; Matthews, R. P.; Welton, T.; Hunt, P. A., Doubly ionic hydrogen bond interactions within the choline chloride–urea deep eutectic solvent. Physical Chemistry Chemical Physics 2016, 18 (27), 18145-18160.

8.8 Supporting Information

Table S8.1. β and α relaxations of DES/PVOH and PG/PVOH films along with pure PVOH.

Sample	β Relaxation (°C)	α Relaxation (°C)
PVOH	55	76
5wt% ChCl:MA DES	43	72
10wt% ChCl:MA DES	36	62
15wt% ChCl:MA DES	30	56
20wt% ChCl:MA DES	29	40
5wt% PG	38	66
10wt% PG	30	61
15wt% PG	35	67
20wt% PG	36	72

Table S8.2. Summary of tensile properties of DES/PVOH and PG/PVOH films along with pure PVOH.

Sample	Young's Modulus (MPa)	Elongation at Break (%)	Stress at Break (MPa)
PVOH	4472 ± 453	103 ± 17	79 ± 6
5wt% ChCl:MA DES	701 ± 54	229 ± 13	70 ± 3
10wt% ChCl:MA DES	137 ± 16	296 ± 4	61 ± 1
15wt% ChCl:MA DES	48 ± 4	318 ± 4	50 ± 1
20wt% ChCl:MA DES	34 ± 3	343 ± 10	44 ± 3
5wt% PG	1319 ± 74	209 ± 12	70 ± 3
10wt% PG	173 ± 2	248 ± 12	70 ± 9
15wt% PG	146 ± 1	264 ± 2	59 ±4
20wt% PG	144 ± 1	301 ± 11	67 ± 8

Chapter 9. Natural Deep Eutectic Solvent-Plasticized Poly(vinyl Alcohol) Films

(Manuscript in Preparation)

Lin Ju, Dong Guo, Guoliang Liu, and Robert B. Moore*

Department of Chemistry, Macromolecules Innovation Institute, Virginia Polytechnic Institute and State University, Blacksburg, VA 24061, United States

9.1 Abstract

This work provides the first example of the successful plasticization of poly(vinyl alcohol) films using a novel natural deep eutectic solvent, L-arginine : Levulinic acid (Arg:LA), as a plasticizer. Two types of Arg:LA with different molar ratios of L-arginine and levulinic acid, i.e., Arg:LA (1:1) and Arg:LA (1:3), were synthesized to investigate the plasticization effects on the thermal and mechanical properties, as well as water absorption, of PVOH films. Differential scanning calorimetry (DSC) analysis along with dynamic mechanical analysis (DMA) revealed improved chain mobility for Arg:LA (1:3)/PVOH blends, as evidenced by a decreased T_g with increasing plasticizer content, which was in contrast to Arg:LA (1:1)-plasticized PVOH blends exhibiting an increase in T_g. This comparison implied Arg:LA with higher levulinic acid content imparted a more profound plasticization effect. Both Arg:LA (1:1)/PVOH and Arg:LA (1:3)/PVOH blends exhibited T_m and T_c depression. A greater extent of T_m depression was observed for Arg:LA (1:3)-plasticized PVOH film, indicating a higher thermal processability than Arg:LA (1:1)-PVOH blends. Similar T_c depression behavior was observed for these two

series of Arg:LA/PVOH blends, signifying similar crystallizability. In addition, the water uptake of Arg:LA/PVOH films increased with increasing relative humidity, and was independent of plasticizer content in a lower relative humidity (40%) environment. Furthermore, increasing NADES content lead to greatly deceased Young's modulus and highly improved elongation at break, suggesting highly enhanced film ductility compared to unplasticized PVOH film. Arg:LA (1:3)/PVOH films exhibit lower Young's moduli as compared to Arg:LA (1:1) analogues, further implying Arg:LA (1:3) with a higher levulinic acid molar ratio was more effective in plasticizing PVOH.

9.2 Introduction

Natural deep eutectic solvents (NADESs) are mixtures of natural compounds[1-5] (e.g., sugars, sugar alcohols, polyalcohols, organic acids and bases, amino acids) that interact through hydrogen bonding and liquefy if combined in specific molar ratios.[6] The concept of NADESs was first presented by Choi et al.[7] in 2011. They reported a series of common natural products become liquid in certain molar ratios at ambient temperature, and hypothesized such liquids could exist as a third liquid medium in living organisms apart from water and lipids, which can be utilized to explain many biological phenomena. To date, more than 150 NADES combinations have been reported.[1-7] The natural origin of the components (mainly plant primary metabolites, which are taken daily from vegetables or fruit) gives NADESs a great advantage over synthetic ionic liquids (ILs) and deep eutectic solvents (DESs) since NADESs are clearly less toxic and more environmentally friendly.[6-8] NADESs have been actively applied in diverse fields, e.g., extraction of natural ingredients,[5, 8-10] media for enzymatic or chemical reactions,[11-14]

solubilizing non-water-soluble drugs for pharmaceutical purposes,[15-17] cosmetic ingredients,[18] agrochemical uses,[19, 20] etc.

Poly(vinyl alcohol) (PVOH) is one of the most widely used water-soluble polymers in the fields of fibers, films, hydrogels, and adhesives due to its high strength, high hydrophilicity, and good barrier property.[21-24] Given that the melting temperature (T_m) of PVOH is close to its thermal degradation temperature (T_d), the thermal processing of PVOH is limited, and PVOH is processed mainly from an aqueous solution.[25-27] Various types of plasticizers including water,[28-31] alcohols,[32-35] and small organic compounds containing N-H and C=O functionalities[36, 37] have been reported to successfully plasticize PVOH. The functional groups, i.e., OH, NH and C=O, of these plasticizers could form stable hydrogen bonding with the OH groups of PVOH, resulting in reduced degree of intermolecular H-bonding interactions between PVOH chains, thereby diminishing the regularity and the rigidity of polymer chains.[32, 37] It has been reported plasticized PVOH blends display decreased T_m and thus a wider thermal processing window compared to pure PVOH control.[32, 34, 35, 38] In addition, plasticized PVOH films have been demonstrated to exhibit rubber-like elasticity and increased elongation at break compared to unplasticized analogue attributed to the improved mobility of PVOH chains.[34, 35, 38] Practical processing of plasticized PVOH, however, is often limited due to partial evaporation, thermal decomposition, and instability of these plasticizers during extrusion process.[32, 33, 36]

Recently, we reported the successful plasticization of PVOH film using choline chloride : malic acid (ChCl:MA, 1:1 molar ratio) DES as a plasticizer, and demonstrated that ChCl:MA (1:1) DES was more effective in plasticizing PVOH in comparison to

propylene glycol (PG), one the widely studied alcohol-type plasticizer for PVOH.[39] In this work, we report the first investigation of the plasticization effect of a novel NADES, L-arginine : levulinic acid (Arg:LA), on thermal, mechanical, and water absorption properties of PVOH films. The plasticization effect of Arg:LA NADES with two different molar ratios of L-arginine and levulinic acid, i.e., Arg:LA (1:1) and Arg:LA (1:3), was evaluated to establish the structure-property relationship for Arg:LA/PVOH films. The purpose of this work is to provide an insight into these nontoxic, biodegradable NADES/PVOH blends and to evaluate the potential of NADES/PVOH films to be commercially produced for future packaging applications.

9.3 Experimental Section

Materials. Poly(vinyl alcohol) (88% hydrolyzed, M_w = 85K-120K g/mol) and L-Arginine (>98%) were purchased from Acros Organics and were used as received. Levulinic acid (98%) was purchased from Alfa Aesar and was used as received.

Synthesis of L-arginine : Levulinic Acid Natural Deep Eutectic Solvent (Arg:LA NADES). Two Arg:LA NADES mixtures of L-arginine (Arg) and levulinic acid (LA) with 1:1 and 1:3 molar ratios were prepared. Arg and LA were added to a round-bottomed flask equipped with a magnetic stir bar. The flask was placed into an oil bath at 100 °C with constant stirring under argon. A clear liquid was obtained after stirring for about 24 h, and the generated clear NADES mixture was allowed to stir for another 24 h at 100 °C to ensure complete mixing. After cooling to room temperature, the Arg:LA (1:1) mixture remained in glassy state and the Arg:LA (1:3) mixture remained in the clear, viscous liquid state.

Preparation of Arg:LA DES/PVOH Solution Blends. All blends were prepared as 10 wt% solutions in deionized water (i.e., $\text{wt\%} = \frac{Mass_{PVOH} + Mass_{Plasticizer}}{Mass_{Solution\ Mixture}} \times 100\%$). To prepare the blends, PVOH was first dissolved in 40 mL deionized water at 90 °C, and the solution mixture was allowed to stir for about 5 h to ensure complete dissolution. The plasticizer solutions were obtained by dissolving plasticizer in 5 mL deionized water at room temperature after stirring for about 10 min. The plasticizer/PVOH solution blends were prepared by adding the plasticizer solution into the PVOH solution, and the generated solution mixtures were allowed to stir at 90 °C overnight to ensure complete mixing. The blend compositions were designated as wt% plasticizer/wt% PVOH, and four plasticizer/PVOH blend compositions, i.e., 5/95, 10/90, 15/85 and 20/80 (w/w), were prepared. Both Arg:LA (1:1)/PVOH and Arg:LA (1:3)/PVOH solution blends were prepared by the same procedure, and a composition of pure PVOH (without plasticizer) as a control was also prepared.

Solution Casting Method. The generated solution blends were cast onto a glass substrate at room temperature using a doctor blade set to 0.075 inch. The wet films were allowed to first dry at room temperature for 48 h and then at 50 °C for about 2 h. The generated clear films were peeled off from glass substrate, and were further dried under vacuum at 30 °C for 48 h, resulting in a final thickness of 70-90 μm. Kimwipes were utilized to cover these films during drying in the vacuum oven.

Thermogravimetric Analysis (TGA). As-cast films after vacuum drying were utilized for thermal stability analysis. TGA of plasticizer/PVOH films was performed on a TA Instruments TGA Q500 with a heating ramp from ambient temperature to 550 °C at

a heating rate of 10 °C/min under constant nitrogen purging. $T_{d,\ 5\ wt\%}$ corresponded to the temperature at 5% weight loss of the initial sample weight was reported.

Differential Scanning Calorimetry (DSC). As-cast films after vacuum drying were utilized for DSC measurement. A TA instruments Q2000 differential scanning calorimetry (DSC) was used to determine the thermal transitions and crystallization behavior of plasticized PVOH blends. Under a nitrogen atmosphere, the samples (~5–8 mg) prepared in aluminum Tzero hermetic pans were heated from ambient temperature to 200 °C at 10 °C/min, quench cooled to -50 °C at -60 °C/min, reheated from -50 °C to 200 °C at 10 °C/min, and then cooled to 0 °C at -10 °C/min. The glass transition temperature (T_g) and melting temperature (T_m) were determined from the second heating scan after erasing the thermal history; the crystallization temperature (T_c) was investigated from the subsequent cooling scan by using the TA Instruments Universal Analysis software.

Dynamic Mechanical Analysis (DMA). As-cast films after vacuum drying were conditioned in a 40% relative humidity atmosphere at 30 °C for 24 h before measurements. A TA Instruments Q800 DMA in oscillatory tension mode was used to determine the mechanical properties of PVOH blend films as a function of temperature. Samples were ramped at 2 °C/min from -50 °C to 190 °C at a frequency of 1 Hz, an oscillatory amplitude of 15.0 μm, and a static force of 0.01 N to determine the effect of modulus versus temperature. The β and α relaxation were determined from the peaks in tanδ versus temperature.

Water Uptake Measurement. The water uptake behaviors of PVOH films with various NADES contents were studied at relative humidity of 30%, 50%, and 70% at 30 °C. The equilibrium water uptake for each film composition was determined by

conditioning dry films in the humidity chamber for 12 h. The mass of the dry film (W_{dry}) was recorded prior to measurement, and the mass of the wet film (W_{wet}) was recorded to determine the water absorption of PVOH blend films. The reported values are the average of 5 samples for each blend composition. The water uptake was calculated as:

$$\text{Water uptake} = \frac{W_{wet} - W_{dry}}{W_{dry}} \times 100\% \quad (9.1)$$

Tensile Test. Dumbbell-shaped specimens were cut from the vacuum dried as-cast films, and were conditioned in a 40% relative humidity atmosphere at 30 °C for 24 h before measurements. Tensile tests were conducted at ambient relative humidity and room temperature. The specimens were clamped in the tensile fixture with a distance between grips of 26.54 mm, and the width of narrow section of 3.32 mm. The thicknesses of these specimens were accurately measured for each sample using a calibrated caliper, and were approximately ranging from 70 μm to 90 μm. Tensile testing was performed on a 5500R Instron universal testing instrument at a crosshead speed of 5 mm/min. The Young's moduli and elongation at break were reported as an average of five specimens.

9.4 Results and Discussion

9.4.1 Thermal Properties. Thermogravimetric analysis (TGA) was performed to evaluate the thermal stability of Arg:LA (1:1)/PVOH/ and Arg:LA (1:3)/PVOH blends. The TGA thermograms of these two series of plasticized-PVOH blends along with pure PVOH are shown in **Figure S9.1**, and the thermal degradation temperatures, $T_{d,\,5\ wt\%}$ (i.e., the temperature at which 5 wt% weight loss), are compared in **Figure 9.1**. Two weight loss stages are observed on the thermograms of pure PVOH: the first stage starts near 260 °C, consistent with the elimination of the side groups of PVOH; and the second stage

starts near 380 °C, corresponding to the breakdown of PVOH backbone.[40, 41] Based on the graph of wt% versus temperature, it is apparent all Arg:LA/PVOH blends exhibit similar thermal degradation behavior to pure PVOH (**Figure S9.1**). At low NADES content, i.e., 5 wt%, both of the two types of PVOH blends show similar $T_{d,\,5\ wt\%}$ as pure PVOH, while higher NADES contents lead to a shift of $T_{d,\,5\ wt\%}$ to lower temperature region since L-arginine degrade at 236 °C,[42] which is lower than that of pure PVOH ($T_{d,\,5\ wt\%}$ of PVOH = 278 °C). Furthermore, with increasing the DES concentration up to 20 wt%, a more significant decrease in $T_{d,\,5\ wt\%}$ is observed for Arg:LA (1:1) DES/PVOH blends as compared to Arg:LA (1:3)/PVOH blends containing a lower fraction of L-arginine. This comparison signifies the slightly higher thermal stability of Arg:LA (1:3) DES/PVOH blends than that of PVOH blends containing Arg:LA (1:1).

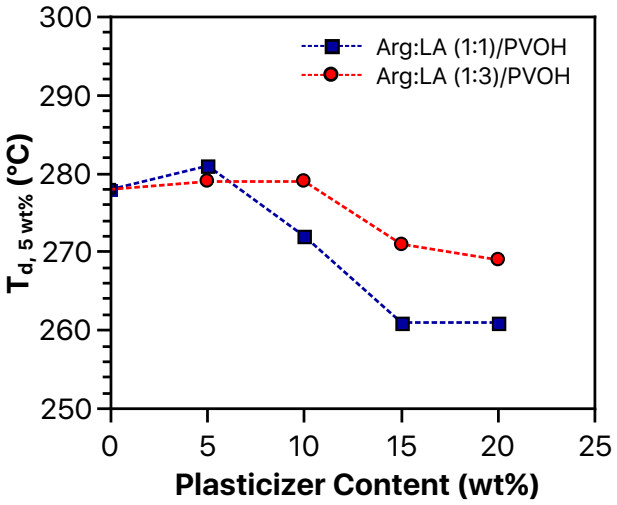

Figure 9.1. $T_{d,\,5\ wt\%}$ (°C) of Arg:LA (1:1)-plasticized (blue squares) and Arg:LA (1:3)-plasticized (red circles) PVOH films as a function of plasticizer content (wt%). TGA analysis was performed at 10 °C/min under nitrogen purge.

Differential scanning calorimetry (DSC) was utilized to provide further insight into the plasticization effect of Arg:LA with different molar ratios of L-arginine and levulinic acid on the thermal properties of PVOH blends. The samples were first heated into the melt and quench cooled to erase thermal history, and then heated into melt again followed by a slow cooling. The second heating thermograms and the subsequent slow cool thermograms of dry Arg:LA (1:1)/PVOH and Arg:LA (1:3)/PVOH blends with varying amounts of plasticizers are shown in **Figures S9.2** and **S9.3**. The heating thermograms for all the blend compositions display two enthalpic events: a glass transition and a melting endotherm; and the subsequent cooling scans reveal a crystallization exotherm. The glass transition temperatures (T_g) for these two sets of NADES/PVOH blends are compared in **Figure 9.2**, and the melting temperatures (T_m) and the crystallization temperatures (T_c) are compared in **Figure 9.3A** and **Figure 9.3B**, respectively.

Given that the glass transition temperature (T_g) reflects the extent of the mobility of polymer chains, it is of interest to investigate the influence of NADES with different molar ratios of L-arginine and levulinic acid on the glass transitions of PVOH blends. **Figure 9.2** provides the comparison of T_g between Arg:LA (1:1)/PVOH and Arg:LA (1:3)/PVOH blends with respect to the wt% of plasticizer. From the graph of T_g as a function of wt% plasticizer, it is evident that Arg:LA (1:3) leads to a significant T_g depression with increasing plasticizer loading, suggesting the successfully plasticization of PVOH using Arg:LA (1:3) NADES as a plasticizer. Note that for pure PVOH, the hydroxyl groups contribute to the stiffness of the polymer chains via hydrogen bonding interaction.[31] Arg:LA (1:3) NADES forms stable hydrogen bonding with the hydroxyl

groups of PVOH, attenuating the hydrogen bonding interactions of PVOH, thus reducing chain stiffness.[28] Consequently, with increasing plasticizer content, Arg:LA (1:3)/PVOH blends exhibit an increased degree of chain mobility, and hence, yield a decreased T_g. In distinct contrast, however, an increased T_g is observed for PVOH blends plasticized with Arg:LA (1:1) containing a higher molar ratio of levulinic acid. Considering that L-arginine has more functional groups that are capable of H-bonding to the OH groups of PVOH than levulinic acid, Arg:LA (1:1) are expected to interact more effectively with PVOH than Arg:LA (1:3), which contains lower molar fraction of L-arginine, affording a more profound T_g depression. This unexpected increase in T_g for Arg:LA (1:1)/PVOH blends is presumably due to the higher glass transition temperature of Arg:LA (1:1) (i.e., 74 °C determined from DSC analysis) than that of pure PVOH (i.e., 63 °C determined from DSC analysis). Thus, unlike Arg:LA (1:3), Arg:LA (1:1) fails to successfully plasticize PVOH.

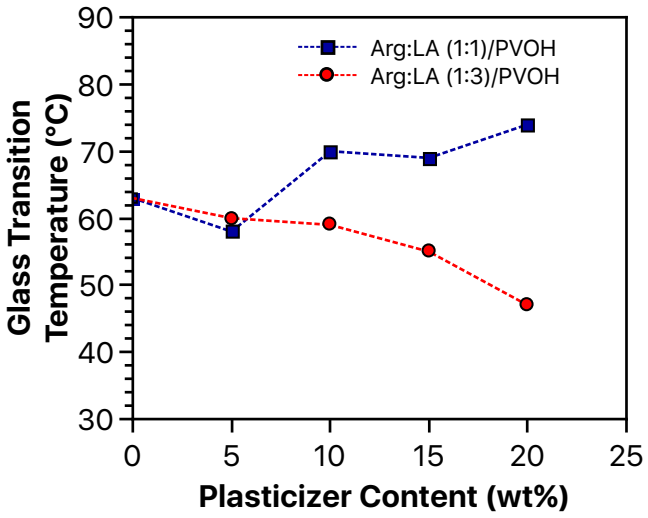

Figure 9.2. Glass transition temperatures of Arg:LA (1:1)-plasticized (blue squares) and Arg:LA (1:3)-plasticized (red circles) PVOH blends versus plasticizer content (wt%).

Dynamic mechanical analysis (DMA) was performed to further elucidate the difference between the glass transitions of Arg:LA (1:1)/PVOH and Arg:LA (1:3)/PVOH blends. To mimic the environmental storage conditions for PVOH film products, these films were conditioned in a 40% relative humidity atmosphere at 30 °C for 24 h prior to measurements. **Figure S9.4** displays the tan δ profiles of these two series of PVOH films. All these films exhibit two mechanical relaxations corresponding to primary (α) relaxation and secondary (β) relaxation.[30, 31, 43] The upper temperature, i.e., α relaxation, is attributed to the glass transition of PVOH, and is attributed to the long-chain segmental motion in the amorphous region.[30, 31, 43] The lower temperature transition, i.e., β relaxation, are not well understood based on the literature. The β relaxation has been related to the movement of polar groups of the polymer that are not hydrogen-bonded to each other.[44] Therefore, the β relaxation of these PVOH films presumably represents water-PVOH or plasticizer-PVOH complex units.

The α and β relaxations for Arg:LA (1:1)- and Arg:LA (1:3)-plasticized PVOH films derived from the tan δ versus temperature curves at different plasticizer concentrations are compared in **Figure 9.3**. With increasing NADES content, α relaxation of Arg:LA (1:1)-plasticized PVOH blends shifts to a higher temperature region, while a decrease in T_g is observed for Arg:LA (1:3)/PVOH blends. This difference in T_g is consistent with the T_g obtained from DSC analysis, and further confirms that Arg:LA NADES with a higher molar ratio of levulinic acid affords a higher

chain mobility. In addition, similar decrease in β relaxation temperature has been observed for both of these two types of PVOH blends. Note that these films were conditioned in a 40% relative humidity atmosphere at 30 °C for 24 h before measurements. Similar water uptake is observed for these two series of PVOH blends at the same relative humidity by a water absorption study, which will be mentioned in the following discussion. Thus, it is reasonable to assume the similar β relaxation is due to the similar water content that imparts a similar effect on the β relaxations of these films.

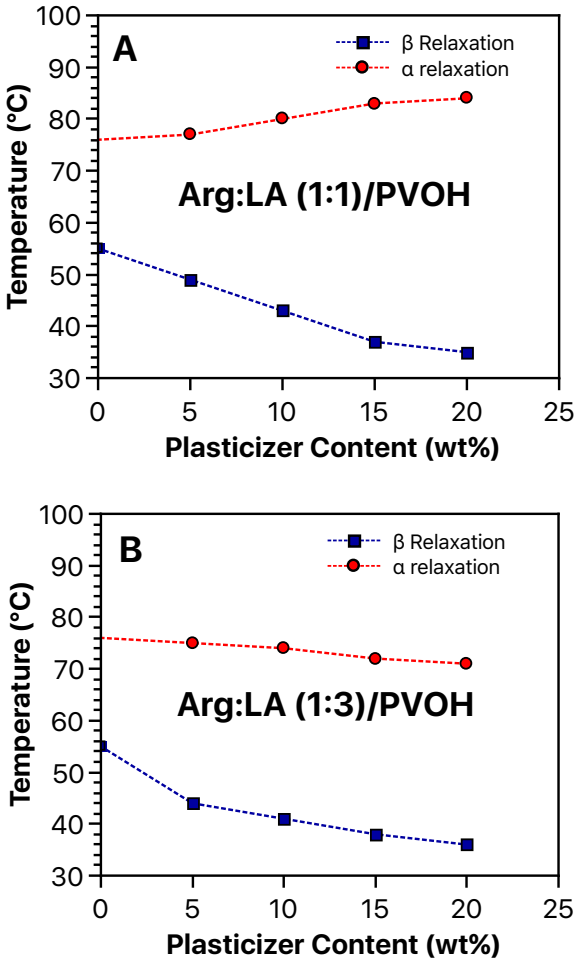

Figure 9.3. β relaxation (blue squares) and α relaxation (red circles) of (A) Arg:LA (1:1)/PVOH and (B) Arg:LA (1:3)/PVOH blends at various plasticizer contents. 1 Hz, 2 °C/min, an oscillatory amplitude of 15.0 μm, and a static force of 0.01 N were employed. The films were conditioned in a 40% relative humidity atmosphere at 30 °C for 24 h before measurements.

Figure 9.4 provides the T_m and T_c of Arg:LA (1:1)/PVOH and Arg:LA (1:3)/PVOH blends with respect to plasticizer content. As expected, both T_m and T_c decrease with increasing NADES concentration. NADES molecules hydrogen-bonded to

the hydroxyl groups of PVOH along the chains are presumably acting as physical defects that are excluded from the crystalline domains. With an increasing defect content, the statistical average length of crystallizable segment decreases, limiting the lamellar thickness.[45-48] Consequently, it is not surprising then that both Arg:LA (1:1)- and Arg:LA (1:3)-plasticized PVOH blends exhibit a T_m depression with increasing plasticizer content. Nevertheless, it is important to note that a more profound T_m depression (about a 20 °C decrease) is observed for 20 wt% Arg:LA (1:3)-plasticized PVOH blend in comparison to Arg:LA (1:1) analogue. This relatively higher T_m of Arg:LA (1:1)/PVOH blend at a higher plasticizer loading may be attributed to the possible phase separation of Arg:LA (1:1) NADES within the polymer matrix that diminishes the H-bonding interaction between NADES and PVOH.[49, 50] Thus, an increase in T_m is observed as a result of decreased number of structural defects. Furthermore, it is important to note that from a practical perspective, the more profound T_m depression of Arg:LA (1:3)/PVOH at 20 wt% NADES concentration suggests a higher thermal processability as compared to Arg:LA (1:1) analogue.

Additionally, the decreased T_c of these two series of Arg:LA/PVOH blends implies lower crystallizability with the addition of Arg:LA NADES. The systematic decrease in T_c reflects a reduction in the rate of crystallization during these non-isothermal scans. Upon cooling from the melt, as the polymer chains attempt to pack into crystalline structures, plasticizers act as interactive defects that are rejected from the growing crystalline interface, thus retarding the crystallization phenomenon to lower temperatures.[46, 48] Moreover, Arg:LA (1:1)/PVOH blends exhibit similar T_c depression as

compared to Arg:LA (1:3)/PVOH blends across all NADES contents, indicating similar crystallizability.

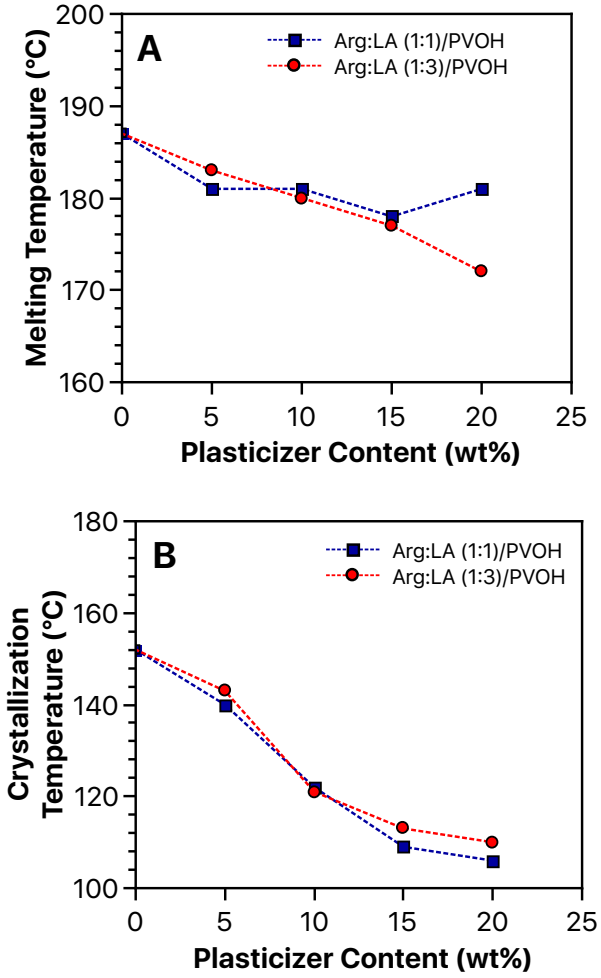

Figure 9.4. (A) Melting temperatures and (B) crystallization temperatures of Arg:LA (1:1)-plasticized (blue squares) and Arg:LA (1:3)-plasticized (red circles) PVOH blends versus plasticizer content (wt%).

9.4.2 Water Absorption. The water absorption performance of Arg:LA (1:1)/PVOH and Arg:LA (1:3)/PVOH blends was examined at different relative humidity (RH) of 30%, 50%, and 70%, and the corresponding equilibrium water uptake data are

compared in **Figure 9.5**. Our previous work[39] examined the water uptake kinetics of pure PVOH, and found the water uptake of PVOH reaches to an equilibrium after conditioning the PVOH film in a certain relatively humidity (relative humidity = 30%, 50%, and 70%) for about 1 h. Thus, in this study, the equilibrium water uptake of Arg:LA/PVOH films were measured after conditioning these films at a certain relative humidity for 12 h. Not surprisingly, higher relative humidity affords higher water uptake due to the hydrophilicity of PVOH matrix. Furthermore, at low relative humidity (i.e., 30% RH), no significant difference between the water uptake of these two series of NADES/PVOH blends is observed across all plasticizer concentrations, while water uptake slightly increases with increasing plasticizer content at higher relative humidity (i.e., 50% RH and 70% RH). This signifies that the water uptake of NADES/PVOH films is independent of plasticizer content in a relatively dry environment. Nevertheless, Arg:LA-plasticized PVOH films absorb less moisture from the environment in comparison to PVOH films plasticized by choline chloride-based deep eutectic solvents (e.g., choline chloride : malic acid),[39] possibly due to the nonionic nature of NADES and the similar polarity between Arg:LA and PVOH.

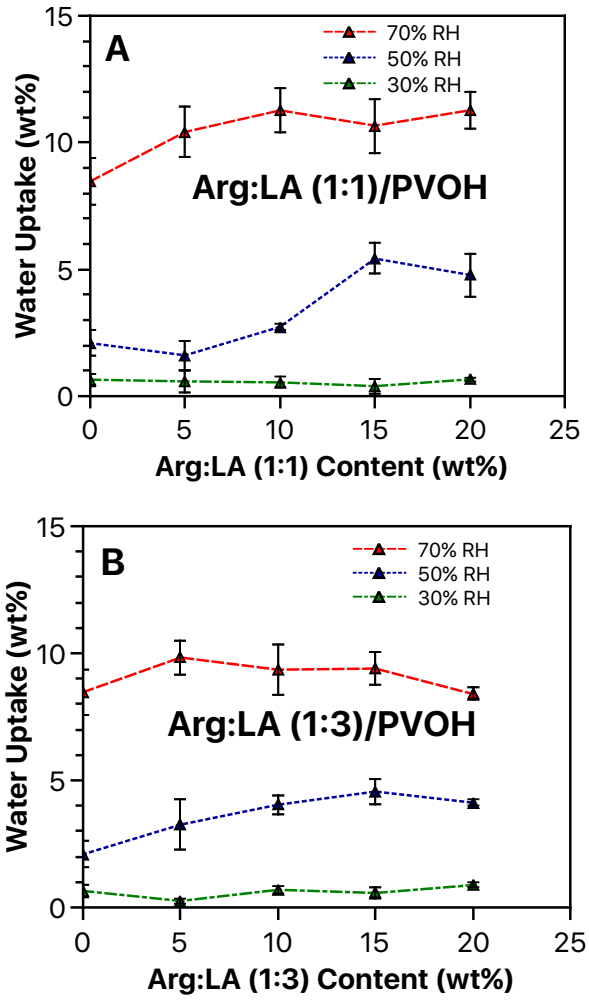

Figure 9.5. Equilibrium water uptake of (A) Arg:LA (1:1)/PVOH and (B) Arg:LA (1:3)/PVOH blends with various plasticizer contents in the relative humidity (RH) of 30%, 50% and 70%. Water uptake values were recorded after conditioning the films in the humidity chamber for 12 h at 30 °C.

9.4.3 Tensile Properties. The plasticization effect of Arg:LA with different molar ratios of L-arginine and levulinic acid on the mechanical properties of PVOH films was investigated using tensile testing. Analysis was performed on as-cast films that were equilibrated in a 40% relative humidity for 24 h prior to measurements. The

representative engineering stress-strain curves of PVOH blends are displayed in **Figure 9.6**, and the corresponding tensile properties, including Young's modulus and elongation at break, are compared in **Figure 9.7A** and **Figure 9.7B**, respectively. The stress-strain curve of pure PVOH film displays an apparent yield point. However, increasing Arg:LA content leads to a diminished yield point, and an absence of yield point is observed at higher plasticizer contents, suggesting rubber-like behavior. This observation reveals that the incorporation of Arg:LA as plasticizer successfully reduces the brittleness of pure PVOH films, thus leading to an enhancement of film ductility. Furthermore, Arg:LA (1:1)/PVOH blends start to exhibit an absence of yield point at 20 wt% of plasticizer, while no yield point is observed for Arg:LA (1:3)/PVOH blends when the plasticizer concentration reaches 10 wt%. This comparison confirms Arg:LA with higher molar ratio of levulinic acid imparts a higher film ductility. This conclusion was also found by the results characterized from DSC and DMA whereby decreased T_g with increasing plasticizer content is observed for Arg:LA (1:3)/PVOH blends.

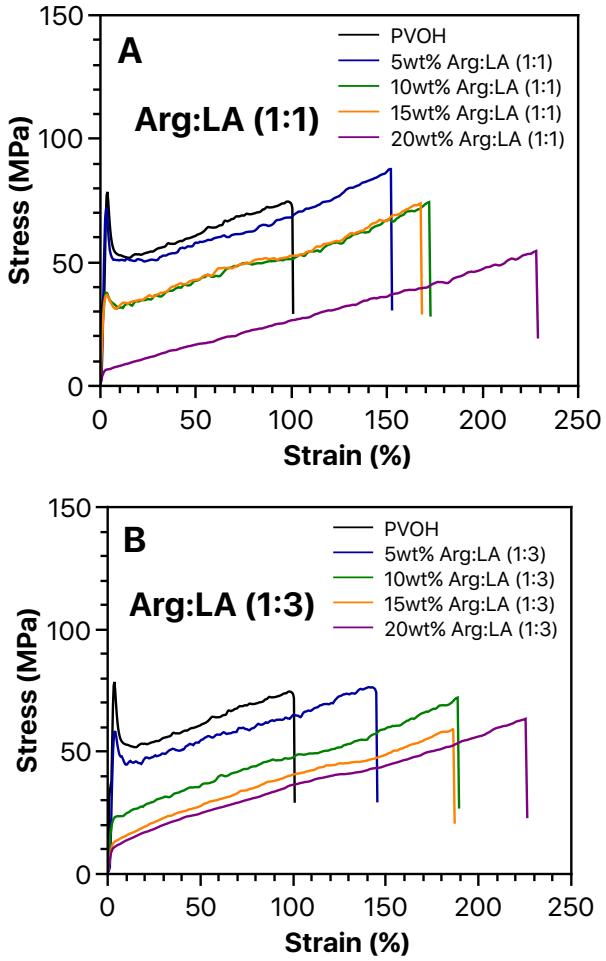

Figure 9.6. Stress-strain curves of (A) Arg:LA (1:1)/PVOH and (B) Arg:LA (1:3)/PVOH films along with pure PVOH film. The films were conditioned in a 40% relative humidity atmosphere at 30 °C for 24 h before measurements. Samples were tested with a crosshead speed of 5 mm/min.

The Young's moduli of Arg:LA-plasticized PVOH films decrease with increasing plasticizer content, and Arg:LA (1:1)/PVOH blends exhibit higher Young's moduli as compared to Arg:LA (1:3) analogues, as shown in **Figure 9.7A**. Young's modulus or elastic modulus is the fundamental measure of the film stiffness, and is associated with the resistance of the film to elastic deformation.[51-53] The lower the Young's modulus, the

lower the stiffness of the films, thus the higher the film ductility.[51-53] This significant decrease in Young's moduli suggests that PVOH films loss their stiffness and become more ductile with the addition of plasticizer. The H-bonding interactions between NADES and the hydroxyl groups of PVOH disrupt the H-bonding interaction of pure PVOH, reducing the chain stiffness and improving the chain mobility, consequently resulting in more flexible networks. Thus, the plasticized PVOH films turn to less resistant to elastic deformation as evidenced by lower Young's moduli. Moreover, the lower Young's moduli for Arg:LA (1:3)/PVOH blends as compared to Arg:LA (1:1)-plasticized PVOH films are in consistent with the T_g depression of Arg:LA (1:3)/PVOH blends, further implying Arg:LA with a higher molar ratio of levulinic acid results a greater chain mobility of PVOH.

The elongation at break of Arg:LA (1:1)/PVOH and Arg:LA (1:3)/PVOH blends is shown in **Figure 9.7B**. The elongation at break increases with increasing NADES content, suggesting improved film ductility. With 20 wt% of Arg:LA incorporated in PVOH, the elongation is improved by more than 100% as compared to pure PVOH control. Elongation at break is defined as the ability of the film to deform before finally breaking, and is related to the chain mobility and film ductility.[51, 52] Consistent with the lower Young's moduli of Arg:LA/PVOH films, the incorporated Arg:LA leads to lower a rigidity of PVOH chains and more ductile films by allowing more chain mobility, thus higher elongation at break than PVOH analogue. Additionally, these two series of Arg:LA/PVOH blends exhibit similar elongation at the same wt% of plasticizer. It is important to note that these blend films were conditioned in 40% relative humidity for 24 h before tensile test, and water has been demonstrated as a plasticizer for PVOH.[28-31] The

similar elongation between these two sets of Arg:LA/PVOH blends is reasonably attributed to the similar equilibrium water content among these blend films.

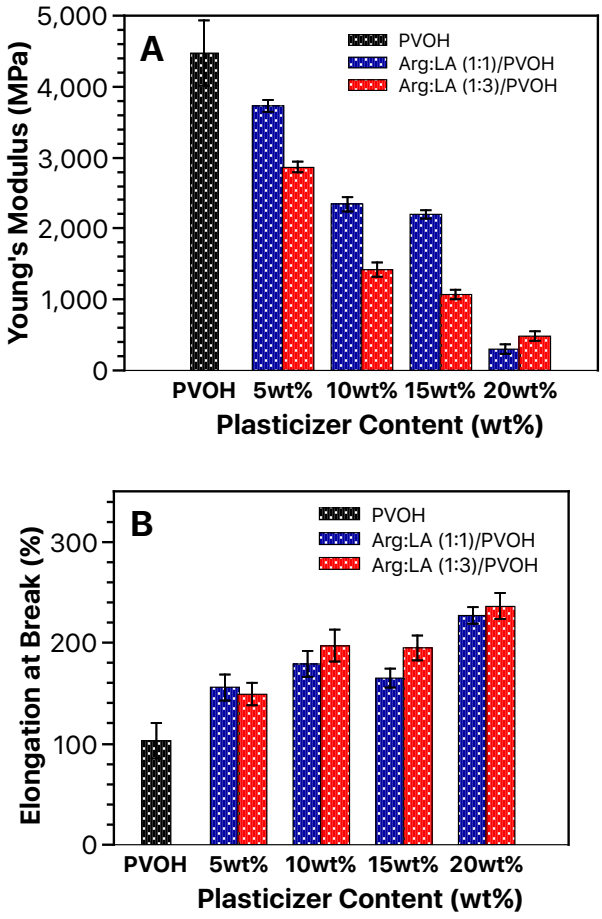

Figure 9.7. (A) Young's modulus and (B) elongation at break of Arg:LA (1:1)-plasticized (blue) and Arg:LA (1:3)-plasticized (red) PVOH films along with pure PVOH (black) as a function of plasticizer content.

9.5 Conclusions

In this work, we have demonstrated the successful plasticization of PVOH using Arg:LA as a plasticizer. Analysis of thermal properties showed T_g, T_m, and T_c depression with increasing plasticizer concentration, implying the effective plasticization of PVOH.

The water uptake study indicated the water uptake of the Arg:LA/PVOH blends were less dependent on the plasticizer content than the choline chloride : malic acid deep eutectic solvent-plasticized PVOH films[39] as reported from our previous work. In addition, Arg:LA-plasticized PVOH films exhibit highly decreased Young's moduli and greatly improved elongation at break, signifying improved film ductility.

The plasticization effects of Arg:LA NADES with different molar ratios of L-arginine and levulinic acid, i.e., Arg:LA (1:1) and Arg:LA (1:3), were also evaluated in this work. Arg:LA with a higher molar ratio of levulinic acid was more effective in plasticizing PVOH in comparison to Arg:LA (1:1). Both DSC and DMA confirmed the significant T_g depression for Arg:LA (1:3)/PVOH blends, while an increased T_g with increasing plasticizer concentration was observed for Arg:LA (1:1)/PVOH blends. The greater plasticization effect of Arg:LA (1:3) was further confirmed by the lower Young's modulus for Arg:LA (1:3)/PVOH films as compared to Arg:LA (1:1) analogues. The relatively lower plasticization effect of Arg:LA (1:1) is presumably due to its higher glass transition temperature than that of PVOH. Overall, this work demonstrated NADES as a nontoxic, sustainable, and biodegradable plasticizer is a promising candidate to improve the thermal processability and film ductility of PVOH, and confirmed the potential of NADES/PVOH films for future applications in the packaging market of health-related products.

9.6 Acknowledgements

The authors gratefully acknowledge Proctor & Gamble Company for providing funds (460080) to support the efforts of this project.

9.7 References

1. Bakirtzi, C.; Triantafyllidou, K.; Makris, D. P., Novel lactic acid-based natural deep eutectic solvents: Efficiency in the ultrasound-assisted extraction of antioxidant polyphenols from common native Greek medicinal plants. Journal of Applied Research on Medicinal and Aromatic Plants 2016, 3 (3), 120-127.
2. Huang, Y.; Feng, F.; Jiang, J.; Qiao, Y.; Wu, T.; Voglmeir, J.; Chen, Z.-G., Green and efficient extraction of rutin from tartary buckwheat hull by using natural deep eutectic solvents. Food chemistry 2017, 221, 1400-1405.
3. Jhong, H.-R.; Wong, D. S.-H.; Wan, C.-C.; Wang, Y.-Y.; Wei, T.-C., A novel deep eutectic solvent-based ionic liquid used as electrolyte for dye-sensitized solar cells. Electrochemistry Communications 2009, 11 (1), 209-211.
4. Kokosa, J. M., Selecting an appropriate solvent microextraction mode for a green analytical method. In Green Extraction Techniques: Principles, Advances and Applications, Comprehensive Analytical Chemistry: 2017; Vol. 76, pp 403-425.
5. Paradiso, V. M.; Clemente, A.; Summo, C.; Pasqualone, A.; Caponio, F., Towards green analysis of virgin olive oil phenolic compounds: Extraction by a natural deep eutectic solvent and direct spectrophotometric detection. Food chemistry 2016, 212, 43-47.
6. Vanda, H.; Dai, Y.; Wilson, E. G.; Verpoorte, R.; Choi, Y. H., Green solvents from ionic liquids and deep eutectic solvents to natural deep eutectic solvents. Comptes Rendus Chimie 2018, 21 (6), 628-638.
7. Choi, Y. H.; van Spronsen, J.; Dai, Y.; Verberne, M.; Hollmann, F.; Arends, I. W.; Witkamp, G.-J.; Verpoorte, R., Are natural deep eutectic solvents the missing link in understanding cellular metabolism and physiology? Plant physiology 2011, 156 (4), 1701-1705.
8. González, C. G.; Mustafa, N. R.; Wilson, E. G.; Verpoorte, R.; Choi, Y. H., Application of natural deep eutectic solvents for the "green" extraction of vanillin from vanilla pods. Flavour and Fragrance Journal 2018, 33 (1), 91-96.
9. Dai, Y.; Rozema, E.; Verpoorte, R.; Choi, Y. H., Application of natural deep eutectic solvents to the extraction of anthocyanins from Catharanthus roseus with high extractability and stability replacing conventional organic solvents. Journal of Chromatography A 2016, 1434, 50-56.
10. Dai, Y.; Witkamp, G.-J.; Verpoorte, R.; Choi, Y. H., Natural deep eutectic solvents as a new extraction media for phenolic metabolites in Carthamus tinctorius L. Analytical chemistry 2013, 85 (13), 6272-6278.
11. Khodaverdian, S.; Dabirmanesh, B.; Heydari, A.; Dashtban-Moghadam, E.; Khajeh, K.; Ghazi, F., Activity, stability and structure of laccase in betaine based natural deep eutectic solvents. International journal of biological macromolecules 2018, 107, 2574-2579.
12. Xu, X.; Guo, Z.; Cheong, L.-Z., Ionic Liquids in Lipid Processing and Analysis: Opportunities and Challenges. Elsevier: 2016.
13. Yang, T.-X.; Zhao, L.-Q.; Wang, J.; Song, G.-L.; Liu, H.-M.; Cheng, H.; Yang, Z., Improving whole-cell biocatalysis by addition of deep eutectic solvents and natural deep eutectic solvents. ACS Sustainable Chemistry & Engineering 2017, 5 (7), 5713-5722.

14. Zhao, H.; Baker, G. A.; Holmes, S., Protease activation in glycerol-based deep eutectic solvents. Journal of Molecular Catalysis B: Enzymatic 2011, 72 (3-4), 163-167.
15. Shamseddin, A.; Crauste, C.; Durand, E.; Villeneuve, P.; Dubois, G.; Durand, T.; Vercauteren, J.; Veas, F., Resveratrol formulated with a natural deep eutectic solvent inhibits active matrix metalloprotease-9 in hormetic conditions. European journal of lipid science and technology 2017, 119 (11), 1700171.
16. Wikene, K. O.; Bruzell, E.; Tønnesen, H. H., Improved antibacterial phototoxicity of a neutral porphyrin in natural deep eutectic solvents. Journal of Photochemistry and Photobiology B: Biology 2015, 148, 188-196.
17. Wikene, K. O.; Rukke, H. V.; Bruzell, E.; Tønnesen, H. H., Investigation of the antimicrobial effect of natural deep eutectic solvents (NADES) as solvents in antimicrobial photodynamic therapy. Journal of Photochemistry and Photobiology B: Biology 2017, 171, 27-33.
18. Jeong, K. M.; Ko, J.; Zhao, J.; Jin, Y.; Yoo, D. E.; Han, S. Y.; Lee, J., Multi-functioning deep eutectic solvents as extraction and storage media for bioactive natural products that are readily applicable to cosmetic products. Journal of cleaner production 2017, 151, 87-95.
19. Huang, Y.; Feng, F.; Chen, Z.-G.; Wu, T.; Wang, Z.-H., Green and efficient removal of cadmium from rice flour using natural deep eutectic solvents. Food chemistry 2018, 244, 260-265.
20. Zahrina, I.; Nasikin, M.; Krisanti, E.; Mulia, K., Deacidification of palm oil using betaine monohydrate-based natural deep eutectic solvents. Food chemistry 2018, 240, 490-495.
21. DeMerlis, C.; Schoneker, D., Review of the oral toxicity of polyvinyl alcohol (PVA). Food and chemical Toxicology 2003, 41 (3), 319-326.
22. Finch, C. A., Polyvinyl alcohol: properties and applications. Wiley London: 1973.
23. Finch, C. A., Polyvinyl alcohol: developments. 1992.
24. Sakurada, I., Polyvinyl alcohol fibers. CRC Press: 1985; Vol. 6.
25. Bolto, B.; Tran, T.; Hoang, M.; Xie, Z., Crosslinked poly (vinyl alcohol) membranes. Progress in polymer science 2009, 34 (9), 969-981.
26. Goodship, V.; Jacobs, D., Polyvinyl alcohol: materials, processing and applications. Smithers Rapra Technology: 2009; Vol. 16.
27. Assender, H. E.; Windle, A. H., Crystallinity in poly (vinyl alcohol). 1. An X-ray diffraction study of atactic PVOH. Polymer 1998, 39 (18), 4295-4302.
28. Hodge, R.; Bastow, T.; Edward, G.; Simon, G.; Hill, A., Free volume and the mechanism of plasticization in water-swollen poly (vinyl alcohol). Macromolecules 1996, 29 (25), 8137-8143.
29. Hodge, R.; Edward, G. H.; Simon, G. P., Water absorption and states of water in semicrystalline poly (vinyl alcohol) films. Polymer 1996, 37 (8), 1371-1376.
30. Park, J. S.; Park, J. W.; Ruckenstein, E., A dynamic mechanical and thermal analysis of unplasticized and plasticized poly (vinyl alcohol)/methylcellulose blends. Journal of applied polymer science 2001, 80 (10), 1825-1834.
31. Park, J. S.; Park, J. W.; Ruckenstein, E., On the viscoelastic properties of poly (vinyl alcohol) and chemically crosslinked poly (vinyl alcohol). Journal of applied polymer science 2001, 82 (7), 1816-1823.

32. Cho, Y. H.; Kim, B. C.; Dan, K. S., Effects of propylene glycol on the physical properties of poly (vinyl alcohol) solutions and films. Macromolecular research 2009, 17 (8), 591-596.
33. Jiang, X.; Jiang, T.; Zhang, X.; Dai, H.; Zhang, X., Melt processing of poly (vinyl alcohol) through adding magnesium chloride hexahydrate and ethylene glycol as a complex plasticizer. Polymer Engineering & Science 2012, 52 (10), 2245-2252.
34. Mohsin, M.; Hossin, A.; Haik, Y., Thermal and mechanical properties of poly (vinyl alcohol) plasticized with glycerol. Journal of Applied Polymer Science 2011, 122 (5), 3102-3109.
35. Mohsin, M.; Hossin, A.; Haik, Y., Thermomechanical properties of poly (vinyl alcohol) plasticized with varying ratios of sorbitol. Materials Science and Engineering: A 2011, 528 (3), 925-930.
36. Hong, P.-D.; Chou, C.-M.; He, C.-H., Solvent effects on aggregation behavior of polyvinyl alcohol solutions. Polymer 2001, 42 (14), 6105-6112.
37. Ni, F.; Wang, G.; Zhao, H., The effects of urea and caprolactam on the molecular mechanisms and elastic modulus of polyvinyl alcohol (PVA): A molecular dynamics simulation study. Journal of the mechanical behavior of biomedical materials 2018, 87, 10-18.
38. Chen, G.; Chen, N.; Li, L.; Wang, Q.; Duan, W., Ionic liquid modified poly (vinyl alcohol) with improved thermal processability and excellent electrical conductivity. Industrial & Engineering Chemistry Research 2018, 57 (15), 5472-5481.
39. Lin Ju, Z. M., Dong Guo, Guoliang Liu, and Robert B. Moore, Comparison of Plasticization Effects of Deep Eutectic Solvent and Propylene Glycol on the Physical Properties of Poly(vinyl Alcohol) Films. Manuscript in preparation.
40. Ballistreri, A.; Foti, S.; Montaudo, G.; Scamporrino, E., Evolution of aromatic compounds in the thermal decomposition of vinyl polymers. Journal of Polymer Science: Polymer Chemistry Edition 1980, 18 (4), 1147-1153.
41. Holland, B.; Hay, J., The thermal degradation of poly (vinyl alcohol). Polymer 2001, 42 (16), 6775-6783.
42. Weiss, I. M.; Muth, C.; Drumm, R.; Kirchner, H. O., Thermal decomposition of the amino acids glycine, cysteine, aspartic acid, asparagine, glutamic acid, glutamine, arginine and histidine. BMC biophysics 2018, 11 (1), 2.
43. Nishio, Y.; Manley, R. J., Cellulose-poly (vinyl alcohol) blends prepared from solutions in N, N-dimethylacetamide-lithium chloride. Macromolecules 1988, 21 (5), 1270-1277.
44. Pramoda, K.; Liu, T., Effect of moisture on the dynamic mechanical relaxation of polyamide-6/clay nanocomposites. Journal of Polymer Science Part B: Polymer Physics 2004, 42 (10), 1823-1830.
45. Noble, K. F.; Noble, A. M.; Talley, S. J.; Moore, R. B., Blocky bromination of syndiotactic polystyrene via post-polymerization functionalization in the heterogeneous gel state. Polymer Chemistry 2018, 9 (41), 5095-5106.
46. Ju, L.; Pretelt, J.; Chen, T.; Dennis, J. M.; Heifferon, K. V.; Baird, D. G.; Long, T. E.; Moore, R. B., Synthesis and characterization of phosphonated Poly (ethylene terephthalate) ionomers. Polymer 2018, 151, 154-163.

47. Fahs, G. B.; Benson, S. D.; Moore, R. B., Blocky sulfonation of syndiotactic polystyrene: a facile route toward tailored ionomer architecture via postpolymerization functionalization in the gel state. Macromolecules 2017, 50 (6), 2387-2396.
48. Anderson, L. J.; Yuan, X.; Fahs, G. B.; Moore, R. B., Blocky Ionomers via Sulfonation of Poly (ether ether ketone) in the Semicrystalline Gel State. Macromolecules 2018, 51 (16), 6226-6237.
49. Jang, J.; Lee, D. K., Plasticizer effect on the melting and crystallization behavior of polyvinyl alcohol. Polymer 2003, 44 (26), 8139-8146.
50. Sakellariou, P.; Rowe, R.; White, E., An evaluation of the interaction and plasticizing efficiency of the polyethylene glycols in ethyl cellulose and hydroxypropyl methylcellulose films using the torsional braid pendulum. International journal of pharmaceutics 1986, 31 (1-2), 55-64.
51. McHugh, T. H.; Krochta, J. M., Sorbitol-vs glycerol-plasticized whey protein edible films: integrated oxygen permeability and tensile property evaluation. Journal of agricultural and food chemistry 1994, 42 (4), 841-845.
52. Jantrawut, P.; Chaiwarit, T.; Jantanasakulwong, K.; Brachais, C.; Chambin, O., Effect of plasticizer type on tensile property and in vitro indomethacin release of thin films based on low-methoxyl pectin. Polymers 2017, 9 (7), 289.
53. Roberts, R.; Rowe, R., The Young's modulus of pharmaceutical materials. International journal of pharmaceutics 1987, 37 (1-2), 15-18.

9.8 Supporting Information

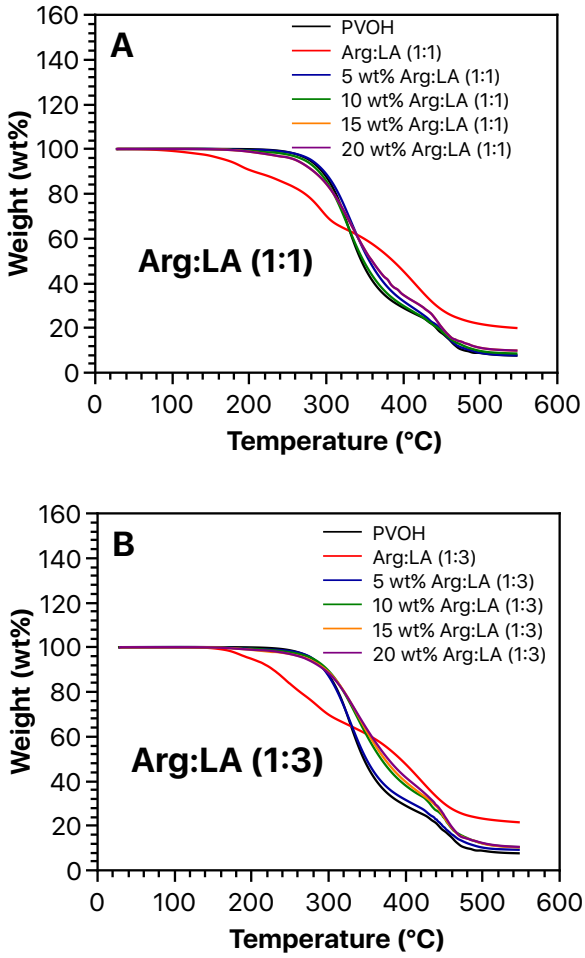

Figure S9.1. Thermogravimetric analysis (TGA) thermograms of (A) Arg:LA (1:1)/PVOH blends, and (B) Arg:LA (1:3)/PVOH blends. TGA analysis was performed at 10 °C/min under nitrogen purge.

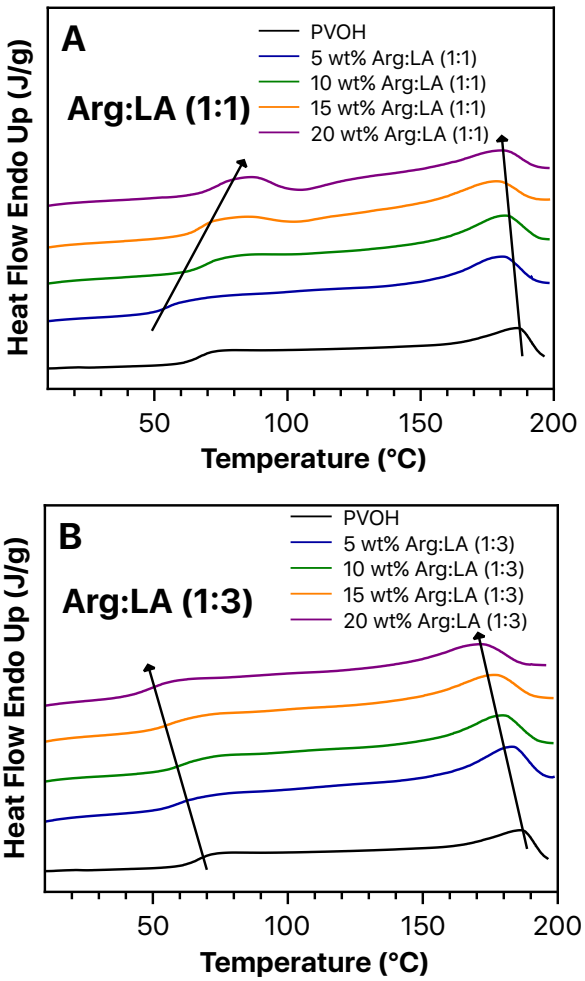

Figure S9.2. DSC heating scans of (A) Arg:LA (1:1)/PVOH blends, and (B) Arg:LA (1:3)/PVOH blends. Second heat reported with a heating rate of 10 °C/min after quench cooling (-60 °C/min) from the 200 °C.

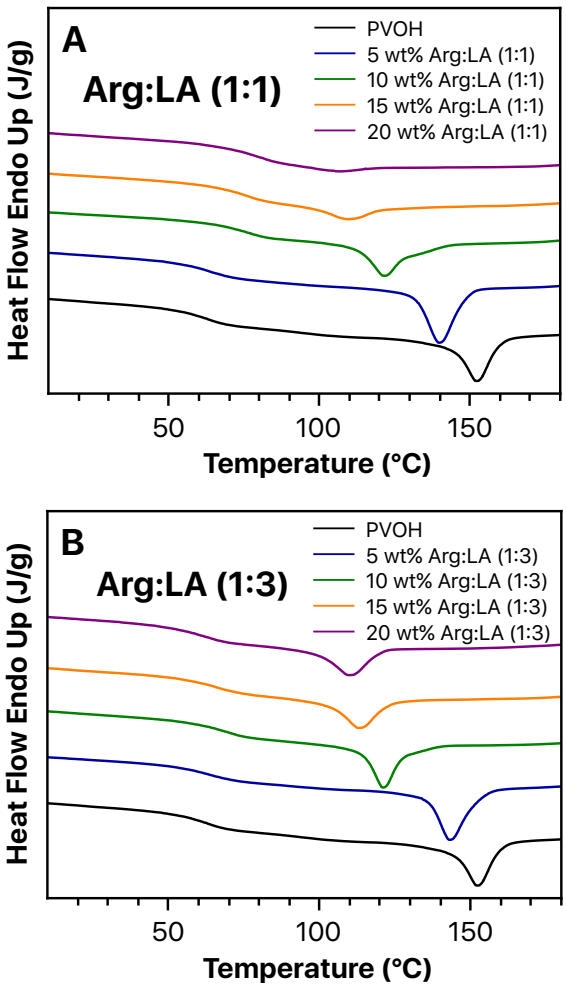

Figure S9.3. DSC cooling scans of (A) Arg:LA (1:1)/PVOH blends, and (B) Arg:LA (1:3)/PVOH blends. Subsequent cooling reported with a cooling rate of -10 °C/min after heating to 200 °C.

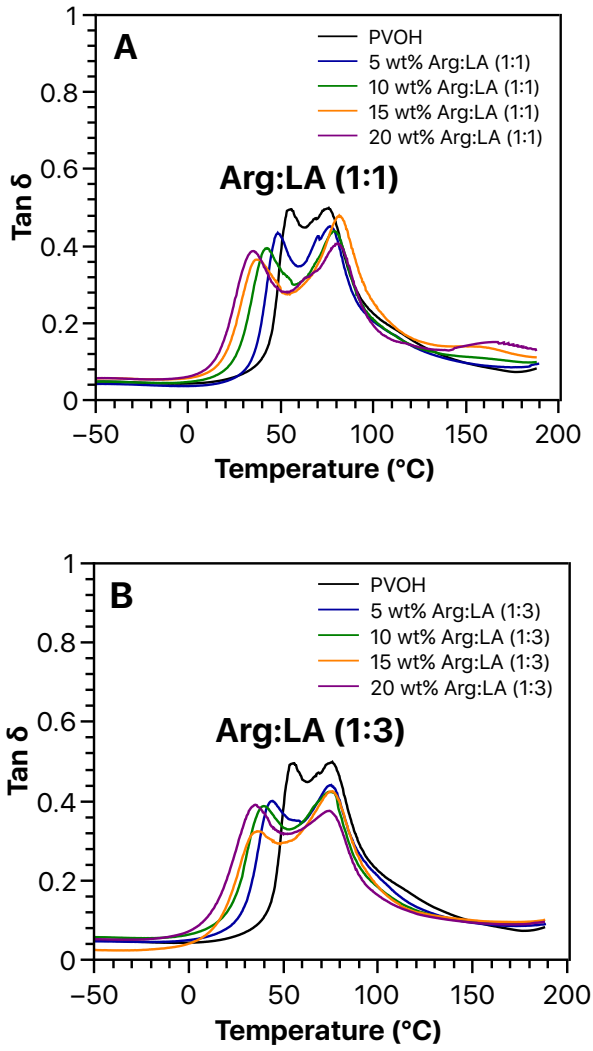

Figure S9.4. Tan δ of (A) Arg:LA (1:1)/PVOH and (B) Arg:LA (1:3)/PVOH films at various plasticizer contents. 1 Hz, 2 °C/min, an oscillatory amplitude of 15.0 μm, and a static force of 0.01 N were employed. The films were conditioned in a 40% relative humidity atmosphere at 30 °C for 24 h before measurements.

Chapter 10. Overall Conclusions

Poly(ethylene terephthalate) (PET) and polystyrene ionomers bearing monovalent sulfonate and divalent phosphonate pendant ions have been successfully synthesized, and the influence of pendant ions on the properties of PET and polystyrene ionomers have been evaluated. The divalent phosphonate pendent ions have been shown to generate stronger ionic associations, consequently providing a stronger physically crosslinked network in phosphonated ionomers as compared to sulfonated analogues. This conclusion was evidenced by higher glass transition temperatures, longer relaxation time, and higher zero-shear viscosity for phosphonated ionomers than SPS ionomers containing the same mol% of ionic monomers. The results from morphology analysis of polystyrene ionomers indicated larger ionic aggregates with higher charge density were generated from the associated phosphonate groups as compared to the sulfonate groups, further suggesting the stronger physical crosslinked network formed in phosphonated ionomers. In addition, it is interesting to note that PET ionomers containing small amounts of divalent phosphonate pendant ions exhibited improved crystallizability and faster crystallization kinetics as compared to SPET ionomers, possibly attributed to the higher nucleation density in PPET.

PPET ionomers with divalent phosphonate pendant ions were more effective at compatibilizing polyester/polyamide blends in comparison to SPET ionomer containing monovalent sulfonate pendant ions. Both SPET/PETG/MXD6 and PPET/PETG/MXD6 blends were prepared using a solution mixing method to enable thin film characterization. The compatibilization effect of monovalent sulfonate and divalent phosphonate pendant

ions was compared with respect to mol% of ionic monomers and mol% of pendant ions, respectively. The comparison on a mol% of ionic monomers basis demonstrates the PPET/PETG/MXD6 blends require 6 times fewer ionic monomers to achieve the same compatibility of polyester/polyamide blends relative to blends compatibilized with the conventional SPET ionomer. On a per mol pendant ion basis, the phosphonate ions have been found to be 3 times more effective at compatibilizing polyester/polyamide blends relative to sulfonate ions. Given the superior compatibilization effect for the divalent phosphonate pendant ions, PPET ionomer is an attractive compatibilizer for various polyester/polyamide blend systems.

The effective compatibilization of melt-mixed PET/MXD6 blends using PPET ionomer as a minor-component compatibilizer was confirmed. Evidence of the effective compatibilization was provided by the reduced MXD6 domain dimension and diminished nucleating effect of smaller MXD6 domain size on the crystallization behavior of PET with increasing mol% of phosphonated ionic monomers in the polyester matrix. Compatibilization of PET/MXD6 blends greatly improved optical properties for biaxially oriented blend films attributed reduced MXD6 platelet size. A significant decrease on the oxygen permeability of biaxially oriented PET/MXD6 blends was observed. The smaller MXD6 platelets at higher phosphonated monomer concentrations increased tortuosity of oxygen diffusion pathway, leading to an increase in diffusivity, thus a reduced permeability.

The successful plasticization of PVOH with two types of deep eutectic solvents (DES), i.e., ChCl:MA and Arg:LA, has been demonstrated. ChCl:MA DES/PVOH films exhibited more profound depression in T_g, T_m, and T_c, and enhanced film ductility as

compared to POVH films containing the same amount of propylene glycol. Arg:LA natural DES with the molar ratio of 1:3 was demonstrated as an effective plasticizer for PVOH. The effective plasticization of PVOH using NADES confirmed the potential of NADES/PVOH films for future applications in the packaging market of health-related products.

Chapter 11. Suggested Future Work

11.1 Reactive Extrusion to Generate Carboxylic Acid-Functionalized Acrylonitrile Butadiene Styrene (ABS): Exploration of Thiol-ene Reaction in the Melt State

Reactive extrusion is a method for polymerization or polymer modification by chemical reaction in the melt state. Post-polymerization thiol-ene reaction has been utilized as a method to prepare blocky copolymers and functionalized polymers in solvents.[1-4] Various types of thiol compounds containing carboxylic acid have been developed and are commercially available. The -SH groups on these thiol compounds are expected to react with polymers containing vinyl functionalities to generated ionomers containing carboxylate functionalities. As depicted in **Scheme 11.1**, the vinyl groups from acrylonitrile butadiene styrene (ABS) possess the potential to react with a thiol compound bearing –COOH, 4-mercaptobenzoic acid, to impart carboxylic acid functionalities on ABS. Extrusion temperature, residence time, initiator type, and different structures of thiol compounds will be explored to probe the feasibility of this thiol-ene reaction in the melt state.

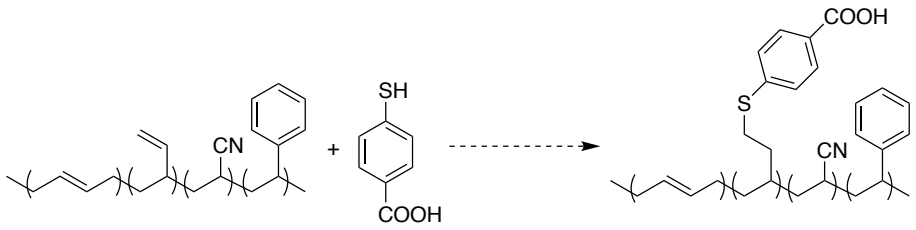

Scheme 11.1. Proposed thiol-ene reaction between ABS and 4-mercaptobenzoic acid.

11.2 Investigation of Desalination Property for Phosphonated Poly(ether ether ketone) (PPEEK) as Water Purification Membrane.

Poly(ether ether ketone) is a promising candidate material for water purification membrane due to its strong thermomechanical properties. Phosphonated PEEK (PPEEK) ionomers are of interest because of the divalent functionalities that make it more charged than ionomers with monovalent functional groups, such as sulfonated PEEK (SPEEK). PPEEK membrane is expected to exhibit improved desalination properties than SPEEK at the same level of functionality. PPEEK ionomers were synthesized by post-polymerization to first generate the ester form, and the Na^+ form was realized by hydrolysis and neutralization (**Scheme 11.2**). PPEEK ionomer films were obtained by solution casting method. Our preliminary results indicated that PPEEK with ion exchange capacity (IEC) of 2.4 meq/g showed similar water uptakes and salt permeability as compared SPEEK with lower IEC of 1.2 meq/g, implying the expected, higher desalination property of PPEEK. Future work will focus on the systematic evaluation of water, ion permeability, and desalination properties of PPEEK films as compared to SPEEK analogues.

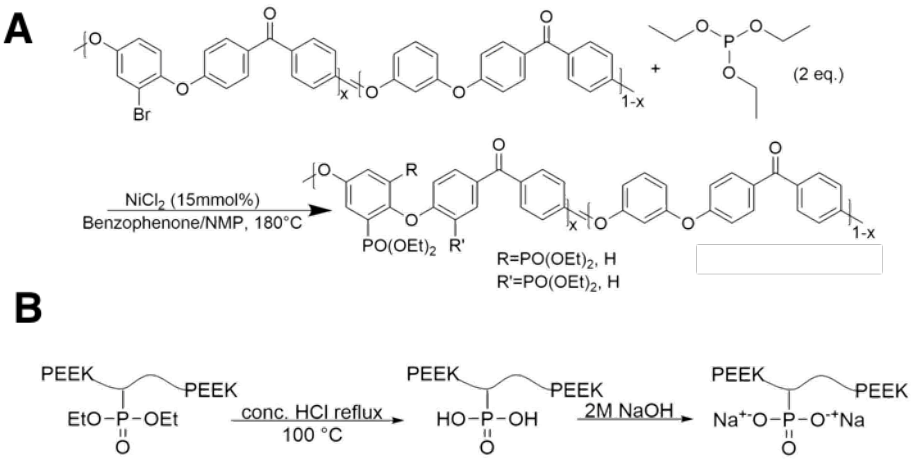

Scheme 11.2. (A) Sythesis of PPEEK in the ester form, and (B) the conversion of the ester form to Na^+ form.

11.3 References

1. Chabanne, L.; Pfirrmann, S.; Lunn, D. J.; Manners, I., Controlled thiol–ene post-polymerization reactions on polyferrocenylsilane homopolymers and block copolymers. Polymer Chemistry 2013, 4 (7), 2353-2360.
2. Hall, D. J.; Van Den Berghe, H. M.; Dove, A. P., Synthesis and post-polymerization modification of maleimide-containing polymers by 'thiol-ene'click and Diels–Alder chemistries. Polymer International 2011, 60 (8), 1149-1157.
3. Lowe, A. B., Thiol-ene "click" reactions and recent applications in polymer and materials synthesis. Polymer Chemistry 2010, 1 (1), 17-36.
4. Singha, N. K.; Gibson, M. I.; Koiry, B. P.; Danial, M.; Klok, H.-A., Side-Chain Peptide-Synthetic Polymer Conjugates via Tandem "Ester-Amide/Thiol–Ene" Post-Polymerization Modification of Poly (pentafluorophenyl methacrylate) Obtained Using ATRP. Biomacromolecules 2011, 12 (8), 2908-2913.